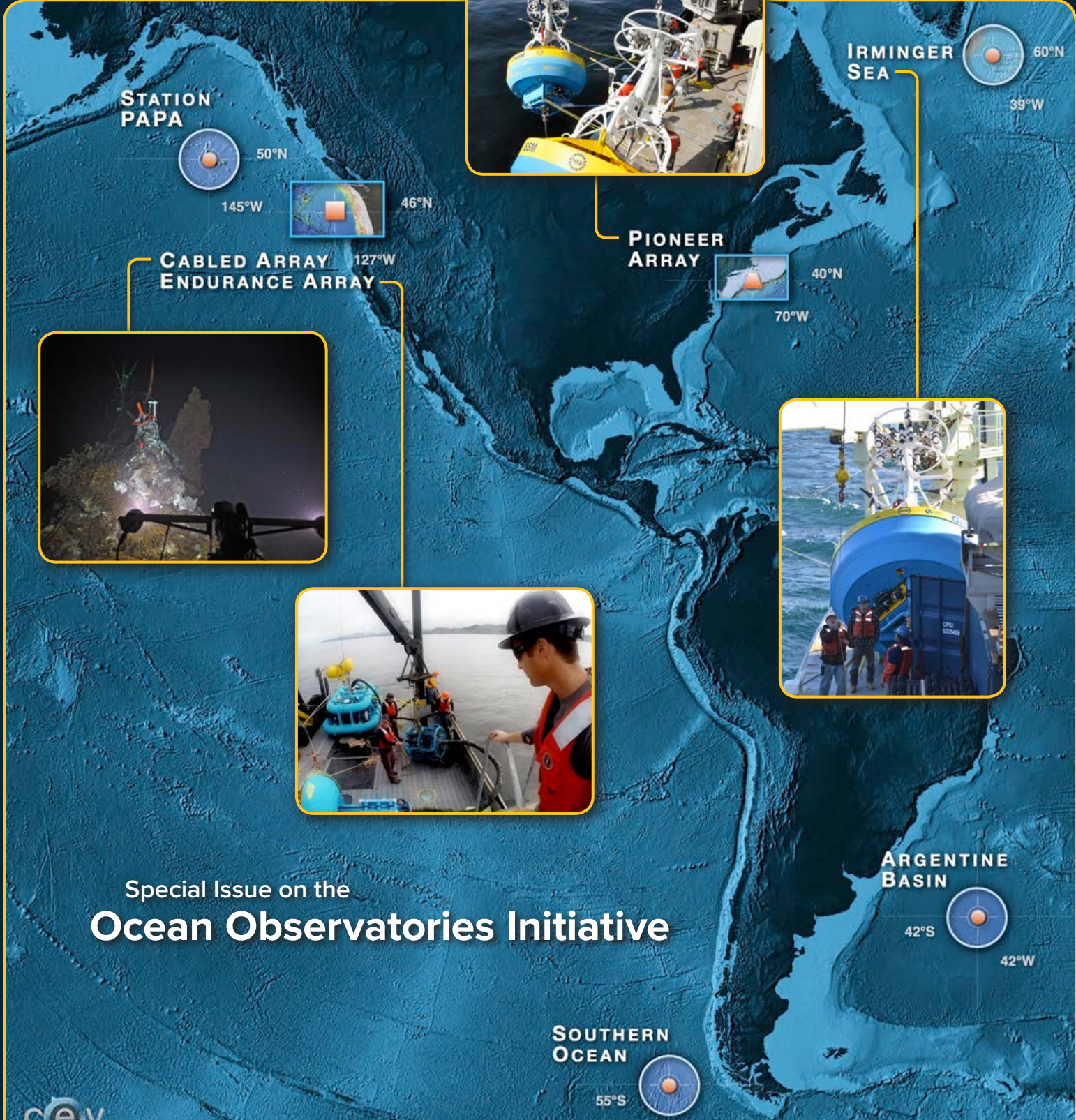


Oceanography

VOL.31, NO.1, MARCH 2018



Special Issue on the
Ocean Observatories Initiative



Content is copyright protected and provided for personal use only - not for reproduction or retransmission.

For reprints please contact the Publisher.

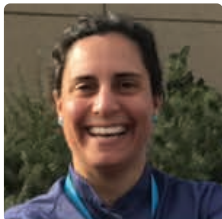


SEA·BIRD
SCIENTIFIC



See Us at Booth 113

Sea-Bird Scientific Presentations at the 2018 Ocean Sciences Meeting



Kim Martini, Ph.D., Senior Oceanographer

Dynamic Corrections for Sea-Bird Surface Temperature Salinity Sensors (STS) on ARGO Profiling Floats

Monday, February 12, 2018; 4:00-6:00 PM, Oregon Convention Center, Poster Hall



David J. Murphy, MS, Director of Science

Determination of Conductivity Cell Compressibility for Argo Program CTDs and MicroCATs

Tuesday, February 13, 2018; 4:00-6:00 PM, Oregon Convention Center, Poster Hall



Charles W. Branham, Ph.D., Senior Chemist

Field Validation of ISFET Based Ocean pH Sensors

Wednesday February 14, 2018; 4:00-6:00 PM, Oregon Convention Center, Poster Hall



Ian Walsh, Ph.D., Director of Science

Nutrient and Estuarine Processes Driven by Hurricane Irma Recorded by the Indian River Lagoon Observatory Network of Environmental Sensors

Friday, February 16, 2018; 3:36-3:48 PM, Oregon Convention Center, F151

Measuring Calibration and Field Variance Scales in Oceanographic Optical Instrumentation Data for Quality Assurance

Tuesday, February 13, 2018; 4:00-6:00 PM, Oregon Convention Center, Poster Hall

+1 425 643 9866 | seabird@seabird.com | seabird.com



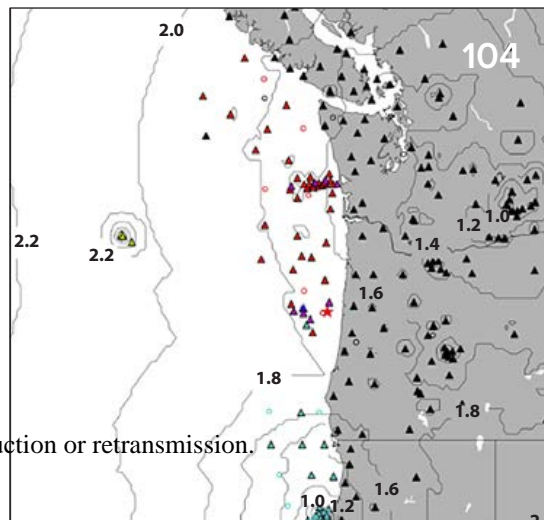
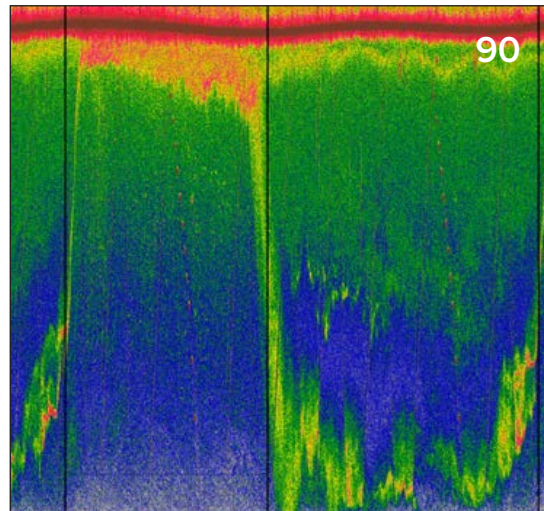
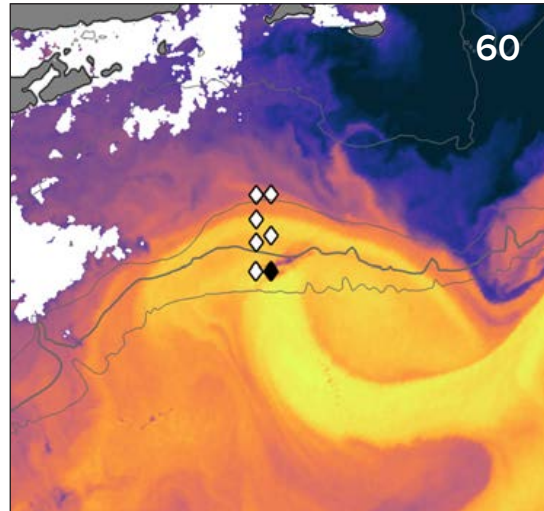
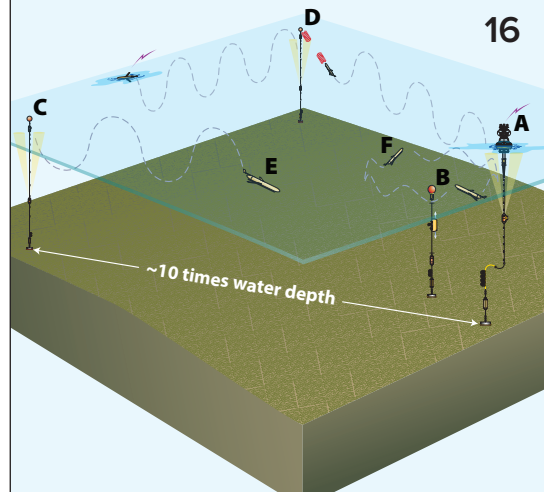
Content is copyright protected and provided for personal use only - not for reproduction or retransmission.

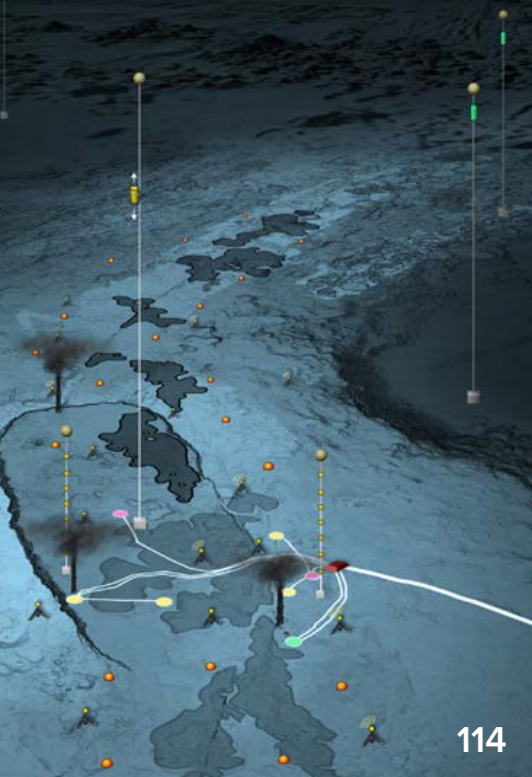
For reprints please contact the Publisher.

contents

SPECIAL ISSUE ON
The Ocean Observatories Initiative

- 12** **FROM THE GUEST EDITORS.** Introduction to the Special Issue on the Ocean Observatories Initiative
By L.M. Smith, T.J. Cowles, R.D. Vaillancourt, and S. Yelisetti
- 16** **The Ocean Observatories Initiative**
By L.M. Smith, J.A. Barth, D.S. Kelley, A. Plueddemann, I. Rodero, G.A. Ulises, M.F. Vardaro, and R. Weller
- 36** **Sidebar > Accessing OOI Data**
By M.F. Vardaro and J. McDonnell
- 38** **On the Relationship Between the Global Ocean Observing System and the Ocean Observatories Initiative**
By E. Lindstrom
- 42** **The North Atlantic Biological Pump: Insights from the Ocean Observatories Initiative Irminger Sea Array**
By H.I. Palevsky and D.P. Nicholson
- 50** **Deep Convection in the Irminger Sea Observed with a Dense Mooring Array**
By M.F. de Jong, M. Oltmanns, J. Karstensen, and L. de Steur
- 60** **The Changing Nature of Shelf-Break Exchange Revealed by the OOI Pioneer Array**
By G. Gawarkiewicz, R.E. Todd, W. Zhang, J. Partida, A. Gangopadhyay, M.-U.-H. Monim, P. Fratantoni, A. Malek Mercer, and M. Dent
- 71** **Sidebar > SeaView: Bringing Together an Ocean of Data**
By K. Stocks, S. Diggs, C. Olson, A. Pham, R. Arko, A. Shepherd, and D. Kinkade
- 72** **Atmospheric and Offshore Forcing of Temperature Variability at the Shelf Break: Observations from the OOI Pioneer Array**
By K. Chen, G. Gawarkiewicz, and A. Plueddemann
- 80** **Temporal and Spatial Dynamics of Physical and Biological Properties along the Endurance Array of the California Current Ecosystem**
By F. Henderikx Freitas, G.S. Saldías, M. Goñi, R.K. Shearman, and A.E. White
- 90** **Warm Blobs, Low-Oxygen Events, and an Eclipse: The Ocean Observatories Initiative Endurance Array Captures Them All**
By J.A. Barth, J.P. Fram, E.P. Dever, C.M. Risien, C.E. Wingard, R.W. Collier, and T.D. Kearney
- 98** **Power from Benthic Microbial Fuel Cells Drives Autonomous Sensors and Acoustic Modems**
By C.E. Reimers and M. Wolf
- 104** **The Role of the Ocean Observatories Initiative in Monitoring the Offshore Earthquake Activity of the Cascadia Subduction Zone**
By A.M. Tréhu, W.S.D. Wilcock, R. Hilmo, P. Bodin, J. Connolly, E.C. Roland, and J. Braumiller





114 The Recent Volcanic History of Axial Seamount: Geophysical Insights into Past Eruption Dynamics with an Eye Toward Enhanced Observations of Future Eruptions

By W.S.D. Wilcock, R.P. Dziak, M. Tolstoy, W.W. Chadwick Jr., S.L. Nooner, D.R. Bohnenstiehl, J. Caplan-Auerbach, F. Waldhauser, A.F. Arnulf, C. Baillard, T.-K. Lau, J.H. Haxel, Y.J. Tan, C. Garcia, S. Levy, and M.E. Mann

124 A Tale of Two Eruptions: How Data from Axial Seamount Led to a Discovery on the East Pacific Rise

By M. Tolstoy, W.S.D. Wilcock, Y.J. Tan, and F. Waldhauser

127 Sidebar > Axial Seamount Biology Catalog

By K. Bigham

128 Deep-Sea Volcanic Eruptions Create Unique Chemical and Biological Linkages Between the Subsurface Lithosphere and the Oceanic Hydrosphere

By R.L. Spietz, D.A. Butterfield, N.J. Buck, B.I. Larson, W.W. Chadwick Jr., S.L. Walker, D.S. Kelley, and R.M. Morris

136 Sidebar > Get Engaged with the Ocean Observatories Initiative

By G.A. Ulses, L.M. Smith, and T.J. Cowles

138 Education and Public Engagement in OOI: Lessons Learned from the Field

By J. McDonnell, A. deCharon, C.S. Lichtenwalner, K. Hunter-Thomson, C. Halversen, O. Schofield, S. Glenn, C. Ferraro, C. Lauter, and J. Hewlett

147 Sidebar > Seastate: Experiential C-STEM Learning Through Environmental Sensor Building

By D.S. Kelley and D. Grünbaum

DEPARTMENTS

05 QUARTERDECK. The Squirrely Thing About Knowledge

By E.S. Kappel

07 FROM THE PRESIDENT. On Mentoring of Graduate Students

By A.C. Mix

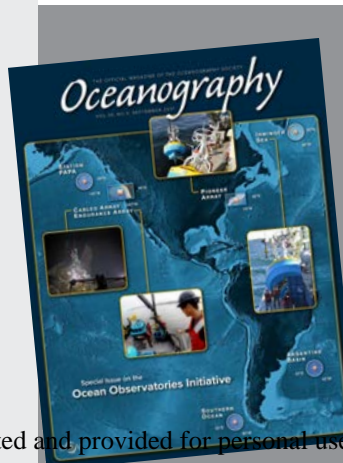
08 RIPPLE MARKS. Icon of Chesapeake Winter Still Graces the Bay

By C.L. Dybas

148 THE OCEANOGRAPHY CLASSROOM. Are You a Marine Major or Minor?

By S. Boxall

150 CAREER PROFILES. Heather Havens, Vice President, Program Development, National Defense Industrial Association • Andreas Krupke, Scientist III, Verification & Validation Department, Thermo Fisher Scientific



ON THE COVER

The Ocean Observatories Initiative (OOI) is a National Science Foundation major research facility operated as a community resource, providing continuous delivery of ocean and seafloor data from the coast to the open ocean in the Atlantic and the Pacific. The map shows the locations of the seven OOI arrays (image credit: OOI Cabled Array program & the Center for Environmental Visualization, University of Washington). Inset photos show infrastructure from the Coastal, Global, and Cabled Arrays (clockwise from top): deployment of a Pioneer Array Coastal Surface Mooring from R/V *Atlantis* (credit: OOI Pioneer Array Program, WHOI); Irminger Sea Global Surface Mooring waits on the deck of R/V *Knorr* for deployment (credit: OOI Global Array Program, WHOI); Endurance Array Coastal Surface Mooring components await deployment (credit: OOI Global Array Program, OSU); digital still camera deployed on Axial Seamount captures the El Gordo hydrothermal vent and attached OOI Cabled Array instrumentation (credit: NSF-OOI/UW/ISS, Dive R1839, V15).

For reprints please contact the Publisher.

The Oceanography Society was founded in 1988 to advance oceanographic research, technology, and education, and to disseminate knowledge of oceanography and its application through research and education. TOS promotes the broad understanding of oceanography, facilitates consensus building across all the disciplines of the field, and informs the public about ocean research, innovative technology, and educational opportunities throughout the spectrum of oceanographic inquiry.

OFFICERS

PRESIDENT: Alan Mix
PRESIDENT-ELECT: Martin Visbeck
PAST-PRESIDENT: Susan Lozier
SECRETARY: Susan Cook
TREASURER: Susan Banahan

COUNCILLORS

AT-LARGE: Dennis McGillicuddy
APPLIED TECHNOLOGY: James Girton
BIOLOGICAL OCEANOGRAPHY: Charles H. Greene
CHEMICAL OCEANOGRAPHY: Peter Sedwick
EDUCATION: Carolyn Scheurle
GEOLOGY AND GEOPHYSICS: Richard Murray
PHYSICAL OCEANOGRAPHY: Magdalena Andres
STUDENT REPRESENTATIVE: Stefanie Mack

EXECUTIVE DIRECTOR

Jennifer Ramarui

CORPORATE AND INSTITUTIONAL MEMBERS

BAKER DONELSON
» <https://www.bakerdonelson.com>
SEA-BIRD SCIENTIFIC
» <https://sea-birdscientific.com>
TELEDYNE RD INSTRUMENTS
» <http://www.teledynemarine.com/rdi>

CONTACT INFO

The Oceanography Society
1 Research Court, Suite 450
Rockville, MD 20850 USA
t: (1) 301-251-7708
f: (1) 301-251-7709
email: info@tos.org
<https://tos.org>

EDITOR

Ellen S. Kappel
Geosciences Professional Services Inc.
5610 Gloster Road
Bethesda, MD 20816 USA
t: (1) 301-229-2709
ekappel@geo-prose.com

ASSOCIATE EDITORS

Margaret L. (Peggy) Delaney
University of California, Santa Cruz
delaney@ucsc.edu

Charles H. Greene
Cornell University
chg2@cornell.edu

Kiyoshi Suyehiro
Yokohama Institute for Earth
Sciences, JAMSTEC
suyehiro@jamstec.go.jp

Peter Wadhams
University of Cambridge
p.wadhams@damtp.cam.ac.uk

ASSISTANT EDITOR

Vicky Cullen
PO Box 687
West Falmouth, MA 02574 USA
t: (1) 508-548-1027
vcullen@whoi.edu

CONTRIBUTING WRITER

Cheryl Lyn Dybas
cheryl.lyn.dybas@gmail.com

DESIGN/PRODUCTION

Johanna Adams
johanna-adams@cox.net

Oceanography contains peer-reviewed articles that chronicle all aspects of ocean science and its applications. The journal presents significant research, noteworthy achievements, exciting new technology, and articles that address public policy and education and how they are affected by science and technology. The overall goal of *Oceanography* is cross-disciplinary communication in the ocean sciences.

Oceanography (ISSN 1042-8275) is published by The Oceanography Society, 1 Research Court, Suite 450, Rockville, MD 20850 USA. ©2018 The Oceanography Society Inc. All rights reserved. Permission is granted for individuals to copy articles from this magazine for personal use in teaching and research, and to use figures, tables, and short quotes from the magazine for republication in scientific books and journals. There is no charge for any of these uses, but the material must be cited appropriately.

Republication, systemic reproduction, or collective redistribution of any material in *Oceanography* is permitted only with the approval of The Oceanography Society. Please contact Jennifer Ramarui at info@tos.org.

Hands-On Oceanography

[https://tos.org/
hands-on-oceanography](https://tos.org/hands-on-oceanography)



Interested in Undergraduate and Graduate Education?

Check out Oceanography's Hands-On Oceanography page <https://tos.org/hands-on-oceanography> that contains peer-reviewed activities that will help you teach fundamental oceanography concepts in undergraduate and graduate classrooms.

Check Out Our Career Profiles Page!

<https://tos.org/career-profiles>

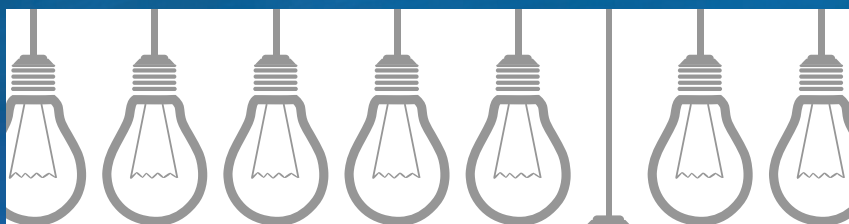
In each issue, *Oceanography* magazine publishes "career profiles" of marine scientists who have pursued successful and fulfilling careers outside of academia. These profiles are intended to advise ocean sciences graduate students about career options other than teaching and/or research in a university setting. They also include wisdom on how to go about the job search.

We have over 50 profiles of ocean scientists on our web page.
Check them out!



Do you have suggestions on who to profile?

Please send their contact information to ekappel@geo-prose.com. Self-nominations are accepted.



**Looking for *Insight*
on education?**



Visit The Oceanography Classroom

<https://tos.org/classroom>

Oceanography's education columnists share their wisdom and insight in The Oceanography Classroom each issue. Go to <https://tos.org/classroom> where you can find all published columns.



**THE
OCEANOGRAPHY
SOCIETY**
tos.org

Content is copyright protected and provided for personal use only - not for reproduction or retransmission.

For reprints please contact the Publisher.

UPCOMING IN *Oceanography*

Special Issues

June 2018

Ocean Warming

September 2018 — Double Issue

- 1. Mathematical Aspects of Physical Oceanography**
- 2. Gulf of San Jorge, Patagonia, Argentina**

December 2018

**Scientific Ocean Drilling:
Looking to the Future** (tentative)

Call for Submissions

In addition to the special issues articles, *Oceanography* solicits and publishes:

- Peer-reviewed articles that chronicle all aspects of ocean science and its applications
- News and information, meeting reports, hands-on laboratory exercises, career profiles, and book reviews
- Editor-reviewed articles that address public policy and education and how they are affected by science and technology
- Breaking Waves articles that describe novel approaches to multidisciplinary problems in ocean science

<https://tos.org/oceanography>

The Squirrely Thing About Knowledge



On this gray winter day, I look out my family room window at the suet feeder I just filled. Although I set this wintertime feeder out for the birds—and even make my own suet (please contact me if you'd like the recipe)—I know that the main beneficiaries of the food are the squirrels. With that knowledge, I devise my own pitiful defenses against these clever and dexterous rodents, using twist-ties to prevent the squirrels from opening the feeder, and slathering hot-pepper-infused shortening on the line from which the feeder hangs to provide a lasting mouthful of fire. In the end, the birds and I are the losers. The squirrels always prevail.

Watching the birds and squirrels leads to thoughts about observation and experimentation. Those tools are the basis of conducting science, but non-scientists use those same skills in solving everyday problems at work and at home. A driver looks at the fuel gauge that is near empty and calculates whether she can make it to the next gas station. A shopper compares prices and features on a new refrigerator to decide which one to purchase. A vacationer checks the weather at his destination to know what clothes to pack. A cook finds substitutes for missing ingredients when preparing a recipe. A homeowner investigates the source of a leak when she sees a stain on the ceiling. And yet, the same people who solve problems every day in their work and home lives somehow reject the results of the same process of observation and experimentation when those results are generated by universities, government agencies, and other components of Big Science. Why?

One of the great challenges of our time is educating the public that they are scientists and mathematicians and engineers each and every day, and that academic and government scientists aren't strange people who possess some set of magical skills and work in secret laboratories. Along with that understanding may come less fear and more appreciation of science and less resistance to policy solutions that may involve short-term sacrifice for the sake of the long-term health of our planet. If people saw themselves as problem solvers, and saw scientists as fellow citizens who are just trying to determine, on a larger scale, whether the fuel gauge is nearing empty, we might be able to tackle pressing social and environmental issues in a more congenial manner. Perhaps we can start by together solving that knotty problem of keeping squirrels away from bird feeders, and then continue our collaborations on thornier issues.

Ellen S. Kappel

Ellen S. Kappel, Editor



Help TOS Fulfill Its Mission!

*Recognizing excellence, disseminating knowledge,
promoting communication*

The Oceanography Society welcomes financial contributions of any size to help support the Society's mission of disseminating knowledge of oceanography and its application through research and education, promoting communication among oceanographers, and providing a constituency for consensus-building across all the disciplines of the field. Contributions are welcome in one or more of the following areas:

- **COSTARS: Career Opportunity/Student Travel and Research Support** – Supporting travel for graduate students to conferences and other institutions and organizations
- **Student Fund** – Supporting programs such as the TOS Mentoring Program
- **Early Career Fund** – Supporting participation in career-enhancing activities
- **TOS General Fund** – Used for greatest needs, as recommended by the TOS Council

To contribute go to <https://tos.networkforgood.com>



CALL FOR NOMINATIONS

TOS Fellows Program

<https://tos.org/tos-fellows>

Recognizing Individuals Who Have Attained Eminence in Oceanography Through Their Outstanding Contributions to the Field of Oceanography or Its Applications

The origins of The Oceanography Society are rooted in bringing together and recognizing individuals from all fields of oceanography, representing the broad interests of members in research, engineering, industry, policy, and education, and the diversity and international nature of the society. TOS members from all areas of oceanography will be considered for the Fellows Program. A recommendation for advancement to TOS Fellow is appropriate after an individual has been a TOS member for at least three years, depending on his or her contributions to the field.

The main criteria for being elected a TOS Fellow are outstanding and sustained contributions, and devotion to the broad field of oceanography, commensurate with the founding principles of the Society.

Nominations Deadline » October 31, 2018

Learn More » <https://tos.org/tos-fellows>

On Mentoring of Graduate Students

Last year, The Oceanography Society started a mentoring program to provide guidance to graduate students on how to survive graduate school and find a satisfying career pathway. Academic “elders” paired with co-mentors from industry and government conduct monthly teleconferences with small groups of students. Susan Lozier initiated this TOS program following her term as president, building on her experience with the Mentoring Physical Oceanography Women to Increase Retention (MPOWIR) program (<http://mpowir.org>), which addresses some of the “leaky pipeline” issues for women in physical oceanography. (You can read more about MPOWIR and its positive impact on the field as a whole in previous issues of *Oceanography*, e.g., Lozier 2005, 2009; Coles et al., 2011; Clem et al., 2014.)

Using MPOWIR as model, TOS began its own prototype program with two mixed-gender mentoring groups whose members span all the fields of ocean science and technology and are drawn from a wide range of universities across the United States. In the future, we hope to expand the program internationally. By combining participants from many institutions, we hope to foster networks of young scientists who will build the future of ocean sciences. As one of the participating members, here I share some early results of this experiment.

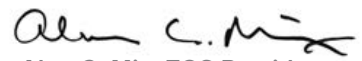
The initial premise of the TOS program is that the mentors will provide sage advice to the graduate students about career pathways, among other topics. Certainly, we’ve done some of that. We have had some interesting discussions about networking, and have read some practical guidebooks on productive networking. We’ve talked a bit about writing and speaking and how to use storytelling techniques to get a message across. We’ve addressed time management, and of course we’ve talked about concerns regarding finding satisfying employment after graduate school. But it is also true that the students are mentoring the mentors, teaching us about what they need. It is far too easy for academic faculty to forget what it was like to be a graduate student, but hearing the students’ concerns is enlightening. While a graduate school experience can be good if an advisor is patient, fair, thoughtful, and responsive to students, not every advisor provides students with the training necessary for future success as a faculty member, such as how to deal with graduate students or how to teach effectively.

Some universities now have mentoring programs, but certainly not all. I recently reviewed the web pages of most of the oceanographic programs in the United States and a few abroad, and found several programs that have senior faculty serve as

mentors for junior faculty. These programs are a great start, but these same pages offer relatively little about best practices in mentoring graduate students, or training the students to become future mentors. Despite promotion and tenure dossiers that require applicants to write about their philosophy of education related to teaching and mentoring, these web pages lack any statements about institutional philosophies or practices. This is odd.

There is no single way to be a good mentor—we all have unique strengths and personalities that we bring to the task—but some attention paid to this most important (most joyful, most frustrating, and most rewarding) faculty task will go a long way toward improving our programs. For faculty members who might like to start exploring some of these general mentoring issues, I recommend the *MPOWIR Handbook* (Clem et al., 2016). Within TOS, we plan to build on our prototype program. Over the next few years, we anticipate producing some general materials on best practices in mentoring of graduate students. I hope that our institutions will use, adapt, or build on these guidelines. As we develop TOS guidelines for mentoring in ocean sciences, I welcome input from faculty members and programs that have addressed mentoring issues. Perhaps a start in shining a light on mentoring would be for TOS to initiate some mechanisms to reward high-quality mentoring; my own institution has a student-administered award for mentoring that is one of the highest honors a faculty member can receive.

For me, participating in the TOS mentoring program is reassuring in that it reinforces my view that the future of ocean sciences will be in great hands as the young generation of students and early career scientists steps up and takes the reins. I look forward to learning more as the TOS program continues.



Alan C. Mix
Alan C. Mix, TOS President

REFERENCES

- Clem, S., S. Legg, S. Lozier, and C. Mouw. 2014. The impact of MPOWIR: A decade of investing in mentoring women in physical oceanography. *Oceanography* 27(4) supplement:39–48, <https://doi.org/10.5670/oceanog.2014.113>.
- Clem, S., C. Mouw, and S. Legg. 2016. *MPOWIR Handbook*. Available at: <http://mpowir.org/wp-content/uploads/2017/01/MPOWIR-Handbook.pdf>.
- Coles, V., L. Gerber, S. Legg, and S. Lozier. 2011. Commentary: Mentoring groups—A non-exit strategy for women in physical oceanography. *Oceanography* 24(2):17–20, <https://doi.org/10.5670/oceanog.2011.43>.
- Lozier, M.S. 2005. A community effort toward the retention of women in physical oceanography. *Oceanography* 18(1):35–38, <https://doi.org/10.5670/oceanog.2005.68>.
- Lozier, M.S. 2009. Conference report: A successful first Pattullo Conference. *Oceanography* 22(1):224–225, <https://doi.org/10.5670/oceanog.2009.25>.

Icon of Chesapeake Winter Still Graces the Bay

BY CHERYL LYN DYBAS

PHOTOS BY ILYA RASKIN

"They came back. This winter." Biologist Donald Webster's voice has a wistful note, wondering if the king of ducks, as the beautiful, crimson-headed canvasback is known, will return to rule Chesapeake Bay in future seasons.

Bundled in parka, gloves, and hat, Webster, waterfowl coordinator for the Maryland Department of Natural Resources, raises his binoculars near a seawall at the confluence of the Chesapeake and the Choptank River in Cambridge, Maryland. The overlook is a mecca for wintering canvasbacks and other ducks. Chesapeake Bay is the largest estuary in the United States and one of the most productive water bodies in the world, attracting myriad waterfowl species.

"Canvasbacks, the ducks everyone comes to see, are usually here in force by Christmas, sometimes by Thanksgiving," Webster says. "They stay through early to mid-March, then they're gone, heading north to nesting grounds."

SKEINS OF WATERFOWL

On this late January morning with calm winds and temperatures that hover just above freezing, the canvasbacks' red heads stand out in quiet, winter-dark waters. The ducks glide near the seawall, where a dozen photographers jostle for the quintessential shot of an iconic Chesapeake species. "This place is known as the 'wall of shame,'" laughs Webster, "because it's almost too easy to get great canvasback pictures here."

After the warm winter of 2015–2016 and its low numbers of canvasbacks, they've arrived in large flocks this season (2016–2017).

Chesapeake skies fill with migrating ducks—canvasbacks, buffleheads, greater and lesser scaup, and many others—from December through March. The bay is the Atlantic Coast's most important waterfowl migration and wintering area. The Chesapeake and its 19 major tributaries offer refuge to 24 species of ducks as well as Canada geese, greater snow geese, and tundra swans.

"Long-term worsening of the bay's water quality, however, and loss of habitat, especially the grasses so many of these birds depend upon, have contributed to declines in wintering waterfowl populations," says Webster.

SEESAWING GRASS ESTIMATES

An estimated 97,433 acres (400 km²) of submerged aquatic vegetation (SAV) remained in the bay and its tributaries in 2016, down from historic levels that may have reached more than 600,000 acres (2,500 km²).

There's good news, however, in the 2016 estimate. It's an 8% increase over 2015, and more than twice the SAV in the bay in 2013.

In 2011, the Chesapeake's SAV declined to 48,195 acres (195 km²), a result of the effects of Hurricane Irene and Tropical Storm Lee. The storms sent a flood of sediment cascading down rivers and into the bay. After 2011, conditions became relatively dry, reducing the flow of grass-smothering sand and mud. More sunlight reached submerged grasses, allowing them to rebound. In return, the SAV filtered runoff, helping keep Chesapeake waters clear.

Forty years ago, SAV reached what may be its lowest point in parts of the bay. Another major storm, Tropical Storm Agnes in 1972, nearly wiped out the SAV at Susquehanna Flats, an expansive bed of grasses where the Susquehanna River



widens into the Chesapeake. The rush of flood water from the roiling Susquehanna uprooted grasses at the Flats' edges and deposited sediment there, blocking sunlight and photosynthesis. Then the storms of 2011 exacerbated the damage.

But the grasses fought back. Their blades impeded the river's flow enough to prevent erosion of the beds' inner cores. "SAV modified its environment in ways that improved its growth," says biologist Cassie Gurbisz of St. Mary's College of Maryland. "That ability likely serves as a mechanism of SAV resilience."

The plants create clear water in the middle of the beds, which promotes their growth and improves water clarity. When clean water sluices out of an SAV bed's center into the surrounding bay, more light is available for the grasses to grow, allowing them to shoot up faster.

Gurbisz and colleagues published the results of a study of storm-related SAV loss and resilience in 2016 in the journal *Estuaries and Coasts*. Coauthors of the paper are Michael Kemp and Lawrence Sanford of the University of Maryland Center for Environmental Science, and Robert Orth of the Virginia Institute of Marine Science.

DUCK FEAST TO FAMINE

Over the bay's history, SAV has floundered and flourished. Canvasbacks have followed suit. As recently as 1950, half the continent's population of canvasbacks—more than a quarter million—wintered in the Chesapeake, relying on aquatic grasses as favored food sources.

During Colonial times, as many as one

million of the ducks may have spent wintertime on the bay. In the nineteenth century, their abundance and, to many, good taste, made them a favored selection in many East Coast restaurants, says Matt Kneisley, regional director for the Northeast Atlantic Flyway at the Delta Waterfowl Foundation, a waterfowl conservation and hunting organization.

Canvasbacks congregate in large flocks on open waters, leading to easy—too easy—harvesting. By the end of the nineteenth century, commercial hunters with batteries of weapons went after rafts of the ducks, often killing dozens with one shot. The "cans," as hunters call them, were shipped by boxcar to markets from Baltimore to Boston. Such market hunting was outlawed with the passage of the Migratory Bird Treaty Act of 1918.

"Canvasbacks were a favored quarry because their meat was considered the tastiest of all the ducks due to their consumption of wild celery," writes Guy Baldassarre in the 2014 edition of *Ducks, Geese and Swans of North America*.

Adds Kneisley, "Large beds of wild celery once attracted thousands of the ducks to Susquehanna Flats and elsewhere on the upper bay." Then a decline in the Chesapeake's water quality greatly reduced the amount of wild celery. Tropical Storm Agnes was the final blow. "After the storm, wild celery was virtually impossible for canvasbacks to find," says Kneisley.

The ducks switched their foraging efforts

to small clams on the Chesapeake's shallow bottom. But a less nutritious diet of shellfish such as Baltic clams may affect the ducks' winter survival rates.

A COMMON FUTURE

Annual January bird counts, Webster says, "give us a very good picture of how much declines in SAV have affected wintering waterfowl."

Half a century ago, four to five million ducks, geese, and swans spent time on Chesapeake Bay during the winter. Now, that number is less than one million, according to results from a midwinter waterfowl survey. The nationwide count has taken place every year since the 1950s.

Survey teams of biologists from the Maryland Department of Natural Resources and the US Fish and Wildlife Service fly transects to make visual estimates of waterfowl along the Chesapeake and the nearby Atlantic coast. In 2017, the teams counted 812,600 ducks, geese, and swans, higher than the 663,000 birds observed in 2016 and similar to the five-year average of 795,240, says Webster.

Estimates of canvasbacks in 2017 were 75,100; in 2016, 19,800; and in 2015, 64,200. Sixty years earlier, in 1955, 225,450 canvasbacks were sighted. The last time the canvasback count exceeded 100,000 was in 1967: 133,100.

Nonetheless, says Webster, "this is one of the best places on Earth to see waterfowl in winter and as they migrate in and out during fall and spring."

In a Currier and Ives view of Chesapeake Bay in winter, canvasbacks and other waterfowl species linger near a seawall in Cambridge, Maryland.



From afar, canvasbacks and redheads may be challenging to distinguish. Canvasbacks have black bills; redheads' bills are blue. Here, the lead duck is a redhead. The two following are canvasbacks. They're making their way along Chesapeake Bay to a spot near Cambridge, Maryland (pictured, previous pages).



ON THE FLY

Most birds in North America move with the seasons, but "perhaps because waterfowl are more visible than other species in migration, they epitomize this phenomenon," wrote Frank Bellrose in the first edition of *Ducks, Geese and Swans of North America*, published in 1980.

Only a few waterfowl species, such as Florida ducks, are nonmigratory. In the southern parts of their ranges, wood ducks and hooded mergansers are resident throughout the year. Some groups of mallards, Canada geese, and common eiders migrate only short distances or not at all when conditions for staying put are favorable.

On the whole, however, waterfowl make "tremendously long migratory flights," Bellrose wrote.

Lesser snow geese and pintails that breed in Siberia spend the winter in the Central Valley of California. Black brant that nest along Queen Maud Gulf in the Canadian Arctic migrate to Baja California. Pintails and American wigeons, most of which come from Alaska, regularly winter in the Hawaiian Islands.

Migrating waterfowl fly continuously unless forced to land by exhaustion or bad weather. Some species make nonstop flights as long as 4,800 kilometers. Most waterfowl migrate at speeds of 64 to 97 kilometers per hour. A flight of 3,200 kilometers at 80 kilometers per hour would take a duck about 40 hours.

"We humans can't keep a plane in the air that long," Webster says. "Waterfowl in migration perform quite a feat."

Ducks fly at altitudes ranging from a meter above the ocean to more than six kilometers. The lowest migratory flights, according to Bellrose, are those of sea ducks like eiders.

Other species fly high enough to clear the peaks of the Rocky Mountains, some of which exceed 4.3 kilometers. In general, the longer the flight, the higher the altitude.

THE ULTIMATE MIGRATORS

Why do waterfowl migrate, and how do they find their way? Most ducks wouldn't survive northern winters. The waters where they breed freeze over, making food impossible to find. However, they migrate as short a distance as possible to find open water and food.

If nature provides a nearby alternative, waterfowl are quick to notice. When hurricanes opened densely vegetated coastal marshes in Louisiana, for example, tens of thousands of ducks responded by wintering there rather than continuing across the Gulf of Mexico to the Yucatán Peninsula.

"In acquiring their navigational abilities," Bellrose wrote, "each species of waterfowl has evolved different cues and degrees of dependence on them. Mallards that migrate short distances show a different use of sun and star cues than do blue-winged teal, for example, which migrate much farther."

Waterfowl heavily depend on landscapes as they navigate across the continent, which works fine during daylight hours. But scientists have noted cases in which ducks flying at night have overshot their intended stopping points, only to

retrace their routes the next day.

Ducks also migrate across trackless regions with few clues. And they fly on nights so darkened by clouds that the places where land meets water are nearly invisible. Landscape alone, therefore, can't be the only way in which waterfowl find their way south or north.

Although scientists don't know all the answers, they believe that waterfowl and other birds have internal clocks enabling them to adjust to the changing position of the sun in the sky, and that the birds can follow star patterns to find direction.

Some species can navigate at night even within cloud layers, without reference to landscape or celestial clues. Evidence suggests that they use Earth's magnetic field when other sources are unavailable.

Most waterfowl migrate along corridors, the well-known "flyways." Four major routes pass through the United States: the Pacific Flyway, which runs north-south along the West Coast; the Mississippi Flyway, which leads from the bays of northern Canada and the Arctic to the Gulf of Mexico; the Central Flyway from northwestern Canada to Central America and the Yucatán Peninsula; and the Atlantic Flyway, which funnels waterfowl from central and eastern Canada along the Atlantic Coast to Florida. Chesapeake Bay is a major duck stop along the Atlantic flyway.

BIRD NURSERY

About half North America's ducklings, including many of the Chesapeake's wintering ducks, began life in the prairie



Waterfowl wintering on the Chesapeake depend on submerged aquatic vegetation such as wild celery. When that's not available, some species turn to shellfish like Baltic clams. Clockwise from upper left: Lesser scaup; mallards and American wigeon; canvasbacks; American wigeon; mixed flock of canvasbacks and lesser scaup; and a lone redhead.

pothole region, an area that extends from the Midwest into Canada.

As the ice sheets of the last glacial period retreated northward, tens of thousands of landlocked icebergs were left in their wakes, writes Michael Furtman in *On the Wings of a North Wind: The Waterfowl and Wetlands of North America's Inland Flyways*.

As these icebergs melted, Furtman states, "they became the foundation of the prairie potholes. An estimated 10 million glacially carved depressions once pockmarked the landscape of the prairie pothole region of the United States and Canada." The potholes evolved into a habitat so enticing that more than 130 bird species have used a single pothole.

Ducks were likely among the first residents. With millions of potholes from which to choose, waterfowl had plenty of room to find nesting sites.

"The diversity of potholes, ranging from small spring ponds to large permanent wetlands, provided ducks with the various

habitats necessary for each specific stage in their breeding and brood-rearing cycles," Furtman states.

As the glaciated land gave way to farmland, however, the number of potholes decreased, especially over the last 40 years. In North Dakota's pothole region, where as many as 100 wetland basins per 2.5 km² once existed, "60 percent of the original 5 million acres [20,000 km²] of wetlands have been lost," Furtman reports. "Ninety-five percent of that loss is attributable to agriculture."

IS PAST PROLOGUE?

If agriculture isn't challenge enough for waterfowl during their nesting seasons, rising global temperatures may result in more frequent and severe droughts in the

prairie pothole region, with a devastating effect on breeding ducks.

Webster has witnessed the result.

"Decades ago," he says, "the Chesapeake was full of wintering canvasbacks. But no more. I'd like to see the days again when their dark red heads stretched as far as you could see."

Canvasbacks and the many other ducks that winter on the bay have come a long way to get there, Webster says. "The least we can do is show them some hospitality by making sure their environment is healthy."

Otherwise, he says, the Chesapeake's winter waterfowl spectacle may vanish, the seawall along the Choptank indeed becoming a wall of shame as the last canvasbacks' wingbeats fade into silence.

Cheryl Lyn Dybas (cheryl.lyn.dybas@gmail.com), a Fellow of the International League of Conservation Writers, is a contributing writer for *Oceanography* and a marine ecologist and science journalist. She also writes about science and the environment for *National Geographic*, *BioScience*, *Ocean Geographic*, *Canadian Geographic*, *National Wildlife*, *Yankee*, and many other publications.



Introduction to the Special Issue on the Ocean Observatories Initiative

By Leslie M. Smith, Timothy J. Cowles,
Robert D. Vaillancourt, and Subbarao Yelisetti

INTRODUCTION

The Ocean Observatories Initiative (OOI) is a National Science Foundation (NSF)-funded major research facility operated as a community resource to provide continuous observations of the ocean and seafloor from several key locations. The data collected, maintained, and disseminated by OOI addresses large-scale scientific challenges such as coastal ocean dynamics, climate and ecosystem health, the global carbon cycle, and linkages among seafloor volcanism and life. The system was designed to grow as it incorporates new technologies and accommodates novel research ideas and approaches proposed by individual research scientists. Unlike most facilities, the OOI is mostly operated remotely; engagement by the user community is online through dedicated cyberinfrastructure. The OOI allows scientists unprecedented access to ocean data collected in remote locations and delivers it at high temporal and spatial resolutions, in near-real time, when practicable ([Smith et al.](#)).

What follows in the pages of this special issue of *Oceanography* brings readers, in many cases, the results of the first scientific studies using the diverse and unique data sets collected from the OOI's Coastal, Global, and Cabled Arrays. The articles and sidebars highlight unique features of this facility, focusing on key OOI data and science themes, community-developed tools, and ways that OOI

data can provide the environmental and observational context for initializing and designing novel research and technologies. The articles examine ocean processes across multiple dimensions, revealing previously difficult-to-capture phenomena on temporal scales from seconds to years and spatial scales from centimeters to kilometers.

OBSERVATIONS ACROSS SCALES

The continuously operating OOI permits sampling of short-lived, episodic events, enabling scientists to be in the “right place at the right time,” such as capturing the 2.5-minute window of the total solar eclipse in 2017 ([Barth et al.](#)) or watching the progression of the 2015 Axial Seamount eruption in near-real time ([Wilcock et al.](#)). Capturing events as they occur provides key insights into preconditions, initial onset, and event evolution often missed by traditional sampling approaches and platforms. Data collected at OOI sites before, during, and after events can enhance understanding of other events where previously only after-event information was collected. For example, OOI data recorded during the 2015 Axial Seamount eruption led to a new interpretation of the cause of a 2006 eruption in the equatorial Pacific ([Tolstoy et al.](#)). Real-time monitoring of an event also enables scientists to quickly mobilize to collect additional samples.



For example, [Spietz et al.](#) conducted a rapid response cruise following the 2015 Axial Seamount eruption to sample microbial communities surrounding the eruption site. Real-time sampling and near real-time data access are also critical for earthquake monitoring ([Tréhu et al.](#))

In some cases, the OOI provides the first year-round observations at previously sparsely sampled locations. For example, insight into mixed layer processes during winter in the Irminger Sea provided a key missing link for understanding the biological pump in the subarctic Atlantic Ocean ([Palevsky and Nicholson](#)). During the 25 years of the OOI's planned lifetime, it will be possible to examine decadal dynamics, such as the El Niño-Southern Oscillation in the Northeast Pacific and the Arctic Oscillation in the North Atlantic. We are still years from extracting decadal dynamics from the OOI data, but shorter, multiyear-scale phenomena are now being observed, such as the “warm blob” event in the Northeast Pacific as well as the seasonal formation of hypoxia ([Barth et al.](#)).

Detailed spatial coverage within each OOI array permits examination



Photo credits: (a) NSF-OOI/UW/CSSF
 (b) OOI Pioneer Array Program, WHOI
 (c) OOI Cabled Array Program, UW: V15
 (d) OOI Pioneer Array Program, WHOI
 (e) OOI Endurance Array Program, OSU

of patchy phenomena such as heat balance ([Chen et al.](#)) and warm core rings ([Gawarkiewicz et al.](#)) in the Northwest Atlantic, and the juxtaposing forces of upwelling and riverine freshwater input in the Northeast Pacific ([Henderikx Freitas et al.](#)). On a larger scale, the OOI provides data to support regional-scale observations of phenomena among multiple OOI arrays, such as tracing the warm blob from the Gulf of Alaska to Oregon coastal waters ([Barth et al.](#)). Additionally, OOI data can aid in regional spatial analyses, such as in the Irminger Sea ([de Jong et al.](#)), when used in concert with data from other nearby observatories, and off the coast of New England ([Stocks et al.](#)), where a diversity of data sets and sampling assets are available.

OVERVIEW AND GLOBAL CONTEXT

This *Oceanography* special issue begins with an overarching summary of the OOI ([Smith et al.](#)) that describes its scientific motivations and overall design, outlines its infrastructure, and provides details of how data are collected, transmitted, processed, quality controlled, and distributed. Further details of data access can be found in the [Vardaro and McDonnell](#) sidebar. [Lindstrom](#) highlights how the OOI fits into the broader global ocean observing efforts, not only through its contribution of data but also through

its commitment to driving and providing a testbed for technological innovation in ocean observing platform and sensor design. [Reimers and Wolf](#) exemplify this commitment, wherein authors describe their novel Benthic Observer powered by energy harvested with a benthic microbial fuel cell. This autonomous platform offers a potential low-cost alternative for benthic boundary layer observations. These platforms were deployed next to an Endurance Array Cabled Benthic Experiment Package off the coast of Oregon during OOI maintenance cruises in order to compare and validate their data.

GLOBAL IRMINGER SEA ARRAY

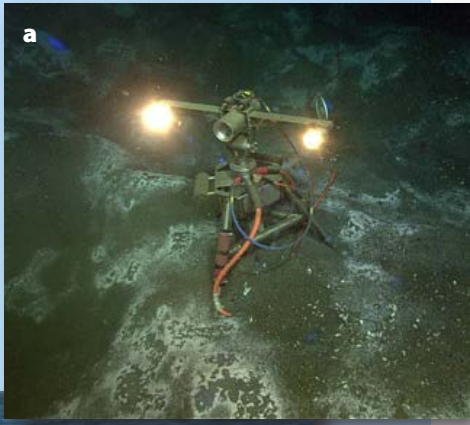
Two articles in this special issue highlight the Global Irminger Sea Array off the coast of Greenland. In the first article, [Palevsky and Nicholson](#) synthesize biogeochemical sensor data from the first two years of operations at the array. These data provide the first simultaneous year-round observations of biological carbon cycling processes in both the surface ocean and the seasonal thermocline in this critical region of the subpolar North Atlantic. These data show significant mixed layer net autotrophy during the spring bloom, respiration in the seasonal thermocline during the stratified season, and subsequent ventilation during winter convective mixing. The results represent a

measurable reduction in potential carbon sequestration, highlighting the importance of year-round observations to accurately constrain the biological pump in the subpolar North Atlantic.

In the second article, [de Jong et al.](#) further investigate deep mixing and convection in the subpolar North Atlantic. In this study, the authors use observations from the OOI Irminger Sea mooring array in combination with other nearby moorings (an 86×35 km domain) to evaluate spatial differences in the cycles of deep convection and restratification off southern Greenland over two annual cycles. Although surface forcing was observed to be stronger in the northern portion of the domain, the deeper convection occurred in the southern portion of the domain. The OOI moorings in the north were subject to intermittent lateral advection, via eddies and filaments, of slightly warmer water from the Irminger Current. These events initiated more frequent restratification in the north than occurred in the southern portion of the domain. The findings point to the critical importance of mesoscale resolution of overturning and atmospheric forcing at frequent intervals within an annual cycle.

COASTAL PIONEER ARRAY

To the south, off the coast of New England, exchange processes across the continental shelf and slope are examined using Pioneer Array data. [Gawarkiewicz et al.](#)



b



c



examine shelf-slope exchange processes that were previously difficult to study at the appropriate temporal and spatial resolution. In this study, the authors report that coastal ocean dynamics are changing rapidly, with more frequent extreme events of warm, salty Gulf Stream waters intruding onto the shelf and penetrating further onshore than previous studies suggested. A better understanding of these exchanges is critical as these warm, salty intrusions can potentially have large impacts on commercial fisheries, ecosystems, and storm intensity.

Using the capability of the Pioneer Array to capture multiscale processes, **Chen et al.** demonstrate the scale dependence of the heat balance at the southern New England shelf break, and show the importance of advective processes in the overall heat balance over the continental shelf and slope. Knowledge of the temperature variability and heat budget of the outer continental shelf and shelf break region are fundamentally important to understanding the influence of climate change in the coastal ocean as well as the direct economic impact on the harvesting of living marine resources.

Finally, the **Stocks et al.** sidebar places the Pioneer data in a regional context, highlighting the SeaView Pioneer Array data collection. One of three SeaView thematic collections, the Pioneer collection is a free resource for obtaining nearby oceanographic data that are integrated and reformatted in the SeaView repository for ease of download and use.

COASTAL ENDURANCE ARRAY

On the other side of the continent, coastal processes are examined in the Northeast Pacific off the coast of Oregon and Washington. **Henderikx Freitas et al.** present a multi-year, multiplatform study of the cross- and along-shelf patterns of river flow, upwelling, and chlorophyll dynamics. Satellite observations—traditionally used to study the area—are compared to in situ OOI Endurance Array mooring and glider data. In situ observations

from OOI instrumentation reveal chlorophyll concentrations of similar magnitude between Oregon and Washington coasts, contrasting with satellite data, which consistently show higher chlorophyll concentrations off the Washington coast. The authors suggest that observed elevated chromophoric dissolved organic matter (CDOM), likely from the nearby Columbia River plume, may help to explain the differences between satellite-derived chlorophyll and in situ observations. This preliminary report demonstrates the strength of the approach of using multiplatform, multiyear data sets to understand complexity within this dynamic coastal system.

Barth et al. describe three phenomena with durations that span from minutes to years to demonstrate the unique ability of these platforms to capture ocean phenomena that vary across a wide range of timescales: (1) a diel biological response to the total eclipse of the sun on August 21, 2017, where a layer of zooplankton was observed to vertically migrate upward during the midday total solar eclipse in what is a typical nighttime response to diminished light, (2) the devastating effects of a seasonal-scale hypoxic event in July off the central Oregon coast on a population of Dungeness crabs, and (3) the appearance and multiyear persistence of an anomalously warm upper-ocean feature in the Northeast Pacific, the warm blob.

CABLED ARRAY

The OOI Cabled Array spans the Juan de Fuca Plate in the Northeast Pacific, providing observations both at an offshore seafloor spreading center with its active underwater volcano, Axial Seamount (**Wilcock, et al.**), and at the Cascadia subduction zone closer to the coast (**Tréhu et al.**).

Tréhu et al. provide background on the Cascadia subduction zone, highlighting some of its unusual aspects, such as past great earthquakes. The Cascadia subduction zone is fairly quiet during interseismic times, which makes monitoring

the earthquake-producing zone a challenge. The authors use available offshore seismic data, including from the OOI, to demonstrate the benefits of using offshore data in detection and accurate location of small magnitude earthquakes in this region. They show that the quality of data from buried OOI seismometers is better than that from campaign style ocean bottom seismometer deployments. The authors make the case for obtaining real-time ocean bottom seismic recordings to improve earthquake monitoring offshore of the Cascadia margin, rather than depending only on data from instruments recovered after several months on the seafloor.

Several papers capture various aspects of the 2015 Axial Seamount eruption, the first undersea volcanic eruption observed in real time. **Wilcock et al.** provide a comprehensive analysis of Axial Seamount using data from the OOI Cabled Array system. Cabled Array seismic data show that inflation and deflation are accommodated by fault motions beneath the caldera, and eruptions appear to occur at a predictable level of inflation. The authors also compare the 2015 Axial volcanic eruption results with two historical eruptions from 1998 and 2011, and conclude by discussing how the observatory might be enhanced prior to the next eruption. **Tolstoy et al.** show how the real-time observations of the 2015 Axial Seamount eruption described by **Wilcock et al.** inspired a fresh look at older data recorded at the East Pacific Rise, and led to new discoveries. They compare geophysical signals leading up to and during eruptions at both locations, and note the difference in timing of the magmatic tremor. They conclude that one of the eruptions appears to have initiated from a “tearing” of the seafloor due to plate spreading (East Pacific Rise), while the other initiated from the more typical buildup of magma pressure observed in volcanic systems (Axial Seamount). Lastly, **Spietz et al.** present the results from a rapid response cruise following the same 2015 eruption. They report post-eruption changes in the

chemical and microbiological properties of the water column with an elevated level of presumed chemosynthetic microbial lineages. This study relied on OOI data for the locations of seismic events and activity to identify sampling sites, further demonstrating the necessity of real-time detection for future biological studies.

EDUCATION AND PUBLIC ENGAGEMENT

As described in the articles and sidebars of this issue, there are a variety of ways to engage with the OOI system and its data (enumerated in **Ulses et al.**). In addition to its utility for the oceanographic community, the OOI is a resource for the educational community. **McDonnell et al.** provide valuable insights into the development and application of software tools for educators wishing to engage students with real-time data. The authors use the outcomes of the development and testing process to illustrate successful pedagogical approaches using OOI data in classroom settings. **Bigham** describes the digital catalog of deep-sea creatures built by undergraduates from video and still imagery collected by remotely operated vehicles at the Axial Seamount Cabled Observatory. The Axial Seamount Biology Catalog project engaged students in the research process, provided a wealth of seagoing experiences, and led to the creation of a one-of-a-kind resource for Northeast Pacific biology intended for scientists, educators, news agencies, and documentary producers. An overview of the Seastate project by **Kelley and Grünbaum** focuses on student-driven design, building, and implementation of sensors to address locally relevant environmental problems. In this project, K20 teachers and students are trained to improve their computing, science, technology, engineering, and mathematics (C+STEM) knowledge.

SUMMARY

This special issue of *Oceanography* provides an initial view of the breadth and scope of scientific analysis and evaluation

made possible by the data flowing from the extensive OOI infrastructure. The articles illustrate the value the OOI and its data offer the scientific community, including opportunities to:

- Observe phenomena across multiple temporal and spatial scales
- Capture rare and episodic events
- Create long-term data records in previously poorly sampled ocean regions
- Make observations of patchy distributions of materials, energy fluxes, and processes
- Augment OOI observations with those from other ocean observing assets (e.g., remote sensing, shipboard, Argo profiling floats, US Geological Survey river gauges)
- Provide a testbed for technological innovation, extending the capabilities of present assets and instrumentation
- Enhance learning opportunities with real-time ocean observations

We encourage readers of this special issue to build upon this list, and extend the opportunities for the use of OOI data to address compelling scientific, educational, and societal issues. ☰

ACKNOWLEDGMENTS

We thank all of our authors and reviewers for their contributions to this special issue. It has been amazing to read about the novel and diverse work being conducted by the OOI user community. We thank the OOI Scientific Oversight Committee (Deb Kelley, Bob Weller, Al Pluedemann, and Jack Barth), the OOI Data Manager (Michael Vardaro), and those in the OOI Program Management Office (Greg Ulses and Sue Banahan) for their guidance, support, and editorial assistance. We are indebted to Ellen Kappel and her team at *Oceanography* magazine for their help in making these manuscripts a beautiful reality.

AUTHORS

Leslie M. Smith (lsmith@oceanleadership.org) is OOI Science Communicator, Consortium for Ocean Leadership, Washington, DC, USA. **Timothy J. Cowles** is Professor Emeritus, Oregon State University, Corvallis, OR, USA. **Robert D. Vaillancourt** is Associate Professor of Oceanography, Millersville University, Millersville, PA, USA. **Subbarao Yelisetti** is Assistant Professor of Geophysics, Texas A&M University-Kingsville, Kingsville, TX, USA.

ARTICLE CITATION

Smith, L.M., T.J. Cowles, R.D. Vaillancourt, and S. Yelisetti. 2018. Introduction to the special issue on the Ocean Observatories Initiative. *Oceanography* 31(1):12–15, <https://doi.org/10.5670/oceanog.2018.104>.

The Ocean Observatories Initiative

By Leslie M. Smith, John A. Barth, Deborah S. Kelley, Al Plueddemann, Ivan Rodero, Greg A. Ulles, Michael F. Vardaro, and Robert Weller

ABSTRACT. The Ocean Observatories Initiative (OOI) is an integrated suite of instrumented platforms and discrete instruments that measure physical, chemical, geological, and biological properties from the seafloor to the sea surface. The OOI provides data to address large-scale scientific challenges such as coastal ocean dynamics, climate and ecosystem health, the global carbon cycle, and linkages among seafloor volcanism and life. The OOI Cyberinfrastructure currently serves over 250 terabytes of data from the arrays. These data are freely available to users worldwide, changing the way scientists and the broader community interact with the ocean, and permitting ocean research and inquiry at scales of centimeters to kilometers and seconds to decades.

INTRODUCTION

The ocean is a dominant influence on Earth's habitability and is the primary trade route for commerce, yet it is still largely unexplored. Observational ocean data available in real time are needed to examine global issues such as sea level rise, ocean acidification, climate change, and fisheries decline. Beneath the ocean's surface, seafloor volcanism and plate tectonics continue to shape ocean basins, and associated earthquakes and tsunamis have the potential to severely impact coastal areas. Unusual creatures thrive in the extreme environments of hydrothermal vent fields at mid-ocean ridges and within methane seeps along continental margins. A better understanding of processes that occur within these dynamic environments requires long-term observations at centimeter to kilometer scales.

Recent advances in observational and computational technologies are transforming how oceanographers study and interact with the global ocean (e.g., Lindstrom, 2018, in this issue). Examples include advances in

underwater robotic capabilities, molecular biological techniques, and submarine telecommunications technologies (e.g., Lee et al., 2017). Increasingly, expeditionary, ship-based research is being augmented by the persistent presence of instrumented drifters, autonomous instrumented vehicles, buoys, and cabled observatories (e.g., Rudnick et al., 2017; Spietz et al., 2018, in this issue). New and innovative instruments are also being developed that may solve power issues that hamper long-term data collection in the ocean (e.g., Reimers and Wolf, 2018, in this issue). To answer the call for long-term, continuous ocean observations (NSF, 2001), in 2009 the National Science Foundation (NSF) funded construction and operation of the Ocean Observatories Initiative (OOI).

This article provides an overview of the OOI program. The first section describes the scientific motivation and overall design of each array. The second section provides a detailed description of the different types of moorings, profilers, autonomous vehicles, and seafloor

instrumentation used in the OOI. The third section outlines data flow from ocean platforms and instrumentation to users and discusses quality control procedures. The article concludes with a discussion of collaborative opportunities and future directions.

SCIENTIFIC MOTIVATION AND OVERALL DESIGN

The science requirements for the OOI were developed through Request for Assistance proposals and numerous community workshops, and with input from the approximately 90-member OOI Science and Technical Advisory Committee (Schofield and Tivey, 2004; Daly et al., 2006). The marine infrastructure was designed and constructed to meet these scientific requirements. The OOI is currently composed of five arrays spanning the North Atlantic and Northeast Pacific Oceans (Figure 1). Initial construction included two additional arrays in the Southern Hemisphere (red boxes, Figure 1), but deployments at those arrays were suspended in December 2017. Data collected at all of the OOI arrays, including the two Southern Hemisphere arrays that operated for 34 months, are available through the OOI Data Portal (<https://ooinet.oceanobservatories.org>).

Each of the OOI Arrays was designed and constructed to address large-scale scientific challenges. **Coastal Arrays** (Endurance and Pioneer) provide observations important for understanding

coastal ocean dynamics, ecology, and biogeochemistry. **Global Arrays** (Irminger Sea, Station Papa, Argentine Basin, and Southern Ocean) provide sustained open-ocean observations in high-latitude areas that have been historically sparsely sampled due to severe weather and energetic surface wave conditions. Data collected in these coastal and global areas address science questions related to ocean-atmosphere exchange, climate variability, ocean circulation, ecosystems, the global carbon cycle, turbulent mixing, and biophysical interactions. The **Cabled Array** spans the Juan de Fuca Plate in the Northeast Pacific where it continuously monitors volcanic activity, methane seeps, hydrothermal vents, and submarine earthquakes, as well as biological, chemical, and physical processes in the overlying water column. This array spans coastal to blue-water environments and includes electro-optical submarine cables that provide power, bandwidth, and two-way communication to seafloor and water column instrumentation.

An overarching goal of the OOI infrastructure is to provide sustained measurements for 25 years. Key operational objectives identified for the OOI program include: (1) real-time to near-real-time data availability as practicable, (2) two-way communication links allowing for control of the instrumentation, (3) additional power and bandwidth to support scientific instrumentation added by community investigators, and (4) adaptive sampling capabilities to respond to episodic or frequent events (e.g., episodic phytoplankton blooms, thin layer development, submarine eruptions, earthquakes, and frequent storms).

An important component of the OOI is its Education and Public Engagement (EPE) Implementing Organization, which has built an educational cyberinfrastructure and developed tools that allow undergraduates easy access to OOI data, images, and video (McDonnell et al., 2018, in this issue). In addition, OOI data have ignited student-led initiatives, such as the Axial Seamount Biology

Catalog (Bigham, 2018, in this issue). Because OOI data are free and openly available, they have been used in educational programs not related to the OOI such as the University of Washington's Seastate (Kelley and Grünbaum, 2018, in this issue).

By increasing accessibility to ocean data and research, augmenting cruise-based studies, aiding in model calibration, and fueling innovative studies through the addition of novel instrumentation to the existing OOI infrastructure, the OOI is transforming ocean science.

Coastal Endurance Array

The Coastal Endurance Array is located in the Northeast Pacific Ocean off the coasts of Oregon and Washington (Figure 1).

The array is designed to capture annual and decadal variability of ocean properties across a range of temporal and spatial scales. The Endurance Array uses instrumented fixed and mobile platforms over the continental shelf and slope to cover the Northern California Current and the eastern boundary current of the North Pacific. The array also includes cabled infrastructure on its Oregon Line.

SCIENTIFIC MOTIVATION

Climate and ocean anomalies affect the Northeast Pacific on interannual and interdecadal timescales. Interannual variability forced by the El Niño-Southern Oscillation at the equator influences upper-ocean stratification, ocean currents, and local winds traveling through

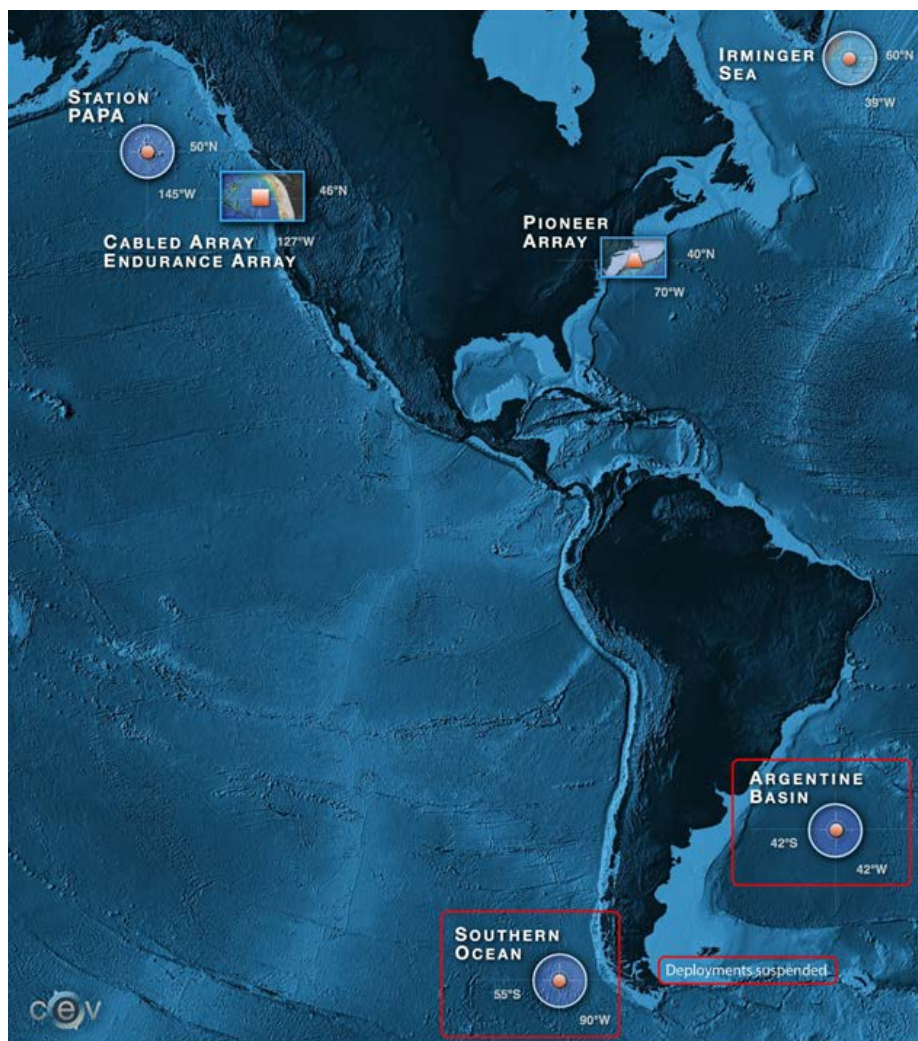


FIGURE 1. Map of Ocean Observatories Initiative (OOI) array locations. Note that deployments at the Southern Hemisphere arrays (outlined in red) were suspended as of December 2017. Credit: OOI Cabled Array program & the Center for Environmental Visualization, University of Washington

both ocean and atmosphere (Huyer et al., 2002). Over longer timescales, the Pacific Decadal Oscillation affects the region (Peterson and Schwing, 2003).

A combination of ocean observatories facilitates tracking of such climate and ocean phenomena across the Northeast Pacific. The Endurance Array is part of a broader regional observatory network that includes the OOI Cabled Array, the OOI Station Papa Array augmented by US National Oceanic and Atmospheric Administration (NOAA) assets, and the Ocean Networks Canada NEPTUNE and

VENUS arrays. One example of the network's effectiveness occurred during late 2013 and early 2014 when an anomalous "warm blob" was observed forming in the Gulf of Alaska; it was subsequently tracked by OOI assets as it spread to the US/Canadian west coast (Bond et al., 2015; McCabe et al., 2016; McKibben et al., 2017; Barth et al., 2018, in this issue).

Wind-driven upwelling and downwelling and the Columbia River plume (the largest source of freshwater to the US west coast) seasonally affect plankton productivity along Oregon and

Washington coasts (Henderikx Freitas et al., 2018, in this issue). These Northeast Pacific waters are home to a diverse range of profitable fisheries that rely on nutrients upwelled into the euphotic zone to drive phytoplankton blooms that form the base of the food web. In recent years, Northeast Pacific phenomena impacting human and ocean health have included (1) hypoxic and anoxic events (Grantham et al., 2004; Chan et al., 2008), (2) increasing ocean acidification (Feely et al., 2008; Barton et al., 2012; Chan et al., 2017), and (3) harmful algal blooms (Trainer et al., 2009). The Endurance Array is collecting abundant data in this region so that researchers can better understand the causes, timing, and consequences of such phenomena, ultimately leading to actions by decision-makers that will mitigate their effects.

LOCATION AND DESIGN

The Endurance Array includes gliders and two lines of moorings: the Oregon Line, off the coast of Newport, Oregon (44.6°N), and the Washington Line, off Grays Harbor, Washington (47°N) (Figure 2). The site of the Oregon Line was selected for its proximity to the historic Newport Hydrographic Line that has been sampled regularly since 1961 (Huyer et al., 2007). Additionally, an oceanographic mooring has been maintained 16 km offshore of Newport since 1999 (Boyd et al., 2000), and autonomous underwater gliders have sampled on the Newport Hydrographic Line since 2006 (Mazzini et al., 2014). Data from these historical observations have contributed to our understanding of coastal upwelling, regional manifestations of El Niño and La Niña, and interdecadal variability due to the Pacific Decadal Oscillation. The Washington Line was selected to provide a companion line to the north, focusing on an area affected by the Columbia River plume.

Each of the Endurance Array lines has three sites that sample distinct regions (Figure 3): (1) the "Inshore" site on the inner shelf ($\sim 25\text{--}30$ m water depth, 4–6 km from shore); (2) the "Shelf"

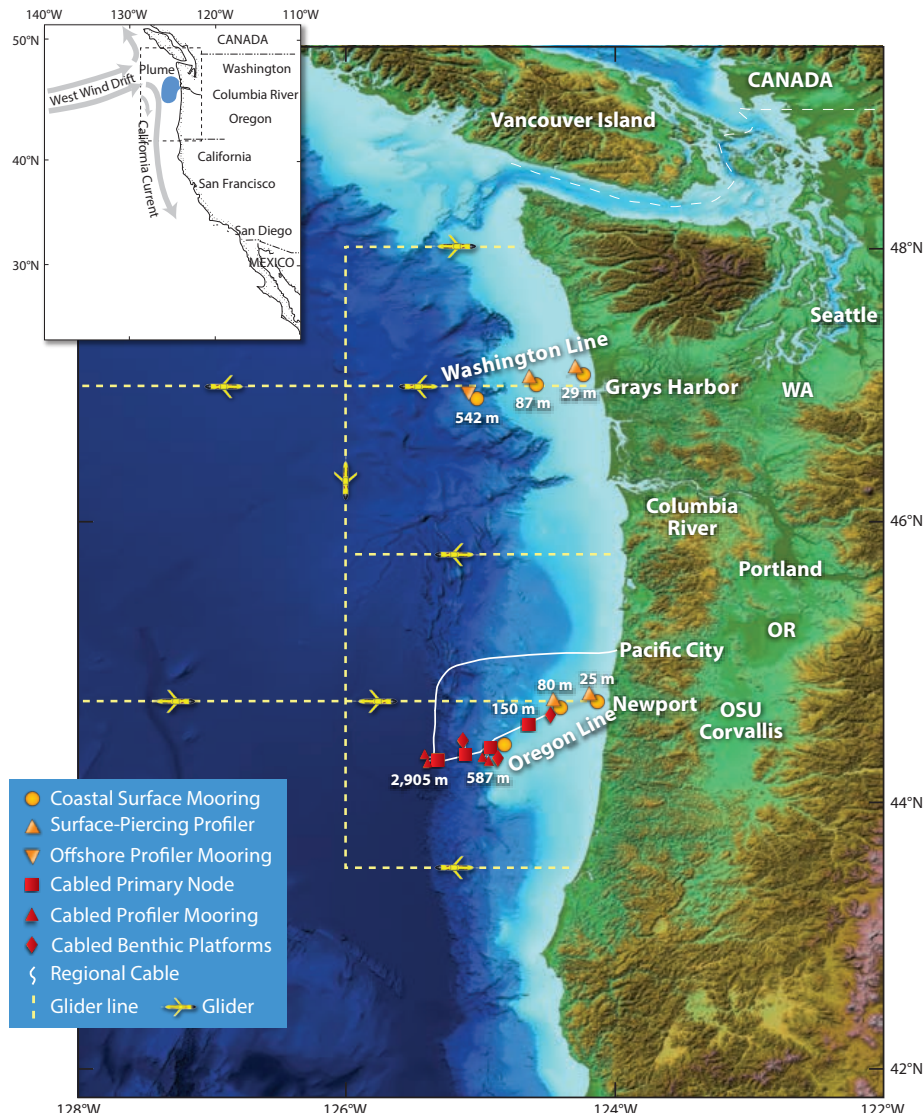


FIGURE 2. Map of the Endurance Array located in the Northeast Pacific, north and south of the Columbia River. Fixed platforms are shown as either stand-alone (orange) or attached to a seafloor cable (red). Primary backbone cable, shown by a thin white curve, heads offshore from Pacific City, Oregon, before turning south to create the Cabled Array off Newport, Oregon (note the primary cable to Axial Seamount is not shown; see Figure 7). Coastal glider sampling lines are shown as dashed yellow lines. Credit: OOI Endurance Array Program, Oregon State University

site (~80–90 m depth, 20–30 km from shore); and (3) the “Offshore” site on the continental slope (~500–600 m depth, 60–65 km from shore). In the inner shelf, wind, waves, and river plumes influence circulation and stratification, and the ocean connects to the sandy shores and rocky intertidal reefs. The shelf is a region of upwelling fronts, alongshore jets, plankton blooms, and stretches of seafloor with near-bottom hypoxia. At the offshore site on the continental slope, zooplankton migrate on a diurnal basis from a few hundred meters to the surface, wind-stress curl and offshore eddies interact with the coastal circulation, and a subsurface undercurrent moves poleward.

Instrumented platforms deployed at the Endurance Array are designed to measure critical interfaces in the coastal ocean from the seafloor to the sea surface and from the coastal boundary to the continental shelf break. Each site contains a Coastal Surface Mooring and one of four types of profiler moorings: a Coastal Profiler Mooring, a Coastal Surface-Piercing Profiler Mooring, a Cabled Deep Profiler Mooring, or a Cabled Shallow Profiler Mooring. Cabled instrumented seafloor packages and profiler moorings are deployed along the Oregon Line at the Offshore and Shelf sites. Underwater glider observations span 500 km from northern Washington (~48°N) to Coos Bay, Oregon (~43°N) as they sample along five east-west transects from 20 m isobaths to 126°W (out to 128°W on the transects off the Oregon and Washington Lines) and one north-south transect along 126°W (Figure 2).

Coastal Pioneer Array

The Pioneer Array is located over the continental shelf and slope in the Northwest Atlantic Ocean south of New England (Figure 1). It contains fixed and mobile platforms to sample processes near the shelf-break front, a characteristic feature of the Middle Atlantic Bight. The Array is centered near the front and samples the nearby shelf waters inshore and the slope sea offshore.

SCIENTIFIC MOTIVATION

The Middle Atlantic Bight shelf-break front, a region of high biological productivity, is representative of buoyancy-driven systems found on broad shelves worldwide. It is a persistent oceanographic front associated with the changing bathymetry that separates relatively cold, fresh continental shelf water to the north from relatively warm, salty oceanic water to the south. This dynamic environment permits investigation of key features of coastal processes and ecosystems.

Large horizontal and vertical gradients

in water properties are associated with the shelf-break front. The frontal region has significant along- and cross-shelf fluxes of heat, freshwater, nutrients, and carbon that control the characteristics of water masses and the ecosystem at the shelf break, over the continental shelf inshore of the front, and in the slope sea offshore. Despite several decades of research, we have a limited understanding of the processes that control the dynamics and ecosystem interactions at the shelf-break front. Many of these processes are short-lived and occur

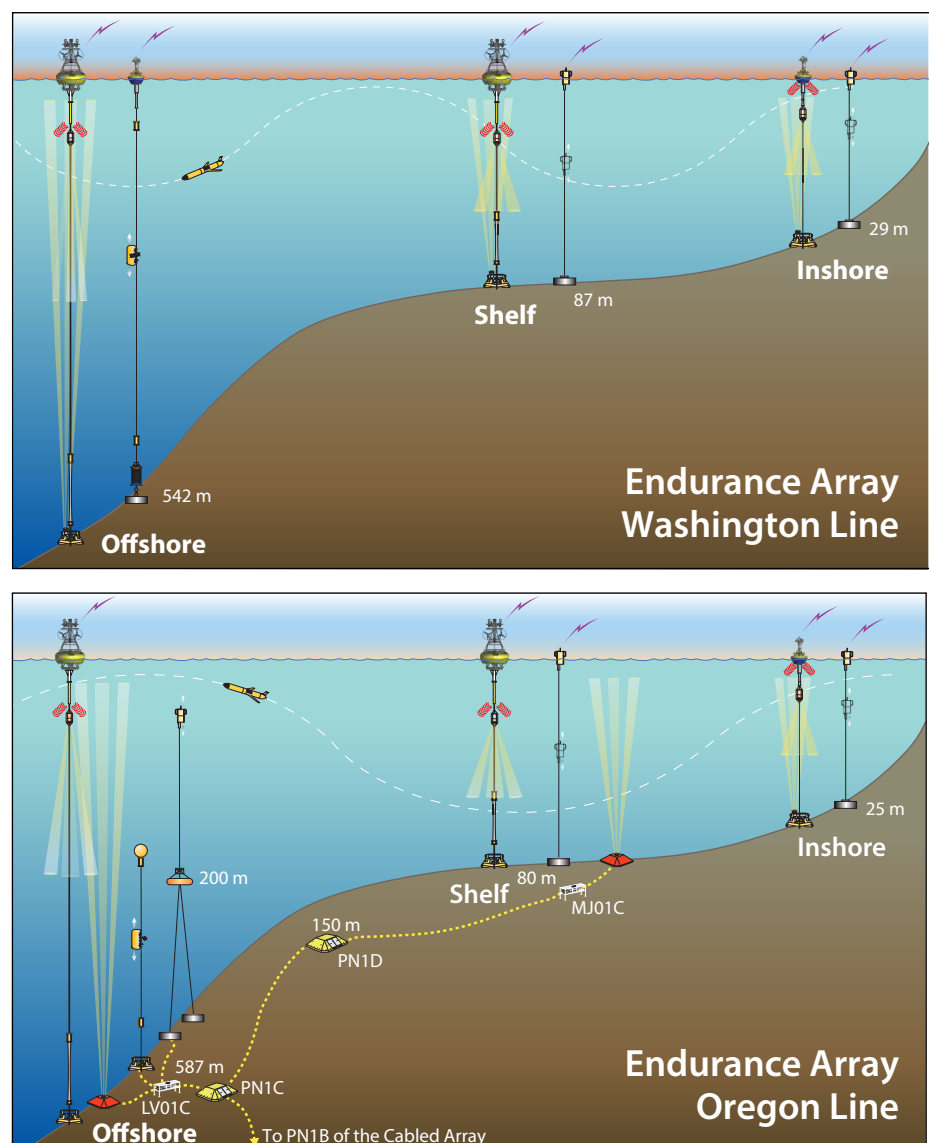


FIGURE 3. Cross sections of the Endurance Array Lines off Grays Harbor, Washington (top), and Newport, Oregon (bottom). Several of the Newport Line platforms are attached to the seafloor cable (yellow dashed curve). The surface buoys and the surface-piercing profilers communicate to shore via satellite. The glider path is notional; individual profiles are much closer together than depicted. Credit: OOI Endurance Array Program, Oregon State University

over a broad range of spatial and temporal scales, making them difficult to measure (Gawarkiewicz et al., 2018, in this issue). To achieve significant progress toward understanding these processes, a new approach was needed that combined rapid sampling (hours to days) on multiple spatial scales (meters to hundreds of kilometers) simultaneously. Additionally, sustained observations through multiple seasonal and annual cycles are critical in order to capture intermittent processes controlling air-sea flux and mixing events (Chen et al., 2018, in this issue).

The OOI Pioneer Array collects data that enables scientists to examine how shelf/slope exchange processes structure the physics, chemistry, and biology of continental shelves. The 2011 Shelf Slope Processes Workshop (Gawarkiewicz et al., 2012) emphasized the importance of tackling this issue and recommended focusing on four areas: (1) nutrient and carbon

cycling over the outer continental shelf and upper continental slope; (2) abundance, distribution, and biodiversity of phytoplankton near the shelf break; (3) controls on the abundance and distribution of marine organisms at higher trophic levels; and (4) extreme events including winter storms and hurricanes.

LOCATION AND DESIGN

The Middle Atlantic Bight shelf-break front extends from Nova Scotia, Canada, to Cape Hatteras, North Carolina, USA. The Pioneer Array's location along the shelf break south of New England allows isolation of frontal processes from those associated with other features such as canyons, river outflows, and the Gulf Stream. Importantly, prior research provided detailed information about the horizontal, vertical, and temporal scales of the area's complex physical processes as the Pioneer Array was being designed.

The core of the Pioneer Array is a rectangular, uncabled seven-site mooring array that spans the shelf break (Figure 4). The five primary components of the cross-shelf array are at 95, 127, 135, 147, and 450 m water depths. Primary sites located at 95 m and 450 m have paired "upstream" sites located to the east (they are "upstream" relative to the mean flow over the shelf) to provide observations across a horizontal gradient. The mooring array spans along- and across-shelf distances of 9 km and 47 km, respectively, and moorings are separated from each other by distances of 9.2 km to 17.5 km. To provide multiscale observations of the outer shelf, shelf-break frontal region, and slope sea, the mooring array is supplemented by 10 mobile platforms: six coastal gliders, two profiling gliders, and two autonomous underwater vehicles (AUVs). Coastal gliders are used to monitor the slope sea and outer shelf in order to resolve Gulf Stream rings, eddies, and meanders as they contact the shelf-break front. Profiling gliders are used as "virtual moorings" at the Central and Inshore sites in the summer. The overall glider operating area is $185 \text{ km} \times 130 \text{ km}$, roughly centered on the mooring array (Figure 5). The nominal AUV missions are two $14 \text{ km} \times 47 \text{ km}$ rectangles, with the along-shelf rectangle intersecting the inshore end of the mooring array and the cross-shelf rectangle encompassing the mooring array.

The Pioneer mooring array includes three Coastal Surface Moorings with fixed instruments and either five (in summer) or seven (in winter) Coastal Profiler Moorings with profiling instruments. The Offshore site is continuously occupied by both a Coastal Surface Mooring and a Coastal Profiler Mooring in near proximity (typical separation 1 km). In winter, the Inshore and Central sites each contain both a Coastal Surface Mooring and a Coastal Profiler Mooring (profiling gliders replace the Coastal Profiler Moorings in summer). The remaining four sites are each continuously occupied by a Coastal Profiler Mooring.

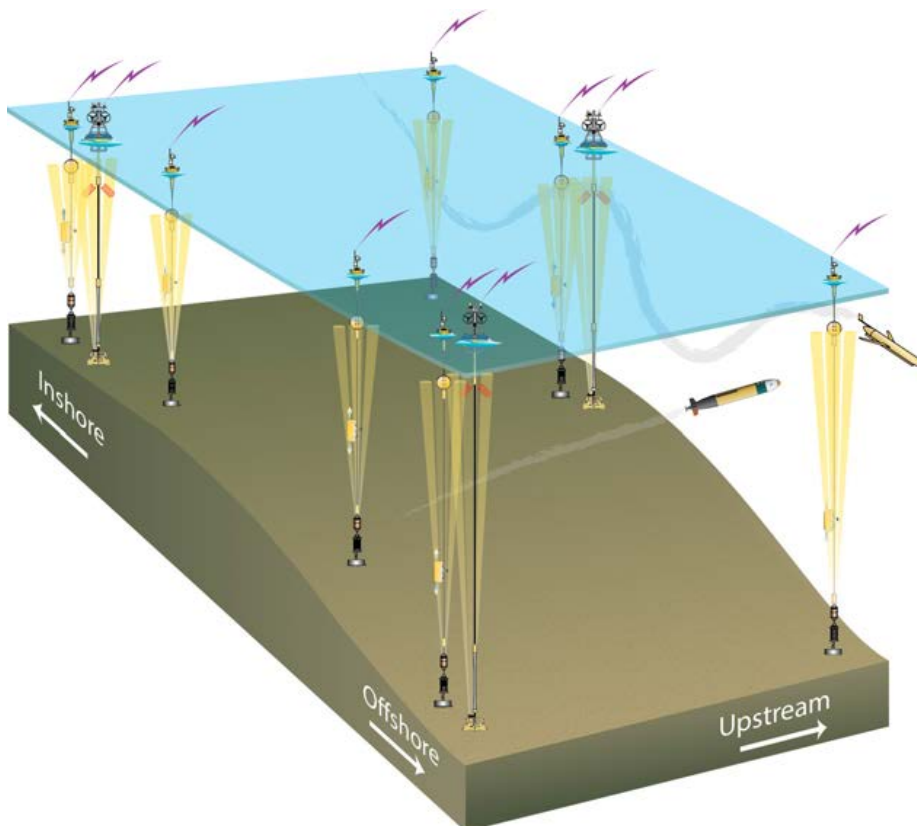


FIGURE 4. Schematic of the Pioneer Array (not to scale). Ten moorings occupy seven sites spanning the shelf break south of New England. Three sites—Inshore, Offshore, and Central (right center)—are occupied by mooring pairs. At two sites—Inshore and Central—the profiler moorings are replaced by profiling gliders in summer. A fleet of six gliders survey the area near and offshore of the moorings, while autonomous underwater vehicle (AUV) missions are conducted near the moored array. Credit: OOI Pioneer Array Program, Woods Hole Oceanographic Institution

Global Arrays

The four original high-latitude, open-ocean OOI Global Array sites (Figure 1) were located in the Irminger Sea (60°N , 39°W), the Southern Ocean (55°S , 90°W), the Argentine Basin (42°S , 42°W), and the Gulf of Alaska (Station Papa; 50°N , 145°W). These sites were selected not only for their individual scientific merit, but also to ensure that these locations would provide observations for contrasting biological and biogeochemical regimes. (As noted earlier, deployments have been suspended at the two Southern Hemisphere arrays—Southern Ocean and Argentine Basin.)

Three goals guided the design of the Global Arrays: (1) observation of the full water column and sea surface; (2) sampling of physical, biological, and biogeochemical variables; and (3) sampling of eddy variability and processes. These sites collectively address global-scale scientific challenges, including understanding of ocean circulation, the carbon cycle, and climate.

SCIENTIFIC MOTIVATION FOR THE GLOBAL IRMINGER SEA ARRAY

The Irminger Sea site is a region with high wind and large surface waves, strong atmosphere-ocean exchanges of energy and gases, deepwater formation, CO₂ sequestration, high biological productivity, an important fishery, and a climate-sensitive ecosystem.

The large-scale thermohaline circulation in the subarctic Atlantic is a fundamental feature of global ocean circulation and a response to the equator-to-pole asymmetry in atmospheric forcing of the ocean. Some of the strongest atmospheric forcing occurs at the site of the Global Irminger Sea Array southeast of Greenland. For decades, shipboard sampling has documented water column freshening in the Denmark Straits and Faroe-Shetland Channel region of the high-latitude North Atlantic (Dickson et al., 2002). International attention has focused on the potential impact of this freshening on deep convection in the

region (de Jong et al., 2018, in this issue) as it may affect large-scale thermohaline circulation globally. The Irminger Sea Array provides data for studies of this thermohaline circulation, specifically, deepwater formation processes, regional air-sea interactions, the role of ocean mesoscale and three-dimensional processes in water mass transformation, and ongoing freshening. Year-round sampling captures episodic and strong forcing events likely missed in the historical record of intermittent shipboard sampling.

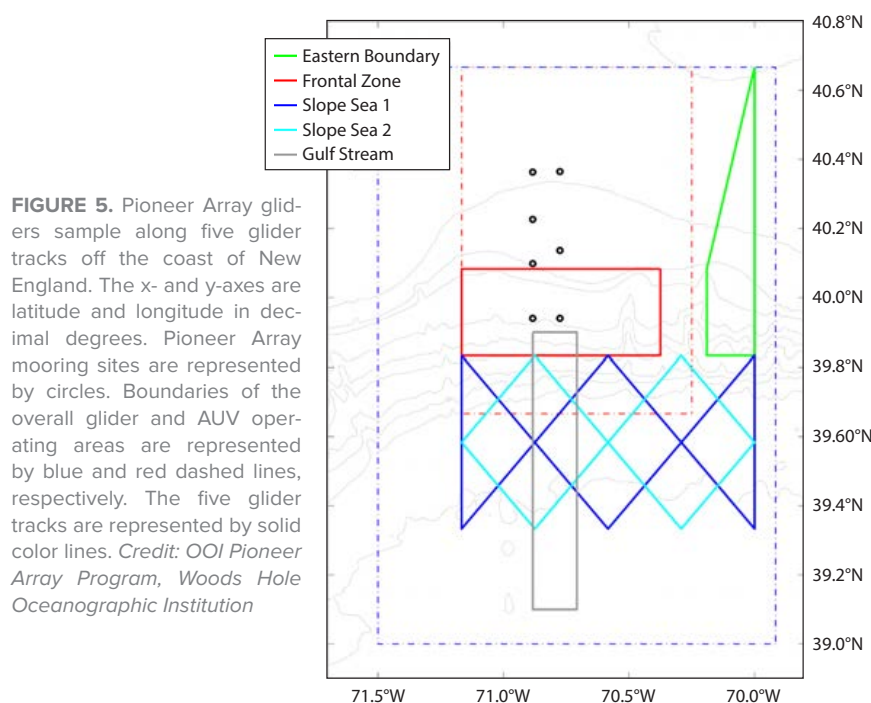
The Irminger Sea region is also of high interest because of the role it plays in the global carbon cycle. This ocean region is known as a strong carbon sink that supports an annual spring diatom bloom (Takahashi et al., 2002; Sabine et al., 2004; Palevsky and Nicholson, 2018, in this issue). Profound effects of high climate variability on ecosystems here include copepod species composition changes (Gislason et al., 2014) and the poleward migration of marine species (Sundby et al., 2016).

SCIENTIFIC MOTIVATION FOR THE GLOBAL STATION PAPA ARRAY

The Gulf of Alaska site is co-located with Station Papa (50°N , 145°W). Unlike other

OOI Global Array locations, this area has a long ship-based observational history. Station Papa was first occupied in 1949 by a United States weather ship and in 1950 by a Canadian weather ship. After these ships were discontinued, Canadian oceanographers began in 1981 to maintain a shipboard sampling line in the region. Persistent moored occupation of the site began in 2007 with an installation by the NOAA Pacific Marine Environmental Laboratory (PMEL). The OOI Global Profiler Mooring is co-located with the PMEL Surface Mooring.

The OOI Station Papa Array adds a contrasting regime to the other global arrays. Anthropogenic CO₂ influence is the lowest of the four global nodes, biological productivity is likely limited by iron (though it has a productive fishery), and it has the lowest eddy variability of the global sites. Over longer timescales, the Pacific Decadal Oscillation influences the area. Additionally, though anthropogenic CO₂ influence is low, the area around Papa has been found to be extremely vulnerable to ocean acidification (Mathis et al., 2015). The Global Station Papa Array adds to a broader suite of observations in the Northeast Pacific by providing observational continuity through



the OOI Cabled and Coastal Array to the south, and nearby Ocean Networks Canada arrays.

SCIENTIFIC MOTIVATION FOR THE SOUTHERN OCEAN ARRAY

Prior to deployment suspension (December 2017), the Southern Ocean Array was located in the high-latitude Southern Pacific (55°S , 90°W), west of the southern tip of Chile in an area of large-scale thermohaline circulation, intermediate water formation (e.g., Sloyan et al., 2010), and CO_2 sequestration. This location provided data for weather and ocean model initialization and verification in a data-sparse region. It also permitted examination of the links between the Southern Ocean and the Antarctic (National Academies of Sciences, Engineering, and Medicine, 2015), including strengthening westerly winds and their role in increased upwelling of warmer waters around the Antarctic continent's ice shelves.

This Southern Ocean Array provided a contrast to the Irminger Sea site in terms of biological and climatic conditions. Unlike the Irminger Sea site, the macronutrient-rich Southern Ocean has lower biological productivity due to iron

limitation (Morrissey and Bowler, 2012). Additionally, whereas climate models point to a warmer and fresher water column in the Irminger Sea, they suggest a cooling of surface waters off southern Chile at the Southern Ocean site.

SCIENTIFIC MOTIVATION FOR THE GLOBAL ARGENTINE BASIN ARRAY

Prior to deployment suspension (December 2017), the Argentine Basin site was located at 42°S , 42°W . This site was selected to explore the global carbon cycle because of its high biological productivity. Though primary productivity in the region is thought to be iron-limited, Li et al. (2008) suggest that these micronutrients are supplied by periodic dust deposition originating from the nearby continent.

The Argentine Basin is characterized by strong currents and elevated levels of eddy kinetic energy. These currents persist to the seafloor, impacting suspended particulate matter (Richardson et al., 1993) and generating seafloor mud waves (Flood and Shor, 1988). Eddy kinetic energy levels are similar to those in the Gulf Stream (Stammer, 1997), allowing for investigation of mesoscale variability

and its role in ocean processes. There is ongoing interest in the interaction of different water masses in the region and exchange between gyres of mass, heat, and salt (e.g., Jullion et al., 2010).

GLOBAL ARRAY LOCATION AND DESIGN

The overall design and construction of the global arrays focused on sampling the full water column as well as spatial structure and variability. Each global array consists of a triangular set of moorings, with the sides of the triangle having a length roughly 10 times the water depth (Figure 6). This spacing was based on the characteristics of the mesoscale variability in each region using satellite ocean color and altimetry. The global array design consists of a combination of three mooring types: the paired Global Surface and subsurface Global Profiler Moorings are at one corner of the triangle, with the other two corners occupied by subsurface Global Flanking Moorings. The paired Surface and Profiler Moorings at the apex of the triangle collect samples from the sea surface to the seafloor.

Two types of gliders are deployed within the array: open-ocean gliders sample spatial variability within and around the moored array, and vertically profiling gliders make vertical profiles near the Profiler Mooring. Gliders deployed at the Global Array sites have the additional role of being messengers between the three subsurface moorings and shore.

Cabled Array

The OOI Regional Cabled Array is located off the coast of Oregon and extends across the Juan de Fuca Plate (Figure 1). The array hosts instruments on the seafloor and on moorings that include instrumented mobile platforms to promote integrated investigations spanning (1) coastal ecosystems and methane seeps west of Newport, Oregon; (2) the Cascadia subduction zone; (3) blue water environments >500 km offshore; and (4) the Juan de Fuca mid-ocean ridge

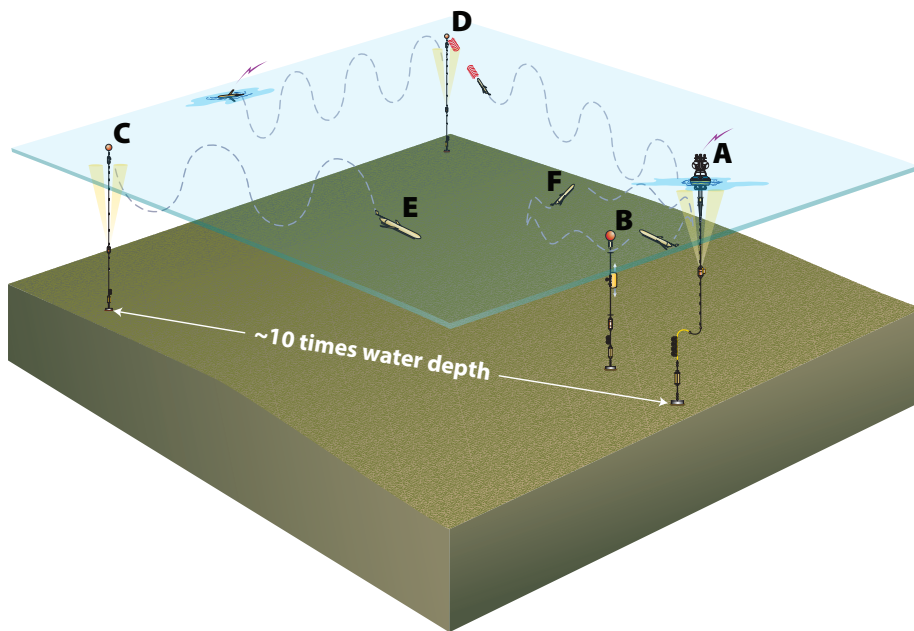


FIGURE 6. Schematic of an OOI Global Array, showing the (A) Global Surface Mooring, (B) Global Profiler Mooring, and (C and D) Flanking Subsurface Moorings. Open-ocean gliders (E) sample spatial variability within and around the moored array while profiling gliders (F) make vertical profiles near the Profiler Mooring. Credit: OOI Global Array Program, Woods Hole Oceanographic Institution

spreading center (Kelley et al., 2014). The decadal time-series observations supported by the Regional Cabled Array allow in-depth study of globally significant oceanographic processes, including biogeochemical cycles, fisheries and climate forcing, tsunamis, ocean dynamics, carbon flux from the seafloor to the hydrosphere, life in extreme environments, and plate tectonics.

The Regional Cabled Array focuses on two areas on opposite sides of the Juan de Fuca Plate—the continental margin and Axial Seamount (Figure 7). Within the continental margin, infrastructure is located at four sites: (1) just off the continental slope near the Cascadia subduction zone, (2) on the continental slope at Southern Hydrate Ridge (an area with active methane hydrates), and along the Endurance Array Oregon Line at the (3) Offshore, and (4) Shelf sites. On the far west side of the Juan de Fuca Plate, infrastructure is located within the active caldera of Axial Seamount and at its base.

SCIENTIFIC MOTIVATION FOR THE CABLED CONTINENTAL MARGIN ARRAY

The Slope Base site (2,900 m depth) is located seaward of the continental slope, west of Newport, Oregon (Figure 7). This is one of a few locations where geophysical instruments are located close together, with one set on the oceanic side (Juan de Fuca Plate) of the subduction zone and the other on the North American Plate, atop the accretionary prism (Southern Hydrate Ridge; e.g., see Tréhu et al., 2018, in this issue). These geophysical observations assist in the detection of seismic and tsunami events associated with earthquakes along the Cascadia subduction zone. This site also contains seafloor infrastructure and instrumented moorings designed to observe the deeper portions of the California Current off the continental slope, movement of fluids across the continental slope, and flow over rough topography (Barth et al., 2018, in this issue).

Southern Hydrate Ridge (780 m depth; Figure 7) is located in a region of buried deposits of methane hydrate and, more rarely, hydrates exposed on the seafloor (Torres et al., 2004; Bangs et al. 2011; Suess, 2014). Here, seeps emit methane-rich fluids, and their bubble plumes reach >400 m above the seafloor, possibly supporting life in the upper water column (Philip et al., 2016). It is critical to quantify the flux of this powerful greenhouse gas from the seafloor to the hydrosphere and atmosphere to understand carbon-cycle dynamics and its contribution to global warming. These seeps also support dense benthic colonies of methane-metabolizing microbes, and animals with methane and hydrogen sulfide utilizing symbionts (Boetius and Suess, 2004).

Further up the slope from Southern Hydrate Ridge (Figure 8), a fiber-optic cable connects to the Offshore (600 m depth) and Shelf (80 m depth) sites of the Coastal Endurance Array. This extended footprint of the Regional



FIGURE 7. The Regional Cabled Array infrastructure spans the Juan de Fuca Plate with one 521 km long backbone cable connecting infrastructure located at the base (PN3A) and the summit (PN3B) of Axial Seamount ($45^{\circ}56'N$; $129^{\circ}59'W$), and another southern line that connects infrastructure at the base of the continental margin (Slope Base – PN1A), the active methane seep site at Southern Hydrate Ridge (SHR) 10 km north of the Primary Node PN1B, and the Oregon Offshore (PN1C) and Shelf sites (see Figure 2). A 17 km cable connects PN1D to the shelf site. Primary cables are buried ~1 m beneath the seafloor to 1,500 m water depth. A highly expandable plan includes arrays at the Blanco Transform Fault and at the subduction zone off of Grays Harbor. A 5 km cable extends from the Mid-Plate node (5A), allowing easy expansion in the future to the Grays Harbor site. Credit: University of Washington and Center for Environmental Visualization

Cabled Array permits further examination of the California Current's eastern boundary current regime, collecting data on ocean processes from the coastal zone through their transition into the ocean basin interior, and outward to the pelagic North Pacific.

SCIENTIFIC MOTIVATION FOR THE CABLED AXIAL SEAMOUNT ARRAY

Axial Base (2,700 m depth), located >350 km offshore at the base of Axial Seamount, is in an open-ocean environment that permits collection of data linking ocean dynamics, climate, and ecosystem response from basin to regional scales (Figure 7). Here, large-scale currents interact, including the North Pacific Current, the subpolar gyre, and the northern end of the California Current. These currents transport heat, salt, oxygen, and biota, crucial elements of the region's ecosystem. Their variability results from a combination of short-term changes in tides and winds and longer-term climate phenomena that act at interannual (El Niño) to decadal (Pacific Decadal Oscillation) timescales. Additional focus

at Axial Base is on monitoring plate-scale seismicity and local earthquakes associated with magma migration within Axial Seamount, seafloor spreading events along the Juan de Fuca Ridge, and far-field earthquakes.

The infrastructure at the summit of Axial Seamount (1,500 m deep) makes it the most advanced underwater volcanic observatory in the world ocean (Kelley et al., 2014; Kelley, 2017). The volcano rises 1,100 m above the surrounding abyssal plain and is the most magmatically robust system on the Juan de Fuca Ridge. Seismic data indicate that there is a significant magma reservoir beneath the volcano, with the highest melt concentrations occurring at depths of 2.5–3.5 km (Arnulf et al., 2014). The volcano erupted in 1998, 2011, and April 2015 (Chadwick et al., 2006; Nooner and Chadwick, 2016; Wilcock et al., 2016, 2018, in this issue; Tolstoy et al., 2018, in this issue). Using data from this site, scientists examine formation and alteration of oceanic crust, the relationships between seismic activity and fluid flow in diffuse and black smoker sites, and how changes in fluid temperature and

chemistry impact microbial and macrofaunal communities (Kelley et al., 2014).

A highlight of the networked array on Axial Seamount was live detection of the April 24, 2015, eruption marked by a 10-hour seismic crisis involving >8,000 earthquakes (Wilcock et al., 2016), an approximately 2.4 m collapse of the seafloor (Nooner and Chadwick, 2016), more than 30,000 explosive events (Wilcock et al., 2016), and lava flows reaching 127 m in thickness.

CABLED ARRAY LOCATION AND DESIGN

The OOI Regional Cabled Array includes two backbone cables extending from a shore station in Pacific City, Oregon (Figure 7). One branch extends approximately 480 km due west to the Axial Seamount site. The second branch extends 208 km southward near the base of the Cascadia subduction zone at 2,900 m water depth and then turns east, extending 147 km to 80 m water depth offshore Newport, Oregon.

Seven Primary Nodes are distributed across these two backbone cable

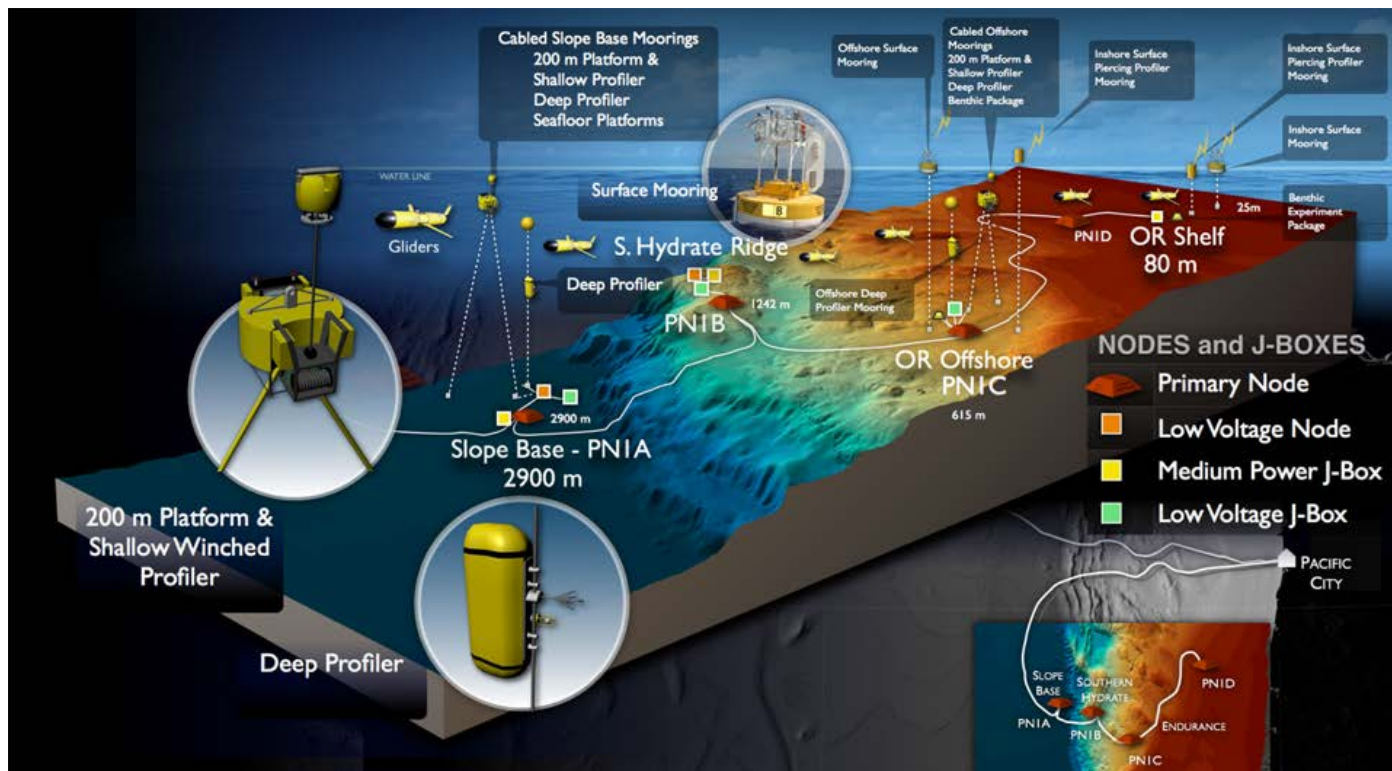


FIGURE 8. Schematic showing OOI cabled and uncabled infrastructure off the coast of Oregon from the base of the continental slope up onto the shelf. Credit: University of Washington and the Center for Environmental Visualization

lines—four covering the Slope Base to Oregon Shelf sites, one at mid-plate, and two at Axial Seamount (Figure 7). Primary Nodes distribute power (8 kW) and bandwidth (10 Gbs) between secondary infrastructure at each site and the shore. Secondary infrastructure provides access to key observational sites. This infrastructure includes 33,000 m of extension cables, 18 low- and medium-power junction boxes and low-voltage nodes (Figures 7, 8, and 9), and >140 instruments of more than 30 types.

Geophysical sensors located at Slope Base, Southern Hydrate Ridge, and Axial Seamount include seismometers and low-frequency hydrophones. At Axial Seamount, these instruments are coupled with pressure-tilt devices to monitor inflation and deflation of the volcano (Wilcock et al., 2018, in this issue). Biogeochemical and physical sensors, including a digital still camera, a mass spectrometer, acoustic Doppler current profilers (ADCPs),

two benthic flow meters, an osmotic fluid sampler, and seismometers, are used at Southern Hydrate Ridge to examine gas hydrate formation and destruction, and links between seismic activity and methane release. For studies of volcanic and hydrothermal processes associated with hydrothermal vents at Axial Seamount, a high-definition video camera, a long-duration fluid sampler, and a three-dimensional thermistor array are located at the actively venting >250°C chimney called Mushroom in the ASHES hydrothermal field (Kelley et al., 2016; Knuth et al., 2016).

Some of the most technologically advanced instrumentation is located within the International District Hydrothermal Field, including a mass spectrometer to measure the volatile chemistry of diffuse fluids, adaptive diffuse fluid and microbial DNA samplers, and instruments to measure high-temperature vent fluid and volatile chemistry. A digital still

camera provides images, and a seismometer, a bottom-pressure tilt instrument, and a current meter are located nearby.

Cabled mooring sites include Slope Base, Endurance Oregon Offshore, and Axial Base. Each site hosts a Cabled Deep Profiler and a Shallow Profiler Mooring (McRae, 2016). The instrumented moorings and associated seafloor infrastructure are designed to allow measurement of global and local currents, megaplumes, ocean chemistry, heat content, thin layers, and biological parameters. Examples of cabled mooring instrumentation include broadband hydrophones, five-beam and 150 kHz ADCPs, digital still cameras, zooplankton samplers, fluorometers, current meters, and sensors for pH, $p\text{CO}_2$, nitrate, CTD-dissolved oxygen (O_2), optical attenuation, spectral irradiance, and photosynthetically active radiation (PAR). Expansion capabilities are built into the mooring assembly for addition of new technologies, and

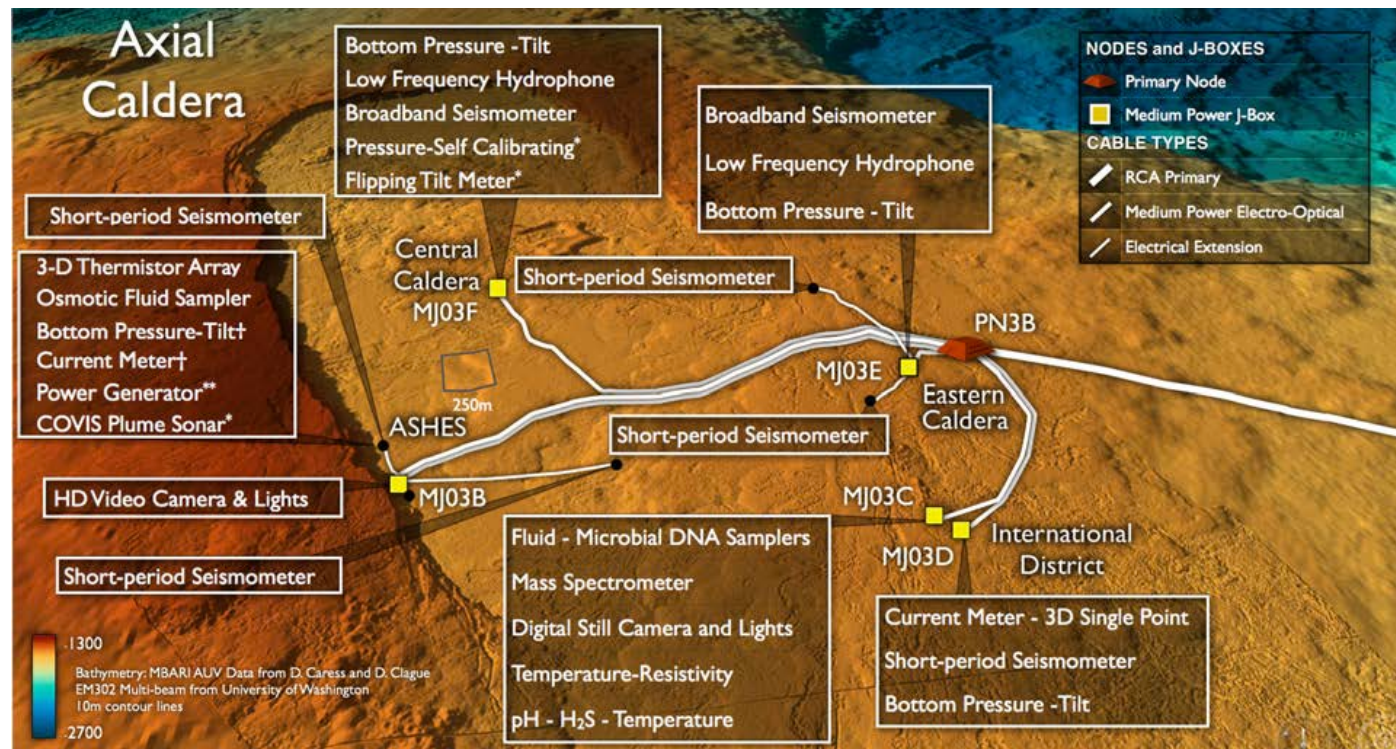
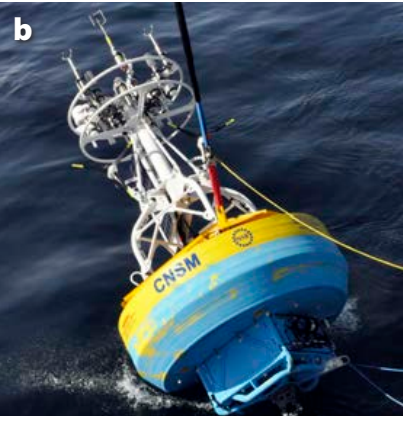


FIGURE 9. Schematic of the cabled infrastructure on Axial Seamount's caldera. The caldera is located at a water depth of ~1,500 m. Its walls rise ~100 m above the surrounding seafloor and it is ~3 km across. Primary Node PN3B provides power and bandwidth to a diverse array of instrumentation to study the most active volcano on the Juan de Fuca Ridge. Five medium-power junction boxes provide power and two-way communications to geophysical, geochemical, and biological instruments to examine linkages among volcanic and hydrothermal processes. New instrumentation was added in 2017 through National Science Foundation (NSF) principal investigator funding, including a CTD and a bottom pressure-tilt instrument. Additional infrastructure funded through NSF and the Office of Naval Research will be added in 2018, including a sonar to image hydrothermal plumes (Cabled Observatory Vent Imaging Soar, COVIS), two new geodetic instruments that include a flipping tilt meter and a self-calibrating pressure sensor, and a camera and platform to examine power generation from hydrothermal vents. Credit: University of Washington and the Center for Environmental Visualization



two-way communications enable rapid responses to ocean events. A complementary set of seafloor instruments for documenting near-bottom and water-column processes includes a 150 kHz ADCP, a low-frequency hydrophone (Slope and Axial Base), a broadband hydrophone (Endurance Offshore and Shelf), an optical attenuation sensor, a CTD-O₂, and a HPIES (Horizontal Electric Field, Pressure and Inverted Echo Sounder). In addition, a suite of geophysical instruments includes a broadband seismometer, a low-frequency hydrophone, a current meter, a pressure sensor, and a temperature sensor.

PLATFORMS

The five actively deployed OOI arrays (Figure 1) in the original OOI infrastructure plan together contain 71 instrumented platforms supporting approximately 760 deployed instruments. This system offers over 200 unique data products, allowing scientists to study oceanographic phenomena from the seafloor to the air-sea interface on scales of centimeters to kilometers and seconds to decades.

In this section, we summarize the infrastructure within the OOI to provide context for design decisions. For engineering schematics and greater details of implementation of the designs of the OOI infrastructure, please visit the OOI website (<http://oceanobservatories.org>).

FIGURE 10. (a,b) Images of Coastal Surface Mooring components. (a) The surface buoy (CNSM) is lowered to the water before the quick release (yellow line) is pulled. (b) The multi-function node (ISSM) goes into the water. (c) The Global Surface Mooring surface buoy is equipped with solar panels and wind generators for charging lead-acid batteries. Instrumentation on the 5 m tower includes two bulk meteorological packages, a direct covariance flux system, and antennae for the telemetry systems. (d,e) Components of a Coastal Profiler Mooring. (d) The blue-bottomed Surface Buoy (OSPM) is prepared for deployment with two tag lines and a quick release line. (e) The yellow Wire-Following Profiler slides out along the wire rope with the motor disengaged while the buoy trails behind the ship. Credit: OOI Pioneer and Global Array Programs, Woods Hole Oceanographic Institution.

Moorings

Moorings provide high temporal resolution observations in one location either through fixed sensors distributed through depth, or sensors on profilers that repeatedly sample the water column. Most OOI sites consist of an array of moorings, permitting examination of spatial variability across the local domain. OOI moorings include Coastal and Global Surface Moorings along with Flanking Subsurface Moorings, as well as various types of Profiler Moorings (Figures 10, 11, and 12).

COASTAL SURFACE MOORINGS

Coastal Surface Moorings include an instrumented surface buoy with a 3 m tall tower, a near-surface instrument frame (NSIF) deployed at 7 m depth, a mooring riser, and an anchor (Figures 10b and 11). In some cases, instead of a traditional anchor, an instrumented seafloor package, the multifunction node (MFN; Figure 10a), is used. The MFN also incorporates an anchor and anchor recovery system. The surface buoy and tower, NSIF, and MFN are designed to accommodate multiple fixed-depth instruments.

The mooring riser on a Coastal Surface Mooring includes specially designed stretch hoses that allow mechanical extension and compression of the mooring riser while still providing electrical connectivity for power and communication from the buoy to instruments on the NSIF and MFN. The flexible mechanical and electrical mooring riser elements are essential in these coastal environments, which are subject to tidal fluctuations, large waves, and strong winds and currents. At Endurance Inshore locations, where wave events in winter can exceed 20 m, submersible surface buoys are used to allow the buoy to be pulled underwater if the stretch hose reaches its full extent (Paul, 2004).

Large capacity batteries charged by wind and solar power (photovoltaic panels) supply ample power to the OOI Coastal Surface Moorings, and each mooring has Ethernet connectivity from

the buoy to the seafloor. Communication systems on the buoy include GPS for location and timing, two-way satellite telemetry (buoy to shore), and line-of-sight communications (buoy to ship). Overlapping communication systems offer redundancy while providing for near-real-time data telemetry as well as command and control from ship or shore.

The Coastal Surface Moorings include instruments that require significant power, space, and bandwidth—cameras, ADCPs, bioacoustic instruments, and sensors for ocean acidity and carbon dioxide. Coastal Surface Mooring buoys contain standard meteorological sensors that measure wind, air temperature and humidity, solar radiation, and near-surface temperature and salinity. Some buoys have additional instrumentation for measuring surface waves and collecting direct (covariance-based) estimates of momentum and buoyancy flux. The NSIF and MFN carry sensors that measure temperature, salinity, dissolved oxygen, pH, optical properties, and currents. The MFN also carries instruments for bottom pressure and carbon dioxide concentration, and a bioacoustic profiler. Sampling rates for fixed-depth instruments range from 10 sec^{-1} to 1 hr^{-1} to resolve surface wave, internal wave, and tidal variability.

GLOBAL SURFACE MOORINGS

Global Surface Moorings are very similar to their coastal counterparts (Figures 10c and 11), with alterations to handle conditions of open-ocean, high-latitude deployments, where harsh weather and annual maintenance limitations impose additional challenges for sustained operations. These buoys are the only mooring platforms at the OOI Global Arrays with surface expressions. The height of the surface buoy tower is set at 5 m (compared to 3 m for the Coastal Surface Mooring) to account for anticipated sea states and freezing spray. The surface mooring uses chain and wire rope near the surface where instrumentation can be attached, but relies on buoyant and stretchable synthetic rope at depth to

resist the drag forces of currents.

Global Surface Moorings each consist of a surface buoy (Figure 10c) with both meteorological and in-water sensors, an NSIF deployed at 12 m depth (as compared to 7 m on Coastal Surface Moorings), and additional sensors at fixed depths along the mooring riser (Figure 11). The surface buoy supports two redundant bulk meteorological systems and a direct covariance flux system, as well as sensors for irradiance, wave spectra, air-sea $p\text{CO}_2$, dissolved oxygen, nitrate, and fluorescence. The NSIF contains a similar instrument suite to that on the Coastal Surface Moorings plus a velocity sensor. Sensors on the mooring riser are concentrated in

the upper 200 m of the water column, with additional CTD instruments and ADCPs deployed at intervals down to 1,500 m.

The surface buoy is the only platform on each global array capable of supporting satellite telemetry. It incorporates a comprehensive and redundant set of telemetry systems, including fleet broadband. Rechargeable lead-acid batteries, wind turbines, and solar panels support these systems, providing power up to about 200 W for the instrumentation.

FLANKING SUBSURFACE MOORINGS

Flanking Subsurface Moorings are deployed at all global arrays (Figure 11). These moorings are composed of

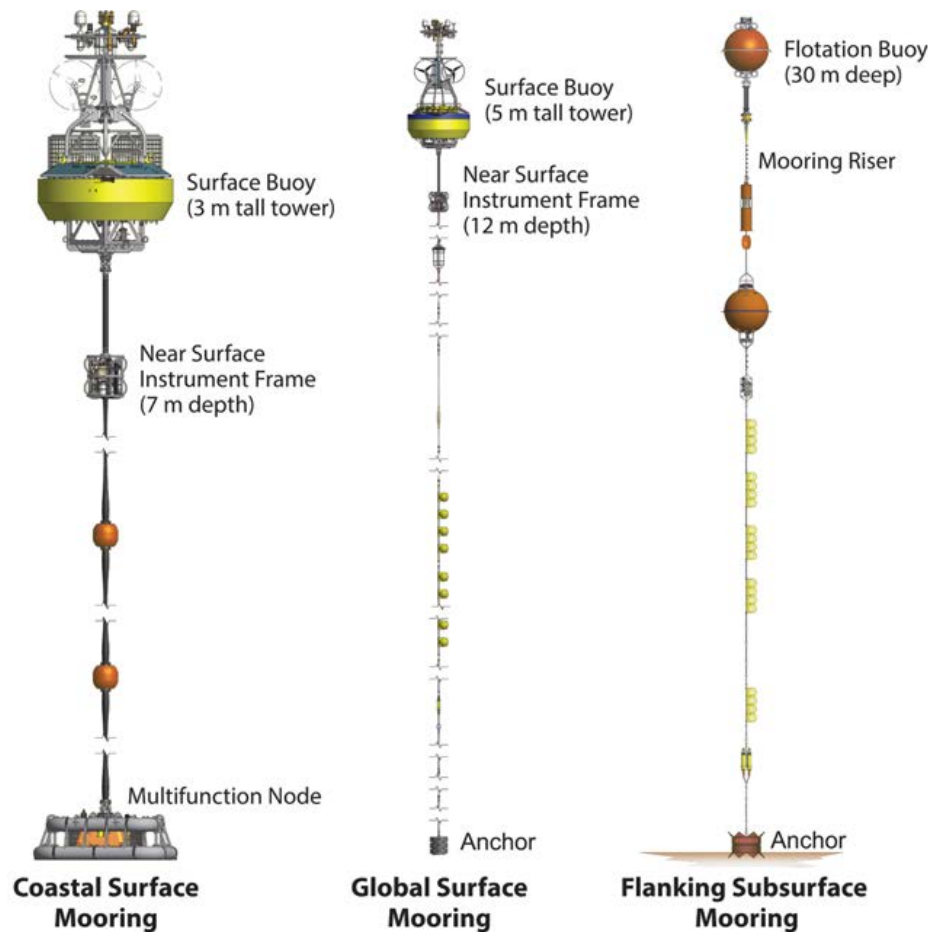


FIGURE 11. Schematics of Surface and Flanking Subsurface Moorings. Coastal Surface Moorings contain an instrumented surface buoy with a 3 m tall tower. A near-surface instrument frame is located at 7 m depth and contains a suite of instrumentation. Each of several Coastal Surface Moorings also have an instrumented multifunction node on the seafloor that also acts as an anchor. The Global Surface Mooring is similar to the Coastal Surface Moorings with a few key differences: the surface buoy tower is taller at 5 m, the near-surface instrument frame is deeper at 12 m, instruments are located along the mooring riser, and there is no multifunction node. The Flanking Subsurface Mooring does not have a surface expression; the top flotation buoy is located at 30 m depth. Instruments are located at fixed depths along its mooring riser.

flotation buoys at approximately 30 m depth and fixed instruments along their mooring risers. CTD, dissolved oxygen, pH, and fluorescence sensors are located just below the subsurface flotation buoys. Additional CTDs are spaced throughout the water column down to 1,500 m depth, and an ADCP is located at 500 m depth. As they do not have a surface expression, these moorings communicate to shore via acoustic links with nearby gliders.

profilers

In many cases, profiler moorings are co-located with surface moorings. Their instrumented platforms move up and down through the water column to collect observations at fine vertical resolution, complementing surface mooring sensor data at discrete depths. The OOI employs five types of profiler moorings: Coastal Profiler Moorings, Global Profiler Moorings, Coastal Surface-Piercing Profiler Moorings, Cabled Deep Profiler Moorings, and Cabled Shallow Profiler Moorings (Figures 8, 10, and 12).

COASTAL PROFILER MOORINGS

Coastal Profiler Moorings contain McLane wire-following profilers with multidisciplinary sensor suites (Figures 10d,e and 12). Coastal Profiler Mooring surface buoys are equipped with communication systems analogous to those of the Coastal Surface Mooring. Unlike Coastal Surface Mooring buoys, however, these do not have scientific instrumentation or power generation; alkaline primary batteries provide the only power source. Wire-following profilers carry low-power instruments that measure temperature, salinity, pressure, water velocity, light, chlorophyll fluorescence, light backscatter from particles, and dissolved oxygen. Below the maximum profiler excursion depth, an ADCP is connected electrically to the mooring wire. Both the profiler package and the ADCP transmit data inductively to a receiver in the surface buoy. Components of an anchor recovery system are configured in line along the mooring riser below the ADCP.

Wire-following profiler instruments

sample at 0.25–2.0 Hz during ascent and descent and are programmed to run along the hydrowire from 28 m below the surface to 28 m above the bottom. At the shallow sites (≤ 150 m), the internal batteries are sufficient for full profiles every 1.5 hours. At deep sites, the profile interval is three hours and every other descent stops at 200 m for Pioneer and is 6–8 hours over the full profiling distance for Endurance. ADCP configurations (e.g., bin depths, pulse repetition rate) vary with water depth; averaging intervals are 15 minutes at the shallow sites and one hour at the deep sites.

GLOBAL PROFILER MOORINGS

The top flotation buoys of the Global Profiler Moorings are located at 150 m depth. They operate in a similar manner to Coastal Profiler Moorings and are co-located with Global Surface Moorings to provide sampling of the full water column (Figure 12). These moorings each contain two wire-following profilers, except for the Irminger Sea Array that only contains one. Profiling instruments on these subsurface moorings move up and down a hydrowire, covering the depths not sampled by the Global Surface Mooring, and include a fluorometer and CTD, velocity, and oxygen sensors. Bioacoustic sonar and an additional CTD are located just below the top flotation buoy. As with Flanking Subsurface Moorings, Global Profiler Moorings communicate to shore via acoustic links with nearby gliders.

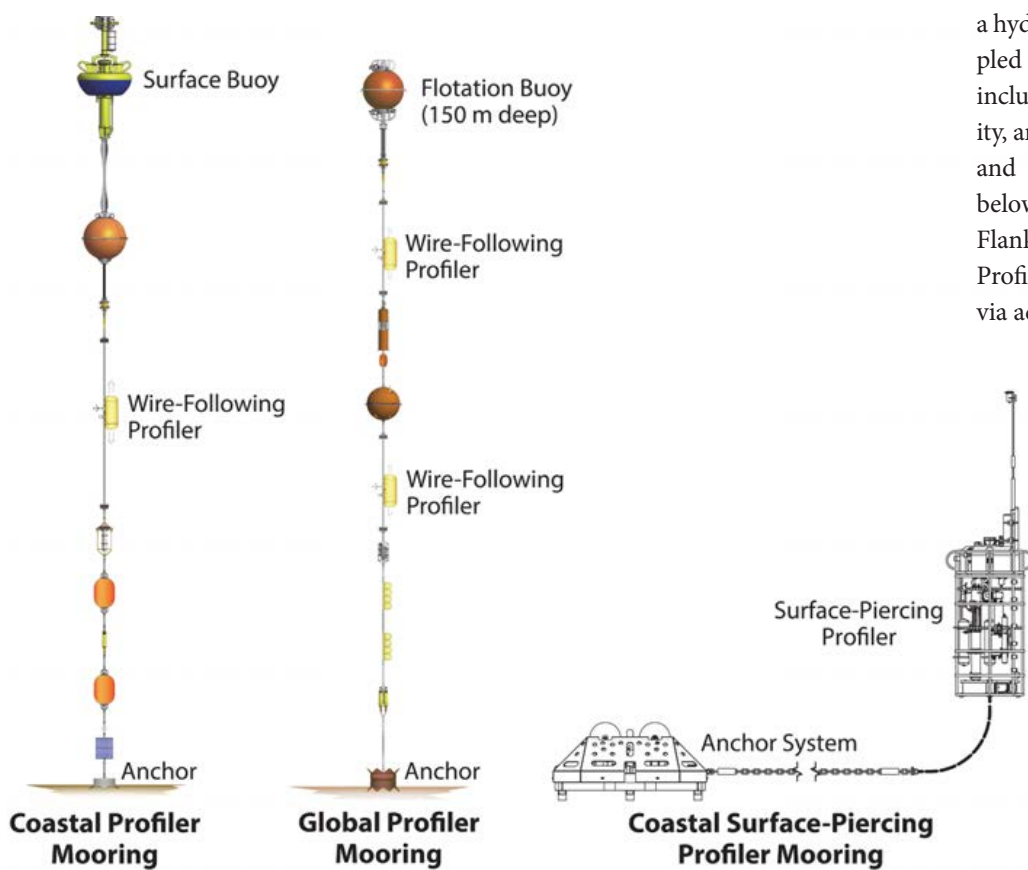


FIGURE 12. Schematics of the OOI profiler moorings. Profiler moorings provide fine vertical resolution observations at fixed locations and are, in many cases, co-located with surface moorings. Coastal Profiler Moorings, Global Profiler Moorings, and Cabled Deep Profilers (see Figure 8) all utilize instrumented wire-following profilers that run along a hydrowire across a set depth interval. Coastal Surface-Piercing Profiler Moorings travel through the water column with a profiler-mounted winch and breach the surface.

CABLED DEEP PROFILER MOORINGS

Cabled Deep Profiler Moorings (Figure 8) operate in a similar manner to Coastal Profiler and Global Profiler Moorings, with wire-following profilers that measure ocean properties across a depth interval. However, the Cabled Deep Profiler Moorings are connected to fiber-optic cables that provide greater power and bandwidth and permit real-time data transmission. The profiler transits the cable at 25 cm s^{-1} . Power and data transfer are provided via an inductive couple at a base docking station with Wi-Fi capabilities. The profiler hosts six instruments: a CTD, a two-wavelength fluorometer, a water velocity meter, a chromophoric dissolved organic matter (CDOM) fluorometer, a dissolved oxygen sensor, and a hyperspectral spectrophotometer. They are located at Slope and Axial Base, and at the Endurance Oregon Offshore site.

COASTAL SURFACE-PIERCING PROFILER MOORINGS

Coastal Surface-Piercing Profiler Moorings are the only OOI profilers that provide data from near the seafloor to the air-sea interface (Figure 12). The profilers travel through the water column controlled by a profiler-mounted winch, then break the surface. While on the sea surface, they telemeter data to shore; while underwater, their status is checked periodically, and command and control from shore occurs via an acoustic modem on a nearby surface mooring. Coastal Surface-Piercing Profiler Moorings carry low-power instruments (e.g., CTD, fluorometric chlorophyll *a*, CDOM concentration, optical backscatter, and dissolved oxygen sensors) as well as higher-power instruments, including sensors for nitrate, light attenuation and absorption, and spectral irradiance.

CABLED SHALLOW PROFILER MOORINGS

Two-legged Shallow Profiler Moorings (Figure 8) are specifically built and designed for the OOI (McRae, 2016). The mooring design is composed of a 200 m

deep, 4 m across platform that houses five to eight instruments, including zooplankton sensors, digital still cameras, and two kinds of ADCPs. The platform also hosts a winched shallow profiler with an instrumented science pod that profiles the upper 200 m of the water column (Figure 8). The science pod carries 10 instruments and conducts missions that include nine trips per day through the water column; automated step functions stop the profiler pod at specific depths, turning instruments on and off that require stationary measurements (e.g., CO_2). Connections to the fiber-optic cable allow missions and parameters to be changed in response to events (e.g., detection of thin layers) through real-time commands from shore. Since 2015, the profilers have logged $>12,000$ cycles with continuous live transmission of data back to shore (see McRae, 2016). The profiler science pod carries the same instruments as the Coastal Surface-Piercing Profiler Mooring plus sensors for pH and $p\text{CO}_2$. The 200 m platform contains a fluorometer, an ADCP and a five-beam ADCP (VADCP), a broadband hydrophone, a CTD, a still camera, and dissolved oxygen and pH sensors. At the Endurance Offshore site, the platform also includes a zooplankton sensor.

Seafloor Technology

PRIMARY NODES

The Cable Shore Station in Pacific City, Oregon, is the terminal for the Cabled Array (Figure 7). Power feed equipment provides constant voltage that permits each cable line to be powered by either the same or a separate power supply.

The two submarine backbone cables connect the shore station to the Primary Nodes, which are distribution centers for extension cables that provide direct access to the specific sites of scientific interest. The backbone cable is comprised of approximately 900 km of telecom industry subsea electro-optical cable that provides 8 kW of power and redundant 10 Gb s^{-1} data communications to each Primary Node (Figure 7). A science interface assembly in each Primary

Node houses five wet-mateable science ports with 1 gigabit Ethernet (GbE) and 375 V capabilities and two high-bandwidth ports (10 GbE, 375 V) for network expansion. Primary Nodes do not contain instrumentation, and are used to convert 10 kVDC primary level voltage from the Shore Station to lower 375 VDC levels and distribute that power and communication to junction boxes distributed around each site.

JUNCTION BOXES AND LOW-VOLTAGE NODES

To access specific experimental sites, junction boxes (Secondary Nodes, designed and built at the University of Washington Applied Physics Laboratory) are connected to the Primary Nodes by extension cables up to approximately 5 km in length (e.g., Figure 9). Each junction box includes eight configurable ports that provide 12, 24, and 48 VDC, and numerous communication capabilities. Pulse per second timing is available on all ports with $\sim 10 \mu\text{s}$ accuracy. Each port can provide either 50 W or 200 W. Extension cables are connected through dry- or ROV wet-mate connectors, with most being wet-mates. Expansion ports provide the ability to connect 375 VDC power and 1 Gbps fiber-optic Ethernet, making the system highly expandable. Each port on a junction box is configured to supply the power needed by an individual instrument or platform (e.g., mooring). Real-time communication to shore allows direct interaction with the ports and instruments that can be used to adjust sampling protocols (e.g., HD camera missions), and to monitor and respond to health and status of the network. The network currently hosts 18 junction boxes, all operational since 2014, which provide power and bandwidth to more than 30 different instrument types (see earlier discussion of instrument types).

BENTHIC EXPERIMENT PACKAGES

The coastal seafloor Benthic Experiment Package, designed at Oregon State University, hosts a variety of oceanographic

instruments for studying the near-bottom, benthic bottom boundary layer. Its slanted sides provide some protection from fishing trawls. The system's core contains an Applied Physics Laboratory-built low-power junction box that provides power and bandwidth communication through the seafloor electro-optical cable. Benthic Experiment Package instruments measure physical (temperature, salinity, pressure, point three-dimensional velocity, water-column profiles of horizontal velocity), chemical (dissolved oxygen, pH, dissolved CO₂), biological (spectral light absorption and attenuation), and acoustic (broadband hydrophone) ocean properties. A digital still camera and a three-frequency (38 kHz, 120 kHz split beam, and 200 kHz) upward-looking bio-acoustic sonar (Barth et al., 2018, in this issue) are also mounted on the Benthic Experiment Package.

Autonomous Vehicles

COASTAL GLIDERS

Coastal gliders (all OOI gliders are Teledyne Webb Slocum gliders; Figure 13) are optimized for continental shelf and slope operations and running along track lines (Figures 2 and 5). Coastal gliders are deployed with two different buoyancy engines that dictate maximum dive depths—either 200 m or 1,000 m. The gliders sample the vertical structure of the ocean from the sea surface to within a few meters of the seafloor or their maximum dive depths. Gliders equipped with 200 m buoyancy engines operate primarily in

the shallow waters over the shelf, and those equipped with 1,000 m buoyancy engines operate primarily over the continental slope. The coastal gliders carry a multidisciplinary sensor suite measuring temperature, salinity, pressure, dissolved oxygen, optical properties, and currents. Data are transmitted to shore from antennae on the gliders via satellite phone.

OPEN-OCEAN GLIDERS

Additional sampling of spatial variability within and around the global moorings is conducted with open-ocean gliders. These gliders sample within the footprint of the moored array, diving to 1,000 m and each carrying a two-wavelength fluorometer, a CTD, and a dissolved oxygen sensor.

PROFILING GLIDERS

Profiling gliders are operated in a manner that maintains the glider near a set location. On the Pioneer Array, gliders replace two Coastal Profiler Moorings in the summer; on the Global Arrays, these gliders sample the upper 200 m of water above the Global Profiler Mooring. Profiling Gliders carry a similar instrument load as their coastal and open-ocean counterparts with the exception that profiling gliders add more comprehensive optical measurements and nitrate sensors.

AUTONOMOUS UNDERWATER VEHICLES

Two AUVs (Hydroid Remus 600; Figure 13) are the primary tools for resolving cross- and along-front structure

within the Pioneer Array, providing transects with horizontal resolution of 1–5 km (varying with water depth) and crossing the ~50 km frontal zone in approximately nine hours.

The two AUVs are rated to 600 m depth and are typically programmed to make consecutive ascents and descents from a few meters below the surface to a few meters above the seafloor. At specified intervals along the track line, the AUV surfaces to obtain a GPS fix and telemeter information to shore. They can also be monitored and controlled acoustically when within a few kilometers of the ship. The primary goal of the AUV missions is to obtain simultaneous, synoptic transects along and across the frontal zone. The AUVs carry sensors to provide the same interdisciplinary measurements as the coastal gliders, plus optical nitrate instruments.

Operations and Maintenance

Teams of technicians, scientists, and engineers operate OOI platforms and sensors around the clock. For uncabled arrays, platform performance, battery voltages, and available power from the surface wind and solar energy collectors are closely monitored. Should there be insufficient power to execute the full sampling schedule and/or telemetry to shore, adjustments are made to ensure the health of the platform and associated instruments. System health and status for cabled infrastructure is closely monitored in real time from shore; all

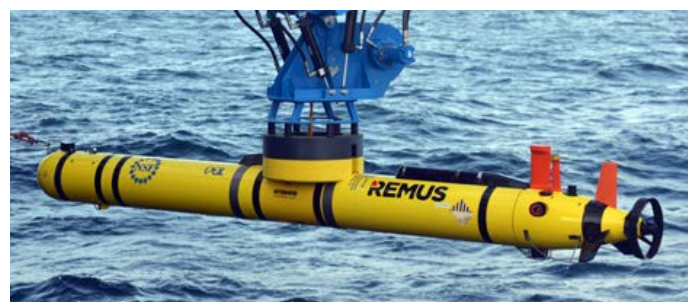


FIGURE 13. (left) Coastal gliders are staged on deck for pre-flight checks via satellite telemetry to the shore lab. (right) An AUV is prepared for deployment using a hydraulic launch and recovery system fitted to R/V *Neil Armstrong*. Credit: OOI Pioneer Array Program, Woods Hole Oceanographic Institution

instruments operate on full sampling capacity. Battery status is not a consideration because of the connection to the high-power telecommunication cables. Gliders are tracked in near-real time, and adjustments are made in the targeted waypoints to keep the gliders as close as possible to their planned tracklines while contending with ocean currents, winds, and buoyant river plumes. Across the facility, instruments and platforms are monitored for safety, functionality, and basic data quality.

The degradation of mooring components, biofouling of instruments, and depletion of batteries on the uncabled profiler moorings are the main drivers of the OOI moored array maintenance schedule. After recovery, buoys and other durable components of the mooring riser are refurbished for reuse. Wire rope and mooring hardware such as shackles and links are replaced with new material for each “turn” (a recover/redeploy operation). Instruments, data controllers, and loggers are refurbished, recalibrated, and tested before redeployment on a subsequent mooring turn.

Coastal Array servicing includes two turn cruises per year, in spring and fall, typically conducted on US University-National Oceanographic Laboratory System (UNOLS) vessels. These cruises focus on mooring and glider turns. During each cruise, newly refurbished moorings are deployed within a few hundred meters of the existing mooring sites. Calibration casts are done alongside the moorings with a ship’s CTD and rosette for collecting water samples at multiple depths for analysis of nutrients, dissolved oxygen, and carbon dioxide. In some cases, the existing mooring and the refurbished mooring operate concurrently for hours to days before the existing mooring is recovered. The CTD casts, bottle samples, and concurrent mooring data are used to check the calibration and drift of the moored sensors.

Smaller vessels are used for servicing the glider fleet deployed at coastal arrays. Coastal gliders have a nominal

endurance of three months. Profiling gliders have a longer hull, which allows for more batteries and thus longer endurance of four to six months. Upon recovery, gliders are returned to the manufacturer for refurbishment and calibration of onboard instrumentation.

As with gliders, Coastal Surface-Piercing Profiler Mooring deployments are limited by battery life and biofouling. Thus, these moorings are maintained with a similar service cycle to gliders—every two to three months. Upon recovery, Coastal Surface-Piercing Profiler Moorings are cleaned, and they undergo minor in-house refurbishment and sensor checks, with major refurbishment done by the vendor annually.

AUVs are deployed from a ship during the Pioneer Array mooring and glider turns; additional cruises may be scheduled to approach the desired AUV mission interval of once per month. AUVs and onboard instrumentation are refurbished annually.

Global Array sites are particularly remote from the United States. Practical considerations of ship time availability and cost limit the service at these sites to once a year. Annual turn cruises of the Global Arrays operate in much the same manner as those of the Coastal Arrays, with deployment of new platforms and instruments and recovery of moorings deployed the previous year scheduled during these cruises.

Cabled infrastructure is serviced once per year using a global-class UNOLS vessel and a remotely operated vehicle (ROV). Typically, about 120 instruments and up to seven junction boxes are turned each year. Instruments that are biofouled or use reagents are turned each year, but instruments such as seismometers and bottom pressure tilt meters remain in place for several years. Cabled Array moorings were specifically designed to stay in place for at least five years, optimizing operations and maintenance costs. The modified McLane profiler vehicle on the Deep Profiler Mooring is recovered and redeployed

annually with an ROV. Similarly, both the instrumented stationary assembly on the 200 m platform and the shallow winched profiler system on the Cabled Shallow Profiler Mooring are turned each year with an ROV.

DATA COLLECTION, PROCESSING, AND DELIVERY

OOI networked sensors collect atmosphere, ocean, and seafloor data at high sampling rates (up to 200 Hz) over years to decades. In total, over 100,000 OOI science and engineering parameters (206 unique data products) from 2,993 data streams, 1,227 instruments (deployed and awaiting turn cruises), 276 nodes, and 89 platforms (including suspended deployments) from every array are available online in the OOI Data Portal (<https://oceanobservatories.org>). The challenge of the OOI Cyberinfrastructure (CI) is to collect, archive, transform, and distribute data from the numerous instruments and platforms across the OOI to the user community in real time or near-real time.

In this section, we describe how data are collected by OOI instruments and platforms, processed by the OOI CI, and then delivered to the OOI user. For specific details of the various means for accessing OOI data, see Vardaro and McDonnell (2018, in this issue).

Sampling Strategies

The OOI sampling strategy was designed to (1) provide consistently sampled long-term decadal data sets, (2) capture short-lived stochastic events at small spatial scales, and (3) permit targeted manipulation to capture specific phenomena. Observation strategies address the temporal and spatial scales of variability that characterize the local environment for each instrument, and the sampling strategy attempts to optimize platform mobility as well as instrument operation.

Further details of sampling strategies across the OOI can be found

in the Observation and Sampling Approach document on the OOI website (<http://oceanobservatories.org/observation-and-sampling-approach>).

From Instrument to User (Data Path)

The OOI Cyberinfrastructure is the pathway from each deployed sensor and platform to the user (Figure 14). The OOI CI design and implementation are based on industry best practices, and use a decentralized, coordinated architecture optimized for data storage and delivery, data security and integrity, and quality of service requirements. The CI's role is to collect, archive, and host raw data, transform the raw data into processed data in science units, maintain and deliver metadata

and cruise data, and provide user support. Ensuring the success of the end-to-end CI system requires continuous monitoring, performance improvements, and data evaluation. The OOI CI currently archives over 250 terabytes of data from the OOI arrays. Since data download services came online in January 2016, users from across the world have downloaded nearly 100 terabytes of data from the OOI arrays.

Raw data (both engineering and science) are gathered from cabled and uncabled instruments and platforms located across the marine networks and transmitted to one of three operation components: Pacific City, Oregon, directly connected to all cabled instruments and platforms; an operations and

management component (OMC) responsible for all uncabled instrument data on the Pacific coast; and an OMC for Atlantic coast-based uncabled instrument data.

Deployed uncabled instruments send a subset of raw data back to shore ("telemetered data") via satellite connection or cellular phone. Once uncabled instruments are brought back to shore after a mooring turn or glider recovery, the complete collected data set is downloaded directly by OOI operators to provide a "recovered" data set. Immediately upon receipt, all raw data are transferred over the Internet to the OOI CI system for processing, storage, and dissemination via the Internet. Installed cabled instruments send data back to shore via electro-optical cables ("streaming data") to the shore station in Pacific City, Oregon. Full resolution data are streamed to shore, including uncompressed HD video (1.5 GB s^{-1}) and broadband hydrophone data at 200 Hz.

From each OMC, data are transferred to two primary CI components located on East and West Coasts for processing, storage, and dissemination. The East Coast CI houses the primary computing servers, data storage and backup, and online data portal interface. The West Coast CI mirrors the East Coast component. The data stored at the three OMCs are continuously synchronized with the data repositories located at the East and West Coast CI sites. Tape storage, a last tier storage that is not dependent on power or cooling, supports longer-term backup and archiving, disaster recovery, and data transport.

The core of the OOI CI software is the uFrame-based OOINet, which implements a service-oriented architecture and integrates a set of data, instrument, and platform drivers as well as data product algorithms to produce data products on demand to the user community. Databases of information about every asset, including predeployment calibration values, cruise information, and deployment configuration, are used by the system to provide all necessary metadata to the graphical user interface upon data delivery.

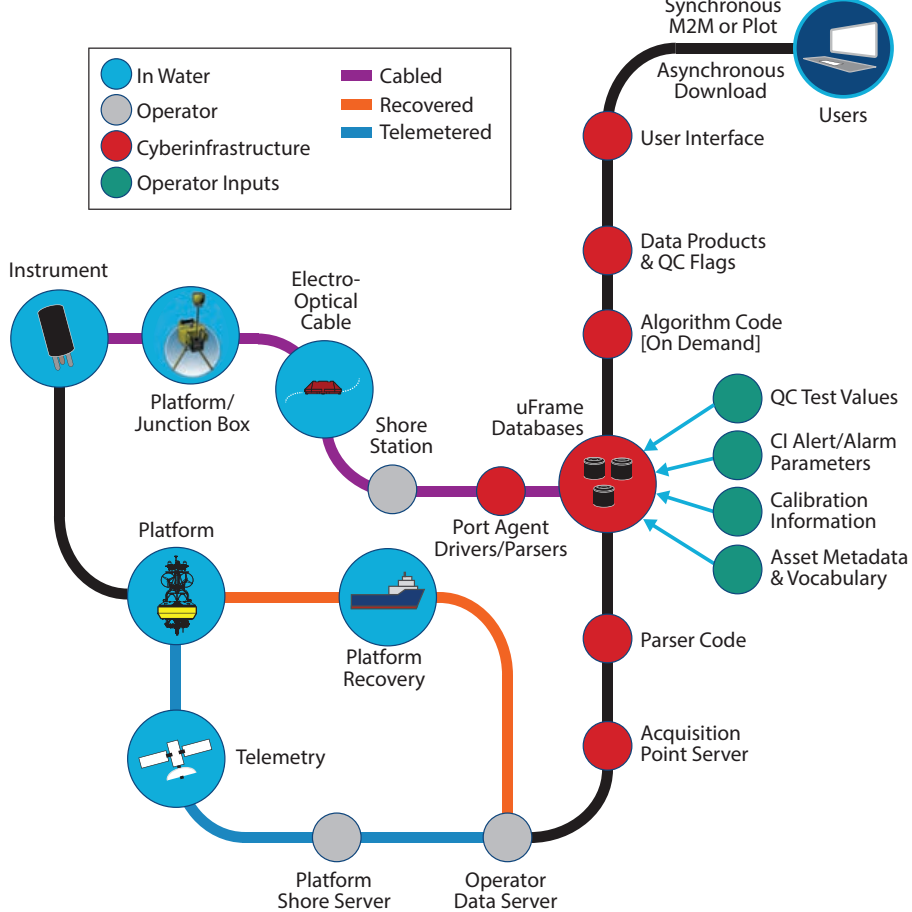


FIGURE 14. The paths of cabled (purple line), telemetered (blue line), and recovered (orange line) OOI data from ocean (in blue) to shoreside operations and management component servers (gray) to the cyberinfrastructure system (red), where raw data are parsed into streams and stored in a database. Parsed data are processed on demand via data product and quality control (QC) algorithms and delivered to the user's desktop. The circles illustrate the major touch points and transformations, as well as the necessary input of metadata and calibration information (green), along the data processing pathway.

Data Quality Control Processes

Oceanographic and engineering data throughout the OOI system are reviewed through manual (human in the loop) and automated quality control procedures. The overall goal is to ensure that the data and metadata delivered by the OOI meet community data quality standards. These standards were designed with the goal of meeting the Integrated Ocean Observing System (IOOS) Quality Assurance of Real Time Ocean Data (QARTOD) standards. Feedback from the user community to identify, diagnose, and resolve data availability and data quality issues is also a critical element of the quality control.

The primary goals of these quality control procedures are to: (1) monitor the operational status of the data flowing through OOINet, (2) ensure the availability of OOI data sets in the system and that they meet quality guidelines, (3) identify data availability and quality issues and ensure they are resolved and communicated to end users, and (4) report operational statistics on data availability, quality, and issue resolution.

To meet these goals, end-to-end data flow from online instruments is checked daily. Any gaps (e.g., instrument, telemetry, or parsing) are investigated during a periodic end-to-end review, as needed. The process includes daily reviews of the operational status, data delivery alerts, issue requests from users, and annotations to notify users of status changes. A set of scripts and necessary tools for quality checks help determine if any telemetered or streamed data have stopped updating and whether the interruption is due to instrument, telemetry, or data transfer issues, or an unknown problem. If the recent data do not appear reasonable (e.g., scientifically valid, correct sampling rate), the data evaluation team ensures that all potential issues are reported and annotated in the OOI Data Portal.

Data from all OOI maintenance cruises are compiled and assessed for completeness to ensure that all necessary information and documentation are added to the system for each cruise.

An Open Access Ocean for All

The OOI CI provides a common operating infrastructure to connect and enable the coordination of operations of the OOI arrays with the scientific and educational pursuits of oceanographic research and other user communities around the globe. This software provides 24/7 connectivity to deliver ocean observing data to anyone with an Internet connection free of charge. For information on how to access OOI data, see Vardaro and McDonnell (2018, in this issue).

MOVING FORWARD THROUGH COLLABORATION

Oceanographic observation is rapidly transforming in this era of technological innovation. In situ observatories and advanced cyberinfrastructure have become critical components for successful integration and collaboration across programs (Lindstrom, 2018, in this issue). Integration across programs comes in many forms, for example, integrating data into existing global and regional data repositories (see Box 1 in Lindstrom, 2018, in this issue).

Co-location of infrastructure provides a unique opportunity for collaboration across observatories and for providing higher data granularity (e.g., Stocks et al., 2018, in this issue). Two moorings of the Global Irminger Sea Array off the coast of Greenland are aligned within the array of the Overturning in the Subpolar North Atlantic Program (OSNAP; Lozier et al., 2017), an international effort to examine meridional overturning circulation in the North Atlantic, a critical component of deepwater formation for the globe. Similarly, the Ocean Station Papa array is co-located with a NOAA PMEL surface mooring and augments the existing long-term time series (since 1949) in the area.

The OOI Cabled Array is located south of its Canadian counterpart, the Ocean Networks Canada array, off the coast of British Columbia. Components of the Ocean Networks Canada array, comprised of 800 km of fiber-optic cable and five instrumented sites, went online in

2009 (Moran, 2013). Together, the US and Canadian cabled arrays span a significant portion of the Juan de Fuca Plate. Hence, they provide a unique opportunity to examine both local and regional co-registered seafloor and water column data in real time toward understanding dynamic processes along the continental margin/subduction zone in the Northeast Pacific, in the middle of the Juan de Fuca Plate, and at the Juan de Fuca seafloor spreading center.

Lastly, OOI data aid in the calibration of global climate and ocean models. For example, collaborations with the World Climate Research Program and its Climate and Ocean: Variability, Predictability and Change (CLIVAR) program examine air-sea fluxes of heat, freshwater, and momentum. Forecasters at the European Centre for Medium-range Weather Forecasts (ECMWF) use Global Array data to examine storms in the Southern Ocean as part of the Year of Polar Prediction Effort by the World Meteorological Organization.

Moving forward, the OOI will maintain and establish new relationships with other national and international observatories.

NSF has committed to support the OOI for 25 years, and is now funding proposals for both new OOI infrastructure and data analysis (Ulses et al., 2018, in this issue). The OOI will periodically undergo a technology refresh to ensure that the latest advances in sensor technology and in ocean observation approaches are included in the system. The OOI already utilizes instrumentation that has never been fielded before—an in situ mass spectrometer, a particulate DNA sampler, and other vent chemistry sensors. As observational technologies advance and innovations continue, the OOI will integrate new technologies into its infrastructure through a publicly advertised proposal process.

The OOI is an ambitious program, designed from its inception to use emerging and leading-edge technology and engineering solutions to investigate science themes focused on our most pressing

and complex global oceanographic challenges. Ongoing input from the scientific community will ensure that all aspects of the OOI—from its deployed sensors and instruments to its CI data discovery, delivery, and display capabilities—adapt and align with changing user requirements and the latest technological advances over the program’s 25-year lifespan. OOI users are encouraged to stay involved and engaged with this program to help inform and shape its future. ☐

REFERENCES

- Arnulf, A.F., A.J. Harding, G.M. Kent, S.M. Carbotte, J.P. Canales, and M.R. Nedimovic. 2014. Anatomy of an active submarine volcano. *Geology* 42:655–658, <https://doi.org/10.1130/G35629.1>.
- Bangs, N.L.B., M.J. Hornbach, and C. Berndt. 2011. The mechanics of intermittent methane venting at South Hydrate Ridge inferred from 4D seismic surveying. *Earth and Planetary Science Letters* 310:105–112, <https://doi.org/10.1016/j.epsl.2011.06.022>.
- Barth, J.A., J.P. Fram, E.P. Dever, C.M. Risien, C.E. Wingard, R.W. Collier, and T.D. Kearney. 2018. Warm blobs, low-oxygen events, and an eclipse: The Ocean Observatories Initiative Endurance Array captures them all. *Oceanography* 31(1):90–97, <https://doi.org/10.5670/oceanog.2018.114>.
- Barton, A., B. Hales, G.G. Waldbusser, C. Langdon, and R.A. Feely. 2012. The Pacific oyster, *Crassostrea gigas*, shows negative correlation to naturally elevated carbon dioxide levels: Implications for near-term ocean acidification effects. *Limnology and Oceanography* 57:689–710, <https://doi.org/10.4319/lo.2012.57.3.0698>.
- Bigham, K. 2018. Axial Seamount Biology Catalog. *Oceanography* 31(1):127, <https://doi.org/10.5670/oceanog.2018.119>.
- Boetius, A., and E. Suess. 2004. Hydrate Ridge: A natural laboratory for the study of microbial life fueled by methane from near-surface gas hydrates. *Chemical Geology* 205:291–310, <https://doi.org/10.1016/j.chemgeo.2003.12.034>.
- Bond, N.A., M.F. Cronin, H. Freeland, and N. Mantua. 2015. Causes and impacts of the 2014 warm anomaly in the NE Pacific. *Geophysical Research Letters* 42:3,414–3,420, <https://doi.org/10.1002/2015GL063306>.
- Boyd, T.J., M.D. Levine, P.M. Kosro, and S.R. Gard. 2000. *Mooring Observations from the Oregon Continental Shelf, April–September 1999: A Component of The Prediction of Wind-Driven Coastal Circulation Project*. Data report 177, COAS Ref. 00-1, College of Oceanic and Atmospheric Sciences, Oregon State University, 202 pp.
- Chadwick, W.W., D.J. Geist, S. Jónsson, M. Poland, D.J. Johnson, and C.M. Meertens. 2006. A volcano bursting at the seams: Inflation, faulting, and eruption at Sierra Negra volcano, Galápagos. *Geology* 34:1,025–1,028, <https://doi.org/10.1130/G22826A.1>.
- Chadwick, W.W., Jr., J.B. Paduan, D.A. Clague, B.M. Dreyer, S.G. Merle, A.M. Bobbitt, D.W. Caress, B.T. Philip, D.S. Kelley, and S.L. Nooner. 2016. Voluminous eruption from a zoned magma body after an increase in magma supply rate at Axial Seamount. *Geophysical Research Letters* 43:12,063–12,070, <https://doi.org/10.1002/2016GL071327>.
- Chan, F., J.A. Barth, C.A. Blanchette, R.H. Byrne, F. Chavez, O. Cheriton, R.A. Feely, G. Friederich, B. Gaylord, T. Gouhier, and others. 2017. Persistent spatial structuring of coastal ocean acidification in the California Current System. *Scientific Reports* 7:2526, <https://doi.org/10.1038/s41598-017-02777-y>.
- Chan, F., J.A. Barth, J. Lubchenco, A. Kirincich, H. Weeks, W.T. Peterson, and B.A. Menge. 2008. Emergence of anoxia in the California current large marine ecosystem. *Science* 319:920–920, <https://doi.org/10.1126/science.1149016>.
- Chen, K., G. Gawarkiewicz, and A. Plueddemann. 2018. Atmospheric and offshore forcing of temperature variability at the shelf break: Observations from the OOI Pioneer Array. *Oceanography* 31(1):72–79, <https://doi.org/10.5670/oceanog.2018.112>.
- Daly, K., R. Jahnke, M. Moline, R. Detrick, D. Luther, G. Matsumoto, L. Mayer, and K. Raybould. 2006. *Report of the D&I Workshop, 27–30 March 2006*. Joint Oceanographic Institutions, Consortium for Ocean Research and Education, and the National Science Foundation, Washington, DC, http://oceanleadership.org/wp-content/uploads/2009/07/ooi_di_report_final.pdf.
- de Jong, M.F., M. Oltmanns, J. Karstensen, and L. de Steur. 2018. Deep convection in the Irminger Sea observed with a dense mooring array. *Oceanography* 31(1):50–59, <https://doi.org/10.5670/oceanog.2018.109>.
- Dickson, B., I. Yashayaev, J. Meincke, B. Turrell, S. Dye, and J. Holfort. 2002. Rapid freshening of the deep North Atlantic Ocean over the past four decades. *Nature* 416:832–837, <https://doi.org/10.1038/416832a>.
- Flood, R.D., and A.N. Shor. 1988. Mud waves in the Argentine Basin and their relationship to regional bottom circulation patterns. *Deep Sea Research Part A* 35:943–971, [https://doi.org/10.1016/0198-0149\(88\)90070-2](https://doi.org/10.1016/0198-0149(88)90070-2).
- Feeley, R.A., C.L. Sabine, J.M. Hernandez-Ayon, D. Ianson, and B. Hales. 2008. Evidence for upwelling of corrosive “acidified” water onto the continental shelf. *Science* 320:1,490–1,492, <https://doi.org/10.1126/science.1155676>.
- Gawarkiewicz, G.G., R.E. Todd, A.J. Plueddemann, M. Andres, and J.P. Manning. 2012. Direct interaction between the Gulf Stream and the shelf-break south of New England. *Nature Scientific Reports* 2:553, <https://doi.org/10.1038/srep00553>.
- Gawarkiewicz, G., R.E. Todd, W. Zhang, J. Partida, A. Gangopadhyay, M.-U.-H. Monim, P. Fratantoni, A. Malek Mercer, and M. Dent. 2018. The changing nature of shelf-break exchange revealed by the OOI Pioneer Array. *Oceanography* 31(1):60–70, <https://doi.org/10.5670/oceanog.2018.110>.
- Gislason, A.P., H. Petursdóttir, and K. Gudmundsson. 2014. Long-term changes in abundance of *Calanus finmarchicus* south and north of Iceland in relation to environmental conditions and regional diversity in spring 1990–2013. *ICES Journal of Marine Science* 71(2):539–2,549, <https://doi.org/10.1093/icesjms/fsu098>.
- Grantham, B.A., F. Chan, K.J. Nielsen, D.S. Fox, J.A. Barth, A. Huyer, J. Lubchenco, and B.A. Menge. 2004. Upwelling-driven nearshore hypoxia signals ecosystem and oceanographic changes in the northeast Pacific. *Nature* 429:749–754, <https://doi.org/10.1038/nature02605>.
- Henderikx Freitas, F., G.S. Saldías, M. Goñi, R.K. Shearman, and A.E. White. 2018. Temporal and spatial dynamics of physical and biological properties along the Endurance Array of the California Current ecosystem. *Oceanography* 31(1):80–89, <https://doi.org/10.5670/oceanog.2018.113>.
- Huyer, A., R.L. Smith, and J. Fleischbein. 2002. The coastal ocean off Oregon and northern California during the 1997–8 El Niño. *Progress in Oceanography* 54:311–341, [https://doi.org/10.1016/S0079-6611\(02\)00056-3](https://doi.org/10.1016/S0079-6611(02)00056-3).
- Huyer, A., P.A. Wheeler, P.T. Strub, R.L. Smith, R. Letelier, and P.M. Kosro. 2007. The Newport line off Oregon: Studies in the North East Pacific. *Progress in Oceanography* 75:126–160, <https://doi.org/10.1016/j.pocean.2007.08.003>.
- Jullion, L., K. Heywood, A.C. Naveira Garabato, and D.P. Stevens. 2010. Circulation and water mass modification in the Brazil-Malvinas confluence. *Journal of Physical Oceanography* 40:845–864, <https://doi.org/10.1175/2009JPO417.1>.
- Kelley, D.S. 2017. Volcanology: Vulcans rule beneath the sea. *Nature Geoscience* 10:251–253, <https://doi.org/10.1038/ngeo2929>.
- Kelley, D.S., J.R. Delaney, and S.K. Juniper. 2014. Establishing a new era of submarine volcanic observatories: Cabling Axial Seamount and the Endeavor Segment of the Juan de Fuca Ridge. *Marine Geology 50th Anniversary Special Volume* 352:426–450, <https://doi.org/10.1016/j.margeo.2014.03.010>.
- Kelley, D.S., J.R. Delaney, and the Cabled Array Team. 2016. NSF’s Cabled Array: A wired tectonic plate and overlying ocean. Paper presented at OCEANS 2016 MTS/IEEE Monterey, September 19–23, 2016, <https://doi.org/10.1109/OCEANS.2016.7761398>.
- Kelley, D.S., and D. Grünbaum. 2018. Seastate: Experiential C-STEM learning through environmental sensor building. *Oceanography* 31(1):147, <https://doi.org/10.5670/oceanog.2018.123>.
- Knuth, F., and A. Marburg. 2016. Automated QA/QC and time series analyses on OOI high-definition video data. Paper presented at OCEANS 2016 MTS/IEEE Monterey, September 19–23, 2016, <https://doi.org/10.1109/OCEANS.2016.7761396>.
- Lee, C.M., T. Paluskiewicz, D.L. Rudnick, M.M. Omard, and R.E. Todd. 2017. Autonomous instruments significantly expand ocean observing: An introduction to the special issue on autonomous and Lagrangian platforms and sensors (ALPS). *Oceanography* 30(2):15–17, <https://doi.org/10.5670/oceanog.2017.211>.
- Li, F., P. Ginoux, and V. Ramaswamy. 2008. Distribution, transport, and deposition of mineral dust in the Southern Ocean and Antarctica: Contribution of major sources. *Journal of Geophysical Research* 113:10207, <https://doi.org/10.1029/2007JD009190>.
- Lindstrom, E. 2018. On the relationship between the Global Ocean Observing System and the Ocean Observatories Initiative. *Oceanography* 31(1):38–41, <https://doi.org/10.5670/oceanog.2018.107>.
- Lozier, M.S., S. Bacon, A.S. Bower, S.A. Cunningham, M.F. de Jong, L. de Steur, B. deYoung, J. Fischer, S.F. Gary, B.J.W. Greenan, and others. 2017. Overturning in the Subpolar North Atlantic Program: A new international ocean observing system. *Bulletin of the American Meteorological Society* 98:737–752, <https://doi.org/10.1175/BAMS-D-16-00571>.
- Mathis, J.T., S.R. Cooley, N. Lucey, S. Colt, J. Ekstrom, T. Hurst, C. Hauri, W. Evans, J.N. Cross, and R.A. Feely. 2015. Ocean acidification risk assessment for Alaska’s fishery sector. *Progress in Oceanography* 136:71–91, <https://doi.org/10.1016/j.pocean.2014.07.001>.
- Mazzini, P.L.F., J.A. Barth, R.K. Shearman, and A. Erofeev. 2014. Buoyancy-driven coastal currents off the Oregon coast during fall and winter. *Journal of Physical Oceanography* 44:2,854–2,876, <https://doi.org/10.1175/JPO-D-14-0012.1>.
- McCabe, R.M., B. Hickey, R. Kudela, K. Lefebvre, N.G. Adams, B.D. Bill, F.M.D. Gulland, R.E. Thomson, W.P. Cochlan, and V.L. Trainer. 2016. An unprecedented coastwide toxic algal bloom linked to anomalous ocean conditions. *Geophysical Research Letters* 43(19):10,366–10,376, <https://doi.org/10.1002/2016GL070023>.
- McDonnell, J., A. deCharon, C.S. Lichtenwalner, K. Hunter-Thomson, C. Halversen, O. Schofield, S. Glenn, C. Ferraro, C. Lauter, and J. Hewlett. 2018. Education and public engagement in OOI: Lessons learned from the field. *Oceanography* 31(1):138–146, <https://doi.org/10.5670/oceanog.2018.122>.

- McKibben, S.M., W. Peterson, A.M. Wood, V.L. Trainer, M. Hunter, and A.E. White. 2017. Climatic regulation of the neurotoxin domoic acid. *Proceedings of the National Academy of Sciences* 114(2):239–244, <https://doi.org/10.1073/pnas.1606798114>.
- McRae, E. 2016. Continuous real time scanning of the upper ocean water column. Paper presented at OCEANS 2016 MTS/IEEE Monterey, September 19–23, 2016, <https://doi.org/10.1109/OCEANS.2016.7761359>.
- Morrissey, J., and C. Bowler. 2012. Iron utilization in marine cyanobacteria and eukaryotic algae. *Frontiers in Microbiology* 3:PMC3296057, <https://doi.org/10.3389/fmicb.2012.00043>.
- National Academies of Sciences, Engineering, and Medicine. 2015. *A Strategic Vision for NSF Investments in Antarctic and Southern Ocean Research*. The National Academies Press, Washington, DC, 154 pp., <https://doi.org/10.17226/21741>.
- NSF (National Science Foundation). 2001. *Ocean Sciences at the New Millennium*. National Science Foundation, Arlington, VA, 151 pp., https://geoprose.com/pdfs/os_millennium_report.pdf.
- Nooner, S.L., and W.W. Chadwick Jr. 2016. Inflation-predictable behavior and co-eruption deformation at Axial Seamount. *Science* 354:1,399-1,403, <https://doi.org/10.1126/science.aaa4666>.
- Palevsky, H.I., and D.P. Nicholson. 2018. The North Atlantic biological pump: Insights from the Ocean Observatories Initiative Irminger Sea Array. *Oceanography* 31(1):42–49, <https://doi.org/10.5670/oceanog.2018.108>.
- Paul, W. 2004. Hose elements for buoy moorings: Design, fabrication and mechanical properties. Woods Hole Oceanographic Institution Technical Report WHOI-2004-06, Woods Hole Oceanographic Institution, Woods Hole, MA, 21 pp.
- Peterson, W.T., and F.B. Schwing. 2003. A new climate regime in Northeast Pacific ecosystems. *Geophysical Research Letters* 30, 1896, <https://doi.org/10.1029/2003GL017528>.
- Philip, B.T., A.R. Denny, E.A. Solomon, and D.S. Kelley. 2016. Time-series measurements of bubble plume variability and water column methane distribution above Southern Hydrate Ridge, Oregon. *Geochemistry, Geophysics, Geosystems* 17:1,182–1,196, <https://doi.org/10.1002/2016GC006250>.
- Reimers, C.E., and M. Wolf. 2018. Power from benthic microbial fuel cells drives autonomous sensors and acoustic modems. *Oceanography* 31(1):98–103, <https://doi.org/10.5670/oceanog.2018.115>.
- Richardson, M.J., G.L. Weatherly, and W.D. Gardner. 1993. Benthic storms in the Argentine Basin. *Deep Sea Research Part II* 40:975–987, [https://doi.org/10.1016/0967-0645\(93\)90044-N](https://doi.org/10.1016/0967-0645(93)90044-N).
- Rudnick, D.L., K.D. Zaba, R.E. Todd, and R.E. Davis. 2017. A climatology of the California Current System from a network of underwater gliders. *Progress in Oceanography* 154:64–106, <https://doi.org/10.1016/j.pocean.2017.03.002>.
- Sabine, C.L., R.A. Feely, N. Gruber, R.M. Key, K. Lee, J.L. Bullister, R. Wanninkhof, C.S. Wong, D.W.R. Wallace, B. Tilbrook, and others. 2004. The oceanic sink for anthropogenic CO₂. *Science* 305:367–371, <https://doi.org/10.1126/science.1097403>.
- Schofield, O., and M.K. Tivey. 2004. Building a window to the sea: Ocean Research Interactive Observatory Networks (ORION). *Oceanography* 17(2):113–120, <https://doi.org/10.5670/oceanog.2004.59>.
- Sloyan, B., L.D. Talley, T. Chereskin, R. Fine, and J. Holte. 2010. Antarctic Intermediate Water and Subantarctic Mode Water formation in the Southeast Pacific: The role of turbulent mixing. *Journal of Physical Oceanography* 40:1,558–1,574, <https://doi.org/10.1175/2010JPO4114.1>.
- Spietz, R.L., D.A. Butterfield, N.J. Buck, B.I. Larson, W.W. Chadwick Jr., S.L. Walker, D.S. Kelley, and R.M. Morris. 2018. Deep-sea volcanic eruptions create unique chemical and biological linkages between the subsurface lithosphere and the oceanic hydrosphere. *Oceanography* 31(1):128–135, <https://doi.org/10.5670/oceanog.2018.120>.
- Stammer, D. 1997. Global characteristics of ocean variability estimated from regional TOPEX/POSEIDON altimeter measurements. *Journal of Physical Oceanography* 27:1,743–1,769, [https://doi.org/10.1175/1520-0485\(1997\)027<1743:GCOOVE>2.0.CO;2](https://doi.org/10.1175/1520-0485(1997)027<1743:GCOOVE>2.0.CO;2).
- Stocks, K., S. Diggs, C. Olson, A. Pham, R. Arko, A. Shepherd, and D. Kinkade. 2018. SeaView: Bringing together an ocean of data. *Oceanography* 31(1):71, <https://doi.org/10.5670/oceanog.2018.111>.
- Suess, E. 2014. Marine cold seeps and their manifestations: Geological control, biogeochemical criteria and environmental conditions. *International Journal of Earth Science* 103:1,889–1,916, <https://doi.org/10.1007/s00531-014-1010-0>.
- Sundby, S., K. Drinkwater, and O.S. Kjesbu. 2016. The North Atlantic spring-bloom system: Where the changing climate meets the winter dark. *Frontiers in Marine Science* 3:28, <https://doi.org/10.3389/fmars.2016.00028>.
- Takahashi, T., S.C. Sutherland, C. Sweeney, A. Poisson, N. Metzl, B. Tilbrook, N. Bates, R. Wanninkhof, R.A. Feely, C. Sabine, and others. 2002. Global sea-air CO₂ flux based on climatological surface ocean pCO₂, and seasonal biological and temperature effects. *Deep Sea Research Part II* 49:1,601–1,622, [https://doi.org/10.1016/S0967-0645\(02\)00003-6](https://doi.org/10.1016/S0967-0645(02)00003-6).
- Tolstoy, M., W.S.D. Wilcock, Y.J. Tan, and F. Waldhauser. 2018. A tale of two eruptions: How data from Axial Seamount led to a discovery on the East Pacific Rise. *Oceanography* 31(1):124–125, <https://doi.org/10.5670/oceanog.2018.118>.
- Torres, M.E., K. Wallmann, A.M. Tréhu, G. Bohrmann, W.S. Borowski, and H. Tomaru. 2004. Gas hydrate growth, methane transport, and chloride enrichment at the southern summit of Hydrate Ridge, Cascadia margin off Oregon. *Earth and Planetary Science Letters* 226:225–241, <https://doi.org/10.1016/j.epsl.2004.07.029>.
- Trainer, V.L., B.M. Hickey, E.J. Lessard, W.P. Cochlan, C.G. Trick, M.L. Wells, A. MacFadyen, and S.K. Moore. 2009. Variability of *Pseudo-nitzschia* and domoic acid in the Juan de Fuca eddy region and its adjacent shelves. *Limnology and Oceanography* 54:289–308, <https://doi.org/10.4319/lo.2009.54.1.0289>.
- Tréhu, A.M., W.S.D. Wilcock, R. Hilmo, P. Bodin, J. Connolly, E.C. Roland, and J. Braunmiller. 2018. The role of the Ocean Observatories Initiative in monitoring the offshore earthquake activity of the Cascadia subduction zone. *Oceanography* 31(1):104–113, <https://doi.org/10.5670/oceanog.2018.116>.
- Ulises, G.A., L.M. Smith, and T.J. Cowles. 2018. Get engaged with the Ocean Observatories Initiative. *Oceanography* 31(1):136–137, <https://doi.org/10.5670/oceanog.2018.121>.
- Vardaro, M.F., and J. McDonnell. 2018. Accessing OOI data. *Oceanography* 31(1):36–37, <https://doi.org/10.5670/oceanog.2018.106>.
- Wilcock, W.S.D., R.P. Dziak, M. Tolstoy, W.W. Chadwick Jr., S.L. Nooner, D.R. Bohnenstiehl, J. Caplan-Auerbach, F. Waldhauser, A.F. Arnulf, C. Baillard, and others. 2018. The recent volcanic history of Axial Seamount: Geophysical insights into past eruption dynamics with an eye toward enhanced observations of future eruptions. *Oceanography* 31(1):114–123, <https://doi.org/10.5670/oceanog.2018.117>.
- Wilcock, W.S.D., M. Tolstoy, F. Waldhauser, C. Garcia, J.J. Tan, D.R. Bohnenstiehl, J. Caplan-Auerbach, R.P. Dziak, A.F. Arnulf, and M.E. Mann. 2016. Seismic constraints on caldera dynamics from the 2015 Axial Seamount eruption. *Science* 354:1,395–1,399, <https://doi.org/10.1126/science.aah5563>.

ACKNOWLEDGMENTS

Funding for the OOI is provided by the National Science Foundation through a Cooperative Support Agreement with the Consortium for Ocean Leadership (OCE-1026342). Pioneer Array and Global Array Moorings and autonomous vehicles are operated by Woods Hole Oceanographic Institution. Endurance Array uncabled moorings and gliders are operated by Oregon State University. All cabled infrastructure is operated by the University of Washington. Cabled Array primary infrastructure and backbone cables were built and installed by L3 MariPro. The cyberinfrastructure and education and public engagement components are operated by Rutgers University.

We thank the many scientists, engineers, technicians, students, captain and crews, field teams, and support staff who have worked on the OOI program. In particular, we thank and acknowledge the following key individuals, in alphabetical order, within the greater OOI Team: Sue Banahan, Leila Belabbassi, Pete Barletto, Peter Brickley, Liz Caporelli, Robert Collier, Michael Crowley, Edward Dever, Jonathan Fram, Lori Garzio, Scott Glenn, Gary Harkins, Mike Harrington, James Housell, Brian Ittig, Aamir Jadoon, Orest Kawka, Tom Kearney, John Kemp, John Kerfoot, William Kish, Friedrich Knuth, Sage Lichtenwalner, Dana Manalang, Paul Matthias, Mike Mulvihill, Kris Newhall, Matt Palanza, Manish Parashar, Don Peters, Janeen Pisciotto, Craig Risien, Oscar Schofield, Michael Smith, Mark Steiner, Mark Stoermer, John Trowbridge, J.J. Villalobos, Sheri White, and Chris Wingard. Additionally, we thank the following individuals who laid the groundwork for the program in key leadership roles: Ken Brink, Peter Milne, Tim Cowles, Kendra Daly, John Delaney, Anthony Ferlaino (dec.), Holly Given, and Mike Kelly.

AUTHORS

Leslie M. Smith (lsmith@oceaneleadership.org) is OOI Science Communicator, Consortium for Ocean Leadership, Washington, DC, USA. **John A. Barth** is Professor and OOI Project Scientist, Oregon State University, Corvallis, OR, USA. **Deborah S. Kelley** is Professor and OOI Chief Scientist, University of Washington, Seattle, WA, USA. **Al Plueddemann** is Senior Scientist, Woods Hole Oceanographic Institution, Woods Hole, MA, USA. **Ivan Rodero** is Associate Research Professor and OOI CI Systems Engineering Program Manager, Rutgers University, New Brunswick, NJ, USA. **Greg A. Ulises** is OOI Director, Consortium for Ocean Leadership, Washington, DC, USA. **Michael F. Vardaro** is OOI Data Manager, Rutgers University, New Brunswick, NJ, USA. **Robert Weller** is Senior Scientist and OOI Co-Principal Investigator, Woods Hole Oceanographic Institution, Woods Hole, MA, USA.

ARTICLE CITATION

Smith, L.M., J.A. Barth, D.S. Kelley, A. Plueddemann, I. Rodero, G.A. Ulises, M.F. Vardaro, and R. Weller. 2018. The Ocean Observatories Initiative. *Oceanography* 31(1):16–35, <https://doi.org/10.5670/oceanog.2018.105>.

SIDE BAR Accessing OOI Data

By Michael F. Vardaro and Janice McDonnell



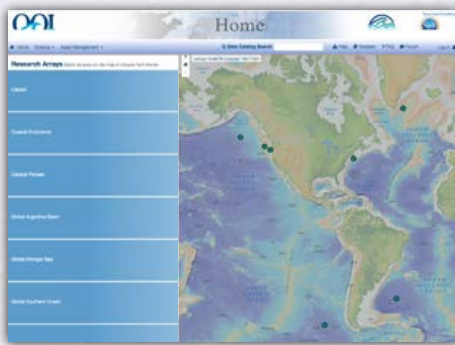
Ocean Observatories Initiative

<http://oceanobservatories.org>

The Ocean Observatories Initiative (OOI) website is the main website for the project. It highlights the science themes, platforms, and instrumentation of the OOI project. It also serves as a hub to access the other OOI sites.

Key Features:

- Events and updates
- Background on science themes
- Explanation of instrumentation and technology
- Information for researchers
- Links to data portal, cruise data, and analytical data pages



OOI Data Portal

<https://ooinet.oceanobservatories.org>

The data portal facilitates access to OOI data for research and education.

Key Features:

- List of OOI sites and platforms, including location and depth information
- Quick looks at data streams
- Ability to plot and download a data set and associated metadata (NetCDF, .csv, .json format)



OOI ERDDAP Server

<https://erddap-uncabled.oceanobservatories.org/uncabled>

A data server that provides a simple, consistent way to download subsets of OOI data sets in common file formats and make graphs and maps.

Key Features:

- Single data request format
- Common file format (with many file type options) and common time format
- RESTful API for scripted data requests
- More information and user manuals available via the landing page



Raw Data Archive

<https://rawdata.oceanobservatories.org/files>

All raw data from all platforms and instruments are stored by OOI, including hydrophones, HD video, and seismometers. A subset of the total stored raw data is delivered via the Raw Data Archive, which allows users to perform their own analyses using their own scripts or software, and to permit operators to confirm status of deployed instrumentation.

Key Features:

- “Raw” indicates data as they are received directly from an instrument, in instrument-specific format
- The archive is a mirror of the repository where all raw data enter the system
- Data in the online archive may be removed for space reasons. These data are never deleted and are available to users upon request.

Core Instrument Analytical Results

The Core Instrument Analytical Results data repository contains processed analytical data and metadata for a subset of Cabled Array instruments that collect fluid or particulate samples that are brought back to shore and analyzed in a laboratory. These instruments are described below, along with links to their associated news, publications, and other resources. Associated images are provided in spreadsheet-based catalogs.

- Ocean-based Water Sampler (OBWS) Data:** This instrument collects long-term pore fluid samples from hydrothermal vents at the International District Vent Field on Axial Seamount. It is connected to the Particulate DNA Sampler (PDS), which has an onboard temperature sensor and which continuously measures vent temperature. The PDS is able to store up to 100 samples for later analysis to determine the presence of specific microorganisms. Samples can be triggered to be sent to the surface to measure biological activity in hydrothermal vents, or to trigger specified intervals. After instrument recovery, laboratory analyses provide chemical characterization of the hydrothermal fluid samples.
- Hydrothermal Vent Fluid Interactive Sampler (HAFIS) Data:** This instrument collects fluid samples from hydrothermal vents at the International District Vent Field on Axial Seamount. It is connected to the Particulate DNA Sampler (PDS), which has an onboard temperature sensor and which continuously measures vent temperature. The PDS is able to store up to 100 samples for later analysis to determine the presence of specific microorganisms. Samples can be triggered to be sent to the surface to measure biological activity in hydrothermal vents, or to trigger specified intervals. After instrument recovery, laboratory analyses provide chemical characterization of the hydrothermal fluid samples.

SOUTHERN HYDRATE RIDGE OOI DATA | ARMED FIELD OBWS DATA | INTERNATIONAL DISTRICT VENT FIELD HAFIS DATA - COMMING SOON

Analytical Data

<http://oceanobservatories.org/core-instrument-analytical-results>

The Core Instrument Analytical Results data repository contains processed analytical data and metadata for a subset of Cabled Array instruments that collect fluid or particulate samples and that are brought back to shore and analyzed in a laboratory.

Key Features:

- Processed analytical results are generally provided in spreadsheet format
- Associated metadata files are presented in .pdf format
- As-deployed images of instruments provided in .jpg format, with image metadata summarized in spreadsheet-based catalogs

Live Video from Axial Seamount

A live video feed from the Axial Seamount is currently available. The video shows a hydrothermal vent field with active venting and mineralization. The video is part of a 14-minute broadcast every 2 hours, starting at 2:00, 5:00, 8:00, and 11:00 EDT/PDT.

LIVE VIDEO from AXIAL SEAMOUNT
14-min Broadcasts Every 2 Hours
2:00, 5:00, 8:00, & 11:00 EDT/PDT

The next live video will occur in: 2 hours, 37 minutes, and 47 seconds

Live Video Feed

<http://oceanobservatories.org/streaming-underwater-video>

Every three hours from 400 km off the Oregon coast and 1.6 km underwater, HD video streams live over the Internet through the OOI's Cabled Array in situ camera system. Video focuses on the 4.3 m tall actively venting hot spring deposit called "Mushroom" located within the ASHES vent field on Axial Seamount.

Key Features:

- Live video occurs during the hours of 2:00, 5:00, 8:00, and 11:00 EDT & PDT, for a duration of 14 minutes
- The camera also records continuously for 24 hours on the 10th and 20th of every month, and 72 hours nonstop from the 1st to 3rd of every month, to examine animal behavior, diurnal/tidal cycles, and other changes in hydrothermal flow

Welcome

The Ocean Education Portal is a collection of prototypes of advance-ocean science systems to measure the physical, chemical, and biological properties of the ocean in real time and on the seafloor. These systems are designed to be used as end-to-end monitoring instruments, providing a integrated view of the ocean environment. The portal provides links to the home of a vast user community including scientists, educators, students, and the general public.

Tools in the Ocean Education Portal provide access for the development of educational data visualizations and translation of OOI science into pedagogical resources such as concept maps and online lessons.

Visualize Data
These visualizations allow you to explore and analyze raw data from sensors on the OOI or sensors such as NOAA's Ocean Observing System. These are great for use in your classroom!

Connect Concepts
This tool will help you connect the concepts taught in your classroom, including mathematics, science, technology, engineering, and art to OOI science.

Create Investigations
This tool will help you design an on-line investigation, including a concept map that can be used to frame the investigation. You can then use the investigation through a series of steps for preparing, creating, and publishing your investigation as part of a larger lesson.

OOI Ocean Education Portal

<http://education.oceanobservatories.org>

The Ocean Education Portal facilitates access for the development of educational data visualizations and translation of OOI science into pedagogical resources.

Key Features:

- Data visualization tools prototypes
- Concept mapping tool
- Ontology tool
- Lesson Lab Builder prototype

Data Explorations

Looking for ways to connect your undergraduates to introductory courses with authentic data?

What are Data Explorations?

We provide a range of quick and easy Data Explorations using authentic, raw data that is relevant to various concepts that are already taught in introductory courses. The Data Explorations are quick (15–20 minute) interactions with data so that you can easily integrate them into your current classroom teaching while increasing your students' understanding of key concepts.

Current Explorations

Exploring Primary Production with Data

Through these activities, we will explore primary production in greater detail. Primary production is the rate at which organisms store energy through the formation of organic matter (carbon-based compounds), using energy derived from solar radiation during photosynthesis or from chemical reactions during chemosynthesis.

Activities | Instructor's Guide

Data Explorations

<http://education.oceanobservatories.org/explorations>

Provides quick (15–20 minute) interactive explorations using authentic OOI data relevant to various concepts taught in introductory oceanography courses. Easily integrated into classroom teaching while increasing students' understanding of key concepts.

Key Features:

- Collection of activities focused on geology, chemistry, and biological productivity
- Pedagogical support (Learning Cycle) to help you frame the data activity in your class lesson.

AUTHORS

Michael F. Vardaro (vardaro@marine.rutgers.edu) is OOI Data Manager, and **Janice McDonnell** is Associate Professor, both at Rutgers University, New Brunswick, NJ, USA.

ARTICLE CITATION

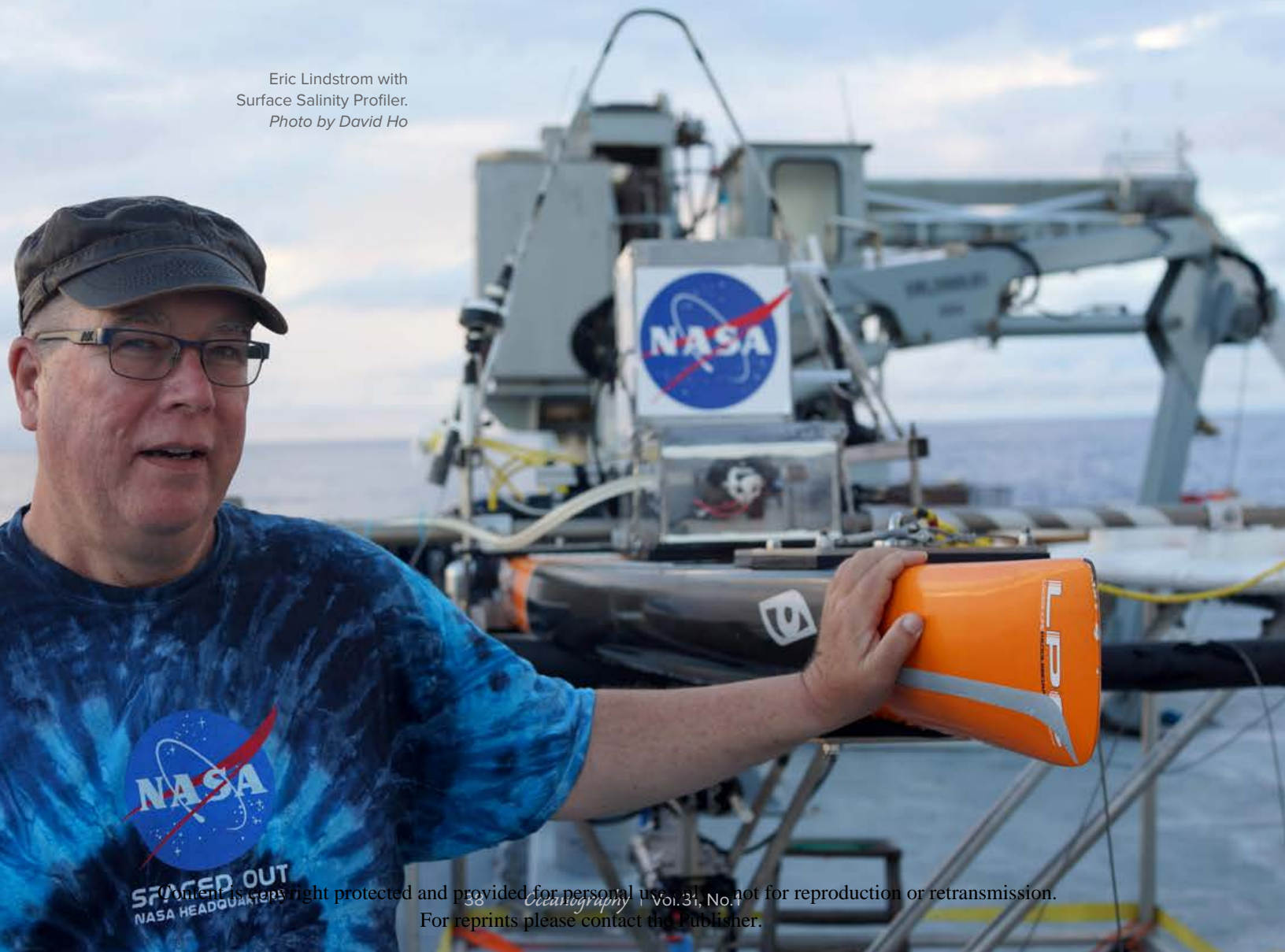
Vardaro, M.F., and J. McDonnell. 2018. Accessing OOI data. *Oceanography* 31(1):36–37, <https://doi.org/10.5670/oceanog.2018.106>.

ON THE RELATIONSHIP BETWEEN THE

Global Ocean Observing System AND THE Ocean Observatories Initiative

By Eric Lindstrom

Eric Lindstrom with
Surface Salinity Profiler.
Photo by David Ho



The Global Ocean Observing System (GOOS; <http://www.goosocean.org>) is an international framework for supporting and sustaining the geographically distributed collection of ocean observations designed to benefit science and society. Observations required to guide an evidentiary-based response by society to environmental change are determined by various international conventions (e.g., United Nations Framework Convention on Climate Change). GOOS, under the Intergovernmental Oceanographic

Commission of UNESCO, seeks to respond to the high-level requirement for ocean observations by managing a suite of global networks that collect observations. These networks include, for example, the global array of nearly 4,000 Argo profiling floats, arrays of about 1,250 surface drifters and 300 precision tide gauges, moorings at dozens of key sites around the planet, and repeat hydrographic lines that replicate the sampling of the World Ocean Circulation Experiment about every 10 years (Figure 1).

Key features of GOOS that make it unique are the ambition to sustain the observing system indefinitely, to make the data freely available to all users, to report data in real time for operational applications where feasible, and to expand the system through promulgation of best practices. To date, GOOS has been successful in providing for a baseline suite of physical measurements of the ocean as a follow-on from the World Ocean Circulation Experiment of the 1990s. It is recognized, however, that science and

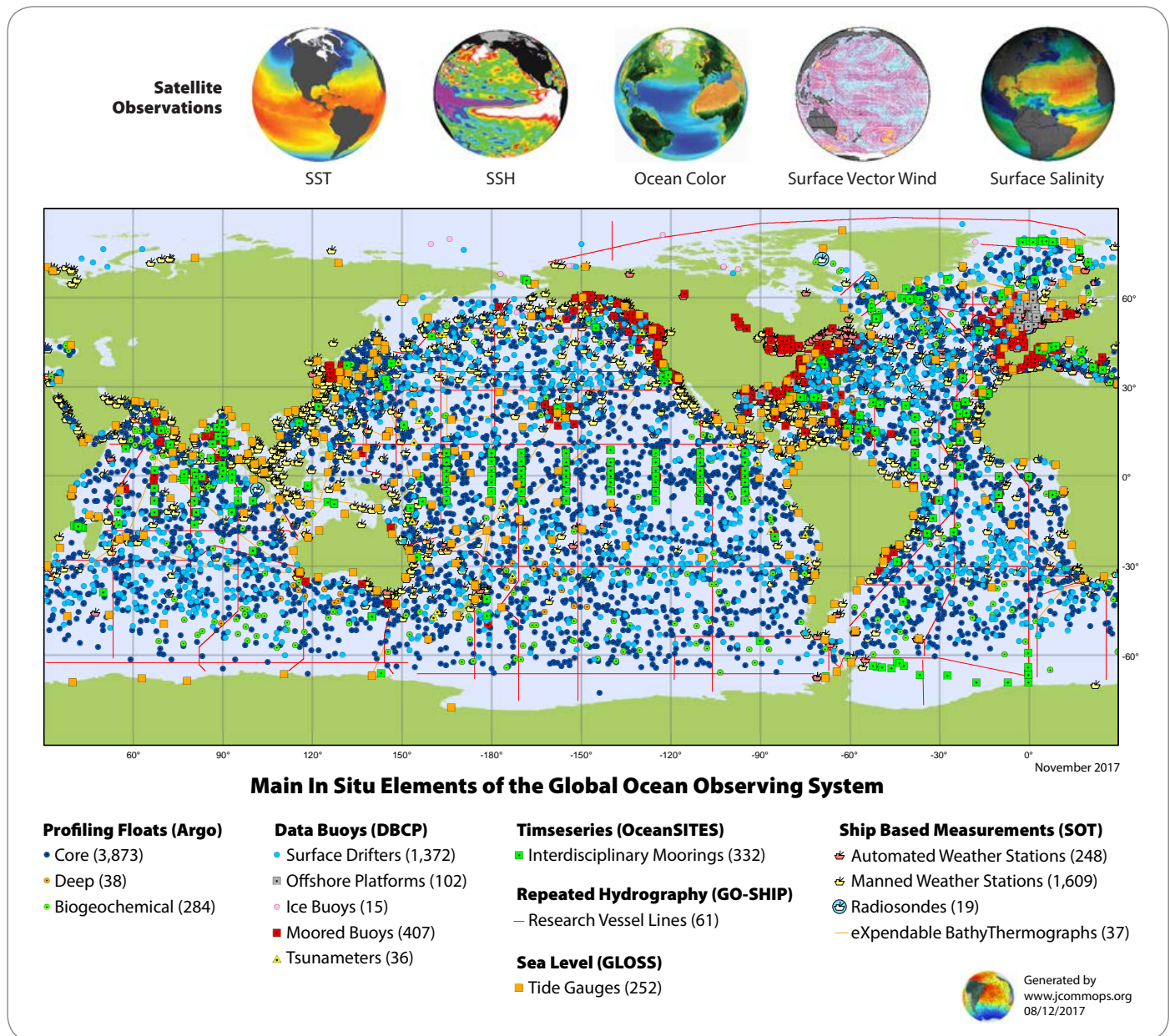


FIGURE 1. Satellite and in situ elements of the Global Ocean Observing System (GOOS).

society require more biogeochemical and biological observations of the ocean than are currently provided by GOOS platforms. The oceanographic community is quite active in sifting through all the various requirements for sustained global observations and their feasibility. Adding more components to a global, permanent, operational observing system is a daunting challenge—politically, financially, and practically. Many questions must be answered with respect to which new measurements are the highest priorities and whether there is a robust sensor technology and sampling platform with which to obtain the measurements. Eventually, nations have to agree to a plan and collect observations using common standards and practices.

The Ocean Observatories Initiative (OOI; <http://oceanobservatories.org>) is an important element within GOOS, despite the fact that it is NOT a global observing system. It does contribute observations to the global system via cabled observatory and moored measurement systems. If there were a weakness in the OOI for

GOOS, it would be a failure to report some key data openly in near-real time for societal uses. I will not dwell here on the valuable data reporting contribution of the OOI to GOOS and science; it a complex area worthy of deeper discussion. The most important OOI contribution may be in promoting and perfecting the next generation of sensors and platforms for global sustained measurement systems, the launching pad for GOOS evolution.

In 2012, with the advent and international agreement to the Framework for Ocean Observing (FOO; <http://www.oceanobs09.net/foo>; Figure 2), GOOS underwent a transformation. It was recognized that GOOS was not only about the collection and use of global ocean observations, but it also had to embrace and develop the ways and means to fulfill new requirements for sustained observations. It was already recognized that much of GOOS was supplied and maintained by the research community, but GOOS had not identified the development pathways for its next generation or evolving observing systems. This outlook,

in broad strokes, was the subject of the Framework for Ocean Observing, which was to provide a set of guidelines for how to mature systems from concept to reality, and globally implement them, based on the proven best practices of GOOS to date. I believe that the OOI is a critical tool for developing the next generation of integrated ocean observing platforms.

Roughly speaking, many of today's oceanography methods focus on using a measurement platform to observe a small number of variables. Most oceanographers would recognize that their tools limit the diversity of observations that they make—despite the great expense and effort to get themselves and/or their observing platforms to far reaches of the ocean. We have yet to perfect autonomous observatories that are truly fit for providing sustained global observations of the disciplinary scope required by the challenges facing society. Argo (<http://www.argo.ucsd.edu>) is one embryonic model for such an observatory, with its evolving subspecies of Deep Argo, Bio-Argo, and Biogeochemical Argo. The OOI represents a pathway for development of cabled observatories, cutting-edge moored observatories, and sophisticated gliders. If GOOS is to be successful and evolve to meet society's need for a comprehensive ocean observing system, the OOI will be a critical element in that evolution. Though there is not space here to enumerate all the potential developments needed to improve a GOOS, I can say that the next generation of improvements within GOOS will build on reliable measurement technologies as now attempted by the OOI. There are numerous frustrations and opportunities: power constraints for autonomous platforms (batteries), cabled platforms and sensors for observing the subtle and crushing signals in the deep ocean, high-bandwidth telemetry through seawater, samplers for the myriad gelatinous forms of life, automated taxonomic identification technology, and robust yet sensitive chemical sensors—the list goes on.

The OOI is highly relevant to

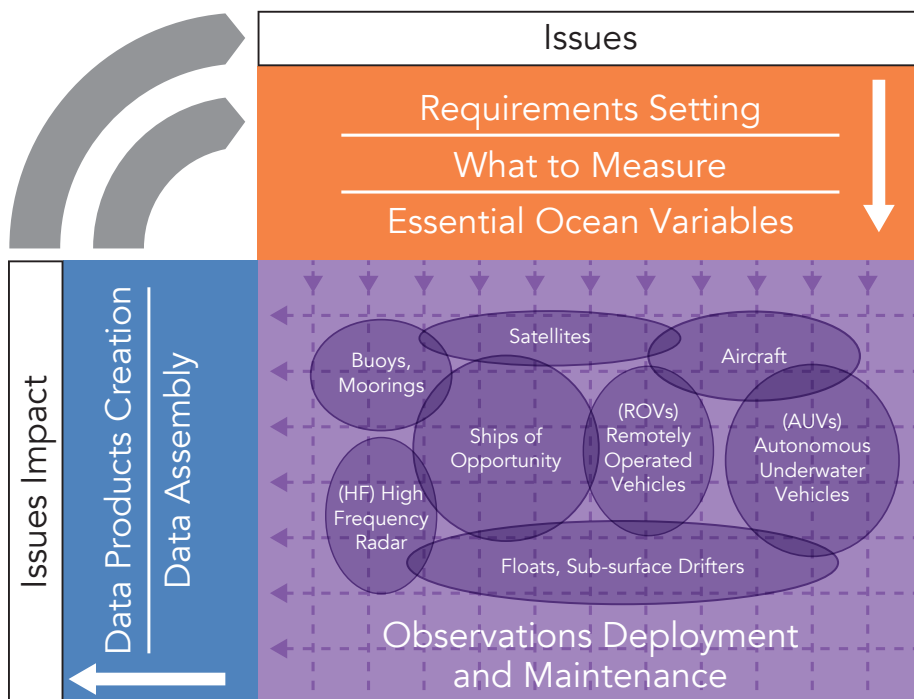


FIGURE 2. Structure of the Framework for Ocean Observing, showing how ocean observing activities fit into the systems model of the Framework and also the critical feedback loop between observing system outputs and science-driven requirements. Observation system examples are illustrative only, not comprehensive.

Box 1. Access to OOI Data from Global and Regional Repositories

In situ observatories, complex cyberinfrastructure, and the need for open access to data are now baseline components of a successful global oceanographic community. Integration and collaboration across programs are imperative. To meet these requirements, Ocean Observatories Initiative (OOI) data have been made available through several existing data repositories, and have been integrated into existing and evolving global and regional visualizations. This allows OOI data not only to be viewed in the greater context of data collected in the area by other programs but also increases its accessibility, as individuals can download through multiple avenues. Currently,

- Coastal Endurance Array mooring data can be viewed through the Northwest Association of Networked Ocean Observing Systems (NANOOS) Visualization System (<http://nvs.nanoos.org>).
- Coastal Pioneer Array mooring data can be viewed through the Mid-Atlantic Coastal Ocean Observing System (MARACOOS) Ocean Map (<http://oceansmap.maracoos.org>).
- OOI glider data have been integrated into the IOOS Glider Data Assembly Center (DAC; <https://gliders.ioos.us>).
- Global Array atmospheric data have been integrated into the World Meteorological Organization's (WMO) Global Telecommunication System (GTS) via the National Data Buoy Center (NDBC; <http://www.ndbc.noaa.gov>).
- Global Array mooring data are available through OceanSITES (<http://www.oceansites.org>).
- Cabled Array seismometer and bottom pressure tilt data are available through the Incorporated Research Institutions for Seismology (IRIS; <http://www.iris.edu>).

Our future is in sustained observations of Earth. Photo by Julian Schanze

such challenges as just articulated. Fundamentally, it has sought to sample a wide range of variables with its sensor platforms. It has sought to bring power to the deep sea. It has enabled long-term term sampling in remote locations through a coherent mix of technology innovations and management skills. The OOI recognized that there is need for a robust cyberinfrastructure to translate observations into usable products and services (Box 1).

It will be very important going forward to find ways for OOI and GOOS to cooperate in meaningful ways to capture OOI innovations into a regularized, internationalized, and economized system such as GOOS. For the most part, GOOS is not “high tech.” It is at its best when the required technologies are easily deployable (e.g., drifter in a cardboard box) but can deliver sophisticated products consumable by all manner of user groups. As GOOS has learned, it is not just about

observing the ocean. We must deliver products and services from those observations to achieve the value that society demands. The OOI is largely tailored to a sophisticated scientific audience. The extension of OOI data products and data services to a wider audience will align nicely with the GOOS objectives.

One way ahead for the synergy of the OOI and GOOS is through joint agreement to the Framework for Ocean Observing (Figure 2) and working together to evolve and improve this Framework. OceanObs’19 (<http://www.oceanobs19.net>) is coming up in less than two years, and it is likely the Framework will be front and center in considering community progress in ocean observing. The OOI can articulate its success to the GOOS community by showing how its developments contribute to the “readiness” of systems to participate in sustained global observations. The GOOS community can take better

note of the progress and development of OOI sensors and platforms by including them in proposals to grow and expand GOOS, thus furthering the overarching GOOS objective to use ocean observations to meet the societal challenges of environmental change. ☐

AUTHOR

Eric Lindstrom (eric.j.lindstrom@nasa.gov) manages the National Aeronautics and Space Administration’s (NASA’s) Physical Oceanography Research Program, NASA Headquarters, Washington, DC, USA, and is serving as co-chair of the steering committee for the Global Ocean Observing System from 2012–2017.

ARTICLE CITATION

Lindstrom, E. 2018. On the relationship between the Global Ocean Observing System and the Ocean Observatories Initiative. *Oceanography* 31(1):38–41, <https://doi.org/10.5670/oceanog.2018.107>.

The North Atlantic Biological Pump

INSIGHTS FROM THE OCEAN OBSERVATORIES INITIATIVE IRMINGER SEA ARRAY

By Hilary I. Palevsky
and David P. Nicholson



ABSTRACT. The biological pump plays a key role in the global carbon cycle by transporting photosynthetically fixed organic carbon into the deep ocean, where it can be sequestered from the atmosphere over annual or longer time scales if exported below the winter ventilation depth. In the subpolar North Atlantic, carbon sequestration via the biological pump is influenced by two competing forces: a spring diatom bloom that features large, fast-sinking biogenic particles, and deep winter mixing that requires particles to sink much further than in other ocean regions to escape winter ventilation. We synthesize biogeochemical sensor data from the first two years of operations at the Ocean Observatories Initiative Irminger Sea Array of moorings and gliders (September 2014–July 2016), providing the first simultaneous year-round observations of biological carbon cycling processes in both the surface ocean and the seasonal thermocline in this critical but previously undersampled region. These data show significant mixed layer net autotrophy during the spring bloom and significant respiration in the seasonal thermocline during the stratified season ($\sim 5.9 \text{ mol C m}^{-2}$ remineralized between 200 m and 1,000 m). This respired carbon is subsequently ventilated during winter convective mixing ($>1,000 \text{ m}$), a significant reduction in potential carbon sequestration. This highlights the importance of year-round observations to accurately constrain the biological pump in the subpolar North Atlantic, as well as other high-latitude regions that experience deep winter mixing.

Photo credit: Sheri White, © Woods Hole Oceanographic Institution

INTRODUCTION

Export of biologically fixed organic carbon from the surface to the deep ocean, known as the biological pump, plays an important role in the global carbon cycle (Volk and Hoffert, 1985). Photosynthesis by marine phytoplankton fixes carbon dioxide into organic carbon at a global rate of $\sim 50 \text{ Pg yr}^{-1}$ (Field et al., 1998). A fraction of this fixed organic carbon escapes being respired by organisms in the surface ocean and is transferred as sinking particles, by mixing of dissolved and suspended organic matter, and by vertical animal migration to the ocean interior, where it is sequestered from the atmosphere on time scales of months to centuries (Volk and Hoffert, 1985; DeVries et al., 2012). This process of biological carbon export is commonly known as the biological pump because it transfers carbon against a concentration gradient from the surface to the deep ocean, which maintains an inorganic carbon reservoir ~ 45 times that of the atmosphere (Volk and Hoffert, 1985; Sarmiento and Gruber, 2006; Caias et al., 2013).

Current understanding suggests that anthropogenic carbon uptake to date has been predominantly driven by the abiotic solubility pump as the surface ocean equilibrates with rising atmospheric CO_2 concentrations, rather than by biological carbon cycling (Sabine and Tanhua, 2010). However, estimates of the current global rate of carbon transfer from the surface ocean to the interior via the biological pump, amounting to $\sim 6\text{--}13 \text{ Pg C yr}^{-1}$ (Laws et al., 2011; Siegel et al., 2014), significantly exceed the current rate at which the ocean absorbs atmospheric CO_2 , estimated at $2.6 \pm 0.5 \text{ Pg C yr}^{-1}$ (Le Quéré et al., 2016), indicating that even a small perturbation to the biological pump could have a large influence on the global carbon cycle. Changes to the strength of the biological pump would also influence the distribution of nutrients and oxygen in the ocean, with broad implications for ocean ecosystems.

In order to effectively monitor and predict future changes to the ocean's

biological pump, accurate baseline measurements of current rates of biological carbon export are necessary to validate rates predicted by remote-sensing algorithms and global climate models (e.g., Stukel et al., 2015; Palevsky et al., 2016b), as well as to refine our understanding of the processes controlling the biological pump. Our current understanding is limited, however, by the difficulty of measuring biological carbon export and the processes that drive it over the entire annual cycle. Our most detailed understanding of the biological pump and its role in the ocean carbon sink comes from time-series sites with robust sampling programs for both primary and export production, often with additional observations of ecosystem composition and structure useful for determining mechanistic controls on export (e.g., Church et al., 2013). However, these existing time-series sites are representative of only a small fraction of the global ocean (estimated at 9%–15% of the total ocean area; Henson et al., 2016), and year-round study sites are largely limited to the subtropical and tropical ocean, while high-latitude sites are sampled predominantly during the spring and summer productive season.

Year-round sampling of the biological pump is especially critical in high-latitude regions because a large fraction of the carbon exported seasonally during

the spring and summer can be brought back to the surface and ventilated during deep winter mixing. For the biological pump to effectively sequester carbon from the atmosphere on annual or multi-annual timescales, organic material must sink deep enough to escape being entrained back into the deepest winter mixed layers. If sinking organic carbon is remineralized (converted from organic to inorganic carbon by respiration) within the seasonal thermocline (the portion of the water column below the seasonally stratified mixed layer but above the depth of deepest annual mixing), this carbon can ventilate back to the atmosphere as CO_2 when entrained into the wintertime mixed layer (Figure 1). Observational estimates based on year-round surface measurements in deep mixing regions in the western North Pacific, northeastern Atlantic, and subpolar North Atlantic indicate that 40%–90% of the organic carbon exported from the seasonally stratified mixed layer is subsequently ventilated during winter mixing (Körtzinger et al., 2008; Quay et al., 2012; Palevsky et al., 2016a). The rate of carbon sequestration below the winter ventilation depth depends not only on export from the euphotic zone during the productive season but also on respiration rates within the seasonal thermocline and the depth of physical mixing the subsequent winter.

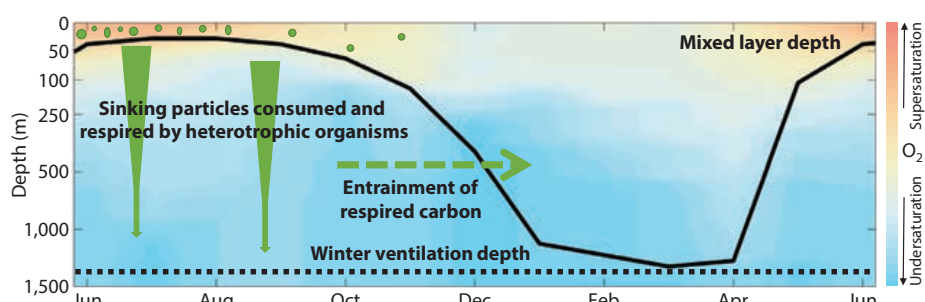


FIGURE 1. Schematic seasonal cycle of organic carbon export and winter ventilation in the subpolar North Atlantic (oxygen saturation and mixed layer depth based on World Ocean Atlas 2013 data for the OOI Irminger Sea Array site). Phytoplankton growth in the spring and summer leads to export from the seasonally stratified mixed layer. This surface net autotrophy is evident in mixed layer oxygen supersaturation. However, much of the seasonally exported carbon is remineralized in the seasonal thermocline and entrained back into the mixed layer during deep winter mixing. This ventilates the respiration carbon (and waters undersaturated with oxygen due to net respiration) back to the atmosphere. In order for carbon to be sequestered on annual or longer time scales, it must sink below the winter ventilation depth prior to remineralization.

In this paper, we focus on the Irminger Sea region of the subpolar North Atlantic as a case study of the high-latitude biological pump. The subpolar North Atlantic is a strong carbon sink region where the biological carbon pump's annual cycle features two pronounced and competing processes: a spring diatom bloom that produces large, fast-sinking particles, and deep winter mixing that ventilates carbon remineralized in the seasonal thermocline back to the atmosphere (Figures 1 and 2a). The Ocean Observatories Initiative (OOI) Irminger Sea Array of moorings and gliders provides a unique opportunity to study the subpolar North Atlantic biological carbon pump throughout the year within the context of an unprecedented density of biogeochemical, physical, and bio-optical sensors operating for multiple years at high temporal resolution. We synthesize data from the OOI Irminger Sea Array's first two years of operation, illustrating the full annual cycle of biologically driven carbon cycling processes in both the surface ocean and the seasonal thermocline in this globally significant and previously undersampled high-latitude region.

THE SUBPOLAR NORTH ATLANTIC AND THE IRMINGER SEA

Anthropogenic carbon has accumulated in the North Atlantic at approximately three times the global average rate (Sabine

et al., 2004; Khatiwala et al., 2009), making it a region of critical importance for understanding the ocean's role in carbon cycling. Deepwater formation in the subpolar North Atlantic enhances the ability of the ocean to absorb carbon abiotically via the solubility pump (Sabine and Tanhua, 2010), and also increases the sequestration time for biologically exported carbon that reaches below the winter ventilation depth (DeVries et al., 2012). However, the amount of carbon sequestered annually by the biological pump and its role in driving ocean carbon uptake in the subpolar North Atlantic is not well constrained (Sanders et al., 2014).

A dominant feature of the subpolar North Atlantic seasonal cycle is the large, diatom-dominated spring phytoplankton bloom (Figure 2a; for a review of the bloom and its drivers, see Behrenfeld and Boss, 2014). Many prior studies have documented high rates of primary production and organic carbon export from the surface ocean during the bloom (e.g., Buesseler et al., 1992; Quay et al., 2012). Fast-sinking particles and aggregates can transfer this organic carbon to depth, with significant particle fluxes observed between the base of the euphotic zone and 1,000 m (Antia et al., 2001; Briggs et al., 2011; P. Martin et al., 2011). Dissolved and suspended organic matter can also be transferred from the surface mixed layer to the thermocline by episodic mixing followed by

restratification (Dall'Olmo et al., 2016). However, this organic matter must penetrate below the deepest winter mixing depth in order not to be remineralized in the seasonal thermocline and ventilated back to the atmosphere during the subsequent winter (Figure 1; Oschlies and Kahler, 2004; Körtzinger et al., 2008; Quay et al., 2012).

The Irminger Sea, located between Greenland and Iceland (Figure 2a), experiences both the large spring bloom and deep winter mixing characteristic throughout the North Atlantic subpolar gyre. Strong wintertime atmospheric forcing over the Irminger Sea cools the surface ocean and drives winter convective mixing to depths of up to 1,400 m, forming a water mass that extends throughout the mid-depth North Atlantic (Pickart et al., 2003; de Jong et al., 2012; de Jong and de Steur, 2016; de Jong et al., 2018, in this issue). There is significant interannual variability in Irminger Sea convective mixing, with the deepest mixing occurring during years with the strongest surface cooling (associated with the positive phase of the North Atlantic Oscillation; de Jong and de Steur, 2016). There is also significant interannual variability in the magnitude and timing of the spring bloom, with satellite ocean color observations showing a delayed bloom and lower maximum chlorophyll *a* concentrations in positive phase North Atlantic Oscillation years

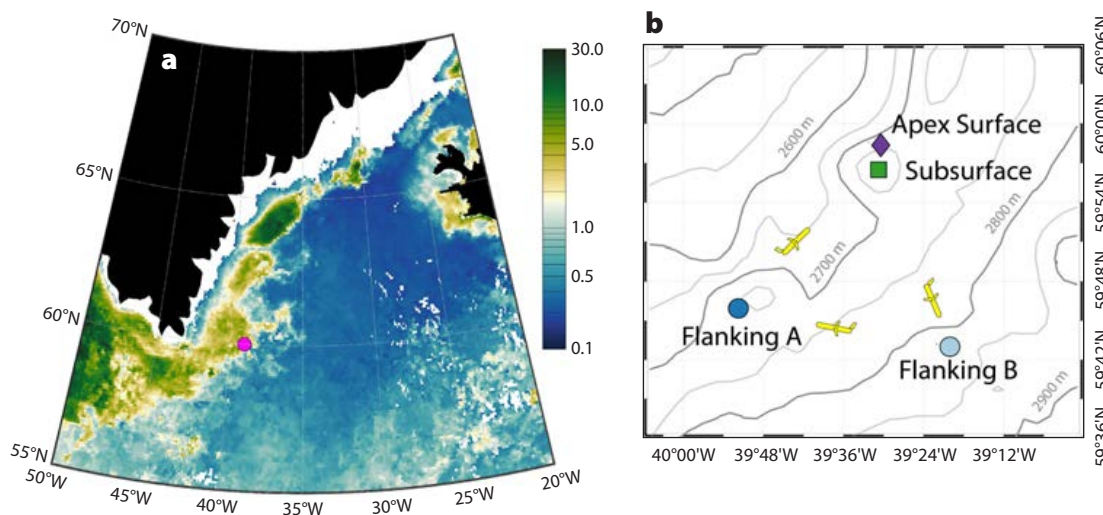


FIGURE 2. (a) Sea surface chlorophyll *a* ($\mu\text{g L}^{-1}$; 9 km MODIS Aqua) in the Irminger Sea from May 2015. The pink dot indicates the location of the OOI Irminger Sea Array. (b) Configuration of moorings and gliders at the OOI Irminger Sea Array, overlaid on bathymetric contours.

that have stronger cooling and deeper mixing (Henson et al., 2006, 2009). This interannual variability in bloom dynamics and physical forcing likely also influences the amount of carbon seasonally exported from the surface ocean, remineralization rates in the seasonal thermocline, and the fraction of seasonally exported carbon ventilated during winter mixing. However, these connections cannot yet be disentangled, because long-term observations have historically been limited to physical properties and satellite ocean color, without corresponding tracers of the biological pump. The picture of the Irminger Sea biological pump presented here, based on the first two years of data from the OOI Array, provides an initial snapshot of the system within the context of longer-term interannual variability, which this new time series will enable us to resolve through continued collection of biogeochemical data over the coming years.

OOI IRMINGER SEA ARRAY

The OOI Irminger Sea Array was first deployed in September 2014, beginning an ongoing time series of observations planned to continue for 25 to 30 years. The array is arranged in a triangular configuration (nominally 20 km a side), with an Apex surface mooring co-located with a subsurface profiler mooring at the north point of the triangle and two flanking moorings located at the southern corners (Figure 2b). Up to three open-ocean gliders continually transit around the array triangle, diving from the surface to 1,000 m. Annual summertime cruises recover all moorings and gliders from the previous year and deploy replacements, as well as conduct shipboard calibration casts for sensors on all moorings and gliders.

Here, we synthesize data collected over the first two years of OOI Irminger Sea Array deployment (September 2014–July 2016) to trace organic carbon production, remineralization, and ventilation. We focus in particular on dissolved oxygen, as stable response Aanderaa

optode model 4831 oxygen sensors are located on all moorings and gliders within the OOI Array, and provide a continuous picture of biologically mediated surface and subsurface carbon cycling. To provide physical and biological context, we interpret these oxygen data alongside temperature and salinity data collected on all moorings and gliders, and chlorophyll *a* concentrations determined from surface mooring fluorometers (see online Supplementary Text for full details on all data included in this analysis).

DISSOLVED OXYGEN DATA FROM THE OOI ARRAY

Dissolved oxygen is a commonly used tracer of the biological pump because it records the balance between rates of photosynthesis and respiration. In a net autotrophic system, photosynthesis dominates over respiration, leading to net biological production of dissolved oxygen that is stoichiometrically related to net production of organic carbon. Conversely, in a net heterotrophic system, oxygen losses due to respiration dominate and are stoichiometrically related to net consumption of organic carbon by remineralization. Abiotic processes of air-sea gas exchange and physical mixing also influence dissolved oxygen concentrations in the ocean, so interpretation of dissolved oxygen data to examine the effects of biological processes requires us to disentangle these separate influences.

Quantitative interpretation of dissolved oxygen sensor data requires that sensors be calibrated to account for two primary sources of error: (1) rapid drift from factory calibrations prior to deployment, and (2) in situ drift after deployment (D'Asaro and McNeil, 2013; Takeshita et al., 2013; Bittig and Körtzinger, 2015, 2017; Johnson et al., 2015; Bushinsky et al., 2016). Details of these corrections are provided in the Supplementary Text. We correct for pre-deployment drift using discrete samples for dissolved oxygen collected during the deployment cruises and measured using shipboard Winkler titrations, which remain

the gold standard for accurate dissolved oxygen measurements. This enables us to determine sensor-specific gain corrections (Figure S1, Table S1). We correct for in situ drift by assuming that oxygen concentrations on deep isotherms (2,000 m and below) should be stable over time, and that observed oxygen change at these depths represents sensor drift (Figure S2, Table S2).

The surface mixed layer oxygen measurements are subject to greater uncertainty than the thermocline measurements due to greater uncertainty in their pre-deployment drift gain corrections and the faster drift of optodes measuring surface properties (Tables S1 and S2). We therefore do not use surface oxygen measurements to calculate air-sea oxygen flux or net community production, which require highly accurate surface oxygen measurements (Emerson and Bushinsky, 2014). Further study with more accurately constrained surface dissolved oxygen measurements will be needed to determine the relative roles of air-sea oxygen flux, biological production, and physical influences on mixed layer dissolved oxygen. Here, we qualitatively interpret the mixed layer seasonal cycle and focus quantitative interpretation on the spring bloom signal that is large enough to overwhelm uncertainty and on the more accurately constrained measurements of the seasonal thermocline from the profiler mooring.

SEASONAL CYCLE IN THE SURFACE OCEAN

The Irminger Sea surface mixed layer ranges from <30 m during the stratified summer season to depths of >1,000 m during winter, and shows a pronounced seasonal cycle in physical, biological, and chemical properties (Figure 3). Sea surface temperatures range from late winter minima of 3.5°–3.6°C to summer maxima of 9.5°C (Figure 3a). Previous analysis shows that the winter of 2014–2015 in the Irminger Sea was characterized by exceptionally strong atmospheric forcing associated with a high North Atlantic

Oscillation index, which drove unusually strong surface cooling and deep winter convection as compared with the previous 12 years, pre-conditioning the region for similarly deep mixing in the winter of 2015/2016 (de Jong and de Steur, 2016; de Jong et al., 2018, in this issue). The spring bloom is evident in elevated surface chlorophyll *a* concentrations from April to early June in both 2015 and 2016 (Figures 2a and 3b).

Observed mixed layer dissolved oxygen concentrations can be interpreted by comparison with oxygen concentrations expected if the surface ocean were in equilibrium with the atmosphere (equilibrium O₂ in Figure 3c). Throughout the winter months, surface oxygen concentrations remain below saturation, indicating ventilation of oxygen-undersaturated deeper waters with a net respiration signature. Oxygen undersaturation persists until the beginning of the spring bloom, when surface oxygen rapidly increases in tandem with the increase in chlorophyll *a*. Once oxygen

concentrations reach supersaturation in late April 2015, they remain supersaturated through early October. This, as well as chlorophyll *a* concentrations elevated above baseline values (Figure 3b), suggests that productive conditions of surface net autotrophy extend throughout this period.

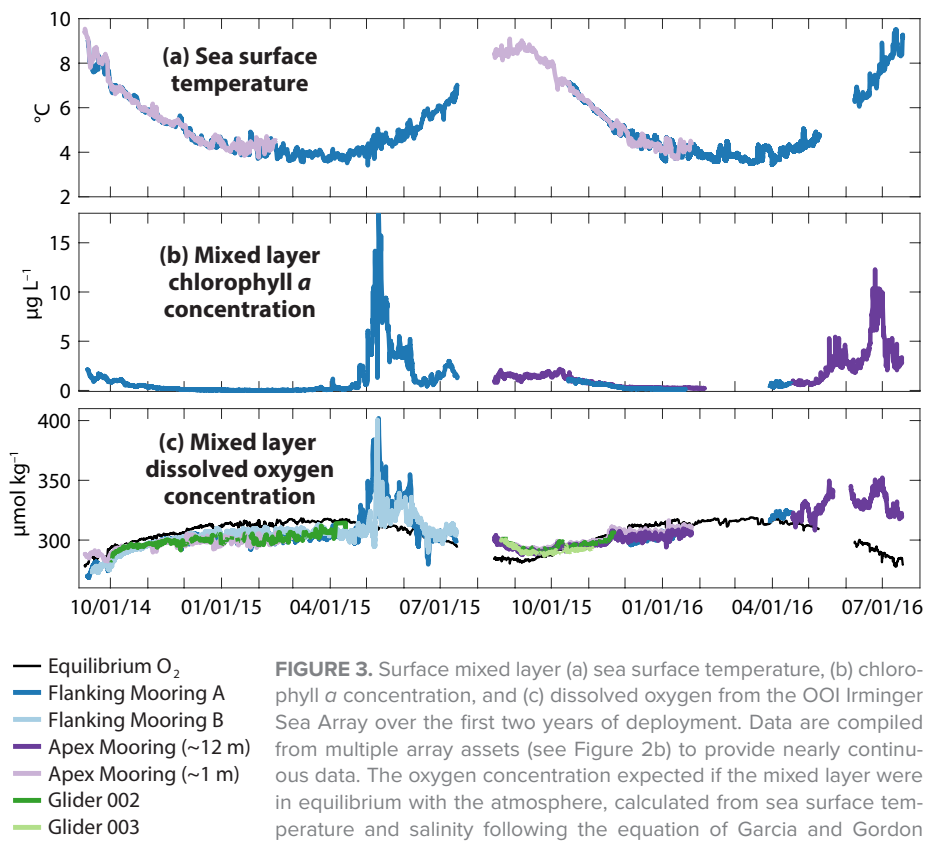
Although oxygen measurements are not sufficiently accurate to estimate the total net community production (NCP) in the surface mixed layer, the rapid increase in dissolved oxygen during the 2015 spring bloom from a baseline value of $305 \pm 2 \mu\text{mol kg}^{-1}$ during April 1–10 to a maximum value of $402 \mu\text{mol kg}^{-1}$ on May 11 reflects an increase in the mixed layer oxygen inventory of $\sim 3.0 \text{ mol m}^{-2}$ integrated through the $\sim 30 \text{ m}$ mixed layer at the time of the oxygen maximum. This increase in oxygen inventory places a lower bound (neglecting oxygen flux to the atmosphere) on the mixed layer NCP during this initial bloom period equivalent to net production of $\sim 2.1 \text{ mol C m}^{-2}$, or $70 \text{ mmol C m}^{-2} \text{ d}^{-1}$ (based on a O₂:C ratio

of 1.4; Laws, 1991). Previous estimates of oxygen flux to the atmosphere during the subpolar North Atlantic spring bloom are of comparable magnitude (Quay et al., 2012, and references therein), suggesting that the total NCP during the bloom is likely considerably greater than our lower bound estimate.

SEASONAL CYCLE OF THERMOCLINE RESPIRATION AND WINTER VENTILATION

Observations below the mixed layer allow us to see the seasonal evolution of respiration and ventilation within the seasonal thermocline. Profiler mooring temperature data (Figure 4a) were compared with sea surface temperature (Figure 3a) to determine the base of the mixed layer ($\Delta 0.2^\circ\text{C}$ from the sea surface temperature; de Boyer Montégut et al., 2004). During the stratified spring and summer season, the profiler mooring's surface-most measurements are well below the mixed layer (i.e., the uppermost temperature measurements from the profiler mooring are more than 0.2°C cooler than the sea surface). As the mixed layer deepens in fall and winter, the surface mixed layer penetrates into the seasonal thermocline and ventilates waters that were isolated from contact with the atmosphere during the stratified season. In both 2014 and 2015, mixed layers first reached to 200 m depth in mid-November, with ventilation extending deeper into the water column and progressively eroding seasonal stratification through the winter (red lines in Figure 4).

The dates of initial winter ventilation (the time that the mixed layer first penetrates to a given depth within the thermocline) correspond with a rapid increase in dissolved oxygen concentration at depth as the oxygen-undersaturated thermocline waters are exposed to the atmosphere (Figure 4b,c). Once ventilation has penetrated to a given depth, oxygen concentrations at that depth continue to increase throughout the period of winter convection until stratification is reestablished in spring (Figure 5). Because the



depth of active mixing often decreases in spring prior to stratification of the mixed layer defined based on physical properties, the date of re-stratification in spring is defined based on the maximum oxygen concentration at a given depth (yellow dots in Figure 5, shown for all depths as the yellow lines in Figure 4).

Respiration in the seasonal thermocline is evident in the oxygen decrease over the stratified season (Figure 5). These layers are isolated from contact with the atmosphere, and the seasonal-scale influence of advection is low because the profiler mooring is located near the center of the gyre where the mean currents are relatively weak (de Jong et al., 2018, in this issue). Thus, oxygen decline over the stratified season reflects respiration of organic matter by heterotrophic organisms. We calculate the respiration over the stratified season at each depth interval as the oxygen decrease from the oxygen maximum at the onset of re-stratification (yellow dots in Figure 5) to the oxygen minimum at the end of the stratified season (cyan dots in Figure 5), yielding total respiration rates for all depths from 200–1,000 m within the seasonal thermocline (Figure 6).

Consistent with previous oxygen-based estimates of subsurface respiration (Martz et al., 2008; Hennon et al., 2016) and with canonical expectations for attenuation of organic matter flux with depth (J.M. Martin et al., 1987), total seasonal respiration is greatest near the top of the thermocline and decreases with depth (Figure 6). The duration of the stratified season over which this respiration occurs increases with depth, as re-stratification begins earlier and winter ventilation begins later deeper in the water column (stratification duration ranges from 194 ± 1 days at depths from 200–300 m to 280 ± 3 days at depths from 750–1,000 m; Figures 4 and 5). The total respiration within each depth interval is stoichiometrically related to an increase in dissolved inorganic carbon due to organic matter remineralization over the course of the stratified season, which is

then ventilated back to the atmosphere during winter. Integrated through the 200–1,000 m layer within the seasonal thermocline, $\sim 5.9 \text{ mol C m}^{-2}$ was remineralized ($8.3 \text{ mol O}_2 \text{ m}^{-2}$ consumed by respiration) over the 2015 stratified season prior to being entrained back into the mixed layer during winter ventilation in 2015/2016. This magnitude of winter ventilation is greater than that previously observed in other deep mixing regions (2.6 mol C m^{-2} in the eastern North Atlantic and 3.6 mol C m^{-2} in the western North Pacific; Körtzinger et al., 2008;

Palevsky et al., 2016a), consistent with the Irminger Sea's stronger spring bloom and deeper winter mixing that enhance the importance of thermocline remineralization and winter ventilation.

CONCLUSIONS

Carbon sequestration via the biological pump can be thought of as a “tug of war” between downward flux of organic matter from the surface during the stratified productive season and upward flux of remineralized organic matter during wintertime ventilation. Both of these

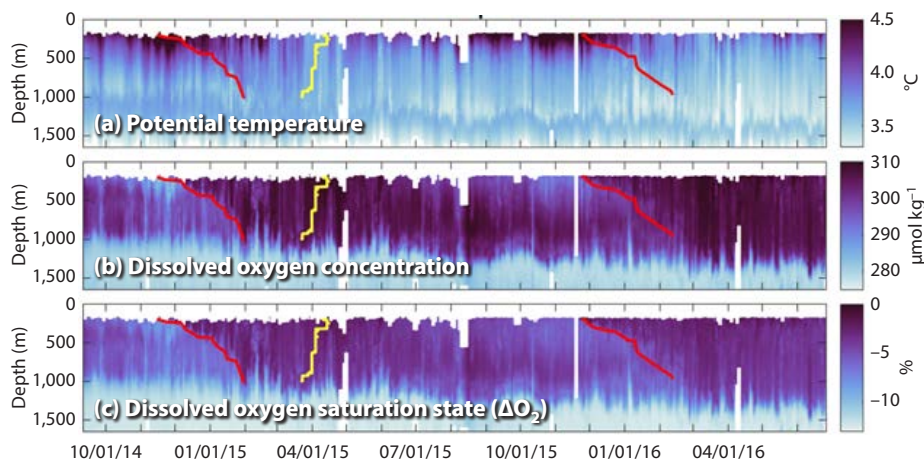


FIGURE 4. Time series of (a) potential temperature, (b) dissolved oxygen concentration, and (c) dissolved oxygen saturation state

$$(\Delta O_2 = \left(\frac{O_2, \text{observed}}{O_2, \text{equilibrium}} - 1 \right) * 100)$$

from the profiler mooring. Red lines indicate the beginning of winter ventilation in each year (determined as the time that the mixed layer first penetrates to a given depth), and yellow lines indicate the end of winter ventilation in 2015 (determined as the date of the late winter-early spring oxygen maximum at each depth; see Figure 5).

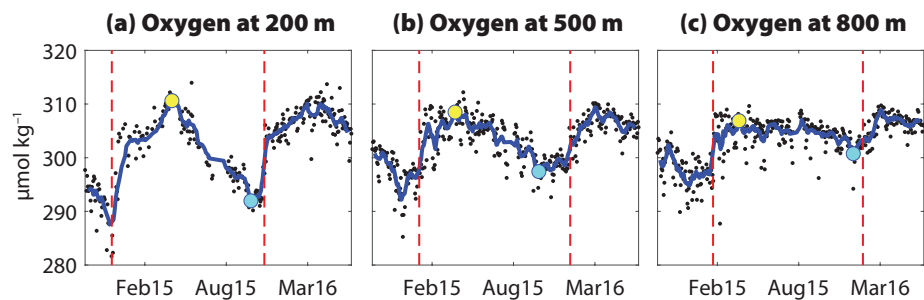


FIGURE 5. Examples of dissolved oxygen time series at (a) 200 m, (b) 500 m, and (c) 800 m depth from the profiler mooring over the first two years' deployment of the OOI Irminger Sea Array. Blue lines show the smoothed time series, determined as a 10-point filtered mean of all dissolved oxygen values gridded to each depth (black points). Red dashed lines indicate the date of initial winter ventilation in each year, determined as the time that the mixed layer first penetrates to the given depth. The end of winter ventilation (cyan dots) in spring 2015 is determined as the maximum dissolved oxygen concentration. The oxygen decrease from the end of winter ventilation (yellow dots) to the minimum oxygen concentration at the end of the stratified season (cyan dots) shows respiration of organic carbon within the seasonal thermocline.

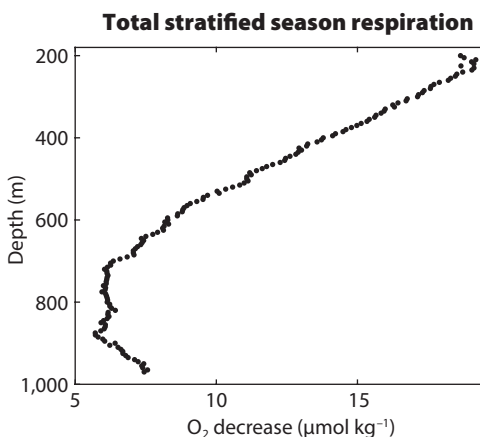


FIGURE 6. Total respiration in the seasonal thermocline (200–1,000 m depth) over the 2015 stratified season, calculated as the oxygen decrease from the end of winter ventilation in spring 2015 to the oxygen minimum at the end of the stratified season (from the yellow to the cyan dots in Figure 5). Thermocline respiration integrated through this full layer is $8.3 \text{ mol O}_2 \text{ m}^{-2}$, representing 5.9 mol C m^{-2} ventilated back to the atmosphere the subsequent winter ($\text{O}_2:\text{C}$ ratio of 1.4; Laws, 1991).

players “tug” especially hard in the subpolar North Atlantic (Figure 1). Data from the first two years of the new OOI Irminger Sea Array provide the first simultaneous observations of the seasonal progression of the biological pump in both the surface mixed layer and the seasonal thermocline in the subpolar North Atlantic Ocean. The spring bloom during April–May each year was associated with a dramatic increase in mixed layer dissolved oxygen, reflecting significant net autotrophic production during this period (Figures 2 and 3). Below the mixed layer, oxygen decline over the 2015 stratified season indicated high remineralization rates within the seasonal thermocline totaling $\sim 5.9 \text{ mol C m}^{-2}$ between 200 m and 1,000 m—greater than the total annual export from the surface in most parts of the ocean (Figures 5 and 6; Emerson, 2014). Deep winter convection extending below 1,000 m ventilated this respiration signature from the seasonal thermocline, maintaining surface dissolved oxygen concentrations below saturation throughout the winter months despite vigorous gas exchange acting to return mixed layer oxygen to saturation (Figures 3c and 4).

These results highlight the importance of accounting for remineralization within the seasonal thermocline and ventilation of respired carbon back to the atmosphere during winter mixing in order to accurately determine the influence of the biological pump on carbon sequestration, particularly in deep convection regions such as the Irminger Sea. However, a

limitation of this analysis is that mixed layer oxygen measurements cannot be calibrated with sufficient accuracy to enable a mass balance calculation of annual net community production at the winter ventilation depth or export from the mixed layer over the stratified season. The accuracy and utility of oxygen measurements from the Irminger Sea and other OOI arrays could be improved by configuring the glider oxygen sensors for in situ air calibration when surfacing between profiles (Nicholson and Feen, 2017), an approach previously proven on long-term Argo float deployments (Johnson et al., 2015; Bushinsky et al., 2016).

Given that winter convection over the initial two years of the OOI Irminger Sea Array’s deployment was significantly deeper than the climatological mean over the previous decade (de Jong and de Steur, 2016), future observations will play an important role in contextualizing the initial look into the Irminger Sea biological pump presented here. Ongoing time-series observations at the OOI Array, ideally with improved calibration of biogeochemical sensors, will enable future analysis of interannual variability in the timing and magnitude of the spring bloom, spring and summer net autotrophy in the surface mixed layer, thermocline remineralization, and winter ventilation. Biogeochemical sensor data from the OOI global arrays and other year-round observing systems (e.g., Biogeochemical Argo floats; Johnson and Claustre, 2016) provide a powerful tool for investigating carbon

cycling throughout the full annual cycle in the previously undersampled high-latitude ocean. ↗

SUPPLEMENTARY MATERIALS

Supplementary Text, Figures S1 and S2, and Tables S1 and S2, include details on all data used in this analysis and are available online at <https://doi.org/10.5670/oceanog.2018.108>.

REFERENCES

- Antia, N., R. Peinert, D. Hebbelin, U. Bathmann, U. Fehner, and B. Zeitzschel. 2001. Basin-wide particulate carbon flux in the Atlantic Ocean: Regional export patterns and potential for atmospheric CO_2 sequestration. *Global Biogeochemical Cycles* 15(4):845–862, <https://doi.org/10.1029/2000gb001376>.
- Behrenfeld, M.J., and E.S. Boss. 2014. Resurrecting the ecological underpinnings of ocean plankton blooms. *Annual Review of Marine Science* 6(1):167–194, <https://doi.org/10.1146/annurev-marine-052913-021325>.
- Bittig, H.C., and A. Körtzinger. 2015. Tackling oxygen optode drift: Near-surface and in-air oxygen optode measurements on a float provide an accurate in situ reference. *Journal of Atmospheric and Oceanic Technology* 32(8):1,536–1,543, <https://doi.org/10.1175/JTECH-D-14-00162.1>.
- Bittig, H.C., and A. Körtzinger. 2017. Technical note: Update on response times, in-air measurements, and in situ drift for oxygen optodes on profiling platforms. *Ocean Science* 13(1):1–11, <https://doi.org/10.5194/os-13-1-2017>.
- Briggs, N., M.J. Perry, I. Cetinić, C. Lee, E. D’Asaro, A.M. Gray, and E. Rehm. 2011. High-resolution observations of aggregate flux during a sub-polar North Atlantic spring bloom. *Deep Sea Research Part I* 58(10):1,031–1,039, <https://doi.org/10.1016/j.dsr.2011.07.007>.
- Buesseler, K.O., P. Michael, H.D. Livingston, and K. Cochrant. 1992. Carbon and nitrogen export during the JGOFS North Atlantic Bloom Experiment estimated from ^{234}Th - ^{238}U disequilibria. *Deep Sea Research* 39(7–8):1,115–1,137, [https://doi.org/10.1016/0198-0149\(92\)90060-7](https://doi.org/10.1016/0198-0149(92)90060-7).
- Bushinsky, S.M., S.R. Emerson, S.C. Riser, and D.D. Swift. 2016. Accurate oxygen measurements on modified Argo floats using in situ air calibrations. *Limnology and Oceanography: Methods* 14:491–505, <https://doi.org/10.1002/lom.31010>.
- Church, M.J., M.W. Lomas, and F. Müller-Karger. 2013. Sea change: Charting the course for biogeochemical ocean time-series research in a new millennium. *Deep Sea Research Part II* 93:2–15, <https://doi.org/10.1016/j.dsr2.2013.01.035>.
- Ciais, P., C. Sabine, G. Bala, L. Bopp, V. Brovkin, J. Canadell, A. Chhabra, R. DeFries, J. Galloway, M. Heimann, and others. 2013. Carbon and other biogeochemical cycles. Pp. 465–570. In *Climate Change 2013 - The Physical Science Basis. Contribution of Working Group I to the Fifth Assessment Report of the Intergovernmental Panel on Climate Change*. T.F. Stocker, D. Qin, G.-K. Plattner, M. Tignor, S.K. Allen, J. Boschung, A. Nauels, Y. Xia, and V. Bex, eds. Cambridge University Press, Cambridge, United Kingdom and New York, NY, USA, <https://doi.org/10.1017/CBO9781107415324.015>.
- D’Asaro, E.A., and C. McNeil. 2013. Calibration and stability of oxygen sensors on autonomous floats. *Journal of Atmospheric and Oceanic Technology* 30:1,896–1,906, <https://doi.org/10.1175/JTECH-D-12-00222.1>.
- Dall’Olmo, G., J. Dingle, L. Polimene, R.J.W. Brewin, and H. Claustre. 2016. Substantial energy input to the mesopelagic ecosystem from the seasonal mixed-layer pump. *Nature Geoscience* 9:820–823, <https://doi.org/10.1038/ngeo2818>.

- de Boyer Montégut, C., G. Madec, A.S. Fischer, A. Lazar, and D. Iudicone. 2004. Mixed layer depth over the global ocean: An examination of profile data and a profile-based climatology. *Journal of Geophysical Research* 109, C12003, <https://doi.org/10.1029/2004JC002378>.
- de Jong, M.F., and L. de Steur. 2016. Strong winter cooling over the Irminger Sea in winter 2014–2015, exceptional deep convection, and the emergence of anomalously low SST. *Geophysical Research Letters* 43(13):7,106–7,113, <https://doi.org/10.1002/2016GL069596>.
- de Jong, M.F., M. Oltmanns, J. Karstensen, and L. de Steur. 2018. Deep convection in the Irminger Sea observed with a dense mooring array. *Oceanography* 31(1):50–59, <https://doi.org/10.5670/oceanog.2018.109>.
- de Jong, M.F., H.M. Van Aken, K. Våge, and R.S. Pickart. 2012. Convective mixing in the central Irminger Sea: 2002–2010. *Deep Sea Research Part I* 63:36–51, <https://doi.org/10.1016/j.dsr.2012.01.003>.
- DeVries, T., F. Primeau, and C. Deutsch. 2012. The sequestration efficiency of the biological pump. *Geophysical Research Letters* 39, L13601, <https://doi.org/10.1029/2012GL051963>.
- Emerson, S. 2014. Annual net community production and the biological carbon flux in the ocean. *Global Biogeochemical Cycles* 28:14–28, <https://doi.org/10.1002/2013GB004680>.
- Emerson, S., and S. Bushinsky. 2014. Oxygen concentrations and biological fluxes in the open ocean. *Oceanography* 27(1):168–171, <https://doi.org/10.5670/oceanog.2014.20>.
- Field, C.B., M.J. Behrenfeld, J.T. Randerson, and P. Falkowski. 1998. Primary production of the biosphere: Integrating terrestrial and oceanic components. *Science* 281(5374):237–240, <https://doi.org/10.1126/science.281.5374.237>.
- Garcia, H.E., and L.I. Gordon. 1992. Oxygen solubility in seawater: Better fitting solubility equations. *Limnology and Oceanography* 37(6):1,307–1,312, <https://doi.org/10.4319/lo.1992.37.6.1307>.
- Hennon, T.D., S.C. Riser, and S. Mecking. 2016. Profiling float-based observations of net respiration beneath the mixed layer. *Global Biogeochemical Cycles* 30:920–932, <https://doi.org/10.1002/2016GB005380>.
- Henson, S.A., C. Beaulieu, and R. Lampitt. 2016. Observing climate change trends in ocean biogeochemistry: When and where. *Global Change Biology* 22:1,561–1,571, <https://doi.org/10.1111/gcb.13152>.
- Henson, S.A., J.P. Dunne, and J.L. Sarmiento. 2009. Decadal variability in North Atlantic phytoplankton blooms. *Journal of Geophysical Research* 114(4):1–11, <https://doi.org/10.1029/2008JC005139>.
- Henson, S.A., I. Robinson, J.T. Allen, and J.J. Waniek. 2006. Effect of meteorological conditions on interannual variability in timing and magnitude of the spring bloom in the Irminger Basin, North Atlantic. *Deep Sea Research Part I* 53:1,601–1,615, <https://doi.org/10.1016/j.dsr.2006.07.009>.
- Johnson, K.S., and H. Claustre. 2016. Bringing Biogeochemistry into the Argo Age. *Eos* 97, <https://doi.org/10.1029/2016EO062427>.
- Johnson, K.S., J.N. Plant, S.C. Riser, and D. Gilbert. 2015. Air oxygen calibration of oxygen optodes on a profiling float array. *Journal of Atmospheric and Oceanic Technology* 32(11):2,160–2,172, <https://doi.org/10.1175/JTECH-D-15-0101.1>.
- Khatiwala, S., F. Primeau, and T. Hall. 2009. Reconstruction of the history of anthropogenic CO₂ concentrations in the ocean. *Nature* 462(7271):346–349, <https://doi.org/10.1038/nature08526>.
- Körtzinger, A., U. Send, R.S. Lampitt, S. Hartman, D.W.R. Wallace, J. Karstensen, M.G. Villagarcía, O. Llinás, and M.D. DeGrandpre. 2008. The seasonal pCO₂ cycle at 49°N/16.5°W in the north-eastern Atlantic Ocean and what it tells us about biological productivity. *Journal of Geophysical Research* 113, C04020, <https://doi.org/10.1029/2007JC004347>.
- Laws, E.A. 1991. Photosynthetic quotients, new production and net community production in the open ocean. *Deep Sea Research* 38(1):143–167, [https://doi.org/10.1016/0198-0149\(91\)90059-O](https://doi.org/10.1016/0198-0149(91)90059-O).
- Laws, E.A., E. D'Sa, and P. Naik. 2011. Simple equations to estimate ratios of new or export production to total production from satellite-derived estimates of sea surface temperature and primary production. *Limnology and Oceanography: Methods* 9:593–601, <https://doi.org/10.4319/lom.2011.9.593>.
- Le Quéré, C., R.M. Andrew, J.G. Canadell, S. Sitch, J.I. Korsbakken, G.P. Peters, A.C. Manning, T.A. Boden, P.P. Tans, R.A. Houghton, and others. 2016. Global carbon budget 2016. *Earth System Science Data* 8:605–649, <https://doi.org/10.5194/essd-8-605-2016>.
- Martin, J.M., G.A. Knauer, D.M. Karl, and W.W. Broenkow. 1987. VERTEX: Carbon cycling in the Northeast Pacific. *Deep Sea Research* 34(2):267–285, [https://doi.org/10.1016/0198-0149\(87\)90086-0](https://doi.org/10.1016/0198-0149(87)90086-0).
- Martin, P., R.S. Lampitt, M.J. Perry, R. Sanders, C. Lee, and E. D'Asaro. 2011. Export and mesopelagic particle flux during a North Atlantic spring diatom bloom. *Deep Sea Research Part I* 58:338–349, <https://doi.org/10.1016/j.dsr.2011.01.006>.
- Martz, T.R., K.S. Johnson, and S.C. Riser. 2008. Ocean metabolism observed with oxygen sensors on profiling floats in the South Pacific. *Limnology and Oceanography* 53(5, part 2):2,094–2,111, https://doi.org/10.4319/lo.2008.53.5_part_2.2094.
- Nicholson, D.P., and M.L. Feen. 2017. Air calibration of an oxygen optode on an underwater glider. *Limnology and Oceanography: Methods* 15:495–502, <https://doi.org/10.1002/lim3.10177>.
- Oschlies, A., and P. Kahler. 2004. Biotic contribution to air-sea fluxes of CO₂ and O₂ and its relation to new production, export production, and net community production. *Global Biogeochemical Cycles* 18, GB1015, <https://doi.org/10.1029/2003GB002094>.
- Palevsky, H.I., P.D. Quay, D.E. Lockwood, and D.P. Nicholson. 2016a. The annual cycle of gross primary production, net community production, and export efficiency across the North Pacific Ocean. *Global Biogeochemical Cycles* 30:361–380, <https://doi.org/10.1002/2015GB005318>.
- Palevsky, H.I., P.D. Quay, and D.P. Nicholson. 2016b. Discrepant estimates of primary and export production from satellite algorithms, a biogeochemical model and geochemical tracer measurements in the North Pacific Ocean. *Geophysical Research Letters* 43:8,645–8,653, <https://doi.org/10.1002/2016GL070226>.
- Pickart, R.S., M.A. Spall, M.H. Ribergaard, G.W.K. Moore, and R.F. Milliff. 2003. Deep convection in the Irminger Sea forced by the Greenland tip jet. *Nature* 424(6945):152–156, <https://doi.org/10.1038/nature01729>.
- Quay, P., J. Stutsman, and T. Steinhoff. 2012. Primary production and carbon export rates across the sub-polar N. Atlantic Ocean basin based on triple oxygen isotope and dissolved O₂ and Ar gas measurements. *Global Biogeochemical Cycles* 26, GB2003, <https://doi.org/10.1029/2010GB004003>.
- Sabine, C.L., R.A. Feely, N. Gruber, R.M. Key, K. Lee, J.L. Bullister, R. Wanninkhof, C. Wong, D.W.R. Wallace, B. Tilbrook, and others. 2004. The oceanic sink for anthropogenic CO₂. *Science* 305:367–371, <https://doi.org/10.1126/science.1097403>.
- Sabine, C.L., and T. Tanhua. 2010. Estimation of anthropogenic CO₂ inventories in the ocean. *Annual Review of Marine Science* 2:175–198, <https://doi.org/10.1146/annurev-marine-120308-080947>.
- Sanders, R., S.A. Henson, M. Koski, C.L. De La Rocha, S.C. Painter, A.J. Poulton, J. Riley, B. Salihoglu, A. Visser, A. Yool, and others. 2014. The biological carbon pump in the North Atlantic. *Progress in Oceanography* 129:200–218, <https://doi.org/10.1016/j.pocean.2014.05.005>.
- Sarmiento, J.L., and N. Gruber. 2006. *Ocean Biogeochemical Dynamics*. Princeton University Press, Princeton, NJ. 526 pp.
- Siegel, D.A., K.O. Buesseler, S.C. Doney, S.F. Sailley, M.J. Behrenfeld, and P.W. Boyd. 2014. Global assessment of ocean carbon export by combining satellite observations and food-web models. *Global Biogeochemical Cycles* 28:181–196, <https://doi.org/10.1002/2013GB004743>.
- Stukel, M.R., M. Kahru, C.R. Benitez-Nelson, M. Decima, R. Goericke, M.R. Landry, and M.D. Ohman. 2015. Using Lagrangian-based process studies to test satellite algorithms of vertical carbon flux in the eastern North Pacific Ocean. *Journal of Geophysical Research* 120:7,208–7,222, <https://doi.org/10.1002/2015JC011264>.
- Takeshita, Y., T.R. Martz, K.S. Johnson, J.N. Plant, D. Gilbert, S.C. Riser, C. Neill, and B. Tilbrook. 2013. A climatology-based quality control procedure for profiling float oxygen data. *Journal of Geophysical Research* 118:5,640–5,650, <https://doi.org/10.1002/jgrc.20399>.
- Volk, T., and M.I. Hoffert. 1985. Ocean carbon pumps: Analysis of relative strengths and efficiencies in ocean-driven atmospheric CO₂ changes. Pp. 99–110 in *The Carbon Cycle and Atmospheric CO₂ Natural Variations Archean to Present*. E.T. Sundquist and W.S. Broecker, eds, Geophysical Monograph Series, vol. 32, American Geophysical Union, Washington, DC.

ACKNOWLEDGMENTS

We are grateful to the many people involved in the planning, deployment, operation, and data management of the Ocean Observatories Initiative, and to the National Science Foundation for OOI funding. We thank Robert Weller, Paul Quay, Robert Vaillancourt, and an anonymous reviewer for constructive feedback that improved the manuscript. Hilary Palevsky acknowledges support from the Postdoctoral Scholar Program at the Woods Hole Oceanographic Institution, with funding provided by the Weston Howland Jr. Postdoctoral Scholarship.

AUTHORS

Hilary I. Palevsky (hpalevsky@whoi.edu) is Postdoctoral Scholar and **David P. Nicholson** is Associate Scientist, both in the Department of Marine Chemistry and Geochemistry, Woods Hole Oceanographic Institution, Woods Hole, MA, USA.

ARTICLE CITATION

Palevsky, H.I., and D.P. Nicholson. 2018. The North Atlantic biological pump: Insights from the Ocean Observatories Initiative Irminger Sea Array. *Oceanography* 31(1):42–49, <https://doi.org/10.5670/oceanog.2018.108>.

Deep Convection in the Irminger Sea Observed with a Dense Mooring Array

By M. Femke de Jong, Marilena Oltmanns,
Johannes Karstensen, and Laura de Steur

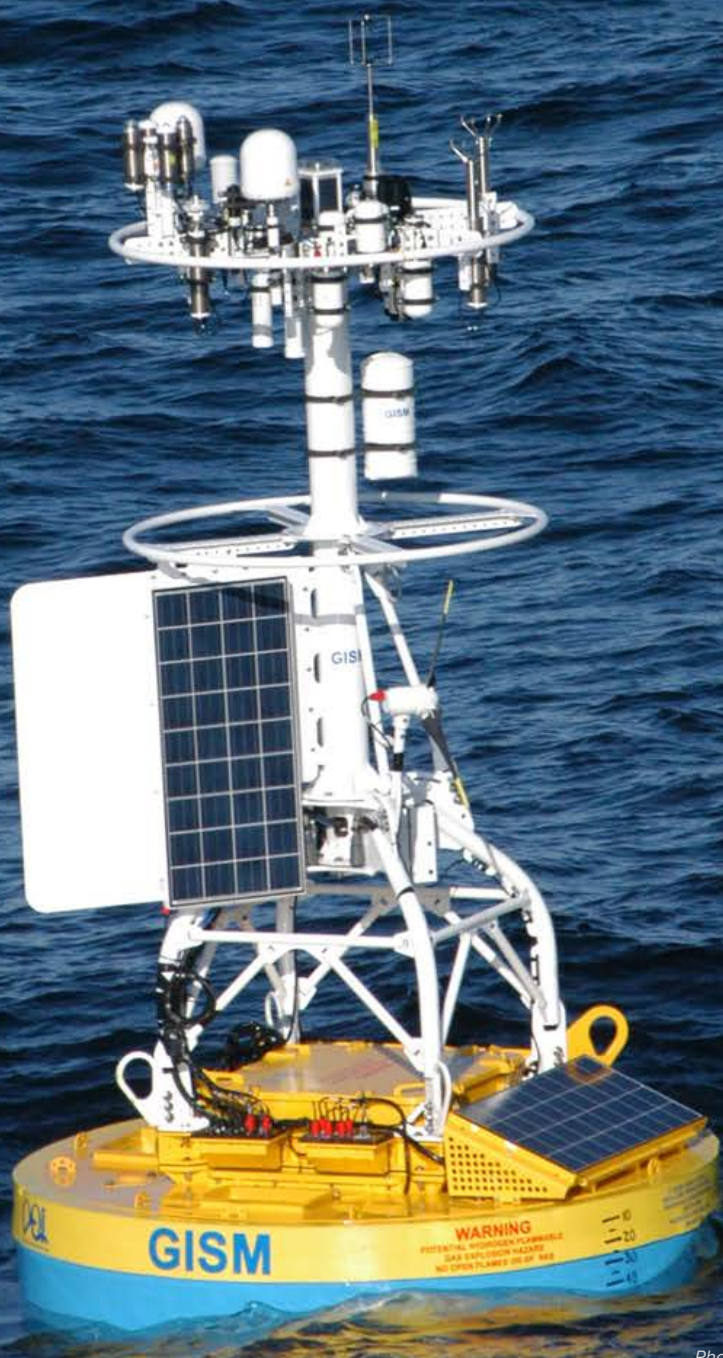


Photo credit: Daniel J. Bogorff

“ Only high-resolution spatial and temporal observations can provide sufficient detail for learning more about the impact of eddies on restratification, and the relationship of restratification to convective mixing. ”

ABSTRACT. Deep convection is a key process in the Atlantic Meridional Overturning Circulation, but because it acts at small scales, it remains poorly resolved by climate models. The occurrence of deep convection depends on weak initial stratification and strong surface buoyancy forcing, conditions that are satisfied in only a few ocean basins. In 2014, one of the Ocean Observatories Initiative (OOI) global arrays was installed close to the Central Irminger Sea (CIS) and the Long-term Ocean Circulation Observations (LOCO) moorings in the central Irminger Sea. These programs' six moorings are located in the center of an area of deep convection and are distributed within a 50 km radius, thus offering detailed insight into spatial differences during the strong convection events that occurred during the winters of 2014/2015 and 2015/2016. Deep mixed layers, down to approximately 1,600 m, formed during both winters. The properties of the convectively renewed water mass at each mooring converge to a common temperature and salinity before restratification sets in at the end of winter. The largest differences in onset (or timing) of convection and restratification are seen between the northernmost and southernmost moorings. High-resolution atmospheric reanalysis data show there is higher atmospheric forcing at the northernmost mooring due to a more favorable position with respect to the Greenland tip jet. Nevertheless, earlier onset, and more continuous cooling and deepening of mixed layers, occurs at the southernmost mooring, while convection at the northern mooring is frequently interrupted by warm events. We propose that these warm events are associated with eddies and filaments originating from the Irminger Current off the coast of Greenland and that convection further south benefits from cold inflow from the southwest.

INTRODUCTION

Ventilation of the ocean's deep layers is a process that combines intense water mass transformation in so-called “deep-water formation areas” and the subsequent export of the waters. Only a limited number of deepwater formation areas have been identified globally, including the Weddell and Ross Seas in the Southern Ocean, the Gulf of Lyon in the Mediterranean, the Greenland Sea, and the Labrador and Irminger Seas in

the North Atlantic. All of these regions are characterized by a marginally stable water column at mid-depth that underlies a seasonally stratified layer above, and strong, although intermittent, surface buoyancy losses. Heat loss is an important contributor to buoyancy loss in all areas. The haline buoyancy flux, which depends on net precipitation and, in some areas, ice melting and freezing (including brine release), is of varying importance.

The deep convection process is

traditionally separated into three stages (Marshall and Schott, 1999, and references therein). The “preconditioning” stage is set by a large-scale (order of 100 km) cyclonic circulation and weak interior ocean stratification. Intense surface buoyancy flux initiates the second, “violent mixing,” stage, which generates localized, intense convective plumes that have similar horizontal and vertical dimensions (order of 1–2 km). As mixing progresses, these cells organize into a larger-scale convective patch (diameter order 100 km) that is characterized by relatively homogenous properties. The third stage, “restratification,” sets in when surface buoyancy flux ceases, and the density front between the convective patch and the stratified environment becomes unstable and breaks down into eddies (on the order of the Rossby deformation radius or roughly 10 km at subpolar latitudes). The net effect of these eddies is a lateral exchange that, together with recurring surface buoyancy gain, reestablishes the upper layer stratification and contributes to the export of water out of the mixed patch.

The processes active during the three stages of deep convection have been directly observed with mixed success and never in a complete sequence that covers all stages and all scales (see Schott and Marshall for a review of the experiment before 1999). In winter, field programs

have made direct observations of convective cells, including early ones (Lazier, 1973; Killworth, 1979). These high-temporal-resolution shipboard observations were generally limited to one location and the duration of a typical field program (a few weeks). Recent intense field programs, executed in the western Mediterranean Sea using ship-based and autonomous observing platforms (glider, moorings), were the first to provide further details about scales and processes for the Mediterranean deep convection across a whole seasonal cycle (Bosse et al., 2016; Houpert et al., 2016; Testor et al., 2017).

In the Irminger and Labrador Seas, which are both part of the North Atlantic Subpolar Gyre, intermittent deep convection contributes to the renewal process, creating the source waters that ultimately supply the upper North Atlantic Deep Water. The first evidence that deep convection occurs in the Irminger Sea was from ship-based observations dating to the beginning of the last century (Nansen,

1912; Sverdrup et al., 1942; Pickart et al., 2003; Våge et al., 2008; de Jong et al., 2012). Post-winter hydrographic sections, executed from the 1970s to 2000s, showed the extent of homogenous water masses in the Irminger Sea. These observations suggested deep convection had occurred during the preceding winter. In order to survey the winter conditions, two observing sites were established in the region at the beginning of the 2000s (Figure 1; Long-term Ocean Circulation Observations [LOCO], Central Irminger Sea [CIS]) with year-round observation through moored sensors and regular ship visits. The CIS site was established in September 2002 by GEOMAR (Kiel, Germany), and the LOCO site was installed one year later in September 2003; the latter has since been maintained by the Royal Netherlands Institute for Sea Research (de Jong et al., 2012).

The preconditioning phase of deep convection includes cyclonic circulation, doming of isopycnals, and large

buoyancy fluxes. However, the location of the maximum doming of the isopycnals in the Irminger Gyre center is not necessarily aligned with the region of maximum wintertime thermal buoyancy loss. Atmospheric variability in this region is characterized by intense and intermittent wind events that can reach surface speeds well above 30 m s^{-1} and that result from the interaction of extratropical cyclones with the high topography of southern Greenland (Moore, 2003). Among these wind events are the so-called “Greenland tip jets” that are associated with enhanced westerly flow around the southern tip of Greenland (Doyle and Shapiro, 1999) at horizontal scales on the order of 200–400 km (Moore and Renfrew, 2005). Tip jets are known to drive significant air-sea heat fluxes in the Irminger Sea, and as such contribute to deep convection in this region (Pickart et al., 2003; Våge et al., 2008).

Depending on the alignment of the regions of the largest buoyancy forcing with those of weak stratification (defining the gyre center), deep convection may regionally vary. In 2013, the Ocean Observatories Initiative (OOI) formalized plans for installing one of its four global arrays in the Irminger Sea. The installation was targeted to improve process understanding of deep convection, and also contribute to the long-term monitoring (multi-annual to decadal) of convection in the region that had been initiated in the early 2000s with the LOCO and CIS moorings. In order to ensure the compatibility of the records already available from LOCO and CIS, the three sites were run simultaneously beginning in the summer of 2014, providing an opportunity to obtain very high sampling density (Figure 1).

The particularly strong and sustained cooling during the winter of 2014/2015 led to record deep mixing in the convection centers of the Labrador (Yashayaev and Loder, 2017) and Irminger Seas, a process that had never been directly observed in this region (de Jong and de Steur, 2016). We used this unique multi-mooring data

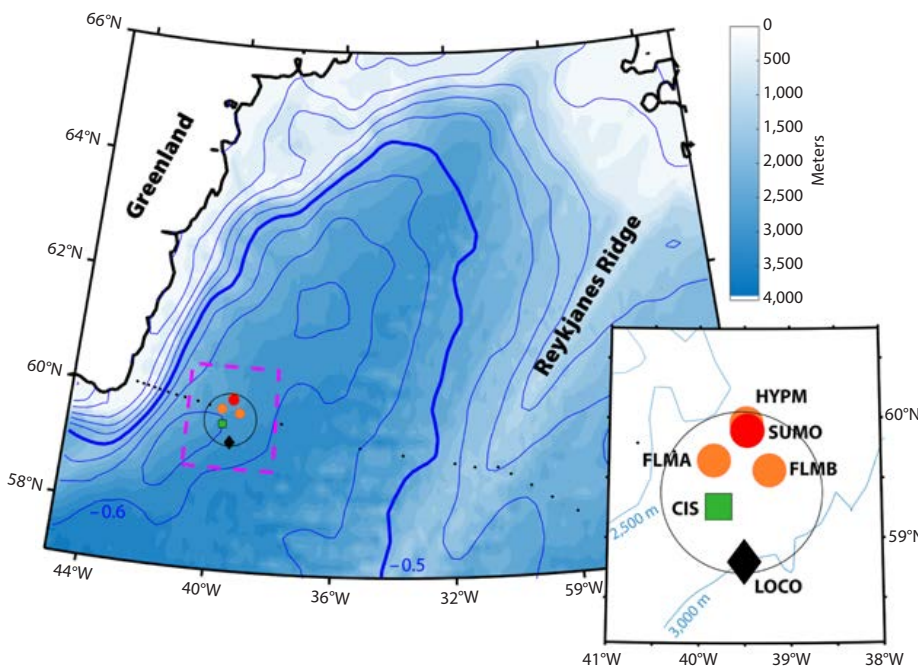


FIGURE 1. Mooring positions in the central Irminger Gyre. Contour lines of absolute dynamic topography (plotted every 0.05 m and averaged from January 1, 2014, to December 31, 2016) indicate the center of the Irminger Gyre. The map at right is closer-up of the magenta dashed box in the left panel. The four Ocean Observatories Initiative (OOI) moorings are indicated by the red and orange circles, with the red circle indicating the surface mooring. The Central Irminger Sea (CIS) and Long-term Ocean Circulation Observations (LOCO) moorings are indicated by a green square and a black diamond, respectively. The six moorings are located within the 50 km radius circle drawn in black. The Overturning in the Subpolar North Atlantic Program (OSNAP) moorings in the Irminger Sea (not part of this study) are indicated by the small black dots.

set collected from 2014 to 2016 to take a detailed look into the onset, spatial evolution, and duration of convection over the winters of 2014/2015 and 2015/2016.

DATA

The OOI Irminger Sea array consists of four individual moorings. Its location was chosen to be close to the maximum doming of isopycnals derived from the contours of dynamic topography and to align with the AR7E World Ocean Circulation Experiment repeat section (Figure 2) as well as the Overturning in the Subpolar North Atlantic Program (OSNAP) array (Lozier et al., 2017). The OOI moorings contain a large variety of sensors that serve various disciplines, but for this study we focus on temperature, salinity, and velocity measurements only. The surface mooring, SUMO, consists of fixed oceanographic instruments that include SBE 37 MicroCAT conductivity and temperature recorders and Teledyne RDI acoustic Doppler current profilers [ADCPs]) along the cable down to 1,500 m, a buoy equipped with meteorological instrumentation, and a telemetric system for near-real-time data transfer. The profiling mooring, HYPMP (59.98°N, 39.48°W), is outfitted with a McLane profiler that traverses the cable between 240 m and 2,400 m depth. Two flanking moorings, FLMA (59.77°N, 39.84°W) and FLMB (59.71°N, 39.32°W), are located 34.8 km apart and each about 28 km from the SUMO (59.93°N, 39.47°W) mooring. FLMA and FLMB contain instruments at discrete depths from 30 m to 2,700 m. Because we are focusing on the surface to intermediate layers affected by convective mixing, we use data from the instrumentation between the sea surface and 2,000 dbar. OOI data used here cover the period from September 10, 2014, to July 18, 2016. Details about the instruments between these levels can be found in Table 1.

The CIS mooring is located 28.6 km south of the OOI FLMA mooring at 59°31.83'N, 39°47.03'W. Before the OOI array installation, CIS was located close

to SUMO/HYPMP. The data analyzed here originate from the thirteenth deployment of the mooring from August 18, 2014, to May 30, 2016. At that time, the mooring was equipped with 15 MicroCATs (14 at various depths between 10 m and 1,500 m and one close to the seafloor; see Table 1), two single-point current meters (1,000 m and 2,953 m depth), and an upward-looking ADCP (150 m depth), as well as an oxygen optode and a fluorometer whose data are not used in this study. All given depths are nominal positions, but instantaneous depths may vary by several hundreds of meters, depending on mooring blow-down. The mooring was deployed with a subsurface head buoy located at about 40 m depth and a surface buoy connected with a 270 m long wire to the head buoy in order to allow the surface module to move with minimal tension on the whole mooring. This “slack wire” had a MicroCAT at 10 m depth and one at 25 m depth to obtain near-surface observational data. The surface telemetry buoy (MI.SAT1; Devologic) broke off on April 7, 2015, and the two instruments in the slack descended to about 300 m depth.

The LOCO mooring is located at 59°12.05'N/39°30.00'W, 37.8 km southeast of the CIS mooring and 58.7 km from the nearest OOI (FLMB) mooring.

The mooring was outfitted with a McLane moored profiler to record daily temperature and salinity profiles between 150 m and 2,500 m depth. The LOCO mooring also contained two downward-looking ADCPs at 150 m and 2,500 m depth as well as a moored CTD near the bottom. Due to a technical failure, the LOCO profiler did not record profiles during the July 2015 to September 2016 deployment.

Mixed-layer depths (MLDs) were derived from the OOI HYPMP and LOCO moored profiling data. These profiles have high vertical resolution, as the profilers record continuously while traveling along the cable. The temporal resolution (20-hour interval for OOI HYPMP, 24-hour interval for LOCO) is limited due to the battery capacity of the profiler. The bottom of the mixed layer was identified from the potential temperature, practical salinity, and potential density profiles. These profiles were smoothed using a running-mean filter with a 25 dbar window to remove instrument noise. MLDs were subsequently determined employing threshold criteria of 0.015°C for temperature, 0.005 for salinity, and 0.0025 kg m⁻³ for potential density, and using the uppermost available measurement at a mooring as a reference. The uppermost measurement had to be shallower than 200 dbar

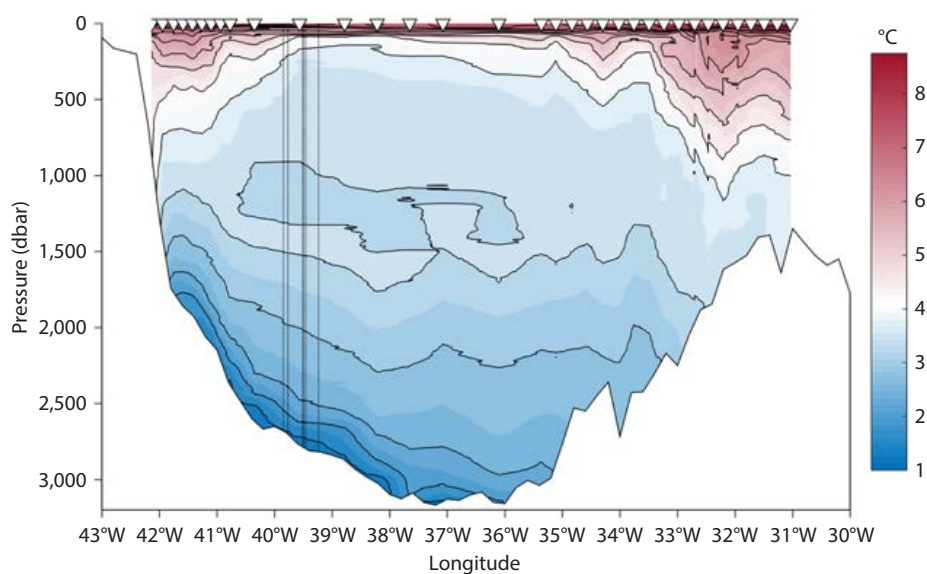


FIGURE 2. Hydrography of the Irminger Sea in summer 2015. Colors indicate potential temperature in degrees Celsius. CTD station locations are marked on the top axis by inverted white triangles. The mooring positions are projected onto the CTD line and shown as black vertical lines.

TABLE 1. Instrumentation on the six moorings used in this study. The Sea-Bird Electronics (SBE) 37, SBE 16plus, and McLane Moored Profiler (MMP) data include temperature, salinity, and pressure. The acoustic Doppler Current profilers (ADCPs) and Aquadopp Deep Water (DW) measure horizontal and vertical water velocities. The Rotating Current Meter (RCM-8) measures only horizontal velocities.

Nominal Depth (m)	OOI HYPM	OOI SUMO	OOI FLMA	OOI FLMB	CIS	LOCO
10		SBE 16plus			SBE3 7	
20		SBE 37				
30			SBE 37	SBE 37	SBE 37	
40		SBE 16plus	SBE 37	SBE 37	SBE 37	
60		SBE 37	SBE 37	SBE 37		
80		SBE 16plus				
90			SBE 37	SBE 37	SBE 37	
100		SBE 37				
130		SBE 16plus	SBE 37	SBE 37		SBE 37/ADCP
140	SBE 37					
150						ADCP
180		SBE37	SBE 37	SBE 37		
230	MMP				SBE 37	
250		SBE37	SBE 37	SBE 37		
310					SBE 37	
350		SBE37	SBE 37	SBE 37		
390					SBE 37	
470					SBE 37	
500		SBE 37/ADCP	SBE 37/ADCP	SBE 37/ADCP		
550					ADCP	
630					SBE 37	
750		SBE 37	SBE 37	SBE 37	SBE 37	
870					SBE 37	
1,000		SBE 37	SBE 37	SBE 37	Aquadopp DW	
1,250					SBE 37	
1,500		SBE 37	SBE 37	SBE 37	SBE 37	
1,700			SBE 37			
1,830				SBE 37		
2,000			SBE 37	SBE 37		
2,500						
2,550						ADCP
2,950					SBE 37/RCM-8	SBE 37

for an MLD to be registered. The resulting MLDs of all three variables had to be within 50 dbar to be accepted, after which the temperature-derived MLDs were chosen as final MLDs.

The temperature profilers from the OOI HYPM and LOCO moored profilers (limited by the uppermost instrument being at ~130 m depth) were extended toward the surface using sea surface temperature (SST) data (Group for High Resolution Sea Surface Temperature [GHRSST] at <https://podaac.jpl.nasa.gov/GHRSST>). GHRSST is a blended product with 0.1° resolution that was validated using the near-surface CTD data from the OOI SUMO mooring (average difference between the instrument time series at 12 m depth, and the SST is 0.085°C).

The moored CTDs on the OOI SUMO, OOI FLMA, OOI FLMB, and CIS moorings offered high temporal resolution (15 min) but limited vertical resolution (up to 250 m). For each mooring, these data were first gridded vertically onto a pressure grid with a 5 dbar interval, and then vertically interpolated. Due to the lack of a sharp transition at the bottom of the MLD in the interpolated MicroCAT data, the timing of mixing events was determined by inspecting the data for layers that have a homogeneous temperature profile and are cooling homogeneously over said layer. The chosen thresholds are $T(z)$ within 0.015°C of the temperature at 10 m depth and temperature change per 15 min interval (dT/dt) within 2.5×10^{-5} °C of the dT/dt at 10 m. The addition of the dT/dt criterion implies that active mixed layers are selected.

Mean velocities were derived for the layer between 200 m and 500 m depth using data from the upward-looking ADCP at ~500 m depth on the OOI SUMO, FLMA, and FLMB moorings and the downward-looking ADCP at ~150 m on the LOCO mooring. At the CIS mooring, we used velocity data from the single-point instrument at ~1,000 m.

The atmospheric forcing was investigated with the European Center for Medium range Weather Forecasting

(ECMWF) reanalysis ERA-Interim (ERA-I; Dee et al., 2011) and the Arctic System Reanalysis (ASR; Bromwich et al., 2016). ASR has a higher horizontal resolution (~15 km) compared to ERA-I (~80 km), yielding an improved representation of the wind and heat flux fields (Moore et al., 2016). Because ASR data are currently available up until 2012 only, we use them to examine the spatial distribution of the heat fluxes during selected tip jet events near the moorings for the period 2000–2012 and then translate those results to the events in the winters 2014/2015 and 2015/2016 identified with ERA-I.

RESULTS

Spatial Variations in Convection

Both the winters of 2014/2015 and 2015/2016 were characterized by strong surface fluxes and deep mixed layers in the Irminger Sea (Figure 3). The 2014/2015 winter was somewhat stronger and lasted longer than the subsequent winter. The October through April mean values from the ERA-I turbulent flux were 178 W m⁻² in 2014–2015 versus 123 W m⁻² in 2015/2016 (Figure 3a). The daily maximum MLD was derived for the six moorings in 2014/2015 and for five moorings in 2015/2016. Despite the substantially lower heat flux in 2015/2016,

mixed layers reached similar depths at the end of that winter, likely due to the extensive removal of stratification during the first winter. The local temperature variability at each mooring as well as the differences between the moorings was high during summer and quickly decreased as MLD depths reached ~250 dbar (Figure 3b,c). Progressive deepening and cooling of the mixed layer did not further reduce the variability in mixed layer properties between the moorings, indicating that a mixed patch, with homogeneous properties over the region enclosing all moorings, had formed at this time.

The velocity fields at the mooring sites,

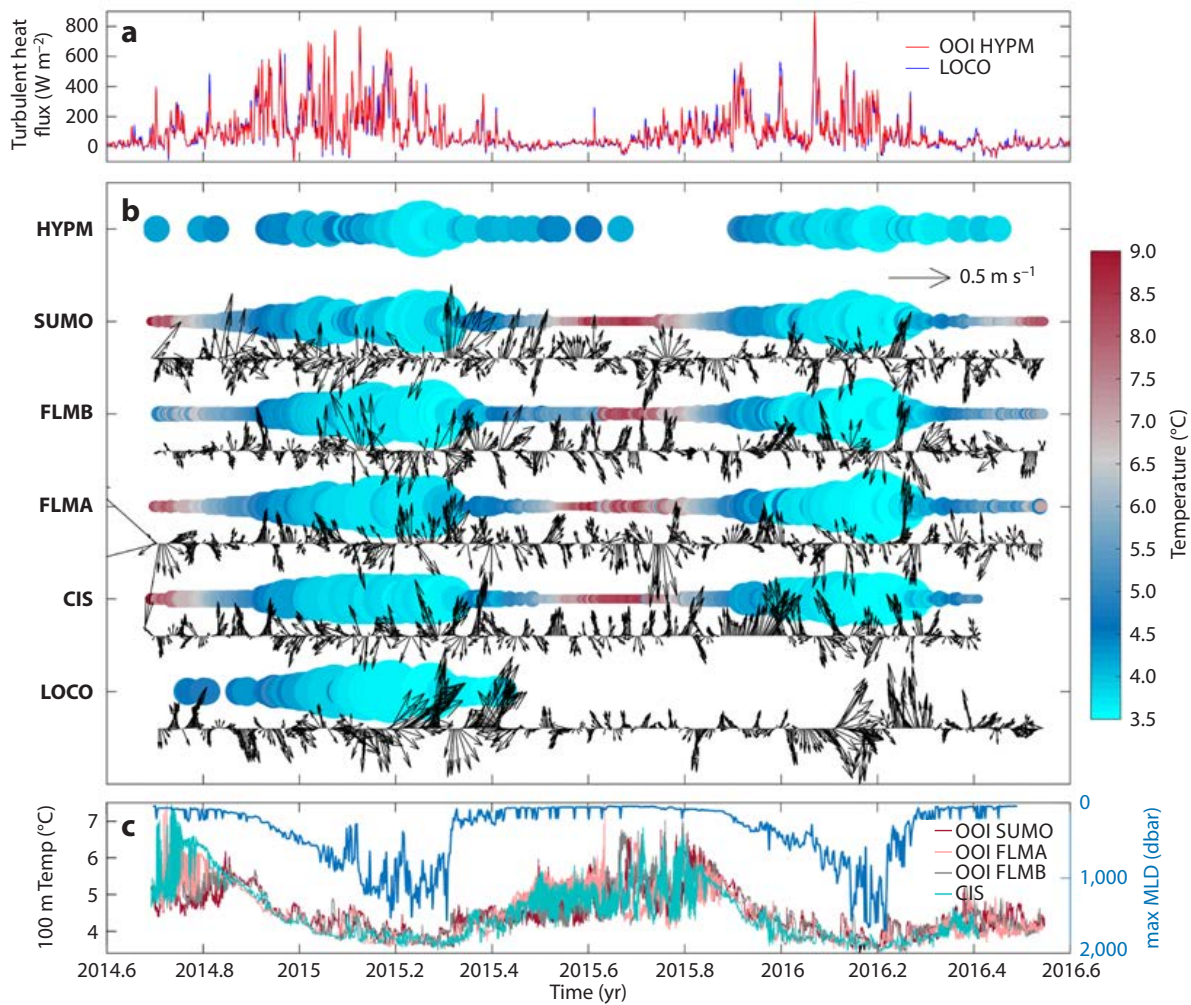


FIGURE 3. Surface fluxes and mixing during the 2014/2016 OOI deployment. (a) Time series of turbulent heat fluxes at the northernmost (red) and southernmost (blue) mooring. Data are derived from the ERA-I reanalysis. (b) Mixed layer depth, temperature, and velocity at the six moorings. Mixed layer depths are indicated by the sizes of the markers, and the mixed layer temperature is indicated with color (values are plotted daily for OOI HYPM and LOCO and thrice daily for OOI SUMO, the two flanking moorings FLMA and FLMB, and CIS). Velocity vectors are plotted every hour. Note that the velocities at the CIS mooring are obtained from a deeper depth (1,000 m rather than ~250 m). (c) Daily maximum mixed layer depth (blue) and the temperature from the four moorings with temperature measurements at 100 m depth.

displayed by the vectors in Figure 3b, showed the proximity to the center of the Irminger Gyre. Mean currents at the moorings were generally weak at the OOI moorings (between 0.6 cm s^{-1} and 1.7 cm s^{-1}) and slightly stronger toward the northeast at the CIS and LOCO moorings (3.5 cm s^{-1} and 4.2 cm s^{-1}). Despite the weak mean flow, the mesoscale field was rich (i.e., the standard deviation in velocity is 19 cm s^{-1} at the OOI moorings, 17 cm s^{-1} at LOCO, and 11 cm s^{-1} at the deeper CIS instrument). Due to the relatively large distance between the moorings compared to the Rossby radius of deformation (order 10 km), there was little coherence between the fluctuations observed at the individual moorings. The magnitude of the mesoscale variability showed a hint of the presence of a seasonal cycle, with larger velocities in winter, mostly evident at LOCO.

Although the overall picture of gradual deepening and cooling of the mixed layers through winter was similar for each mooring, there were striking latitudinal differences. At the northern OOI moorings, cooling and deepening were more

intermittent, intensifying during strong surface fluxes and restratifying whenever the surface fluxes relented. At the southern moorings, CIS and LOCO, cooling and deepening were more sustained.

Of the six moorings, the OOI HYPM and the LOCO moorings were the furthest apart (85.8 km) and were the best examples of lateral contrasts. Bimonthly temperature profiles (Figure 4a) from these two moored profilers were similar at the end of summer, but clear differences appeared in January and February. Mixing and cooling progressed steadily at LOCO, while the upper 600 dbar of the OOI HYPM profiles remained stratified. Below 600 dbar, both the LOCO and HYPM moorings showed a progressive deepening of the temperature inversion, from 900 dbar in September to 1,200 dbar in February. In March and April, deep mixed layers were seen at both moorings, completely removing the temperature inversion. After April, restratification set in at both sites. A thick layer with homogeneous temperature remained at the LOCO mooring, while at the OOI HYPM, restratification appeared to be

stronger, hence changing the temperature profile. Overall, the upper layer temperatures were lower and mixed layers were deeper at the LOCO mooring (Figure 4b).

Spatial Variability in Forcing and Restratiification

Stratification and surface forcing determine the maximum depth of vertical mixing at a given location. The largest wintertime air-sea fluxes take place during individual intense wind events (Holdsworth and Myers, 2015). Using the high-resolution atmospheric reanalysis (ASR), we investigated the long-term spatial distribution of ocean heat loss for the area where the six moorings were deployed. The ASR data showed surprisingly large differences in heat fluxes between the mooring locations, amounting to as much as 200 W m^{-2} (Figure 5a,b). A composite of ~100 tip jet events in 2000 and 2012 showed that the differences between the mooring sites persisted, with stronger heat flux events resulting in larger differences (not shown). Generally, heat losses during tip jet events were larger at the OOI and CIS moorings and weaker at

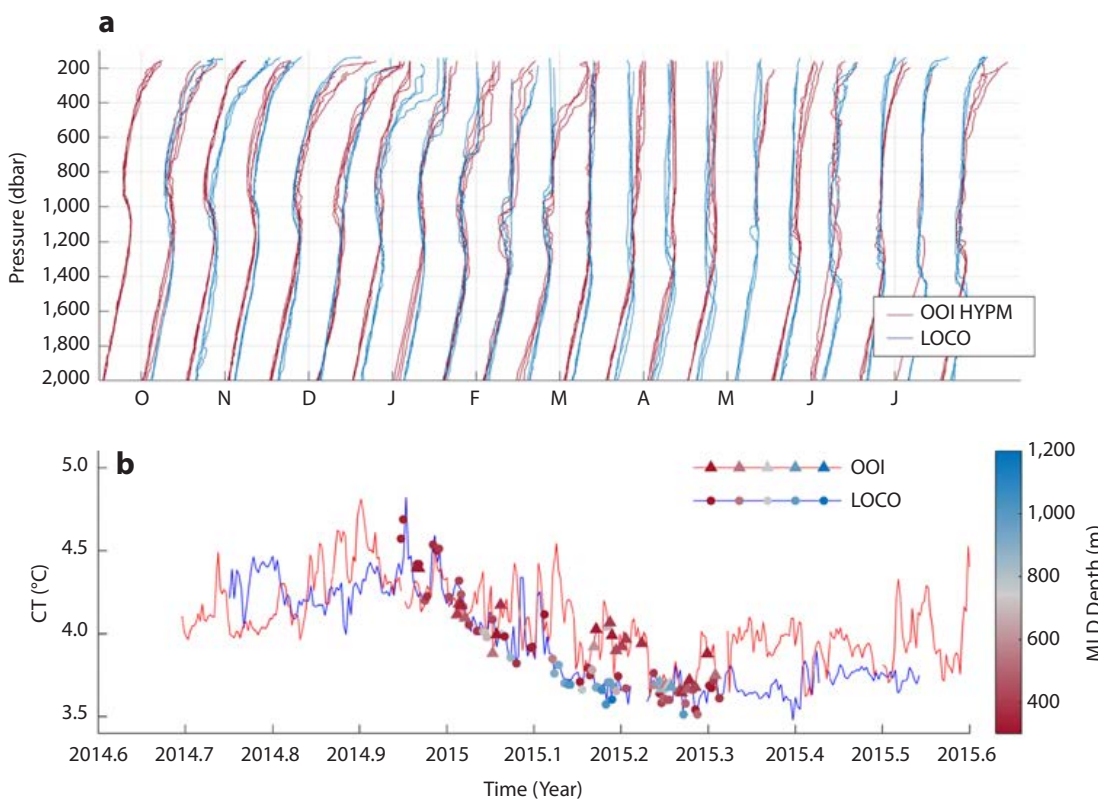


FIGURE 4. (a) Temperature profiles from the OOI (red) and LOCO (blue) moored profilers. Profiles are shown for the first and fifteenth of every month starting on September 15, 2014, for OOI and October 1, 2014, for LOCO. Each set of bimonthly temperature profiles is offset by 1°C . (b) Mean temperature over the 200 m to 500 m layer of the OOI profiles (red) and the LOCO profiles (blue). Scattered markers (triangles for OOI, circles for LOCO) indicate the temperature and the maximum depth of the mid-layer depth (MLD) in color (shown in the color scale) for $\text{MLD} > 200 \text{ dbar}$.

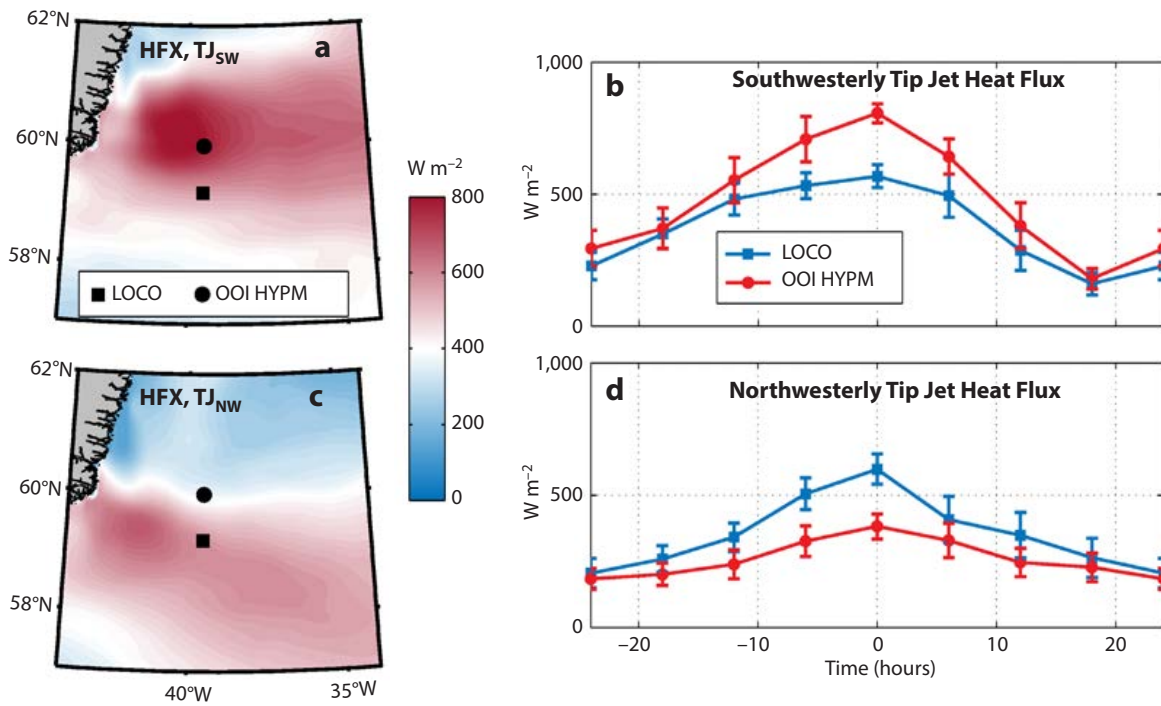


FIGURE 5. (a) Heat-flux composite based on 10 southwesterly tip jet events, obtained from the Arctic System Reanalysis. (b) Evolution of the heat fluxes associated with the southwesterly tip events shown in (a), at the location of the OOI and LOCO moorings, with the error bars indicating the standard error of the mean. (c,d) Same as (a) and (b) but for 10 northwesterly tip jet events. The south- and northwesterly tip jet events were obtained by subsampling the composite of 100 tip jets mentioned in the text.

LOCO, although at times, the heat losses at LOCO exceeded those obtained at CIS and OOI (Figure 5c,d). These wind events, associated with the largest heat losses to the south and classified as northwesterly tip jets (Moore, 2015), were generally less frequent. Both types of tip jet events were not well resolved in the much lower resolution ERA-I fields; in these smoother fields, the differences between fluxes at LOCO and OOI HYPM were reduced to 20 W m⁻² during strong (>200 W m⁻²) cooling events. However, the timing of strong forcing was aligned with temperature homogenization across the array and was also reflected in an increase in the variance of the vertical velocity derived from ADCP data (Figure 6a).

Despite the increased likelihood of stronger surface forcing over the OOI moorings, we observed a shallower MLD in 2014/2015 compared to LOCO, which could mean either that winter was favorable for northerly tip jets or that the OOI site was slightly less favorable for deep convection. While the initial, pre-winter

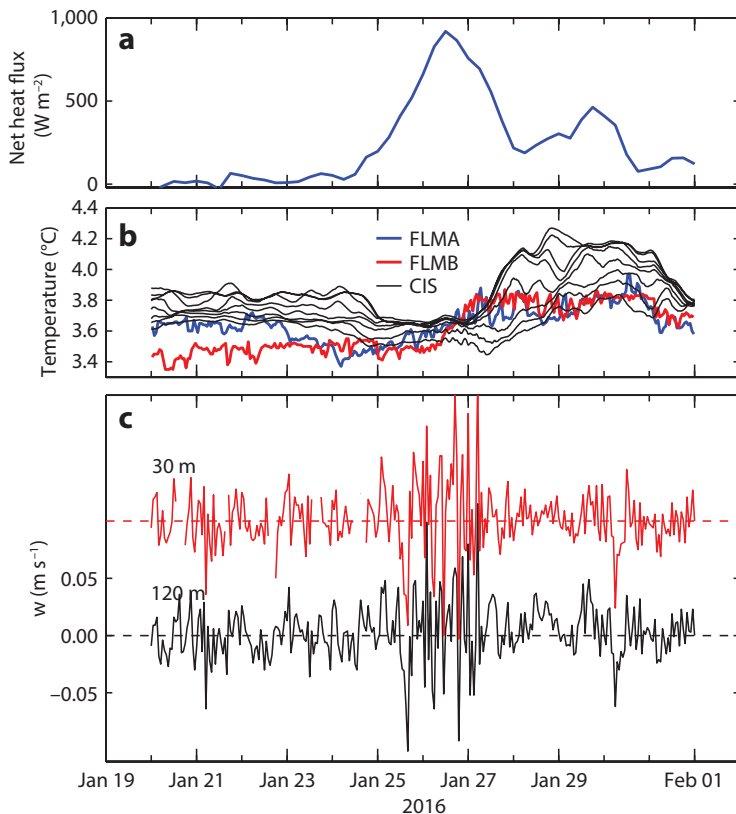


FIGURE 6. (a) ERA-I net heat flux during a tip jet event between January 26 and January 28, 2016. Accompanying (b) temperature from moorings FLMA, FLMB, and CIS, and (c) vertical velocity time series at mooring CIS from two depths of the ADCP.

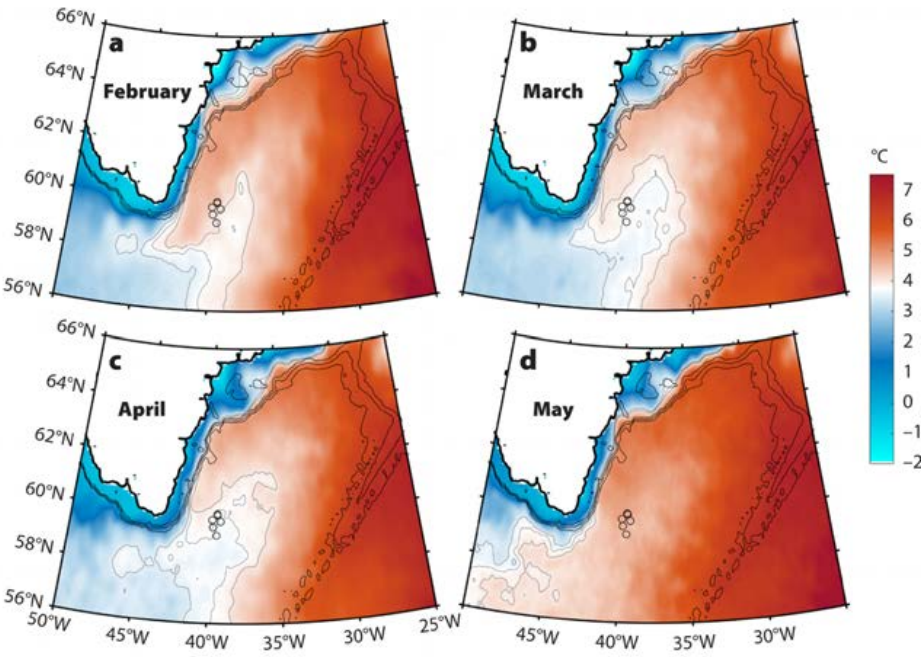


FIGURE 7. Monthly mean sea surface temperature field from the Group for High Resolution Sea Surface Temperature (GHRSST) data set for (a) February, (b) March, (c) April, and (d) May of 2015. Gray contours are drawn for the 3.5°, 3.75°, and 4°C isotherms. The mooring positions are indicated with black circles. Isobaths are drawn for 1,500 m, 1,000 m, and 500 m.

stratification was very similar throughout the area covered by the six mooring (Figure 4a), cooling at the northern OOI HYPM was frequently interrupted by short warming events (Figure 4b). These intermittent events resulted in an average heat content in the upper 1,000 m that was approximately 3% larger at OOI than at the LOCO mooring. This gradient in heat content was also reflected in the increase in SST from south to north: the mean SST over the OOI deployment period was 5.77°C at LOCO, 5.86°C at CIS, and 6.02°C at OOI HYPM. Monthly mean SST through the winter of 2015 shows that the moorings were in the low SST western part of the area (Figure 7). This colder area was east of the center of the Irminger Gyre (Figure 1), as well as east of the region with strongest surface heat fluxes in the ERA-I fields. While surface fluxes were likely dominant in regions of cooling SSTs, this suggests that cooling through advection by colder waters from the southwest may have played a role, as seen at LOCO (time periods 2015.2–2015.4 and 2016.1–2016.3 in Figure 3b) and CIS (at the end of 2015 in Figure 3b).

The Irminger Current advects warmer waters along the cyclonic path around the perimeter of the basin. These warmer waters off the Greenland shelf appeared to strengthen the restratification tendency at the northern OOI mooring (Figure 4b).

DISCUSSION

The two-year data set presented here contains high-resolution data from six moorings deployed in an 86 km × 35 km area in the central Irminger Gyre. Spatial differences observed between the moorings during the winters of 2014/2015 and 2015/2016, which both showed deep (>1,500 dbar) mixed layers, revealed the subtle balance between surface forcing and intermittent restratification during winter. The close proximity of the moorings and nearly identical late summer temperature profiles suggest equal preconditioning at all sites. The more frequent occurrence of stronger tip jet events at the northern moorings has the potential to force deeper and colder mixed layers. However, the stronger surface forcing here was counteracted by frequent restratification through lateral intrusions

from the warm and saline Irminger Current. Fan et al. (2013) studied the occurrence of anticyclonic warm core eddies at the CIS mooring in detail. They proposed two formation regions for the eddies: one west of the Reykjanes Ridge and the other off the East Greenland Irminger Current, near Cape Farewell. The observations presented here clearly suggest that the latter formation region was more important for restratification at the Irminger Sea OOI array.

Only high-resolution spatial and temporal observations can provide sufficient detail for learning more about the impact of eddies on restratification, and the relationship of restratification to convective mixing. These details were not caught in the much sparser Argo profile data. For comparison, there were only two Argo profiles in this area between the moorings during the period October 2014 to April 2015.

Continuation of the OOI moorings in the Irminger Sea will allow the community to study the restratification process in more detail. In addition, OOI surface measurements will allow investigation of the potential impact of freshwater that originates from the Greenland shelf on deep convection, as the influx of freshwater from the Greenland Ice Sheet and the Arctic Ocean is expected to increase with rising atmospheric and oceanic temperatures (Böning et al., 2016). Data from the OOI gliders, whose analysis was outside the scope of this paper, will yield additional insights into lateral scales of variability. Knowledge gained from an integral analysis of the full suite of OOI mooring, surface flux, and glider observations will provide more details about the full convection and restratification cycle, and will contribute significantly to improving our ability to predict deep-water formation. Integrating knowledge about physical processes with the biogeochemical data collected at the OOI array (Palevsky and Nicholson, 2018, in this issue) will lead to further insight into the controls on biological productivity and carbon cycling in the Irminger Sea. ☐

REFERENCES

- Böning, C.W., E. Behrens, A. Biastoch, K. Getzlaff, and J. Bamber. 2016. Emerging impact of Greenland meltwater on deepwater formation in the North Atlantic Ocean. *Nature Geoscience* 9:523–528, <https://doi.org/10.1038/NGEO2740>.
- Bosse, A., P. Testor, L. Houpert, P. Damien, L. Prieur, D. Hayes, V. Taillandier, X. Durrieu de Madron, F. D'Ortenzio, L. Coppola, and others. 2016. Scales and dynamics of submesoscale coherent vortices formed by deep convection in the northwestern Mediterranean Sea. *Journal of Geophysical Research* 121:7,716–7,742, <https://doi.org/10.1002/2016JC012144>.
- Bromwich, D.H., A.B. Wilson, L.-S. Bai, G.W.K. Moore, and P. Bauer. 2016. A comparison of the regional Arctic System Reanalysis and the global ERA-Interim Reanalysis for the Arctic. *Quarterly Journal of the Royal Meteorological Society* 142:644–658, <https://doi.org/10.1002/qj.2527>.
- Dee, D.P., S.M. Uppala, A.J. Simmons, P. Berrisford, P. Poli, S. Kobayashi, U. Andrae, M.A. Balmaseda, G. Balsamo, P. Bauer, and others. 2011. The ERA-Interim reanalysis: Configuration and performance of the data assimilation system. *Quarterly Journal of the Royal Meteorological Society* 137:553–597, <https://doi.org/10.1002/qj.828>.
- de Jong, M.F., and L. de Steur. 2016. Strong winter cooling over the Irminger Sea in winter 2014–2015, exceptional deep convection, and the emergence of anomalously low SST. *Geophysical Research Letters* 43:7,106–7,113, <https://doi.org/10.1002/2016GL069596>.
- de Jong, M.F., H.M. van Aken, K. Våge, and R.S. Pickart. 2012. Convective mixing in the central Irminger Sea: 2002–2010. *Deep Sea Research Part I* 63:36–51, <https://doi.org/10.1016/j.dsr.2012.01.003>.
- Doyle, J.D., and M.A. Shapiro. 1999. Flow response to large-scale topography: The Greenland tip jet. *Tellus A* 51:728–748, <https://doi.org/10.3402/tellusa.v51i5.14471>.
- Fan, X., U. Send, P. Testor, J. Karstensen, and P. Lherminier. 2013. Observations of Irminger Sea anticyclonic eddies. *Journal of Physical Oceanography* 43:805–823, <https://doi.org/10.1175/JPO-D-11-0155.1>.
- Houpert, L., X. Durrieu de Madron, P. Testor, A. Bosse, F. D'Ortenzio, M.N. Bouin, D. Dausse, H. Le Goff, S. Kunesch, M. Labaste, and others. 2016. Observations of open-ocean deep convection in the northwestern Mediterranean Sea: Seasonal and interannual variability of mixing and deep water masses for the 2007–2013 period. *Journal of Geophysical Research* 121:8,139–8,171, <https://doi.org/10.1002/2016JC011857>.
- Holdsworth, A.M., and P.G. Myers. 2015. The influence of high-frequency atmospheric forcing on the circulation and convection of the Labrador Sea. *Journal of Climate* 28:4,980–4,996, <https://doi.org/10.1175/JCLI-D-14-00564.1>.
- Killworth, P.D. 1979. On chimney formation in the ocean. *Journal of Physical Oceanography* 9:531–554, [https://doi.org/10.1175/1520-0485\(1979\)009<0531:OFITO>2.0.CO;2](https://doi.org/10.1175/1520-0485(1979)009<0531:OFITO>2.0.CO;2).
- Lazier, J.R. 1973. The renewal of Labrador Sea Water. *Deep Sea Research* 20:341–353, [https://doi.org/10.1016/0011-7471\(73\)90058-2](https://doi.org/10.1016/0011-7471(73)90058-2).
- Lozier, M., S. Bacon, A. Bower, S. Cunningham, M. de Jong, L. de Steur, B. deYoung, J. Fischer, S. Gary, B. Greenan, and others. 2017. Overturning in the Subpolar North Atlantic Program: A new international ocean observing system. *Bulletin of the American Meteorological Society* 98(4):737–752, <https://doi.org/10.1175/BAMS-D-16-00571>.
- Marshall, J., and F. Schott. 1999. Open-ocean convection: Observations, theory and models. *Reviews of Geophysics* 37:1–64, <https://doi.org/10.1029/98RG02739>.
- Moore, G.W.K. 2003. Gale force winds over the Irminger Sea to the east of Cape Farewell, Greenland. *Geophysical Research Letters* 30, 1894, <https://doi.org/10.1029/2003GL018012>.
- Moore, G.W.K., D.H. Bronwic, A.B. Wilson, I. Renfrew, and L. Bai. 2016. Arctic system reanalysis improvements in topographically forced winds near Greenland. *Quarterly Journal of the Royal Meteorological Society* 142:2,033–2,045, <https://doi.org/10.1002/qj.2798>.
- Moore, G.W.K., and I.A. Renfrew. 2005. Tip jets and barrier winds: A QuickSCAT climatology of high wind speed events around Greenland. *Journal of Climate* 18:3,713–3,725, <https://doi.org/10.1175/JCLI3455.1>.
- Moore, G.W.K., I.A. Renfrew, B.E. Harden, and S.H. Mernild. 2015. The impact of resolution on the representation of southeast Greenland barrier winds and katabatic flows. *Geophysical Research Letters* 42:3,011–3,018, <https://doi.org/10.1002/2015GL063550>.
- Nansen, F. 1912. Das Bodenwasser und die Abkühlung des Meeres. *Internationale Revue der gesamten Hydrobiologie und Hydrographie* 5:1–42, <https://doi.org/10.1002/iroh.19120050102>.
- Palevsky, H.I., and D.P. Nicholson. 2018. The North Atlantic biological pump: Insights from the Ocean Observatories Initiative Irminger Sea Array. *Oceanography* 31(1):42–49, <https://doi.org/10.5670/oceanog.2018.108>.
- Pickart, R.S., F. Straneo, and G.W.K. Moore. 2003. Is Labrador Sea Water formed in the Irminger Basin? *Deep Sea Research Part I* 50(1):23–52, [https://doi.org/10.1016/S0967-0637\(02\)00134-6](https://doi.org/10.1016/S0967-0637(02)00134-6).
- Sverdrup, H.U., M.W. Johnson, and R.H. Fleming. 1942. *The Oceans: Their Physics, Chemistry, and General Biology*. Prentice-Hall Inc., Englewood Cliffs, NJ, USA, 1,060 pp.
- Testor, A. Bosse, L. Houpert, F. Margrerie, L. Mortier, H. Legoff, D. Dausse, M. Labaste, J. Karstensen, D. Hayes, and others. 2017. Multiscale observations of deep convection in the northwestern Mediterranean Sea during winter 2012–2013 using multiple platforms. *Journal of Geophysical Research*, <https://doi.org/10.1002/2016JC012671>.
- Våge, K., R.S. Pickart, G.W.K. Moore, and M.H. Ribergaard. 2008. Winter mixed layer development in the central Irminger Sea: The effect of strong, intermittent wind events. *Journal of Physical Oceanography* 38:541–565, <https://doi.org/10.1175/2007JPO3678.1>.
- Yashayaev, I., and J.W. Loder. 2017. Further intensification of deep convection in the Labrador Sea in 2016. *Geophysical Research Letters* 44:1,429–1,438, <https://doi.org/10.1002/2016GL071668>.

AUTHORS

M. Femke de Jong (femke.de.jong@nioz.nl) is a tenure-track scientist at the Royal Netherlands Institute for Sea Research and Utrecht University, Texel, the Netherlands. **Marilena Oltmanns** is a research scientist and **Johannes Karstensen** is Senior Research Scientist, GEOMAR Helmholtz Centre for Ocean Research Kiel, Kiel, Germany. **Laura de Steur** is a research scientist at the Norwegian Polar Institute, Tromsø, Norway, and the Royal Netherlands Institute for Sea Research and Utrecht University, Texel, the Netherlands.

ARTICLE CITATION

de Jong, M.F., M. Oltmanns, J. Karstensen, and L. de Steur. 2018. Deep convection in the Irminger Sea observed with a dense mooring array. *Oceanography* 31(1):50–59, <https://doi.org/10.5670/oceanog.2018.109>.

ACKNOWLEDGMENTS

The research leading to these results has received funding from the European Union's Horizon 2020 research and innovation program under grant agreement 633211 (AtlantOS) and grant agreement 727852 (Blue-Action), and from the European Union's Seventh Framework Program (FP7/2007–2013) under grant agreement 308299 (NACLIM) and grant agreement 312463 (FixO3). Data from the CIS and LOCO moorings are freely available from the OceanSITES database at <http://www.oceansites.org>. OOI data were obtained from the NSF Ocean Observatories Initiative Data Portal, <http://ooinet.oceanobservatories.org>, downloaded on August 9, 2017. We thank two anonymous reviewers as well as the guest editor, Tim Cowles, for suggestions that improved this manuscript.

The Changing Nature of Shelf-Break Exchange Revealed by the OOI Pioneer Array

By Glen Gawarkiewicz, Robert E. Todd,
Weifeng Zhang, Jacob Partida,
Avijit Gangopadhyay,
Mahmud-Ul-Hasan Monim,
Paula Fratantoni, Anna Malek Mercer,
and Margaret Dent



Photo credit: Ellen Roosen

“ Observations from the OOI Pioneer Array suggest that coastal ocean dynamics are changing rapidly south of New England, with important implications for commercial fisheries, ecosystems, and future storm intensities from both hurricanes and nor’easters. ”

ABSTRACT. Although the continental shelf and slope south of New England have been the subject of recent studies that address decadal-scale warming and interannual variability of water mass properties, it is not well understood how these changes affect shelf-break exchange processes. In recent years, observations of anomalous shelf and slope conditions obtained from the Ocean Observatories Initiative Pioneer Array and other regional observing programs suggest that onshore intrusions of warm, salty waters are becoming more prevalent. Mean cross-shelf transects constructed from Pioneer Array glider observations collected from April 2014 through December 2016 indicate that slope waters have been warmer and saltier. We examine shelf-break exchange events and anomalous onshore intrusions of warm, salty water associated with warm core rings located near the shelf break in spring 2014 and winter 2017 using observations from the Pioneer Array and other sources. We also describe an additional cross-shelf intrusion of ring water in September 2014 to demonstrate that the occurrence of high-salinity waters extending across the continental shelf is rare. Observations from the Pioneer Array and other sources show warm core ring and Gulf Stream water masses intrude onto the continental shelf more frequently and penetrate further onshore than in previous decades.

SHELF-BREAK EXCHANGE AND THE OCEAN OBSERVATORIES INITIATIVE PIONEER ARRAY

Shelf circulation south of New England consists primarily of westward along-shelf flow bounded on the offshore edge by the shelf-break front and jet. The shelf-break front is the boundary between cool, fresh shelf water and warm, salty slope water. The shelf-break front is baroclinically unstable and is frequently populated by large-amplitude frontal meanders (Zhang and Gawarkiewicz,

2015a). A number of recent studies document decadal- to century-scale warming of continental shelf and slope waters in this region, including research in fisheries oceanography and meteorology that focuses on the impacts of warming on commercial fisheries and the potential for storms to strengthen.

An important contributing factor to warming of the continental shelf is the influence of shelf-break exchange processes, particularly those that bring warm, salty water masses from the Slope Sea or Gulf Stream warm core rings onto

the continental shelf. These exchange processes have been difficult to study because decorrelation scales near the shelf break are extremely small both spatially (~10 km) and temporally (~1 day), necessitating high-resolution sampling in both space and time to capture them (Gawarkiewicz et al., 2004). Additionally, variability of the cross-shelf fluxes at the shelf break is much larger than the long-term mean (Chen and He, 2010); thus, long-duration observations are needed to obtain statistically robust estimates of heat and salt fluxes between the continental shelf and the adjoining deep ocean.

Despite its complexity, two important practical applications make this topic important: (1) fisheries management, and (2) storm forecasting and associated public warnings/evacuations. Specifically, the timing and magnitude of episodic warming related to shelf-break exchange events or the cumulative impact of a string of events over a single season could alter critical habitat and affect recruitment success of commercially important species (Sullivan et al., 2005; Bell et al., 2014). Likewise, significant cumulative warming could affect the intensity and severity of storms striking the eastern seaboard (Glenn et al., 2016).

The record warm year of 2012 (Mills

et al., 2013; Chen et al., 2014a) as well as documented warming over decadal timescales (e.g., Forsyth et al., 2015; Pershing et al., 2015) in the Middle Atlantic Bight and Gulf of Maine system raise many important questions regarding shelf-break exchange processes. Increased shelf-break exchange can contribute to continental shelf warming. Warming of the shelf in turn affects cross-shelf density gradients that can change the nature of individual shelf-break exchange processes. This may increase the influence of ocean advective processes relative to air-sea fluxes in contributing to interannual fluctuations of shelf temperatures (e.g., see the discussion of relative contributions between air-sea flux anomalies and ocean advective heat flux anomalies in Chen et al., 2016).

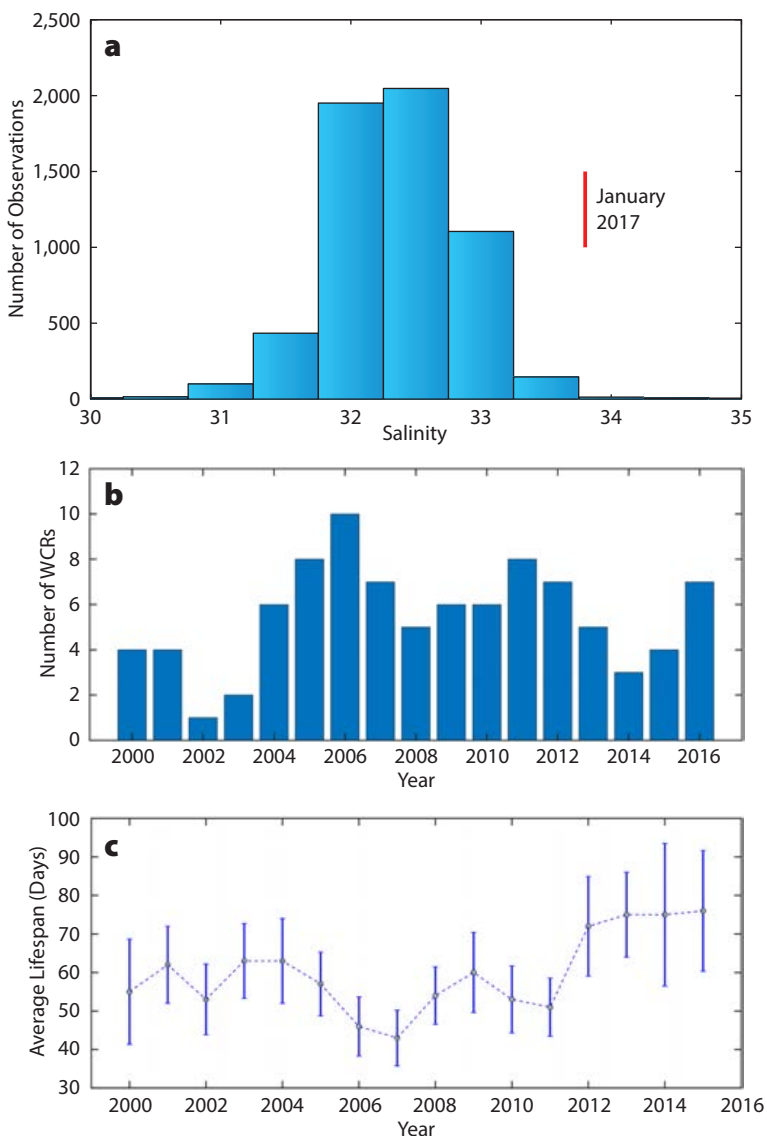


FIGURE 1. (a) A histogram of all salinity observations between 41°N and $41^{\circ}15'\text{N}$ and 70°W and 72°W . The vertical red line denotes the salinity measured in January 2017. (b) The number of warm core rings (WCRs) passing through the Pioneer Array region with a ring center north of $39^{\circ}30'\text{N}$ and within 70°W to 72°W each year from 2000–2016. This census is derived from the Gulf Stream analysis charts published each week by Jenifer Clark (<http://users.erols.com/gulfstrm>). (c) The average lifespan of all rings that pass through the slope region (75°W to 55°W), including the Pioneer Array, is shown with the standard error of the mean lifespan. Note that the warm core rings in the middle panel are a subset of all the warm core rings that were used for the average lifespan computation.

Ocean warming is not the only factor potentially affecting the dynamics of shelf-break exchange in this region. The large-scale spatial pattern of Gulf Stream meandering has changed over the past 20 years. Andres (2016) found that the longitude at which meander amplitudes exceed a specific threshold has been shifting westward since 1995, and large-amplitude meanders now frequently influence the upper continental slope south of New England (e.g., Gawarkiewicz et al., 2012; Ezer et al., 2013). Similarly, a recent census of Gulf Stream warm core rings shows that the average number of warm core rings formed annually from 2000 to 2016 was roughly double that for the time period 1977 to 1999 (Monim, 2017). Surprisingly, the annual frequency of warm core ring formation in the recent period was not correlated with the North Atlantic Oscillation. This is in sharp contrast to the earlier period when the number of rings was well correlated with the phase of the North Atlantic Oscillation (Chaudhuri et al., 2009).

The westward shift in the destabilization point of the Gulf Stream and the increasing number of warm core rings suggest that offshore forcing of the shelf-break region and increasing frequency of ring-shelf interactions may be playing a role in the recent warming of the continental shelf and changes to the continental shelf and slope ecosystem (Hare et al., 2016). Consistent with increasing influence from offshore forcing on the continental shelf, recent hydrographic observations reveal onshore intrusions of salty waters that are at the upper limits of observed values or exceed the range of previously observed values. For example, Ullman et al. (2014) describe a shoreward intrusion of salty bottom water that exceeded the range of historical salinity observations in the vicinity by 1.0 psu. Observations from the Commercial Fisheries Research Foundation (CFRF) Shelf Research Fleet (<http://www.cfrfoundation.org/shelf-research-fleet>) in January 2017 showed salinities in the upper 0.41% of historical observations between latitudes of 41°N and $41^{\circ}15'\text{N}$ and longitudes of 70°W and 72°W (Figure 1a). The historical data were compiled by Christopher Linder of Woods Hole Oceanographic Institution and Maureen Taylor of the National Marine Fisheries Service and are described in Linder et al. (2006). This intrusion of ring water is described further in a later section of this paper.

Since its initial partial deployment in late 2013 and its subsequent commissioning in January 2016, the Ocean Observatories Initiative (OOI) Pioneer Array has collected sufficient observations to begin examining how various physical processes associated with shelf-break exchange may be evolving. A description of the Pioneer Array appears in Smith et al. (2018, in this issue), and recent work of author Gawarkiewicz

and Al Plueddemann will soon yield a detailed discussion of both the final configuration of the array and the scientific motivation for the design choices.

Further examination of Monim's (2017) warm core ring census offers insight into offshore forcing of the shelf-break front. In recent years, a large number of warm core rings, ranging from four to nine per year from 2006 to 2016, have passed through the vicinity of the Pioneer Array (i.e., the ring center was located north of $39^{\circ}30'N$, and within $70^{\circ}W$ to $72^{\circ}W$), frequently affecting the shelf-break front and jet (Figure 1b). The average lifetime of rings along the continental slope ($75^{\circ}W$ – $55^{\circ}W$), including those passing through the Pioneer Array region, has increased in recent years (Figure 1c), allowing for the possibility of longer duration interactions between the rings and the shelf-break jet. (See Gawarkiewicz et al., 2001, for an example of a small ring interacting with the shelf-break jet, and Chen et al., 2014b, for a detailed analysis of a large ring interacting with the shelf-break front in 2006.)

Here, we present new perspectives on the changing nature of shelf-break exchange south of New England. We characterize the mean structure of the shelf-break front using Pioneer Array glider observations and compare the mean during this period to previous studies on decadal variations in slope water mass properties. We then focus on a warm core ring interacting with the shelf-break front in the spring of 2014 when Pioneer Array observations captured a new shelf-deep ocean exchange process (the Pinocchio's Nose Intrusion previously detailed by Zhang and Gawarkiewicz, 2015b), a subsequent rapid shift in shelf-break front location and circulation, and a subsurface filament of shelf-origin water adjacent to the warm core ring. We next combine Pioneer Array observations with measurements collected over the continental shelf by commercial fishermen to characterize the anomalous onshore penetration of warm core ring waters in early 2017. We use observations collected routinely since

1981 by the National Marine Fisheries Service Ecosystem Monitoring (EcoMon) Program to place September 2014 anomalous shelf conditions in a longer-term context. The final section looks ahead to possible impacts of future analyses using Pioneer Array observations.

THE SHELF-BREAK FRONT: A NEW PORTRAIT USING PIONEER ARRAY GLIDER OBSERVATIONS

Before examining recent shelf-break exchange events, it is instructive to consider the mean cross-shelf structure of the shelf-break front from April 2014 to December 2016, a period for which observations from autonomous underwater gliders are available on the Pioneer Array Eastern Boundary (EB) line (Figure 2). The primary science goal of the EB gliders is to measure the inflow of shelf and slope waters, which can be used as upstream boundary conditions

for regional circulation and biogeochemical models. The typical EB glider mission goes back and forth between the 70 m isobath and the 3,000 m isobath (roughly $40^{\circ}24'N$ to $39^{\circ}50'N$). Individual cross-shelf transects are completed in approximately one week. Further details of the glider missions, their scientific justification, and technical attributes may be found in Smith et al. (2018, in this issue) and are evident in recent work of author Gawarkiewicz and Al Plueddemann. A total of 78 distinct glider transects along the EB line are used here to construct mean potential temperature, salinity, and potential density fields. We average observations from individual glider profiles into 5 m vertical bins, then average individual glider transects into horizontal bins of 1 min extent by latitude (1 nm, or 1.852 km), and finally average across transects. The resulting mean fields (Figure 2) are shown only at latitudes occupied by at least 50% of individual transects.

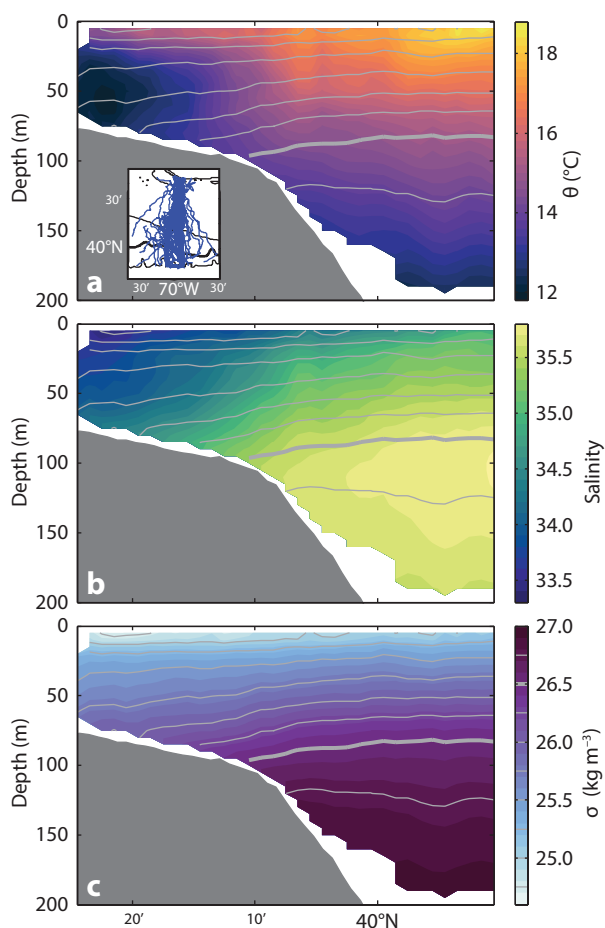


FIGURE 2. Mean transects across the Middle Atlantic Bight shelf break near $70^{\circ}W$ of (a) potential temperature (θ), (b) salinity, and (c) potential density (σ) constructed by averaging observations from gliders surveying along the Pioneer Array's Eastern Boundary line from April 2014 through December 2016. Mean values are shown only at locations where at least 50% of identified glider transects yielded observations. Gray contours in all panels are isopycnals, with a contour interval of 0.25 kg m^{-3} and the 26.5 kg m^{-3} isopycnal bold. The inset in panel a shows the trajectories of the gliders from which observations were used.

Shoreward of the shelf break, the mean temperature, salinity, and density fields from EB glider observations capture expected features of the Middle Atlantic Bight shelf-break frontal region. The shelf-break front itself appears as a transition from cooler, fresher shelf waters to warmer, saltier slope waters, with isopycnals sloping upward offshore to form a retrograde front (i.e., the slope of the isopycnals is in the opposite direction of the

continental slope, the upper 50 m has the warmest temperatures in the region (16°–18°C). Beneath this layer, potential temperatures fall from 16°C to 13°C toward 200 m depth, and salinities reach a local maximum of more than 35.7 near 100 m. Wright and Parker (1976) previously identified these waters as the “upper slope thermostad,” but found temperatures to be 10°–13°C and salinities to be 35–35.6. That these waters were on

destabilization point of the Gulf Stream and the increase in the number of warm core rings since 2000.

RING INTERACTIONS AND SHELF-BREAK EXCHANGE PROCESSES REVEALED BY PIONEER ARRAY OBSERVATIONS

The persistent high-resolution observations provided by the Pioneer Array reveal new aspects of warm core ring interactions with outer shelf circulation. This is illustrated by Pioneer Array observations during the spring of 2014 when warm core ring water masses moved onto the outer continental shelf and shelf water masses extended over the continental slope along the periphery of a warm core ring.

Zhang and Gawarkiewicz (2015b) demonstrated the great potential of the observatory for studying a new form of shelf-break exchange process. By examining observations from the first Pioneer Array glider deployment along the EB line together with satellite-based sea surface temperature measurements, they identified a direct intrusion of warm core ring water onto the outer continental shelf in April–May 2014. The onshore intrusion of ring water represented a type of exchange process that had not been reported previously in the scientific literature, although a similar event was apparent in satellite-based sea surface temperature images from summer 2006. Zhang and Gawarkiewicz (2015b) named this process a Pinocchio’s Nose Intrusion (PNI), as the intrusion had a unique elongated pattern in sea surface imagery that grew in the alongshelf direction.

The Pinocchio’s Nose Intrusion in April–May 2014 measured roughly 30 km wide in the cross-shelf direction and extended at least 150 km alongshelf in two weeks (e.g., Figure 3a). Glider measurements captured the subsurface characteristics of the intrusion, showing that intruding ring water occupied almost the entire water column over the outer shelf (e.g., Figure 3c,e) and was not

“The increase in temperature and salinity over the continental slope is consistent with both the westward shift in the destabilization point of the Gulf Stream and the increase in the number of warm core rings since 2000.”

slope of the bathymetry). The foot of the shelf-break front, identified as the location at which the 26.5 kg m⁻³ isopycnal (Linder and Gawarkiewicz, 1998) intersects the seafloor, is found near the 100 m isobath (approximately 40°12'N), in general agreement with previous, longer-term climatologies (e.g., Linder and Gawarkiewicz, 1998). More recent studies (e.g., Pickart, 2000; Linder et al., 2004; Fratantoni and Pickart, 2007) suggest that the frontal upwelling associated with the shelf-break front is centered on the 26.0 isopycnal, which intersects the seafloor near the 80 m isobath (approximately 40°20'N). The “cold pool” (Houghton et al., 1982), a region of cold water between the seasonal thermocline, the seafloor, and the shelf-break front is apparent shoreward of 40°15'N (Figure 2a), with minimum temperature below 12°C. Salinities within the cold pool range from 33.7 to 34.5 (Figure 2b), which is more saline than the typical salinities near 33 reported previously (e.g., Linder et al. 2006).

Farther offshore over the upper

average warmer and saltier during the April 2014 to December 2016 period suggests more frequent presence over the upper continental slope of waters originating in the Gulf Stream.

The increase in both temperature and salinity over the upper slope is surprising. Greene et al. (2013) and Pickart et al. (1999) describe how two different source regions, from the subpolar north and subtropical south, influence upper slope waters south of New England (see Figure 1 of Greene et al., 2013, for a schematic of the spatial distribution of the various water masses over the slope). The mean fields produced from glider observations along the Pioneer Array EB line (Figure 2) suggest that the subtropical waters of Gulf Stream origin have been dominant over the last several years. This has important consequences for zooplankton distributions and ecosystem dynamics of the shelf-slope system (e.g., Pershing et al., 2015). The increase in temperature and salinity over the continental slope is consistent with both the westward shift in the

a surface-trapped feature entrained by the shelf-break jet. By combining these observations with idealized numerical simulations, Zhang and Gawarkiewicz (2015b) demonstrated that the dynamics of a PNI are inherently nonlinear and that it results from topographically induced vorticity variations of the ring water as it is carried into shallower water. As the ring water moves onshore, it is compressed vertically, and conservation of potential vorticity dictates that the ring water gains anticyclonic vorticity. This causes an enhanced outward-pointing centrifugal force that pushes the ring water further onto the shelf and generates the onshore intrusion. The westward elongation of the PNI is due to the alongshelf advection of momentum, as the intrusion does not

form when nonlinear advective terms are neglected (see details of the momentum balances in Zhang and Gawarkiewicz, 2015b). This process represents a new mechanism for warm core rings interacting with the continental shelf circulation. It is a significant exchange process, as the associated onshore transport of ring water is of the same order of magnitude as shelf-break frontal jet transport. These intrusions of warm, salty waters may have important biogeochemical implications and could facilitate migration of subtropical marine species across the shelf-break barrier and transport low-nutrient surface Gulf Stream ring water into the otherwise productive shelf-break region (Zhang et al., 2013).

A subsequent glider transect along the

EB line demonstrates the rapid shifts in shelf-break hydrography and circulation following the 2014 Pinocchio's Nose Intrusion event (Figure 3d,f). Within the week between repeat glider crossings of the shelf break near $40^{\circ}10'N$ in mid-May 2014, warm salty waters from the PNI were replaced by typical cool and fresh waters as the shelf-break front returned to approximately its mean position (Figure 3d,f) after having been pushed shoreward by the PNI (Figure 3c,e). Vertically averaged currents measured by the gliders indicate a simultaneous shift from westward flow within the PNI near $40^{\circ}10'N$ (Figure 3a) to strong eastward flow south of $40^{\circ}N$ a week later (Figure 3b) as the anticyclonic flow of the warm core ring impinged upon the upper

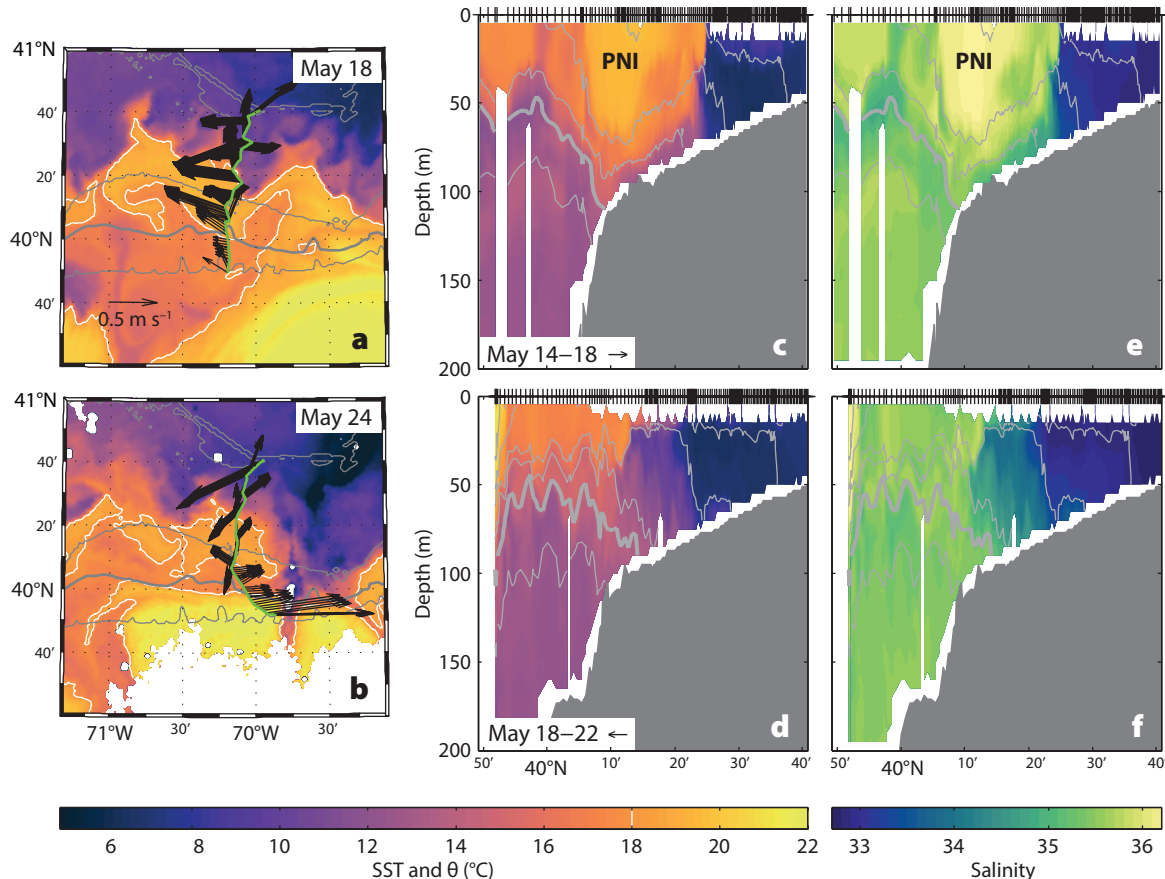


FIGURE 3. Rapid evolution of temperature and salinity near the Middle Atlantic Bight shelf break following the Pinocchio's Nose Intrusion (PNI) in May 2014. Top panels show (a) sea surface temperature with the 18°C isotherm drawn in white to delineate warm core ring water and cross-shelf break distributions of (c) potential temperature and (e) salinity from a Pioneer Array glider while the intrusion was active. PNI denotes the intrusion in (c,e). Lower panels (b,d,f) show the same properties a few days later. In (a) and (b), the trajectory of the glider along the Eastern Boundary line is shown (green), with vectors (black) indicating vertically averaged currents along the glider's trajectory. Gray contours are the 50, 100, 200, and 1,000 m isobaths, with the 200 m isobath bold. In (c–d), isopycnals are shown in gray, with a contour interval of 0.25 kg m^{-3} and the 26.5 kg m^{-3} isopycnal bold. Tick marks on the upper axes denote locations of glider profiles, and arrows show direction of glider motion during the indicated dates.

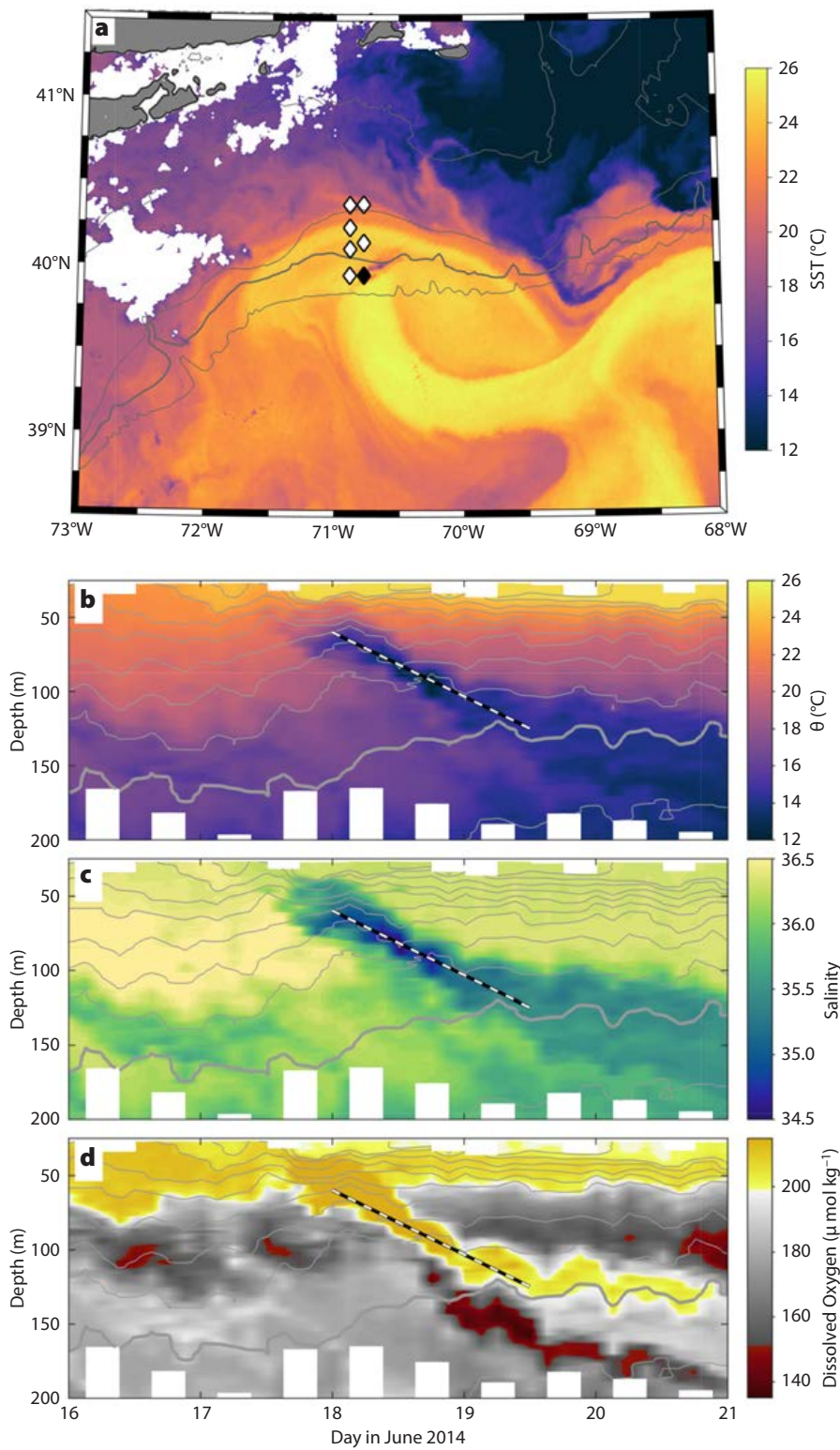


FIGURE 4. (a) Sea surface temperature on June 28, 2014, showing a warm core ring present near the Pioneer Array moorings (diamonds). The location of the Upstream Offshore mooring is shown in black. Time series of (b) potential temperature, (c) salinity, and (d) dissolved oxygen from the Upstream Offshore mooring during June 16–21, 2014, as a filament of shelf water was advected past the mooring. Gray contours in (b–d) are isopycnals, with a contour interval of 0.25 kg m^{-3} and the 26.5 kg m^{-3} isopycnal bold.

continental slope. These observations, together with those discussed by Zhang and Gawarkiewicz (2015b), indicate that the full timescale over which the PNI affected the shelf-break front was approximately one month.

As the same warm core ring continued to impinge upon the shelf break in June 2014, a subsurface filament of shelf-origin water was advected past the Pioneer Array moorings by the complex flows over the upper continental slope that were associated with the warm core ring-shelf-break front interaction (Figure 4b–d). Unlike the surface-visible shelf water streamer transport that is carried around the eastern periphery of the warm core ring (e.g., near $40^\circ\text{N}, 69^\circ20'\text{W}$ in Figure 4a), this subsurface filament of shelf water cannot be seen by satellite.

Moored profiler observations from the upstream-offshore mooring (Figure 4a, black diamond) show the relatively cold, fresh, and high-oxygen signature of shelf waters first reaching the mooring site near 60 m depth on June 18; it is then found at subsequently deeper depths until it arrives at the mooring site near 125 m depth about 1.5 days later (Figure 4b–d, dashed lines) as the northwestern edge of the warm core ring reaches the Pioneer Array moorings. The relatively low temperatures ($<15^\circ\text{C}$) and salinities (<35) within the filament indicate that those waters originated shoreward of the shelf-break front, and the relatively high dissolved oxygen concentration serves as a useful additional tracer that distinguishes shelf waters from slope and ring waters. Note that the upstream-offshore mooring is located near the 500 m isobath and so is seaward of where shelf waters are typically found. The relatively fresh, cold, and oxygen-rich shelf water is eventually found beneath the warmer, saltier, and low-oxygen ring water. The descending signal of shelf water in Figure 4 crosses isopycnals, but this should not be interpreted as observational evidence of a water parcel moving downward across isopycnals. Such cross-isopycnal motion would require substantial mixing to

modify the density of a parcel; however, the temperature, salinity, and oxygen signatures of the shelf water remain intact and do not suggest mixing with adjacent water masses. A likely explanation for the observed descending signal of shelf water is that the mooring sampled the three-dimensional structure of a tilted shelf-water filament as that filament was advected past the mooring by the combined ring and shelf-break flows. Vertically sheared flow, such as that in the shelf-break front, in warm core rings, and in other baroclinic eddies, is effective at producing tilted filaments (e.g., Smith and Ferrari, 2009).

A WARM CORE RING INTRUSION IN WINTER: COMBINING PIONEER ARRAY OBSERVATIONS WITH FISHERMEN-COLLECTED DATA FOR DEEPER INSIGHTS

A warm core ring intrusion onto the Middle Atlantic Bight shelf in the winter of 2017 offered an opportunity to combine Pioneer Array observations with additional in situ observations to examine the shoreward extent of anomalously warm waters over the continental shelf. Sea surface temperature imagery from January 25, 2017, showed an intrusion of warm (10° – 11° C) waters as far north as

$40^{\circ}40'N$ from a warm core ring centered near $39^{\circ}N$, $71^{\circ}20'W$ (Figure 5a). A subsequent sea surface temperature image on February 6 indicated that filaments with surface temperatures of 10° C extended as far north as $41^{\circ}15'N$, in the vicinity of Block Island in Rhode Island Sound (not shown). Block Island is approximately 115 km north of the 100 m isobath, the long-term mean position of the foot of the shelf-break front.

In late January 2017, a Pioneer Array glider surveying along the shelf break near $40^{\circ}N$ (the northern edge of the Frontal Zone [FZ] glider survey pattern; Figure 5a) measured temperatures of

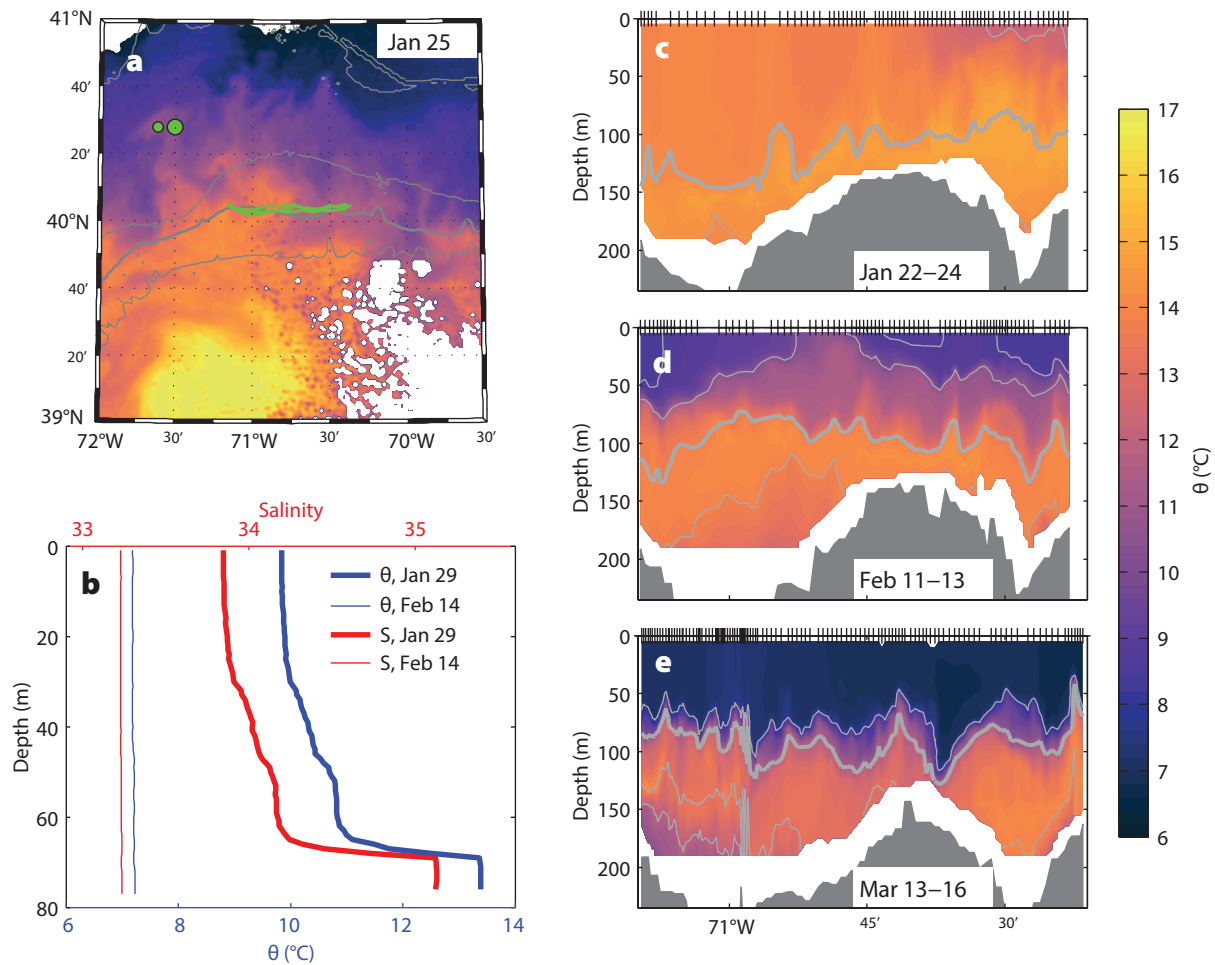


FIGURE 5. The evolution of anomalous conditions on the Middle Atlantic Bight shelf in winter 2017 resulting from a nearby warm core ring. (a) Sea surface temperature for the Pioneer Array region on January 25, 2017. The warm core ring is evident along the southern boundary, with warm water ($>12^{\circ}$ C) extending north of $40^{\circ}20'N$. (b) Potential temperature θ (blue) and salinity (red) profiles over the shelf north of the Pioneer Array from the Commercial Fisheries Research Foundation (CFRF) Shelf Research Fleet during January (thick lines) and February (thin lines) 2017. Warm, salty waters extended onto the shelf, particularly near the bottom, in late January, but not in mid-February. Locations of the CFRF profiles are shown by green circles in (a), with the larger circle corresponding to the January profiles; (c–e) Potential temperature (along the shelf break) from Pioneer Array gliders during (c) January, (d) February, and (e) March 2017, showing substantial cooling as the warm core ring influence diminished. Tick marks on the upper axes in (c–e) denote the locations of individual glider profiles. Glider trajectories, which proceeded westward, are shown in green in (a). Contour lines denote isopycnals.

13°–15°C throughout the water column (Figure 5b). As part of the CFRF Shelf Research Fleet, Rhode Island fishermen collected temperature and salinity profiles near 40°30'N, 71°30'W on January 29 (Figure 5b; thick profiles). These profiles reveal a layer of unusually warm (10°–11°C) and salty (near 34) water in the upper 65 m that overlies a very warm (13.4°C) and salty (35) layer within 10 m of the seafloor. The near-bottom layer is slope water, and the sharp thermal gradient is the shelf-break front near the foot of the front where the high-gradient region intersects the bottom.

It is useful to compare a recent monthly, three-dimensional climatology built from all observations available from 1864 to 2009 (Fleming, 2016) with the observed shelf water mass properties in January 2017. The climatological temperature for the continental shelf for January is 5°C, and the climatological salinity is 33.0. Relative to this climatology, the January 2017 ring intrusion resulted in anomalies of 5°–6°C and 0.8–1.1 salinity units that extended as far north as 41°15'N. As such, the ring intrusion substantially impacted both shelf-water temperature and salinity across virtually the entire continental shelf.

Subsequent Pioneer Array observations and shelf profiles from CFRF fishermen indicate that shelf water properties returned toward normal as the winter of 2017 progressed. By February 14, the water column near 40°30'N, 71°30'W over the mid-shelf was well mixed with a temperature of 7.2°C and salinity of 33.2 (Figure 5b, thin profiles), and a nearly concurrent reoccupation of the glider transect along the shelf break (Figure 5d) showed waters in the upper 50 m around 9°C. Salinity measured at the offshore surface mooring indicated a rapid increase to 35.5 in early January 2017 that slowly decreased to 35.0 in mid-February as the ring intrusion drifted westward toward Hudson Canyon. By mid-March, another occupation of the along-shelf break glider transect showed further cooling throughout the water column, including a surface

mixed layer with temperature near 7°C through the upper 60 m of the water column (Figure 5e).

One consequence of this warm intrusion was the appearance of warm-water fish species that were presumably carried onto the continental shelf in January 2017 as part of this event. A Rhode Island fishermen, Michael Marchetti (F/V *Mister G*, Point Judith, RI), recorded observations and photographs of unusual catch around Block Island in approximately 30 m of water, well inshore of the shelf break. Observed species included Gulf Stream flounder (*Citharichthys arctifrons*) and juvenile black sea bass (*Centropristes striata*), which are not typically found in shallow New England waters during the winter months. Fishermen also reported dramatic changes in Jonah crab (*Cancer borealis*) catch during the warm intrusion. Standardized fisheries surveys (NOAA Northeast Fisheries Science Center trawl survey and Northeast Area Monitoring and Assessment Program trawl survey) do not operate in the winter months, and thus are unable to provide further insights into the biological impacts of this mid-winter warm intrusion. Given the scale of the warm intrusion in January 2017, however, it is likely that the event had major, short-term impacts on ecosystem structure and function. Further research is needed to substantiate these specific ecosystem impacts of the ring intrusion.

HOW UNUSUAL ARE THE RING INTRUSIONS?

The Pioneer Array provides important new perspectives on shelf-break exchange, and observations from the array clearly show that onshore intrusions of warm core ring water masses are penetrating farther onshore than previously noted in historical data or the scientific literature. This is consistent with recent studies described earlier that indicate larger-amplitude Gulf Stream meanders and more frequent warm core rings since the year 2000. However, because the Pioneer Array has only been collecting observations since late 2013, it is difficult

to quantify how unusual the recent ring intrusion events have been since 2013 using Pioneer Array observations alone.

The NOAA National Marine Fisheries Service's EcoMon program has been collecting CTD profiles over the Middle Atlantic Bight shelf between Hudson Canyon and the eastern end of Long Island, New York, since 1981; these long-term measurements allow us to place recent events in context. EcoMon observations are mapped onto a cross-shelf grid based on distance from the 100 m isobaths. Only observations collected during the months of September from 1981 to 2010 were used to calculate the climatological mean values and standard deviations (Figure 6a,b).

A significant intrusion event was identified in observations collected during the September 2014 EcoMon cruise (Figure 6c,d). The 34.0 isohaline outcropped at the 50 m isobath, 70 km shoreward of the shelf break (Figure 6c). In contrast, the surface outcrop of the 34.0 isohaline was located 20 km seaward of the shelf break in the EcoMon climatology (Figure 6a). Note that the slope of the 34.0 isohaline is in the opposite direction in September 2014 (downward offshore) compared to the climatology (upward offshore in the shelf-break front). The 34.0 isohaline intersected the seafloor at the 60 m isobath in September 2014, 50 km shoreward of the shelf break and roughly 30 km shoreward of its climatological position. This shoreward shift in the isohaline surfaces resulted in the mid-shelf salinity being five standard deviations above the climatological mean value in September 2014.

The shelf waters were also much warmer than average during the same time period, with much of the subthermocline water mass ranging from 14°–16°C, compared to climatological averages of 10°–12°C. Thus, the entire shelf was substantially warmer and saltier than average in late summer 2014, consistent with other ring intrusions documented by the OOI Pioneer Array.

LOOKING FORWARD—FUTURE IMPLICATIONS OF OOI PIONEER ARRAY SCIENCE

The OOI Pioneer Array has measured a number of significant shelf-break exchange events from the pre-commissioning deployments in late 2013 to the present. Some of the anomalous water mass properties measured over the continental shelf have rarely been observed in the past. The significant onshore penetration of warm core ring water is particularly likely to have important impacts on the continental shelf ecosystem and the seasonal movements of fish. By combining observations from the Pioneer Array, the CFRF Shelf Research Fleet, and the EcoMon program, we see

that extreme or outlier events with warm, salty intrusions onto the shelf are occurring more frequently and penetrating further onshore than data from historical hydrographic archives would suggest.

We have presented primarily data on the thermohaline signatures of the exchange events. The next stage of Pioneer Array data analysis and modeling is processing and quality control of the velocity measurements from moorings and gliders and the computation of cross-shelf fluxes to characterize heat, salt, and buoyancy fluxes from these events. The ultimate goal will be to parameterize these fluxes based on dynamically important parameters such as the Rossby and Burger numbers, the

maximum jet velocity in the shelf-break jet, and the maximum azimuthal velocities and spatial scales of warm core rings (e.g., Cenedese et al., 2013).

Observations from the OOI Pioneer Array suggest that coastal ocean dynamics are changing rapidly south of New England, with important implications for commercial fisheries, ecosystems, and future storm intensities from both hurricanes and nor'easters. There is an urgent need for focused numerical modeling studies to investigate the dynamics of shelf-break exchange. It is vital to explore the influence of larger, more frequent, and longer-lived warm core rings on the shelf-break front and on continental shelf circulation and ecosystems. Changes to shelf-break exchange may significantly affect nutrient transport between the deep ocean and the continental shelf, with consequences for higher trophic level productivity, including commercially harvested fish. ☐

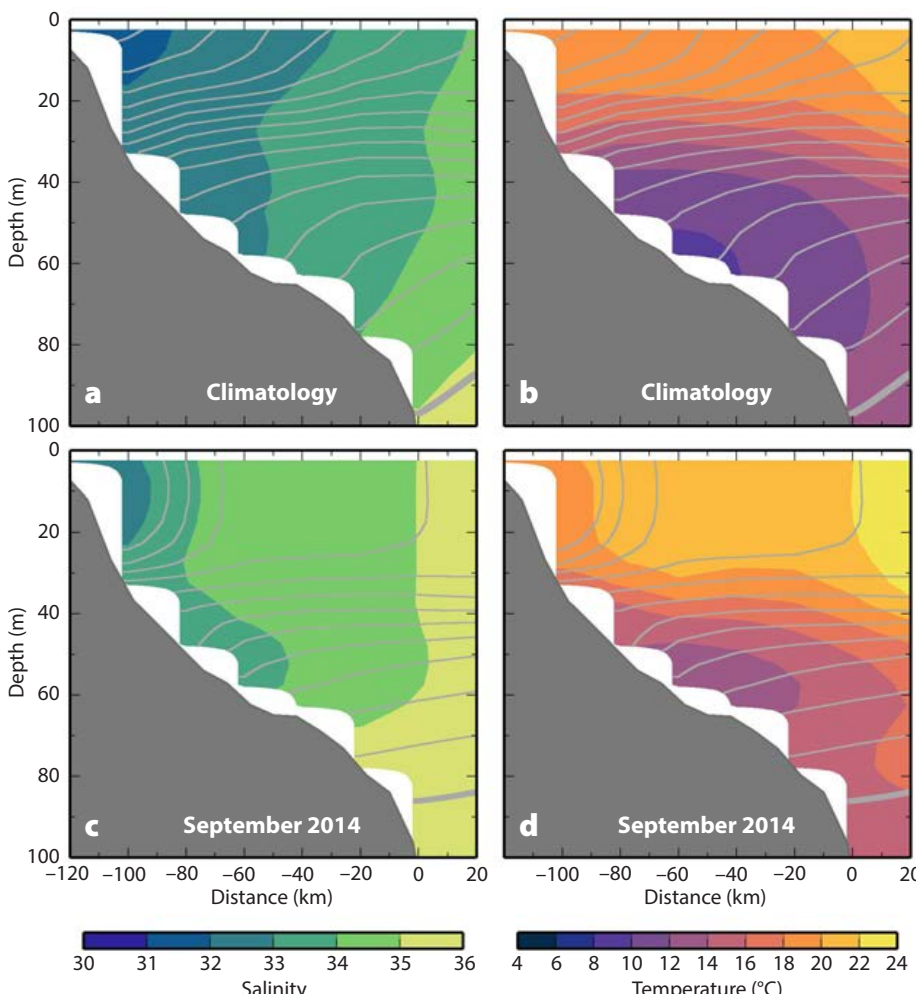


FIGURE 6. Cross-shelf transects of salinity (left panels) and temperature (right panels) from the Ecosystem Monitoring (EcoMon) cruises from NOAA's Northeast Fisheries Science Center. (a–b) Climatological mean fields constructed using observations collected from September cruises from 1981 to 2010. (c–d) Observations collected in September 2014. Gray contours are isopycnals with a contour interval of 0.25 kg m^{-3} and the 26.5 kg m^{-3} isopycnal bold.

REFERENCES

- Andres, M. 2016. On the recent destabilization of the Gulf Stream path downstream of Cape Hatteras. *Geophysical Research Letters* 43:9,836–9,842, <https://doi.org/10.1002/2016GL069966>.
- Bell, R.J., J.A. Hare, J.P. Manderson, and D.E. Richardson. 2014. Externally driven changes in the abundance of summer and winter flounder. *ICES Journal of Marine Science* 71(9):2,416–2,428, <https://doi.org/10.1093/icesjms/fsu069>.
- Cenedese, C., R.E. Todd, G. Gawarkiewicz, and A. Shcherbina. 2013. Offshore transport of shelf water through interaction of vortices with a shelfbreak current. *Journal of Physical Oceanography* 43:905–919, <https://doi.org/10.1175/JPO-D-12-0150.1>.
- Chaudhuri, A.H., A. Gangopadhyay, and J.J. Bisagni. 2009. Interannual variability of Gulf Stream warm core rings in response to the North Atlantic Oscillation. *Continental Shelf Research* 29:856–869, <https://doi.org/10.1016/j.csres.2009.01.008>.
- Chen, K., G.G. Gawarkiewicz, S.J. Lentz, and J.M. Bane. 2014a. Diagnosing the warming of the northeastern US coastal ocean in 2012: A linkage between the atmospheric jet stream variability and ocean response. *Journal of Geophysical Research* 119:218–227, <https://doi.org/10.1002/2013JC009393>.
- Chen, K., and R. He. 2010. Numerical investigation of the Middle Atlantic Bight shelfbreak frontal circulation using a high-resolution ocean hindcast model. *Journal of Physical Oceanography* 40:949–964, <https://doi.org/10.1175/2009JPO4262.1>.
- Chen, K., R. He, B.S. Powell, G.G. Gawarkiewicz, A.M. Moore, and H.G. Arango. 2014b. Data assimilative modeling investigation of Gulf Stream Warm Core Ring interaction with continental shelf and slope circulation. *Journal of Geophysical Research* 119:5,968–5,991, <https://doi.org/10.1002/2014JC009898>.

- Chen, K., Y.-O. Kwon, and G. Gawarkiewicz. 2016. Interannual variability of winter spring temperature in the Middle Atlantic Bight: Relative contributions of atmospheric and oceanic processes. *Journal of Geophysical Research* 121:4,209–4,227, <https://doi.org/10.1002/2016JC011646>.
- Ezer, T., L.P. Atkinson, W.B. Corlett, and J.L. Blanco. 2013. Gulf Stream's induced sea level rise and variability along the US mid-Atlantic coast. *Journal of Geophysical Research* 118:685–697, <https://doi.org/10.1002/jgrc.20091>.
- Fleming, N. 2016. *Seasonal and Spatial Variability in Temperature, Salinity, and Circulation of the Middle Atlantic Bight*. Ph.D. thesis, Rutgers University, 359 pp.
- Forsyth, J.S.T., M. Andres, and G.G. Gawarkiewicz. 2015. Recent accelerated warming of the continental shelf off New Jersey: Observations from the CMV Oleander expendable bathythermograph line. *Journal of Geophysical Research* 120:2,370–2,384, <https://doi.org/10.1002/2014JC010516>.
- Fratantoni, P., and R. Pickart. 2007. The western North Atlantic shelfbreak current system in summer. *Journal of Physical Oceanography* 37:2,509–2,533, <https://doi.org/10.1175/JPO3123.1>.
- Gawarkiewicz, G., F. Bahr, R.C. Beardsley, and K.H. Brink. 2001. Interaction of a slope eddy with the shelfbreak front in the Middle Atlantic Bight. *Journal of Physical Oceanography* 21:2,783–2,796, [https://doi.org/10.1175/1520-0485\(2001\)031<2783:IOASEW>2.0.CO;2](https://doi.org/10.1175/1520-0485(2001)031<2783:IOASEW>2.0.CO;2).
- Gawarkiewicz, G., K. Brink, F. Bahr, R. Beardsley, M. Caruso, J. Lynch, and C.-S. Chiu. 2004. A large-amplitude meander of the shelfbreak front in the Middle Atlantic Bight: Observations from the shelfbreak PRIMER experiment. *Journal of Geophysical Research* 109, C03006, <https://doi.org/10.1029/2002JC001468>.
- Gawarkiewicz, G., R. Todd, A. Plueddemann, and M. Andres. 2012. Direct interaction between the Gulf Stream and the shelf break south of New England. *Scientific Reports* 2, 553, <https://doi.org/10.1038/srep00553>.
- Glenn, S., T. Miles, G. Seroka, Y. Xu, R. Forney, F. Yu, H. Roarty, O. Schofield, and J. Kohut. 2016. Stratified coastal ocean interactions with tropical cyclones. *Nature Communications* 7, <https://doi.org/10.1038/ncomms10887>.
- Greene, C., E. Meyer-Gutbrod, B. Monger, L. McGarry, A. Pershing, I. Belkin, P. Fratantoni, D. Mountain, R. Pickart, A. Proshutinsky, and others. 2013. Remote climate forcing of decadal-scale regime shifts in Northwest Atlantic shelf ecosystems. *Limnology and Oceanography* 58:803–816, <https://doi.org/10.4319/lo.2013.58.3.0803>.
- Hare, J.A., W.E. Morrison, M.W. Nelson, M.M. Stachura, E.J. Teeters, R.B. Griffis, M.A. Alexander, J.D. Scott, L. Alade, R.J. Bell, and others. 2016. A vulnerability assessment of fish and invertebrates to climate change on the northeast US continental shelf. *PLoS ONE* 11(2):e0146756, <https://doi.org/10.1371/journal.pone.0146756>.
- Houghton, R.W., R. Schlitz, R.C. Beardsley, B. Butman, and J. Lockwood Chamberlin. 1982. The Middle Atlantic Bight cold pool: Evolution of the temperature structure during summer 1979. *Journal of Physical Oceanography* 12:1,019–1,029, [https://doi.org/10.1175/1520-0485\(1982\)012<1019:TMABCP>2.0.CO;2](https://doi.org/10.1175/1520-0485(1982)012<1019:TMABCP>2.0.CO;2).
- Linder, C.A., and G. Gawarkiewicz. 1998. A climatology of the shelfbreak front in the Middle Atlantic Bight. *Journal of Geophysical Research* 103:18,405–18,423, <https://doi.org/10.1029/98JC01438>.
- Linder, C.A., G.G. Gawarkiewicz, and R.S. Pickart. 2004. Seasonal characteristics of bottom boundary layer detachment at the shelfbreak front in the Middle Atlantic Bight. *Journal of Geophysical Research* 109, C03049, <https://doi.org/10.1029/2003JC002032>.
- Linder, C.A., G.G. Gawarkiewicz, and M. Taylor. 2006. Climatological estimation of environmental uncertainty over the Middle Atlantic Bight shelf and slope. *IEEE Journal of Oceanic Engineering* 31:308–324, <https://doi.org/10.1109/JOE.2006.877145>.
- Mills, K., A. Pershing, C. Brown, Y. Chen, F.-S. Chiang, D. Holland, S. Lehuta, J. Nye, J. Sun, A. Thomas, and R. Wahle. 2013. Fisheries management in a changing climate: Lessons from the 2012 ocean heat wave in the Northwest Atlantic. *Oceanography* 26(2):191–195, <https://doi.org/10.5670/oceanog.2013.27>.
- Monim, M., 2017. *Seasonal and Inter-annual Variability of Gulf Stream Warm Core Rings from 2000 to 2016*. MS Thesis, University of Massachusetts Dartmouth, 113 pp.
- Pershing, A., M. Alexander, C. Hernandez, L. Kerr, A. Le Bris, K. Mills, J. Nye, N. Record, H. Scannell, J. Scott, and others. 2015. Slow adaptation in the face of ocean warming leads to collapse of Gulf of Maine cod fishery. *Science* 350:809–812, <https://doi.org/10.1126/science.aac9819>.
- Pickart, R. 2000. Bottom boundary layer structure and detachment in the shelfbreak jet of the Middle Atlantic Bight. *Journal of Physical Oceanography* 30:2,668–2,686, [https://doi.org/10.1175/1520-0485\(2001\)031<2668:BBLSAD>2.0.CO;2](https://doi.org/10.1175/1520-0485(2001)031<2668:BBLSAD>2.0.CO;2).
- Pickart, R., T. McKee, D. Torres, and S. Harrington. 1999. Mean structure and interannual variability of the slope water system south of Newfoundland. *Journal of Physical Oceanography* 29:2,541–2,558, [https://doi.org/10.1175/1520-0485\(1999\)029<2541:MSAIVO>2.0.CO;2](https://doi.org/10.1175/1520-0485(1999)029<2541:MSAIVO>2.0.CO;2).
- Smith, K.S., and R. Ferrari. 2009. Production and dissipation of compensated thermohaline variance by mesoscale stirring. *Journal of Physical Oceanography* 39:2,477–2,501, <https://doi.org/10.1175/2009JPO4103.1>.
- Smith, L.M., J.A. Barth, D.S. Kelley, A. Plueddemann, I. Rodero, G.A. Ulses, M.F. Vardaro, and R. Weller. 2018. The Ocean Observatories Initiative. *Oceanography* 31(1):16–35, <https://doi.org/10.5670/oceanog.2018.105>.
- Sullivan, M.C., R.K. Cowen, and B.P. Steves. 2005. Evidence for atmosphere-ocean forcing of yellowtail flounder (*Limanda ferruginea*) recruitment in the Middle Atlantic Bight. *Fisheries Oceanography* 14(5):386–399, <https://doi.org/10.1111/j.1365-2419.2005.00343.x>.
- Ullman, D.S., D.L. Codiga, A. Pfeiffer-Herbert, and C.R. Kincaid. 2014. An anomalous near-bottom cross-shelf intrusion of slope water on the southern New England continental shelf. *Journal of Geophysical Research* 119:1,739–1,753, <https://doi.org/10.1002/2013JC009259>.
- Wright, W., and C. Parker. 1976. A volumetric temperature/salinity census of the Middle Atlantic Bight. *Limnology and Oceanography* 21:563–571, <https://doi.org/10.4319/lo.1976.21.4.0563>.
- Zhang, W., and G. Gawarkiewicz. 2015a. Length scale of the finite amplitude meanders of shelfbreak fronts. *Journal of Physical Oceanography* 45:2,598–2,620, <https://doi.org/10.1175/JPO-D-14-0249.1>.
- Zhang, W., and G. Gawarkiewicz. 2015b. Dynamics of the direct intrusion of Gulf Stream ring water onto the Mid-Atlantic Bight shelf. *Geophysical Research Letters* 42:7,687–7,695, <https://doi.org/10.1002/2015GL065530>.
- Zhang, W.G., D.J. McGillicuddy Jr., and G.G. Gawarkiewicz. 2013. Is biological productivity enhanced at the New England shelfbreak front? *Journal of Geophysical Research* 118:517–535, <https://doi.org/10.1002/jgrc.20068>.

ACKNOWLEDGMENTS

GG, WZ, RT, and MD were supported by the National Science Foundation under grant OCE-1657853. WZ was also supported by grant OCE-1634965. JP is grateful for the support of the Woods Hole Oceanographic Institution Summer Student Fellow Program. AMM was supported by a grant from the MacArthur Foundation. GG and AMM were also supported by a grant from the van Beuren Charitable Foundation for collection and analysis of hydrographic data collected by the CFRF Shelf Research Fleet. Data from the OOI Pioneer Array was obtained from the NSF Ocean Observatories Initiative Data Portal, <http://oceanet.oceanobservatories.org>, as well as from the OOI raw data archive. AG and MM were partially supported by NOAA Grant No. NA11NOS0120038 for implementation of the Mid-Atlantic Regional Association Coastal Ocean Observing System. AG acknowledges the support of Jenifer Clark for the GS-WCR charts, which enabled the census results reported here. Data collected by the CFRF Shelf Research Fleet is available at <http://science.whoi.edu/users/seasoar/cfrfwhoi>. PF acknowledges the NOAA scientists and technicians who coordinated the collection and processing of EcoMon data used in this analysis. The authors thank Frank Bahr and Aubrey Ellertson for their efforts in coordinating and processing Shelf Fleet data as well as the fishermen who collect these data while at sea. We also thank the many dedicated scientists, engineers, and administrators who have worked so hard over more than a decade to make the Pioneer Array a reality.

AUTHORS

Glen Gawarkiewicz (gleng@whoi.edu) is Senior Scientist, **Robert E. Todd** is Associate Scientist, and **Weifeng Zhang** is Associate Scholar, all at Woods Hole Oceanographic Institution, Woods Hole, MA, USA. **Jacob Partida** is an undergraduate at Humboldt State University, Arcata, CA, USA. **Ajvit Gangopadhyay** is Professor and **Mahmud-Ul-Hasan Monim** was Graduate Research Assistant, both at University of Massachusetts Dartmouth, Dartmouth, MA, USA. **Paula Fratantoni** is Research Oceanographer, Northeast Fisheries Science Center, National Marine Fisheries Service, National Oceanic and Atmospheric Administration, Woods Hole, MA, USA. **Anna Malek Mercer** is Executive Director, Commercial Fisheries Research Foundation, Saunderstown, RI, USA. **Margaret Dent** is an undergraduate at Colby College, Waterville, ME, USA.

ARTICLE CITATION

Gawarkiewicz, G., R.E. Todd, W. Zhang, J. Partida, A. Gangopadhyay, M.-U.-H. Monim, P. Fratantoni, A. Malek Mercer, and M. Dent. 2018. The changing nature of shelf-break exchange revealed by the OOI Pioneer Array. *Oceanography* 31(1):60–70, <https://doi.org/10.5670/oceanog.2018.110>.

SIDE BAR SeaView: Bringing Together an Ocean of Data

By Karen Stocks, Steve Diggs, Christopher Olson, Anh Pham, Robert Arko, Adam Shepherd, and Danie Kinkade

The Ocean Observatories Initiative (OOI) supports a comprehensive information management system for data collected by OOI assets, providing access to a wealth of new information for scientists. But what of those wishing to access data from the region of an OOI research array that is not from OOI assets, perhaps to look at longer term trends from before the launch of OOI, or to build a larger regional context? Despite the excellent work of ocean data repositories, finding, accessing, understanding, and reformatting data for use in a desired visualization or analysis tool remains challenging, especially when data are held in multiple repositories.

SeaView (<http://www.seaviewdata.org>) is a US National Science Foundation (NSF) EarthCube effort that works with existing data repositories to create highly integrated thematic data collections in user-requested formats. The project has three related goals:

- **Supporting Scientists.** Driven by input from end-user workshops and interviews, SeaView has produced three thematic data collections, each available as Ocean Data View (ODV) collections and also via a THREDDS Data Server to support R, MATLAB, and Python users. One of these collections focuses on the Pioneer Array region.
- **Strengthening Repositories.** SeaView is helping the ocean data repositories to align their data and processes, to find errors and inconsistencies in the data, and to make ocean data more accessible and easily integrated.
- **Informing EarthCube.** EarthCube (<https://www.earthcube.org>) is an NSF-supported community effort to design and develop the cyberinfrastructure needed to support geosciences in the coming decade. SeaView's experience is informing EarthCube's data integration planning.

To date, SeaView has produced three thematic collections of deeply integrated data pulled from its partner repositories. The Pioneer Array region was selected to support scientists who are developing new research around the OOI array, and because data were available to support the kinds of research prioritized by scientists during SeaView outreach (e.g., biophysical interactions on regional scales). This collection (Figure 1) includes CTD casts from 60+ cruises (11 bottle-calibrated), Northeast Fisheries Science Center Bottom Trawl Survey data, ship tracks, cruise metadata, and links to additional data resources. It supplements the OOI asset data provided through OOI Net. Data sets were selected based on having data within the core Pioneer region of 39.0°N–40.7°N and 69.9°W–71.5°W. For most, the entire data set is provided, including points outside this box. The exception is the Bottom Trawl Survey that, due to its large size, is truncated at 37°N–43°N and 64°W–74°W to match the extent of the other data sets.

A second SeaView collection focuses on the Bermuda Atlantic Time-series Study (BATS) region, providing CTD data from BATS and Hydrostation S, plankton composition, primary productivity, sediment flux, and additional expedition data from the region, all mapped to Rolling Deck to Repository (R2R) cruises and ship tracks. This is the first release of some of these data to the scientific community. A third collection from the Hawaii Ocean Time-series (HOT) region includes CTD and Niskin bottle water sample data from >250 cruises, microbial data from MicrOBIS, and cruise metadata and ship tracks. A fourth collection from the Southern Ocean is in development.

AUTHORS

Karen Stocks (kstocks@ucsd.edu) is Geological Data Center (GDC) Director. **Steve Diggs** is CLIVAR and Carbon Hydrographic Data Office (CCHDO) Technical Manager. **Christopher Olson** is Information Systems Analyst, and **Anh Pham** is Research Assistant, all at Scripps Institution of Oceanography, University of California, San Diego, La Jolla, CA, USA. **Robert Arko** is Rolling Deck to Repository (R2R) Technical Manager, Lamont-Doherty Earth Observatory of Columbia University, Palisades, NY, USA. **Adam Shepherd** is Biological and Chemical Oceanography Data Management Office (BCO-DMO) Technical Director, and **Danie Kinkade** is BCO-DMO Director, both at Woods Hole Oceanographic Institution, Woods Hole, MA, USA.

ARTICLE CITATION

Stocks, K., S. Diggs, C. Olson, A. Pham, R. Arko, A. Shepherd, and D. Kinkade. 2018. SeaView: Bringing together an ocean of data. *Oceanography* 31(1):71, <https://doi.org/10.5670/oceanog.2018.111>.

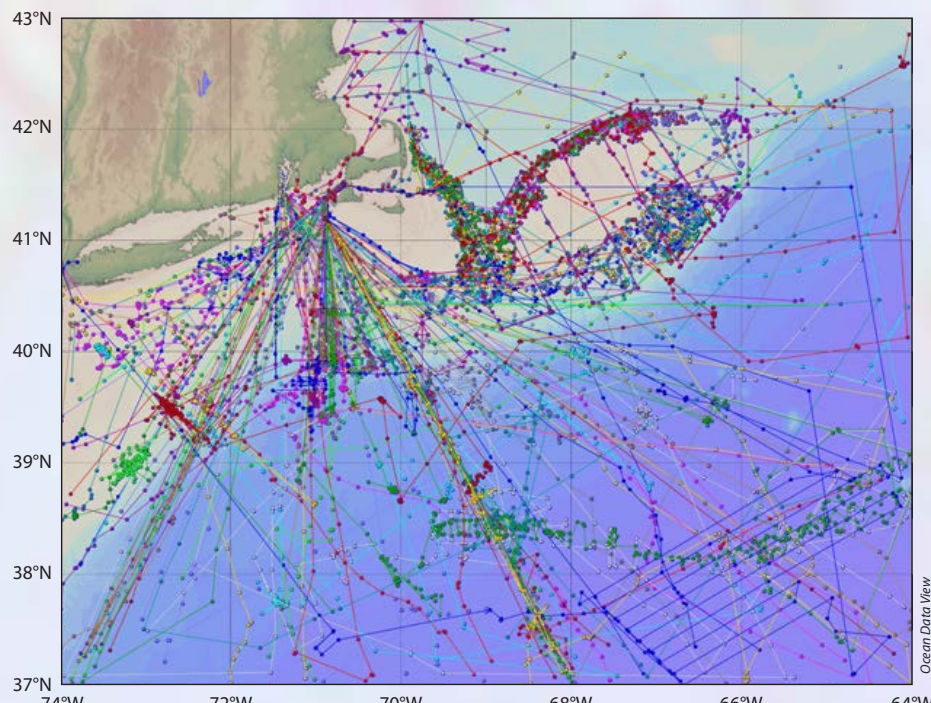


FIGURE 1. Data offered by SeaView's Pioneer region collection include the cruise tracks and station locations mapped here. Map created in ODV (Schlitzer, R., Ocean Data View, <http://odv.awi.de>, 2016)

Atmospheric and Offshore Forcing of Temperature Variability at the Shelf Break

Observations from the OOI Pioneer Array

By Ke Chen,
Glen Gawarkiewicz, and
Albert Plueddemann

ABSTRACT. Knowledge of heat balance and associated temperature variability in the Northwest Atlantic coastal ocean is important for understanding impacts of climate change such as how ocean warming will affect the management of fisheries. Heat balances are particularly complicated near the edge of the continental shelf, where the cross-shelf temperature gradients within the shelf-break front complicate the competing influences of air-sea flux anomalies versus ocean advection. We review the atmospheric and oceanic processes associated with heat balance over the Northwest Atlantic continental shelf and slope, with an emphasis on the scale-dependent nature of the heat balance. We then use data from the Ocean Observatories Initiative (OOI) Pioneer Array to demonstrate heat balance scale dependence at the southern New England shelf break, and the capability of the array to capture multiscale ocean processes. Comparison of the cumulative effects of air-sea heat fluxes measured at the OOI Pioneer Array from May 2015 to April 2016 with the actual temperature change shows the importance of advective processes in overall heat balance near the shelf break.



INTRODUCTION

The coastal ocean of the Northwest Atlantic is affected by both subtropical and subpolar gyres and thus is subject to influences from the Gulf Stream and the Labrador Current. Circulation over the continental shelf includes an equatorward mean flow, which originates in the Labrador Sea (Chapman et al., 1986; Chapman and Beardsley, 1989). Separating the cold/fresh shelf water from the warm/saline slope water are the shelf-break front and the shelf-break jet, which are accompanied by complex shelf-slope exchanges across the shelf break (e.g., Loder et al., 1998). The shelf-break region supports a highly productive ecosystem and commercially valuable fisheries. The importance of understanding the region's ecosystem dynamics and its response to the physical environment has long been recognized (e.g., Fogarty and Murawski, 1998; Ji et al., 2008; He et al., 2011; Mills et al., 2013).

Ocean temperature is a fundamental environmental variable that profoundly influences marine ecosystems. Thus, understanding of the ocean's heat balance and its temperature variability is a long-standing research topic (Beardsley et al., 1985; Lentz et al., 2003a; Brink et al., 2009; Lentz, 2010; Fewings and Lentz, 2011; Connolly and Lentz, 2014). Growing evidence reveals long-term warming of Northwest Atlantic coastal waters (Shearman and Lentz, 2010; Forsyth et al., 2015; Pershing et al., 2015) and extreme warming events such as the ocean heat wave of 2012 (Chen et al., 2014a, 2015). Major shifts across the marine food web associated with such physical changes (e.g., Link and Ford, 2006; Greene and Pershing, 2007; Nye et al., 2009; Lucey and Nye, 2010; Walsh et al., 2015) further challenge ecosystem management (e.g., Mills et al., 2013; Pershing et al., 2015). Better understanding of the heat balance and temperature anomalies has societal and economic importance.

The main processes controlling the Northwest Atlantic coastal ocean heat balance include air-sea heat exchange,

along-shelf advective flux, and cross-shelf advective flux. Each of these three contributions to the heat balance operates on different temporal and spatial scales. This scale-dependent nature of the heat balance often complicates understanding, particularly near the shelf break, where lateral gradients are present.

Fortunately, the Ocean Observatories Initiative (OOI) Pioneer Array (Figure 1) provides observations relevant to the coastal ocean heat balance on the small cross-shelf spatial scales typical of the shelf-break front south of New England. In this article, we briefly review the atmospheric and oceanic processes controlling the heat balance in the Northwest Atlantic coastal ocean, particularly the outer continental shelf and shelf break, with a focus on discussing recent extreme events and interannual variability. Then, we examine a year's worth of data from contrasting locations relative to the shelf-break front to consider both the seasonal cycle and processes contributing to intraseasonal variability. Finally, we discuss future science questions and research opportunities relating to OOI Pioneer Array data.

THE HEAT BALANCE OVER THE OUTER CONTINENTAL SHELF AND SHELF BREAK

Here, we briefly review the processes that affect the heat budget and the temperature variability over the outer continental shelf and shelf break in the Northwest Atlantic coastal ocean, including the Middle Atlantic Bight and the Gulf of Maine, as well as their relationships to large-scale atmospheric and oceanic forcings. These processes include surface air-sea heat flux, along-shelf advection, and shelf-slope exchange. Progress in this area has been limited by the absence of longer-term direct measurements of air-sea fluxes and reliance on reanalysis products with known uncertainty.

Surface air-sea heat flux and along-shelf advective heat flux are the primary drivers of heat balance and temperature variability in the Northwest Atlantic coastal ocean. However, the relative importance

of these two processes in driving temperature changes and the dependence on timescales need clarification. For example, using historical temperature profiles and atmospheric reanalysis products, Lentz (2010) tested the hypothesis that the climatological mean heat balance on the Middle Atlantic Bight continental shelf is between the surface heat flux and the along-shelf advective heat flux resulting from the mean equatorward along-shelf flow. However, he noted that the validity of this simple balance is sensitive to the choice of the meteorological heat flux product. This sensitivity highlights uncertainties associated with the cross-shelf advective flux in the mean heat budget in the Middle Atlantic Bight.

Cross-shelf exchange processes are also important to the heat budget, particularly on an individual event timescale of days to weeks. Note that the mean cross-shelf heat flux in the Middle Atlantic Bight is small (e.g., Lentz, 2010), but the eddy flux (deviation from the mean) over an event timescale can be large. Gulf Stream warm core rings can induce significant cross-shelf transport of shelf water when they impinge upon the shelf break (e.g., Cenedese et al., 2013). Smaller eddies generated by instabilities of the shelf-break front (e.g., Garvine et al., 1988) and frontal meanders (e.g., Gawarkiewicz et al., 2004) can also entrain shelf water. A data-assimilative modeling study by Chen et al. (2014b) shows that one single warm core ring can cause cross-shore heat (and salt) flux much larger than the mean value (Chen and He, 2010). In a companion article, Gawarkiewicz et al. (2018, in this issue) discuss warm core ring intrusions onto the continental shelf observed by the OOI Pioneer Array.

Increasing attention is being given to long-term warming trends in the Middle Atlantic Bight and the increasing influence of offshore forcing that is bringing warmer waters onto the continental shelf because of the potential impacts on fisheries. Examples of such forcing include an increased number of warm core rings on the continental shelf (Monim, 2017), shifts

in the meander pattern of the Gulf Stream (Andres 2016), and the north wall of the Gulf Stream pressing close to the shelf break (Gawarkiewicz et al., 2012; Ullman et al., 2014). Pershing et al. (2015) report accelerated warming of sea surface temperature in the Gulf of Maine during the last decade, which has affected the Atlantic cod fishery. Using XBT data, Forsyth et al. (2015) found accelerated warming of shelf water over the continental shelf off New Jersey. (Interested readers are referred to Figure 1 in Pershing et al., 2015, and Figure 5 in Forsyth et al., 2015, for the long-term warming trends.) Although the exact mechanisms for the accelerated warming in both the Gulf of Maine and the Middle Atlantic Bight remain to be investigated, the Pershing et al. (2015) and Forsyth et al. (2015) papers suggest that both atmospheric and oceanic processes are involved in the accelerated warming. For example, Pershing et al. (2015) showed there was a significant correlation between Gulf of Maine sea surface temperatures and large-scale climate indices, including the Gulf Stream Index, the Atlantic Multidecadal Oscillation, and

the Pacific Decadal Oscillation. Forsyth et al. (2015) showed enhanced warming around the shelf break, indicating the possible role of offshore forcing in displacing the shelf-break front further onshore.

Focusing on the relative contributions of air-sea flux anomalies relative to advective processes, Chen et al. (2016) investigated the interannual variability of winter-spring temperature in the Middle Atlantic Bight using a realistic regional model (5–10 km resolution). They found that seasonal mean temperatures in winter and spring can be estimated using a combination of the initial temperature of the season and mean cumulative air-sea flux. The relative contributions of air-sea flux and ocean advective flux to the evolution of the temperature anomaly (with seasonal cycle removed) varies in each individual year (Chen et al., 2016). Nine of the 12 years considered had temperature anomalies resulting from air-sea flux anomalies, and the other three years had temperature anomalies primarily

resulting from advective processes. It is an open question as to how these relative contributions may change moving forward, given changes in the motions of both the Jet Stream and the Gulf Stream in recent years.

In addition to the long-term warming trend, extreme events have become increasingly common in the Middle Atlantic Bight. The best example is the record warming in 2012. Sea surface temperature in the region was the highest ever recorded (Chen et al. 2015), with a 3°–4°C anomaly that exceeded three standard deviations in both the Middle Atlantic Bight and the Gulf of Maine. The temperature change significantly affected the marine ecosystem (Mills et al., 2013); for example, a northward shift in the distribution of Atlantic cod was observed (Friedland, 2012). Commercial fishermen also reported an increased abundance of squid in the summer of 2012, as well as the appearance of warm-water species not previously seen off southern New England, such as cobia and grouper (Gawarkiewicz et al., 2013). Such an extreme event in the Middle Atlantic Bight was attributed to anomalous atmospheric forcing, which was linked to a northward shift in the Jet Stream position (Figure 2; Chen et al. 2014a, 2015). The anomalously warm atmospheric conditions in the winter of 2011–2012 increased the ocean heat content (and heat content anomaly) and facilitated extreme warm ocean temperatures in spring 2012 (Chen et al. 2014a, 2015), with winter cooling reduced by 50% relative to the mean heat loss from 2000 to 2010. Ocean advection played a secondary role, as it partially damped the heat content anomaly created by the air-sea heat flux (Chen et al., 2015).

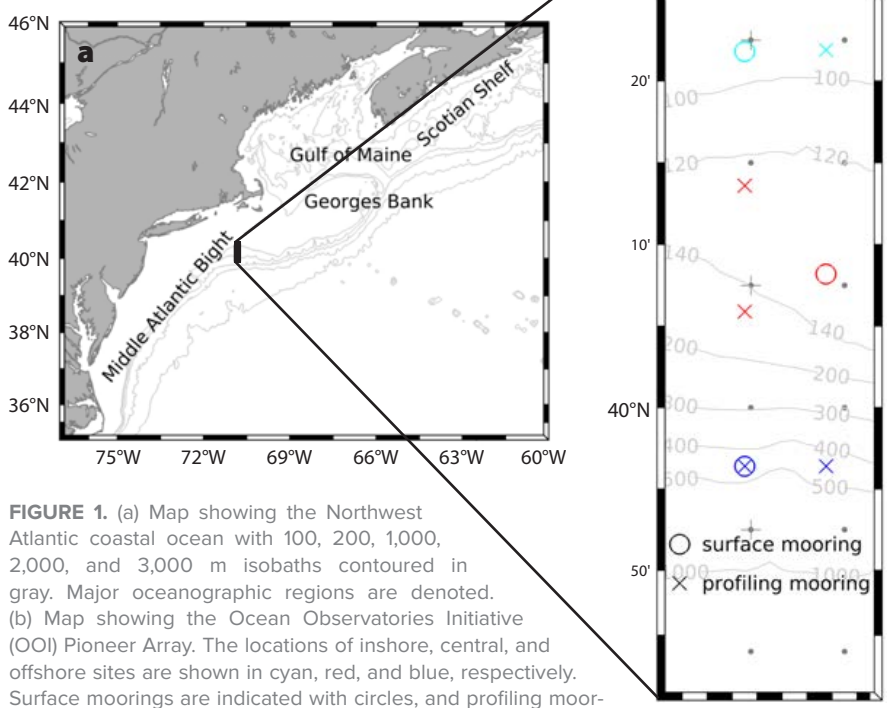


FIGURE 1. (a) Map showing the Northwest Atlantic coastal ocean with 100, 200, 1,000, 2,000, and 3,000 m isobaths contoured in gray. Major oceanographic regions are denoted. (b) Map showing the Ocean Observatories Initiative (OOI) Pioneer Array. The locations of inshore, central, and offshore sites are shown in cyan, red, and blue, respectively. Surface moorings are indicated with circles, and profiling moorings with crosses. Dots and pluses denote the locations of air-sea heat flux grid points for ERA-Interim and temperature/salinity climatology from the World Ocean Atlas.

OBSERVATIONS FROM THE PIONEER ARRAY

The Pioneer Array and Data Processing

The OOI Pioneer Array (Figure 1 and Smith et al., 2018, in this issue) is located off the coast of southern New England. Designed to capture multiscale, inter-

disciplinary processes in the shelf-break region, the Pioneer Array covers the outer shelf, shelf break, and upper slope with three surface moorings, seven profiler moorings, six coastal gliders, and intermittent sections by autonomous underwater vehicles (AUVs). A description of the science motivation and design principles for the Pioneer Array will be available in a forthcoming paper by authors Gawarkiewicz and Plueddemann.

The data used here are from the moored array, including three surface moorings and four profiler moorings at three isobaths near the shelf break: inshore, central, and offshore. The Figure 1 map shows the locations of the moorings. Net air-sea heat flux is collected by bulk meteorology instrument packages (using the COARE v3.5 bulk formula) at three surface moorings, and the depth-averaged temperature is calculated by averaging temperature profiles from the wire-following profilers at corresponding sites: upstream inshore, central inshore, central offshore, and offshore. The CTD on the wire-following profiler takes temperature measurements from 28 m below the surface to 28 m above the bottom (the upper and lower limits are dictated by the mooring design). The surface moorings also record surface water temperature, subsurface temperature at 7 m below surface, and bottom temperature one meter above the seabed. The OOI Data Portal provides two data delivery methods: recovered and telemetered. For each variable at each site, we merge recovered and telemetered data so that the recovered data are prioritized and the telemetered data fill in where the recovered data are not yet available. The net air-sea flux and surface temperature data are averaged to hourly values, and the profiling temperature data are interpolated to the same hourly intervals so that contributions of tidal and other variability are included.

Examination of the availability of heat flux, temperature, and velocity data shows that the inshore and central offshore moorings from May 2015 to April 2016 have the best data coverage. In

the following, we will only focus on the observations from these two sites during this time period.

Heat Flux and Temperature, 2015–2016

The net air-sea heat flux exhibits a strong seasonal cycle, with positive flux into the ocean during the warm months, and

negative flux during the cold months (Figure 3). The daily averaged values from the inshore surface buoy (95 m isobath) range from -775 W m^{-2} to 323 W m^{-2} . The buoy flux compares well with the heat flux from European Centre for Medium-range Weather Forecasts (ECMWF) ERA-Interim global reanalysis at the closest grid point ($70.875^\circ\text{W}, 40.375^\circ\text{N}$).

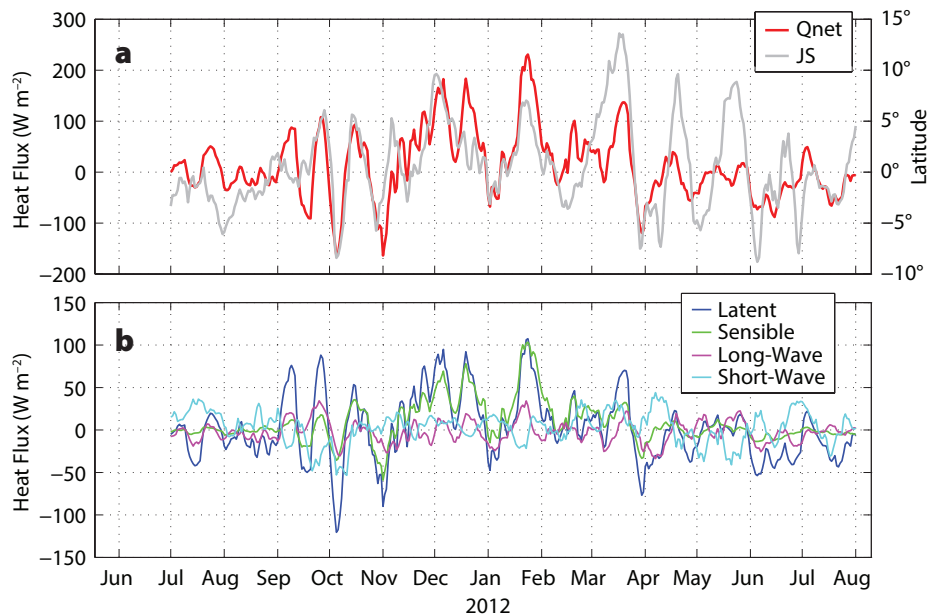


FIGURE 2. (a) The Jet Stream (JS) latitude anomaly (gray) during 2011–2012 and net atmospheric heat flux anomaly from North America Regional Reanalysis (Qnet, red, averaged at National Data Buoy Center buoys 44008, 44025, and 44099 in the Middle Atlantic Bight). (b) Different components of the air-sea heat flux anomaly, including latent heat flux (blue), sensible heat flux (green), long-wave radiation (magenta), and short-wave radiation (cyan). The positive direction is defined as downward (into the ocean). Figure adapted from Chen et al. (2014a)

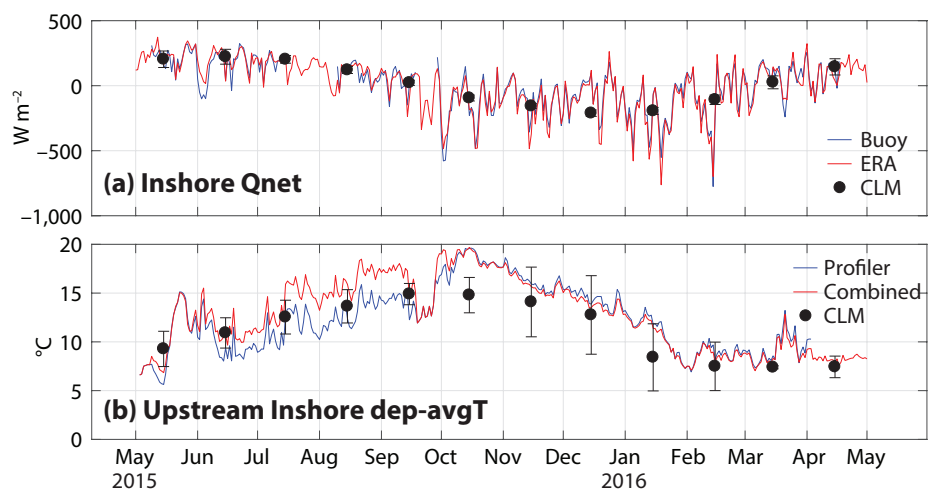


FIGURE 3. (a) Air-sea flux (positive downward) from the inshore surface buoy (blue) and ERA-Interim (red). Black dots indicate the monthly climatology based on ERA-Interim (1979–2016), with the error bar representing one standard deviation for all years. (b) Depth-averaged temperature at the upstream inshore profiler mooring without (blue) and with (red) the combination of surface temperature. Monthly climatology of depth-averaged temperature from WOA 2013 version 2 with the error bar representing one standard deviation during the depth averaging.

The seasonal variation of heat flux from May 2015 to April 2016 generally follows the climatological mean from 1979 to 2016, with larger departures on synoptic timescales during fall and winter, and less so during spring and summer. The strong fluctuations of heat flux during the cooler months are most likely associated with storm activity in the region.

The depth-averaged temperature at the upstream inshore site (9.2 km to the east of the inshore site along the same isobath) has a large seasonal variation, which is consistent with the typical

seasonal cycle over the New England shelf (e.g., Beardsley and Boicourt, 1981; Lentz et al., 2003b, 2010). Over the seasonal scale, the depth-averaged temperature rises from April until October, and decreases to the annual minimum in March. To include the surface variability in the depth-averaged temperature, we also combine the surface water temperature from the inshore surface buoy with the profiling temperature at the upstream inshore site. Linear interpolation was used to fill the values between the surface and the uppermost valid measurement of the

profiling temperature (Figure 4) at the same vertical resolution. Depth averaging then considers all data values for each vertical realization at an hourly interval. As expected, the inclusion of surface temperature increases the depth-averaged value in warmer, stratified months (June through October) by 2°–3°C, and does not change the depth-averaged value in cooler, less stratified months. The depth-averaged temperature at this site is similar to the World Ocean Atlas (WOA) climatology during 2005–2012 at the nearest grid point (70.875°W, 40.375°N) to the west of the upstream inshore site (70.775°W, 40.365°N), although there are notable departures from the climatology during fall and winter (Figure 3b).

At the central site (135 m isobath), net air-sea heat flux exhibits a seasonal cycle similar to that at the inshore site (Figure 5). The buoy air-sea flux values agree well with the ERA-Interim counterpart at the nearest grid point (70.750°W, 40.125°N). The depth-averaged temperature (a combination of profiling temperature at the central offshore mooring and sea surface temperature at the central surface mooring) at the central offshore site (147 m isobaths; 10.2 km from the central site) also shows seasonal variability, although not as significant as that at the inshore site. One notable feature from the depth-averaged temperature record is the anomalously warm temperature in July 2015. The peak temperature is 18°–20°C, about 5°C higher than the climatology (at 70.875°W, 40.125°N) and temperature at the upstream inshore site. Further examination of satellite sea surface temperature imagery reveals that the warm anomaly was associated with a warm core ring, which brought warm and salty water to the outer shelf (Figures 6 and 7). A similar process also occurred in September 2015 when a warm core ring dramatically increased the temperature and salinity at the central offshore site (Figures 6 and 7).

The other notable feature is the anomalously warm temperature from December 2015 to February 2016. The depth-averaged temperature did not go through

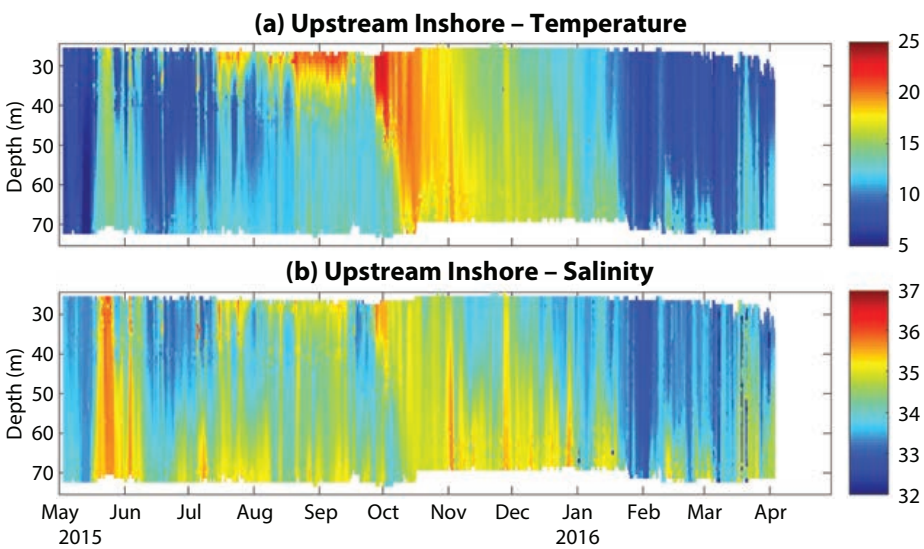


FIGURE 4. Temperature (°C) and salinity record from the upstream inshore wire-following profiler. Data are processed to hourly averages with vertical resolution of one meter.

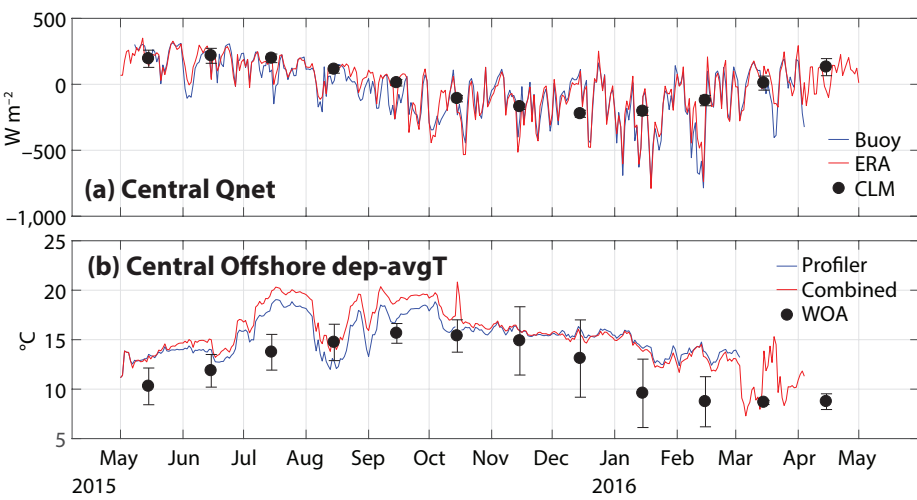


FIGURE 5. (a) Air-sea flux (positive downward) from the central surface buoy (blue) and ERA-Interim (red). Black dots indicate the monthly climatology based on ERA-Interim (1979–2016), with the error bar representing one standard deviation for all years. (b) Depth-averaged temperature at the central offshore profiler mooring without (blue) and with (red) the combination of surface temperature. Monthly climatology of depth-averaged temperature from the World Ocean Atlas with the error bar representing one standard deviation during the depth-averaging.

the typical seasonal cooling (black dots), in contrast with the variability at the upstream inshore site. Chen et al. (2014a) show that reduced cooling in the winter of 2011–2012 caused the extreme warm anomaly in early 2012 over a large region in the Northwest Atlantic coastal ocean. However, the three-month warm anomaly at the central offshore site is less likely to be explained by large-scale reduced cooling (i.e., air-sea heat flux anomaly) because the upstream inshore site, which is only 30 km away, does not exhibit a similar signal. Instead, the long-standing warm anomaly was due to intrusion of warm slope water associated with the Gulf Stream meander and warm core rings (Figure 7), which significantly warmed the continental slope and outer shelf. Considering the small spatial distance, such a contrast in the temporal evolution of the temperature field is remarkable. This contrast explains how the variability of a regional mean (temperature or flux) could be different from that of a single point. The contrasting observations at the inshore and central sites also highlight the importance of resolving the cross-shelf scale of the shelf-break front and frontal processes at the southern New England shelf break, as also suggested by earlier studies (e.g., Lentz et al., 2003b). Local heat balance is critically dependent on the cross-shelf position of the shelf-break front, which may be strongly affected by offshore forcing from warm core rings.

HEAT BALANCE

The time integrated heat balance for the depth-averaged temperature can be written as:

$$\bar{T} = T_0 + Q_{airT} + Q_{hadvT} + Q_{vadvT}, \quad (1)$$

where \bar{T} is the depth-averaged temperature, T_0 is the initial temperature at the beginning of the integration, Q_{airT} is the cumulative air-sea heat flux, Q_{hadvT} is the cumulative horizontal advective flux, and Q_{vadvT} is the cumulative vertical advective flux. For the details of the equation and the data processing, please see the online

supplementary material.

Here, we focus on investigating the one-dimensional balance between the temperature change (the first two terms in Equation 1) and air-sea flux (the third term in Equation 1) and attribute the discrepancies to ocean advective processes. Although the absence of advective fluxes prevents us from closing the budget (we note that velocity data have not yet been

quality controlled; this analysis will be performed in the future), a diagnostic calculation using only atmospheric forcing sheds light on the relative importance of the atmosphere and the ocean in determining temperature variability in the shelf-break region. Over the seasonal timescale, air-sea flux certainly plays an important role in modulating the depth-averaged temperature at both

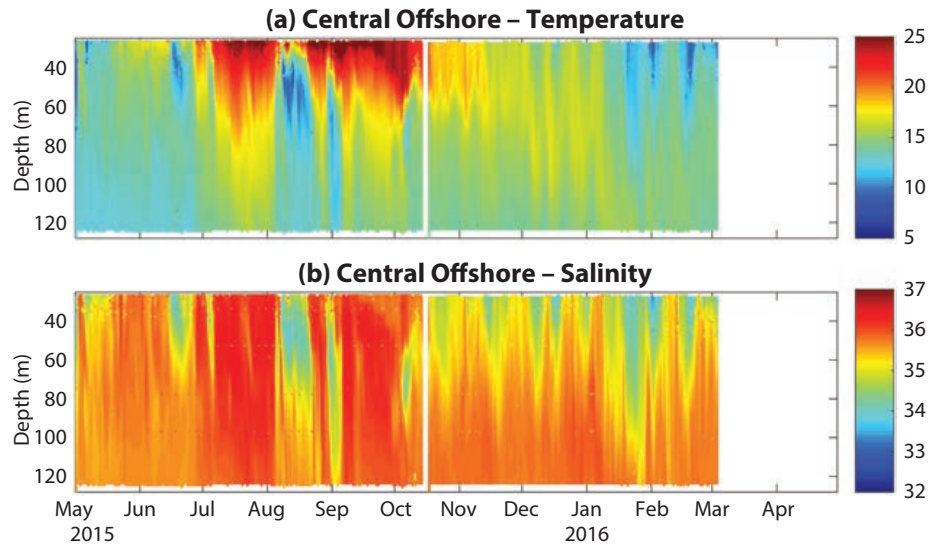


FIGURE 6. Temperature ($^{\circ}\text{C}$) and salinity record from the central offshore wire-following profiler. Data are processed to hourly averages with vertical resolution of one meter.

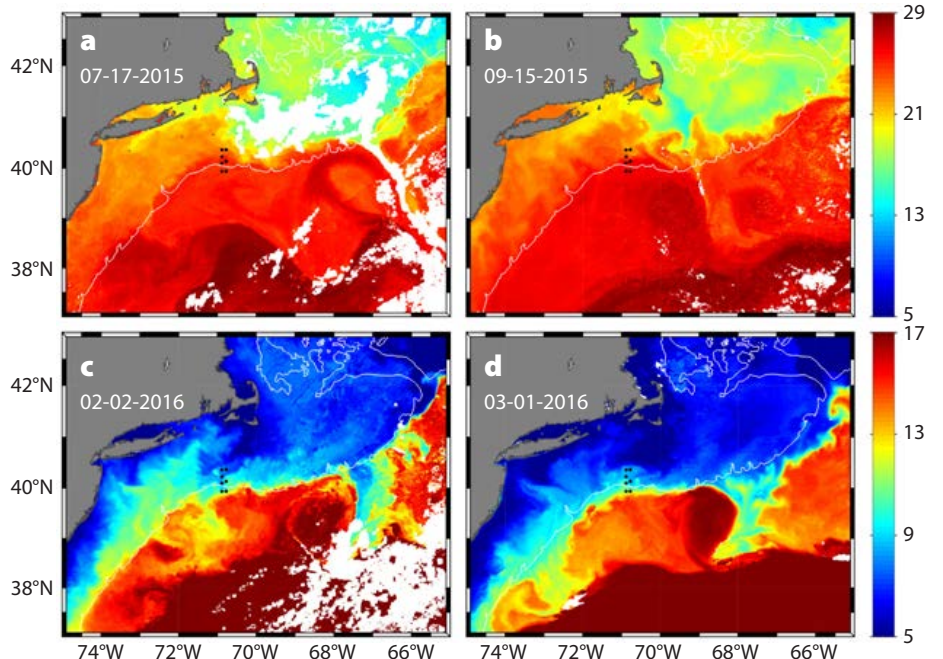


FIGURE 7. Satellite sea surface temperature images showing the impact of warm core rings at the OOI Pioneer Array (black dots). Sea surface temperature data ($^{\circ}\text{C}$) are Advanced Very High Resolution Radiometer (AVHRR) daily averages composite on (a) July 7, 2015, (b) September 15, 2015, (c) February 2, 2016, and (d) March 1, 2016. The white contour is the 200 m isobath. Different color bars (in $^{\circ}\text{C}$) are used for the upper and lower panels.

the upstream inshore and central offshore moorings (Figure 8), consistent with earlier studies over the continental shelf (e.g., Lentz et al., 2003a, 2010; Brink et al. 2009; Chen et al. 2014a). Within a seasonal timescale, the ocean advective flux likely dominates the variability of water column temperature at both the inshore and the central sites. For example, at the central offshore site, the warm anomalies in July 2015 and in early 2016 are primarily the result of advective fluxes associated with warm core ring interactions. Despite the uncertainties in the calculation of depth-averaged temperature and the fact that we did not calculate advective fluxes, the one-dimensional diagnostic calculation in Figure 8 suggests that ocean advective flux can be very important to the heat balance. In particular, intraseasonal variability is dominated by advective processes associated with warm core rings. The calculation of advective fluxes requires depth-dependent along- and cross-shelf temperature gradients and velocities, which are potentially available from the Pioneer Array. Further analysis is needed to better understand the complex ocean advective fluxes in the shelf-break region.

SUMMARY AND FUTURE OUTLOOK

Knowledge of the temperature variability and the heat budget of the outer continental shelf and shelf-break region is important for understanding how climate change is affecting the coastal ocean, in particular, its direct economic impact on the harvesting of living marine resources. Understanding the heat balance relies on the ability to differentiate the underlying atmospheric and oceanic processes, which in this region involves both shelf-break meandering and large-scale forcing from the Jet Stream and the Gulf Stream. The primary drivers of temperature variability depend on the timescale studied, for example, daily, intraseasonal, annual, interannual, or decadal, and the spatial scale, for example, one point to a large control volume. Therefore, interpretation of results needs to consider the appropriate temporal and spatial scales upon which the processes act, which, in the vicinity of the shelf break, may be very small.

The OOI Pioneer Array will undoubtedly provide further insights into the drivers of the heat balance and the role of advective influences, such as warm core ring interactions, on the heat balance at

intraseasonal, seasonal, and interannual timescales. We anticipate gaining a much deeper understanding of heat balance contributions on smaller spatial and temporal scales as oceanographers combine different components of the OOI Pioneer Array data set, such as those from gliders and moored acoustic Doppler current profilers. Even initial analyses are showing that the OOI Pioneer Array resolves the necessary spatial and temporal scales to explore the influences of large-scale atmospheric forcing as well as local shelf-break processes such as frontal meandering.

In addition to improving our understanding of the heat balance in the Northwest Atlantic coastal ocean, data from the OOI Pioneer Array will provide sustained observations of air-sea fluxes necessary for evaluating heat flux products such as OAFlux (Yu and Weller, 2007) and SeaFlux (Curry et al., 2004). Furthermore, keeping a close eye on shelf and slope ocean temperatures is vitally important to understanding changes in the shelf ecosystem and associated fisheries, as well as to examining ocean response and feedbacks to storms affecting the coastal ocean and coastal communities.

Finally, we also hope that a new generation of graduate students and young scientists can be inspired and invigorated by the questions and challenges stimulated by the OOI Pioneer Array. ☐

SUPPLEMENTARY MATERIALS

The Supplementary Materials are available online at <https://doi.org/10.5670/oceanog.2018.112>.

REFERENCES

- Andres, M. 2016. On the recent destabilization of the Gulf Stream path downstream of Cape Hatteras. *Geophysical Research Letters* 43:9,836–9,842, <https://doi.org/10.1002/2016GL069966>.
- Beardsley, R.C., and W.C. Boicourt. 1981. On estuarine and continental-shelf circulation in the Middle Atlantic Bight. Pp. 198–235 in *Evolution of Physical Oceanography*. B.A. Warren and C. Wunsch, eds., The MIT Press.
- Beardsley, R.C., D.C. Chapman, K.H. Brink, S.R. Ramp, and R. Schlitz. 1985. The Nantucket Shoals Flux Experiment (NSFE79): Part 1. A basic description of the current and temperature variability. *Journal of Physical Oceanography* 15:713–748, [https://doi.org/10.1175/1520-0485\(1985\)015<0713:TNSFP>2.0.CO;2](https://doi.org/10.1175/1520-0485(1985)015<0713:TNSFP>2.0.CO;2).
- Brink, K.H., R.C. Beardsley, R. Limeburner, J.D. Irish, and M. Caruso. 2009. Long-term moored array measurements of currents and hydrography over Georges Bank: 1994–1999. *Progress in Oceanography* 82:191–223, <https://doi.org/10.1016/j.pocean.2009.07.004>.

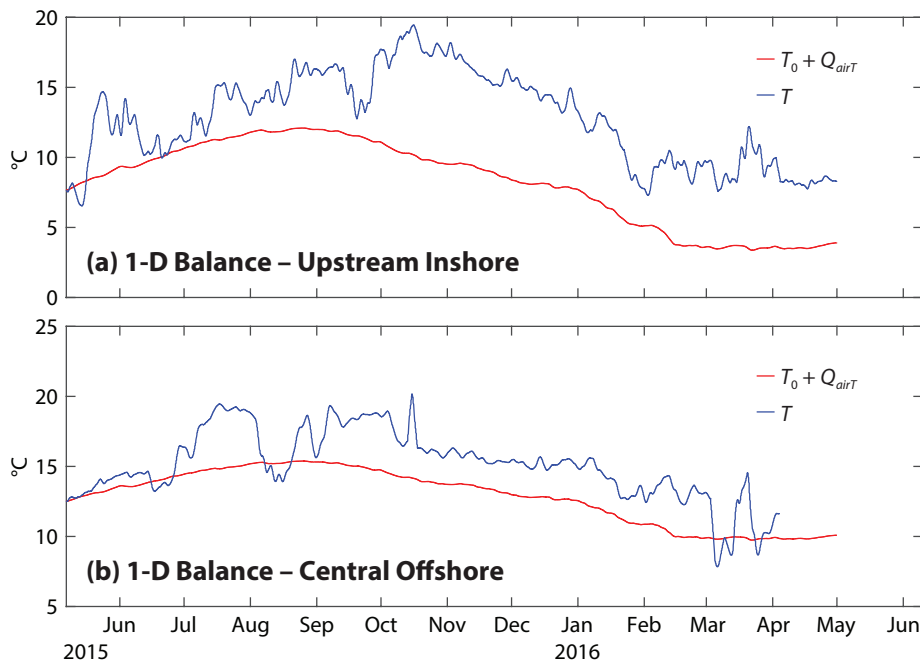


FIGURE 8. Depth-averaged temperature (blue) and the combination of initial temperature and cumulative air-sea heat flux (red) at inshore and central sites from May 2015 to April 2016. All units are °C.

- Cenedese, C., R.E. Todd, G.G. Gawarkiewicz, W.B. Owens, and A.Y. Shcherbina. 2013. Offshore transport of shelf waters through interaction of vortices with a shelfbreak current. *Journal of Physical Oceanography* 43:905–919, <https://doi.org/10.1175/JPO-D-12-0150.1>.
- Chapman, D.C., J.A. Barth, R.C. Beardsley, and R.G. Fairbanks. 1986. On the continuity of mean flow between the Scotian shelf and the Middle Atlantic Bight. *Journal of Physical Oceanography* 16:758–772, [https://doi.org/10.1175/1520-0485\(1986\)016<758:OTCOMF>2.0.CO;2](https://doi.org/10.1175/1520-0485(1986)016<758:OTCOMF>2.0.CO;2).
- Chapman, D.C., and R.C. Beardsley. 1989. On the origin of shelf water in the Middle Atlantic Bight. *Journal of Physical Oceanography* 19:384–391, [https://doi.org/10.1175/1520-0485\(1989\)019<0384:OTCOMF>2.0.CO;2](https://doi.org/10.1175/1520-0485(1989)019<0384:OTCOMF>2.0.CO;2).
- Chen, K., G. Gawarkiewicz, Y.-O. Kwon, and W.G. Zhang. 2015. The role of atmospheric forcing versus ocean advection during the extreme warming of the northeast US continental shelf in 2012. *Journal of Geophysical Research* 120:4,324–4,339, <https://doi.org/10.1002/2014JC010547>.
- Chen, K., G.G. Gawarkiewicz, S.J. Lentz, and J.M. Bane. 2014a. Diagnosing the warming of the northeastern US coastal ocean in 2012: A linkage between the atmospheric jet stream variability and ocean response. *Journal of Geophysical Research* 119:218–227, <https://doi.org/10.1002/2013JC009393>.
- Chen, K., and R. He. 2010. Numerical investigation of the Middle Atlantic Bight shelfbreak frontal circulation using a high-resolution ocean hindcast model. *Journal of Physical Oceanography* 40:949–964, <https://doi.org/10.1175/2009JPO42621>.
- Chen, K., R. He, B.S. Powell, G.G. Gawarkiewicz, A.M. Moore, and H.G. Arango. 2014b. Data assimilative modeling investigation of Gulf Stream warm core ring interaction with continental shelf and slope circulation. *Journal of Geophysical Research* 119:5,968–5,991, <https://doi.org/10.1002/2014JC009898>.
- Chen, K., Y.-O. Kwon, and G. Gawarkiewicz. 2016. Interannual variability of winter-spring temperature in the Middle Atlantic Bight: Relative contributions of atmospheric and oceanic processes. *Journal of Geophysical Research* 121:4,209–4,227, <https://doi.org/10.1002/2016JC011646>.
- Connolly, T.P., and S.J. Lentz. 2014. Interannual variability of wintertime temperature on the inner continental shelf of the Middle Atlantic Bight. *Journal of Geophysical Research* 119:6,269–6,285, <https://doi.org/10.1002/2014JC010153>.
- Curry, J.A., A. Bentamy, M.A. Bourassa, D. Bourras, E.F. Bradley, M. Brunke, S. Castro, S.H. Chou, C.A. Clayson, W.J. Emery, and others. 2004. SEAFLUX. *Bulletin of the American Meteorological Society* 85:409–424, <https://doi.org/10.1175/BAMS-85-3-409>.
- Fewings, M.R., and S.J. Lentz. 2011. Summertime cooling of the shallow continental shelf. *Journal of Geophysical Research* 116, C07015, <https://doi.org/10.1029/2010JC006744>.
- Fogarty, M.J., and S.A. Murawski. 1998. Large-scale disturbance and the structure of marine systems: Fishery impacts on Georges Bank. *Ecological Applications* 8:S6–S22, [https://doi.org/10.1890/1051-0761\(1998\)8\[S6:LDATSO\]2.0.CO;2](https://doi.org/10.1890/1051-0761(1998)8[S6:LDATSO]2.0.CO;2).
- Forsyth, J.S.T., M. Andres, and G.G. Gawarkiewicz. 2015. Recent accelerated warming of the continental shelf off New Jersey: Observations from the CMV Oleander expendable bathythermograph line. *Journal of Geophysical Research* 120:2,370–2,384, <https://doi.org/10.1002/2014JC010516>.
- Friedland, K. 2012. *Ecosystem Advisory for the Northeast Shelf Large Marine Ecosystem. Advisory 2012 - No. 2*. National Marine Fishery Service, Northeast Fishery Science Center, Woods Hole, MA.
- Garvine, R.W., K.C. Wong, G. Gawarkiewicz, R.K. McCarthy, R.W. Houghton, and F. Aikman. 1988. The morphology of shelfbreak eddies. *Journal of Geophysical Research* 93(C12):15,593–15,607, <https://doi.org/10.1029/JC093iC12p15593>.
- Gawarkiewicz, G.G., K. Brink, F. Bahr, R. Beardsley, and M. Caruso. 2004. A large-amplitude meander of the shelfbreak front during summer south of New England: Observations from the Shelfbreak PRIMER experiment. *Journal of Geophysical Research* 109, C03006, <https://doi.org/10.1029/2002JC001468>.
- Gawarkiewicz, G.G., G. Lawson, M. Petruny-Parker, P. Fratantoni, and J. Hare. 2013. *The Shelf Break Ecosystem off the Northeastern United States: Current Issues and Recommended Research Directions*. Report of a workshop sponsored by the Cooperative Institute for the North Atlantic Region (CINAR), January 7–8, 2013, Warwick, RI, 29 pp.
- Gawarkiewicz, G.G., R.E. Todd, A.J. Plueddemann, M. Andres, and J.P. Manning. 2012. Direct interaction between the Gulf Stream and the shelfbreak south of New England. *Scientific Reports* 2:553, <https://doi.org/10.1038/srep00553>.
- Gawarkiewicz, G., R.E. Todd, W. Zhang, J. Partida, A. Gangopadhyay, M.-U.-H. Monim, P. Fratantoni, A. Malek Mercer, and M. Dent. 2018. The changing nature of shelf-break exchange revealed by the OOI Pioneer Array. *Oceanography* 31(1):60–70, <https://doi.org/10.5670/oceanog.2018.110>.
- Greene, C.H., and A.J. Pershing. 2007. Climate drives sea change. *Science* 315:1,084–1,085, <https://doi.org/10.1126/science.1136495>.
- He, R., K. Chen, K. Fennel, G.G. Gawarkiewicz, and D.J. McGillicuddy Jr. 2011. Seasonal and interannual variability of physical and biological dynamics at the shelfbreak front of the Middle Atlantic Bight: Nutrient supply mechanisms. *Biogeosciences* 8:2,935–2,946, <https://doi.org/10.5194/bg-8-2935-2011>.
- Ji, R., C. Davis, C. Chen, and R. Beardsley. 2008. Influence of local and external processes on the annual nitrogen cycle and primary productivity on Georges Bank: A 3-D biological-physical modeling study. *Journal of Marine Systems* 73:31–47, <https://doi.org/10.1016/j.jmarsys.2007.08.002>.
- Lentz, S.J. 2010. The mean along-isobath heat and salt balances over the Middle Atlantic Bight continental shelf. *Journal of Physical Oceanography* 40:934–948, <https://doi.org/10.1175/2009JPO4214.1>.
- Lentz, S.J., R.C. Beardsley, J.D. Irish, J. Manning, P.C. Smith, and R.A. Weller. 2003a. Temperature and salt balances on Georges Bank February–August 1995. *Journal of Geophysical Research* 108, 8006, <https://doi.org/10.1029/2001JC001220>.
- Lentz, S., K. Shearman, S. Anderson, A. Plueddemann, and J. Edson. 2003b. Evolution of stratification over the New England shelf during the Coastal Mixing and Optics study, August 1996–June 1997. *Journal of Geophysical Research* 108(C1), 3008, <https://doi.org/10.1029/2001JC001121>.
- Lentz, S.J., R.K. Shearman, and A.J. Plueddemann. 2010. Heat and salt balances over the New England continental shelf, August 1996 to June 1997. *Journal of Geophysical Research* 115, C07017, <https://doi.org/10.1029/2009JC006073>.
- Link, J.S., and M.D. Ford. 2006. Widespread and persistent increase of Ctenophora in the continental shelf ecosystem off NE USA. *Marine Ecology Progress Series* 320:153–159, <https://doi.org/10.3354/meps320153>.
- Loder, J.W., B. Petrie, and G. Gawarkiewicz. 1998. The coastal ocean off northeastern North America: A large-scale view. Pp. 105–133 in *The Sea, Volume 11: The Global Coastal Ocean—Regional Studies and Syntheses*. A.R. Robinson and K.H. Brink, eds, John Wiley & Sons.
- Lucey, S.M., and J.A. Nye. 2010. Shifting species assemblages in the Northeast US Continental Shelf Large Marine Ecosystem. *Marine Ecology Progress Series* 415:23–33, <https://doi.org/10.3354/meps08743>.
- Mills, K., A.J. Pershing, C.J. Brown, Y. Chen, F.-S. Chiang, D.S. Holland, S. Lehuta, J.A. Nye, J.C. Sun, A.C. Thomas, and R.A. Wahle. 2013. Fisheries management in a changing climate: Lessons from the 2012 ocean heat wave in the Northwest Atlantic. *Oceanography* 26(2):191–195, <https://doi.org/10.5670/oceanog.2013.27>.
- Monim, M. 2017. *Seasonal and Inter-annual Variability of Gulf Stream Warm Core Rings from 2000 to 2016*. Master's thesis, University of Massachusetts Dartmouth, 113 pp.
- Nye, J.A., J.S. Link, J.A. Hare, and W.J. Overholtz. 2009. Changing spatial distribution of fish stocks in relation to climate and population size on the Northeast United States continental shelf. *Marine Ecology Progress Series* 393:111–129, <https://doi.org/10.3354/meps08220>.
- Pershing, A.J., M.A. Alexander, C.M. Hernandez, L.A. Kerr, A. Le Bris, K.E. Mills, J.A. Nye, N.R. Record, H.A. Scannell, J.D. Scott, and others. 2015. Slow adaptation in the face of rapid warming leads to collapse of the Gulf of Maine cod fishery. *Science* 350:809–812, <https://doi.org/10.1126/science.aac9819>.
- Shearman, R.K., and S.J. Lentz. 2010. Long-term sea surface temperature variability along the US east coast. *Journal of Physical Oceanography* 40:1,004–1,016, <https://doi.org/10.1175/2009JPO43001>.
- Smith, L.M., J.A. Barth, D.S. Kelley, A. Plueddemann, I. Rodero, G.A. Ulses, M.F. Vardaro, and R. Weller. 2018. The Ocean Observatories Initiative. *Oceanography* 31(1):16–35, <https://doi.org/10.5670/oceanog.2018.105>.
- Ullman, D.S., D.L. Codiga, A. Pfeiffer-Herbert, and C.R. Kincaid. 2014. An anomalous near-bottom cross-shelf intrusion of slope water on the southern New England continental shelf. *Journal of Geophysical Research* 119:1,739–1,753, <https://doi.org/10.1002/2013JC009259>.
- Walsh, H.J., D.E. Richardson, K.E. Marancik, and J.A. Hare. 2015. Long-term changes in the distributions of larval and adult fish in the northeast US shelf ecosystem. *PLoS ONE* 10(9):e0137382, <https://doi.org/10.1371/journal.pone.0137382>.
- Yu, L., and R.A. Weller. 2007. Objectively analyzed air-sea heat fluxes for the global ice-free oceans (1981–2005). *Bulletin of the American Meteorological Society* 88:527–539, <https://doi.org/10.1175/BAMS-88-4-527>.

ACKNOWLEDGMENTS

KC was partially supported by the National Science Foundation under grant OCE-1435602 and OCE-1634094. GG was supported by the National Science Foundation under grant OCE-1657853. AP was supported by the National Science Foundation through the Cooperative Agreement (subaward) SA9-10 from the Consortium for Ocean Leadership to the Woods Hole Oceanographic Institution. We thank the many scientists and engineers who contributed to the design, construction, and operation of the OOI Pioneer Array for a job well done.

AUTHORS

Ke Chen (kchen@whoi.edu) is Assistant Scientist, **Glen Gawarkiewicz** is Senior Scientist, and **Albert Plueddemann** is Senior Scientist, all in the Physical Oceanography Department, Woods Hole Oceanographic Institution, Woods Hole, MA, USA.

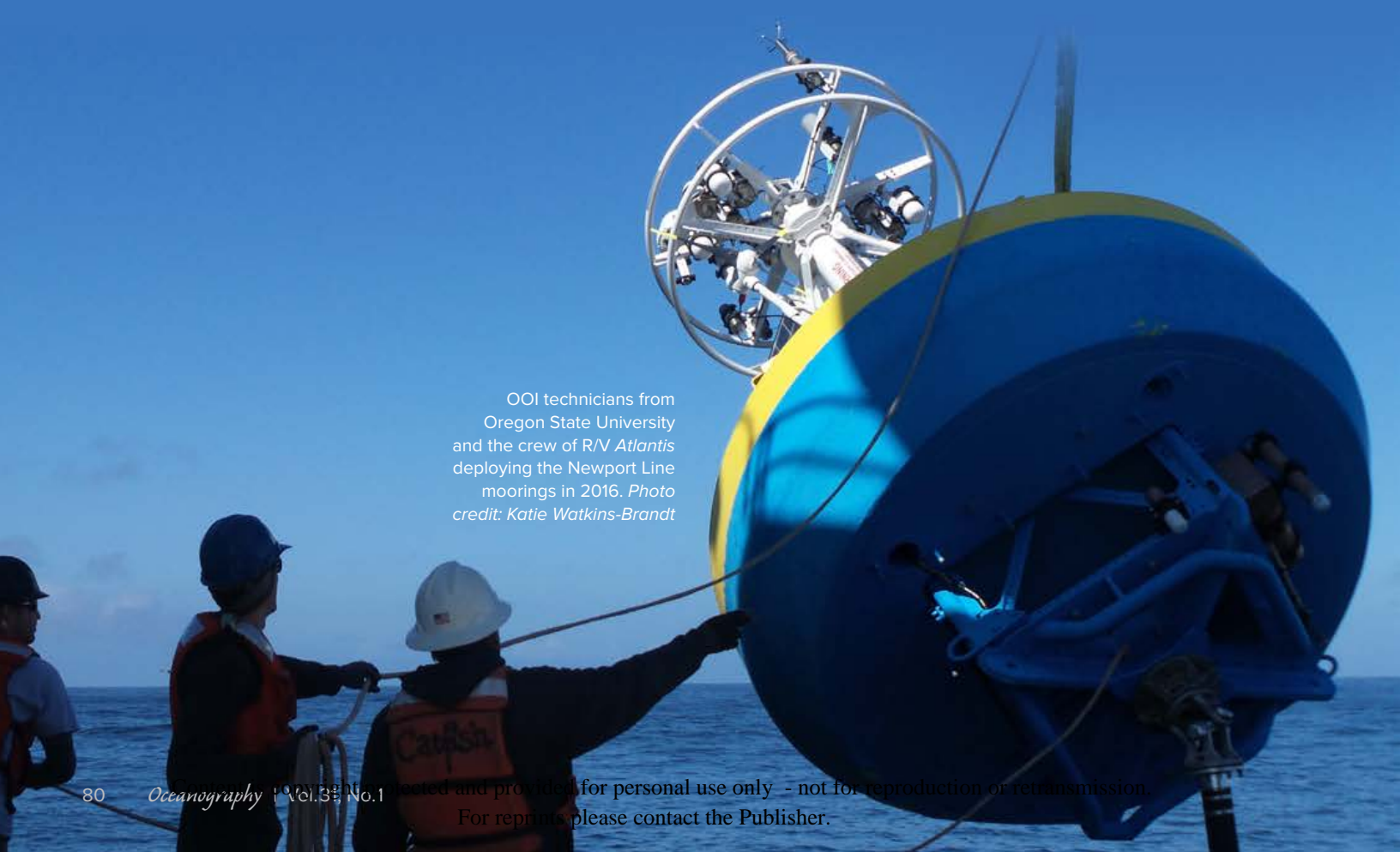
ARTICLE CITATION

Chen, K., G. Gawarkiewicz, and A. Plueddemann. 2018. Atmospheric and offshore forcing of temperature variability at the shelf break: Observations from the OOI Pioneer Array. *Oceanography* 31(1):72–79, <https://doi.org/10.5670/oceanog.2018.112>.

Temporal and Spatial Dynamics of Physical and Biological Properties along the Endurance Array of the California Current Ecosystem

By Fernanda Henderikx Freitas,
Gonzalo S. Saldías,
Miguel Goñi, R. Kipp Shearman,
and Angelique E. White

ABSTRACT. The coastal margin of the Pacific Northwest of the United States is a highly dynamic and productive region. Here, we use satellite, high-frequency mooring, and glider estimates of biologically relevant physical and optical variables to characterize seasonal patterns and latitudinal and cross-shore gradients in particle concentrations between the Washington and Oregon shelves. Consistent with prior research, we find that the Columbia River exerts a strong seasonal influence on the Washington shelf, but smaller coastal rivers and resuspension processes also appear important in determining particle distributions nearshore during winter across the full study region. We find fluorescence-based measurements of chlorophyll to be similar in magnitude across the two shelves over the time period examined, although the much weaker wind stresses off Washington indicate that processes other than upwelling are important determinants of chlorophyll changes in those areas, as previously suggested. These in situ observations contrast with the overall differences observed from satellite data, which consistently show higher chlorophyll concentrations off the Washington coast. This research suggests that latitudinal differences in chromophoric dissolved organic matter may be a partial explanation for perceived trends in satellite-derived chlorophyll. The observations presented are nascent; maturation of temporal and spatial coverage of OOI data sets will be necessary to more conclusively link physical forcing and biogeochemical responses.



OOI technicians from Oregon State University and the crew of R/V *Atlantis* deploying the Newport Line moorings in 2016. Photo credit: Katie Watkins-Brandt

INTRODUCTION

Embedded within the California Current System, the coastal ocean along the Pacific Northwest (PNW) of the continental United States has recently become highly instrumented with the installation of an array of moored and autonomous assets via the National Science Foundation-supported Ocean Observatories Initiative (OOI). The oceanography of this area is complex. Strong temporal and spatial variability in the physics and biogeochemistry of the upper water column is largely the result of wind-driven upwelling and downwelling processes, as well as the freshwater influence of the fourth largest river in North America and other numerous small mountainous rivers. Monitoring changes in the ecological properties of these heterogeneous regions is challenging and requires both synoptic surveys and high-resolution Eulerian time series.

Large-scale upwelling along ocean margins occurs mainly in eastern boundary regimes (e.g., Peru/Chile, Southeast Atlantic, PNW) and is a highly seasonal phenomenon driven by shifts in wind strength and direction. In the PNW, prevailing northerly winds lead to intense upwelling periods when cold, dense, and nutrient-rich waters advected onto the continental shelf reach the euphotic zone (e.g., Huyer, 1983), resulting in enhanced phytoplankton production (e.g., Dickson and Wheeler, 1995) and the formation of biogenic particles (e.g., Wetz and Wheeler, 2003). Wind forcing also drives fluctuations in surface currents, water properties, and sea level, with typical scales of variability on the order of three to 10 days (Hickey and Banas, 2003). Additionally, upwelling-favorable winds drive cross-shelf transport that actively pushes the freshwater plume of the Columbia River southward and offshore of the Oregon shelf in the spring and summer months (Barnes et al., 1972; Hickey et al., 2005; Saldías et al., 2016).

Much less is known about the biogeochemistry of non-upwelling periods, even though these conditions are sustained throughout much of the year.

For example, downwelling-favorable winds and moisture-laden storms prevail along the PNW in fall and winter months, which leads to large fluvial inputs of biogeochemically relevant, land-derived constituents to the coastal ocean, including freshwater (i.e., buoyancy), dissolved inorganic nutrients, and dissolved and particulate organic matter (e.g., Wheatcroft et al., 2010; Goñi et al., 2013). During these periods, the colder waters of the Columbia River are diverted northward over the Washington shelf and slope, altering regional current patterns (Hickey et al., 1998).

Productivity in the PNW has traditionally been assessed from shipboard surveys and satellite data. Studies comparing the productivity patterns of the Washington and Oregon shelves have concluded that absolute chlorophyll (chl) concentrations, a proxy for productivity, as well as the cross-shelf extent of chl signals, are seasonally larger for the Washington shelf despite significantly weaker upwelling winds relative to Oregon (Hickey and Banas, 2003, 2008; Davis et al., 2014). Ware and Thomson (2005) reported similar patterns of increased concentrations of chl, zooplankton, and fish to the north of the California Current System. In these studies, the seeming paradox was attributed to key geographical differences between the two locations, namely (1) the continental shelf is broader in Washington, thus potentially leading to increased residence times for nutrient and phytoplankton-rich waters in the region, (2) the Columbia River, which flows north into the Washington shelf during much of the year, is a potential source of limiting nutrients including iron and silicate, (3) proximity to the Strait of Juan de Fuca in British Columbia, Canada, likely allows for the advection of nutrient-rich waters onto the Washington shelf, and (4) the larger number of submarine canyons off the Washington shelf potentially allows for deeper, nutrient-rich waters to reach areas closer to the surface over the seasons and sustain productivity during weak upwelling periods.

In the following, we summarize long-term satellite estimates of particle distributions for the Washington and Oregon shelves, and raise the importance of considering the contribution of chromophoric dissolved organic matter (CDOM) in the interpretation of productivity patterns from satellite data. Then, we describe latitudinal gradients in temperature, salinity, pigment fluorescence, CDOM, and particle backscattering from high-frequency OOI observations during upwelling and downwelling periods of 2015 and 2016. Finally, we discuss the potential roles of wind-driven upwelling, resuspension processes, and riverine discharge in driving particle distributions across the Washington and Oregon shelves.

METHODS AND DATA SOURCES

OOI Endurance Array

The OOI Endurance Array (<http://oceanobservatories.org/array/coastal-endurance>) provides observations of cross-shelf and along-shelf variability in oceanographic properties off the Oregon and Washington coasts via a set of moorings and autonomous glider surveys (see map in Smith et al., 2018, in this issue). Two cross-shelf moored array lines, the Oregon (OR; Newport Line, ~44.6°N, inshore of 125°W) and Washington (WA; Grays Harbor Line, ~47°N, inshore of 125°W) lines each include inshore, mid-shelf, and offshore moorings at bottom depths of approximately 25, 80, and 600 m. In this work we used in vivo fluorescence-based estimates of chlorophyll (chl, mg m⁻³) and fluorescent-based CDOM (370 ± 20 nm/460 ± 120 nm excitation/emission wavelengths, ppb), volume scattering coefficients at 700 nm (β (124°), m⁻¹ sr⁻¹), water temperature, and salinity data sets from the OR and WA OOI surface mooring sensor packages, nominally sampled at 7 m depth as determined by the OOI mooring design. All available recovered and telemetered data from the January 2015 to March 2017 data period were acquired to improve temporal coverage; no QA/QC flags had

been previously applied to these data. Instances of discrepancies between recovered and telemetered data were observed, in which case the recovered data sets were selected. Personal communication with OOI data managers indicated that these discrepancies were due to “time-of-day” telemetry errors.

Chlorophyll and CDOM data were obtained in scaled units based on OOI pre-deployment calibration coefficients, and only nighttime chl data are used in the analysis to avoid the effects of quenching of chl fluorescence during daylight hours (Müller et al., 2001). Volume scattering coefficients were converted to particulate backscattering coefficients (b_{bp} , m⁻¹) using the relationship $b_{bp} = 2\pi\chi\beta_p(\theta)$, where χ is a dimensionless factor equal to 1.076 based on Sullivan et al. (2013), and the particulate volume scattering β_p is obtained by subtracting the volume scattering of seawater of Zhang et al. (2009) from β . Particulate backscattering is considered a proxy for suspended particles, including phytoplankton, detritus, and sediments (Jonasz and Fournier, 2011). The CDOM instrument configuration is specific for estimation of humic-like dissolved organic matter, and thus is a proxy for land-derived materials transported by rivers (Coble, 1996). Data presented here as daily averages were smoothed using a one-hour moving average filter on log-transformed observations to reduce the effect of high-frequency variability. The minimum values of chl, b_{bp} , and CDOM per mooring were subtracted from each time series to facilitate mooring-to-mooring comparisons, given that OOI biological sensors are not intercalibrated.

Despite the long-term sampling efforts, several sections of data were excluded from the analysis due to low quality of the retrieved outputs. These included raw volume scattering count data between October 2014 and April 2015 for both inshore moorings that were characterized by a repetitive pattern of progressive signal increase up to the upper limit of detection, followed by abrupt drops to

zero values. Similar issues (e.g., maxed-out values possibly associated with bio-fouling) affected several sections of data from these moorings between January and May 2016. Additionally, data density is often more complete for the OR line than the WA time series, which yields large gaps in the comparative data set. For example, only 66 days of data are available for the offshore WA mooring in 2015, compared to 268 days for the offshore OR mooring.

Nearly coincident glider observations from the WA (glider/deployments g386/2, g384/3, and g312/4) and OR (g384/1, g320/2, and g382/2) long Endurance Lines (sampling between 128°W and 125°W) were obtained for the period 2015–2016, totaling about 40 days of data at each line. From these data, we calculated freshwater content (FWC; m), which represents the thickness of freshwater in the water column, as follows:

$$FWC = \int_{-d}^0 \frac{(S_0 - S)}{S_0} dz, \quad (1)$$

where S is salinity, S_0 is the reference salinity of 32.5 for the Columbia River plume (Barnes et al., 1972), and d is the plume thickness according to the depth of S_0 .

Additional glider-derived optical data (chl, CDOM, and b_{bp}) from the short Endurance Lines (sampling between 125°W and 124.3°W) off WA and OR were obtained (g326/1, g247/4, g381/1 and g311/1). Mission configurations consisted of repetitive cross-shore transects, with each deployment lasting between one and two months. Few simultaneous glider deployments were available for WA and OR, or at the times of moored observations. Thus, mean cross-shore sections per deployment were acquired as examples of cross-shore distributions of bio-optical properties during different times of the year at the two lines. A deep offset correction was applied to all glider optical data in order to improve comparisons between data from different gliders (Schmechtig et al., 2014).

Wind stress, significant wave heights, and river discharge measurements were

used to inform potential controls on the observed physical and bio-optical observations. Wind and wave data were obtained from NOAA’s National Data Buoy Center (NDBC) buoys 46041 and 46050 (<http://www.ndbc.noaa.gov>). Hourly Columbia River discharge data were obtained from US Geological Survey gauge 14105700 (<https://nwis.waterdata.usgs.gov>). Monthly discharge totals for 21 small mountainous rivers along the OR-WA coastline were obtained from USGS gauges (Figure 1a). All correlation coefficients (r) shown in this study are considered significant if within the 95% confidence interval.

Satellite Observations of Phytoplankton and Particle Distributions

Monthly satellite retrievals of chlorophyll (chl_{sat}), absorption coefficients of non-algal materials and CDOM at 443 nm (a_{cdom}(443)), and remote sensing reflectances at 555 nm (R_{rs}(555)) from 2003 to 2016 were obtained from NASA MODIS Aqua Level 3 data products (<https://oceancolor.gsfc.nasa.gov>). Here, chl_{sat} (NASA’s OCx algorithm) is considered a proxy for the presence of phytoplankton (e.g., Cullen, 1982). As a proxy for the concentration of CDOM in coastal waters, a_{cdom}(443) was estimated from the Garver-Siegel-Maritorena bio-optical algorithm (Maritorena et al., 2002). R_{rs}(555) is, to first order, a proxy for the influence of low-salinity and sediment-rich river plumes in the coastal PNW (e.g., Thomas and Weatherbee, 2006; Saldías et al., 2016). R_{rs}(555) is correlated with chl_{sat} and presumably plankton biomass in clear oceanic waters not influenced by strong land-ocean interactions.

RESULTS AND DISCUSSION

Latitudinal Gradients in Satellite and Glider Properties and the Impact of Riverine Inputs

The variability in the magnitude and seasonality of river discharge along the Washington-Oregon margin is illustrated in Figure 1a. The dominant and year-round

influence of the Columbia River is clear, with peak discharge in winter and spring as a result of precipitation and melt of the continental snow pack. Columbia River flows are largely regulated by dams, which dampen seasonal discharges and keep summer flows artificially high because of releases from hydroelectric operations. The smaller mountainous rivers that line the PNW margin show winter-time peaks in discharge following seasonal precipitation patterns, with very low flows in the summer. Between November and March, the combined discharge of the 21 gauged small mountainous rivers equals about 30%–50% of the discharge of the Columbia River over the same period, while in the summer months the small rivers are equivalent to less than 10% of the Columbia River discharge. The geographical locations of the WA and OR lines relative to major river inputs help explain some of the patterns discussed in this study. For instance, the WA line is under direct influence of the Columbia River, while the OR line is influenced by a few small mountainous rivers (e.g., Alsea and Yaquina) and is considerably far from the mouths of more important rivers to the south (e.g., Umpqua and Rogue).

Temporal variability of $R_{rs}(555)$ inshore of 125°W (the cross-shore extent of the moored observations) show marked latitudinal differences between Washington and Oregon (Figure 1b). As expected from a relationship between low-salinity river plumes and light scattering (Pak et al., 1970; Palacios et al., 2009), good agreement is observed between the timing of $R_{rs}(555)$ peaks (Figure 1b) and total discharge (Figure 1a). The role of the Columbia River in advecting waters northward along the Washington coast in the first few months of the year, and to the south and outer edges of the OR shelf in the summer, is evident in the $R_{rs}(555)$ fields (Figures 1b and 2a,b). A secondary role for phytoplankton in contributing to increased $R_{rs}(555)$ signals in the summer cannot be disregarded. The cross-shore extent of the offshore advection of the plume during different times of the

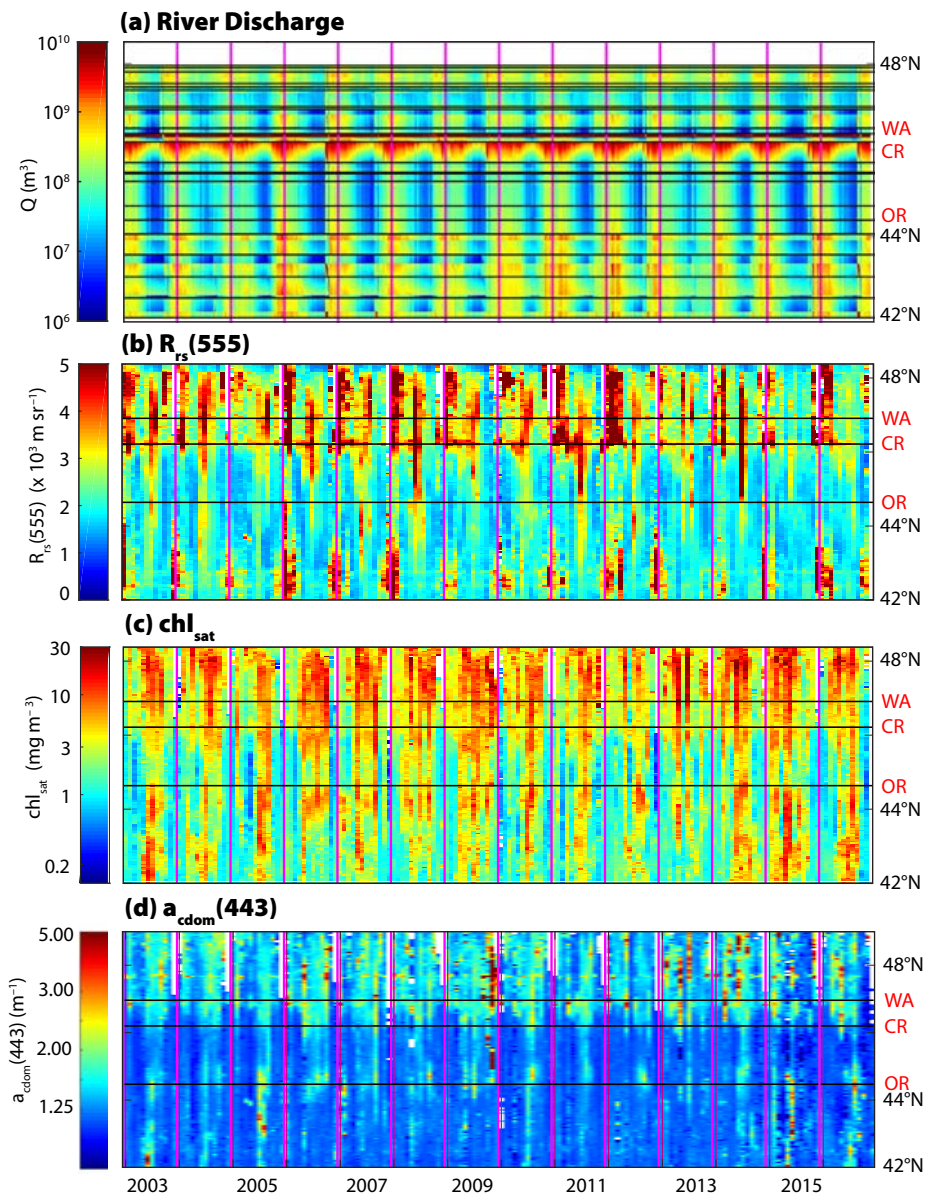
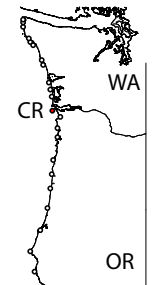


FIGURE 1. Hovmöller plot of (a) integrated monthly water discharge from US Geological Survey stations at the major rivers (horizontal black lines) along the Washington-Oregon coastline, including, from north to south, Calawah, Bogachiel, Hoh, Queets, Quinault, Wynoochee, Satsop, Chehalis, Willapa, Naselle, Columbia, Nehalem, Wilson, Trask, Nestucca, Siletz, Alsea, Siuslaw, Umpqua, South Fork Coquille, Rogue, and Chetco. The location of all river mouths is shown on the map to the right. (b–d) remotely sensed estimates of (b) $R_{rs}(555)$, (c) chl_{sat} , and (d) $a_{cdom}(443)$ from the MODIS-Aqua sensor for coastal waters inshore of 125°W. Note that the discharge data are discrete measurements, and the interpolation along the latitude axis is for visualization purposes only. The vertical magenta lines correspond to January 1.



year is illustrated from glider observations (Figure 3), which reveal times when areas offshore of the OR line experience larger volumes of freshwater compared to the WA line as a result of Columbia River advection.

Discharge from mountainous coastal rivers as a result of high rainfall from

“atmospheric rivers” of moisture (e.g., Warner et al., 2012), particularly to the south of the OR line, also correspond to increases in $R_{rs}(555)$ in winter months (Figure 1a,b). Nonetheless, the observed $R_{rs}(555)$ maxima inshore during fall/winter (Figure 2a,b) likely result from not only discharge patterns along the coast

but also increased particle resuspension processes following storm events, which in this region are marked by coherent changes in winds and surface wave heights (a proxy for mixing; Kniskern et al., 2011; see also Figure 6k–l). Indeed, long-period surface gravity waves have been shown to transport suspended sediments across the shelf and modulate changes in particulate backscattering (i.e., suspended materials) inshore of the 100 m isobath in the absence of strong riverine inputs (Drake and Cacchione, 1985; Henderikx Freitas et al., 2017). Notably, the distance between the coast and the 100 m isobath varies along the Washington–Oregon coastline (i.e., more than 35 km at and north of the WA line, ~32 km at the OR line due to the presence of the Stonewall Bank, and less than 15 km north and south of OR). These differences in shelf configuration may partially explain the overall lower $R_{rs}(555)$ values between 43°N and 46°N in Figure 1b, because offshore waters make up a larger portion of the area east of 125°W in some of those regions.

Temporal variability of chl_{sat} is also large (Figure 1c), with a higher magnitude and broader cross-shelf extent of chl_{sat} along the WA line compared to the

OR line (Figure 2c,d). The coefficient of variation of the annual maximum of chl_{sat} at ~125°W of the OR and WA lines is 34% (range = 3.7–12.9 mg m⁻³) and 70% (range = 8.5–56.8 mg m⁻³), respectively. The maximum in chl_{sat} occurs between June and September at both locations, with OR showing a more distinct seasonal cycle than WA, where relatively high values of chl_{sat} appear to persist for longer periods during the upwelling season (Figure 2c,d). A matchup analysis between in situ chl observations from the OOI moorings and chl_{sat} estimates shows that the satellite data overestimate in situ chl observations closest to the coast (Figure 4a). This is because chl_{sat} algorithms rely on the use of information in the blue region of the reflectance spectrum, which in coastal areas is highly affected by the presence of absorbing aerosols, suspended sediments, and CDOM (Gordon, 1997; Dierssen, 2010). Satellite retrievals of $a_{\text{cdom}}(443)$ show overall larger signals in WA compared to OR (Figure 1d), and similar seasonal cycle patterns to those observed in chl_{sat} (Figure 2e,f). The enhanced cross-shore values in both chl_{sat} and $a_{\text{cdom}}(443)$ at WA during lower productivity months such

as December (Figure 2e) are intriguing, and suggest a role for CDOM contamination in the chl_{sat} retrievals. The notion that phytoplankton, CDOM, and sediments all contribute to chl_{sat} signals implies that the seemingly high chl_{sat} concentrations at WA relative to OR may at least partially be a consequence of the proximity of WA to CDOM-rich sources such as the Columbia River plume and the Grays Harbor outflow (e.g., Palacios et al., 2009, 2012).

Cross-shore glider estimates of CDOM (Figure 3 and 5) suggest a stronger cross-shore gradient in CDOM concentrations off the WA shelf, even at times when larger volumes of freshwater are registered at the OR shelf (i.e., June 2016 in Figure 3o). Certainly, transport, dilution, and other biogeochemical processes that affect CDOM variability need to be considered when comparing distributions at the two sites. Additionally, the large bandwidth of the CDOM fluorometer is tuned to detect CDOM in turbid waters, and thus not suitable for examining subtle changes in this property in clearer ocean conditions further from the coast. Examples of well-resolved coastal glider observations in Figure 5 point to key differences between the cross-shore distribution of bio-optical properties at WA and OR. First, the differences in the bathymetry along the two Endurance Lines may explain the presence of bottom nepheloid layers at WA (as denoted by elevated b_{bp} and near zero chl values along the slope), which suggests that mixing processes may be more important to determining cross-shelf b_{bp} variability at WA than at OR (at least within the sampled region). Second, CDOM distributions over the shelf are notably different at the two locations (particularly in Figure 5b, where observations at the two locations were obtained simultaneously), with patterns in WA suggesting that the nearshore region acts as a source of CDOM. Additional data collected simultaneously along the WA and OR lines would be necessary to determine if these example features hold throughout different seasons and years.

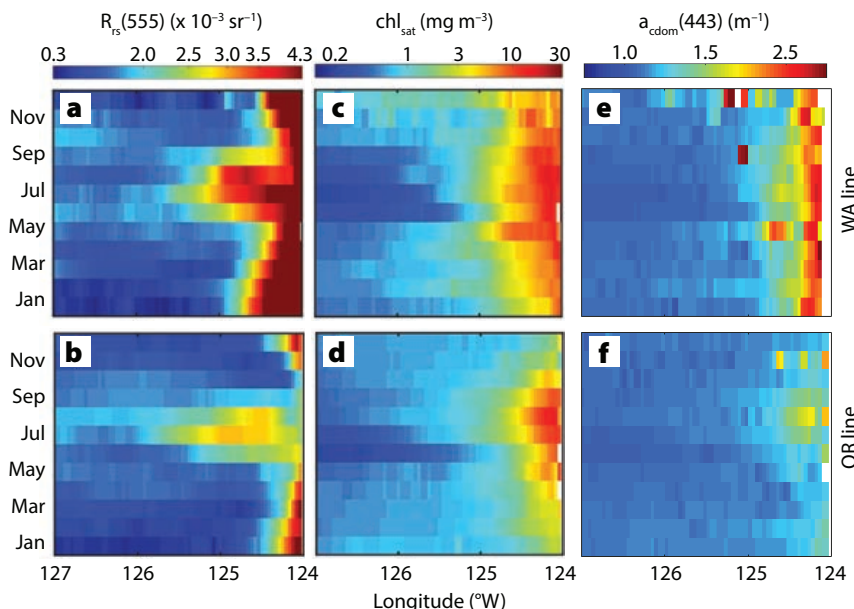


FIGURE 2. Annual mean of (a,b) $R_{rs}(555)$, (c,d) chl_{sat} , and (e,f) $a_{\text{cdom}}(443)$ along the Washington (top panels) and Oregon (bottom panels) Ocean Observatories Initiative Endurance Lines computed using MODIS observations for the 2003–2016 period. Note that $a_{\text{cdom}}(443)$ fails in very turbid coastal waters.

Latitudinal Gradients in Bio-Optical Properties from High-Frequency Moorings

High-frequency measurements from surface moorings expand the observations to the inner shelf regions of WA and OR, and provide temporally resolved observations that allow characterization of the latitudinal differences and interrelationships between bio-optical parameters over the 2015–2016 period (Figure 6). During the observed period, chl maxima at times occur at the mid-shelf sites rather than inshore, possibly following

offshore advection of the upwelling front, whereas minima are generally found further from the coast (Figure 6a,b). In contrast, a more apparent cross-shore gradient is depicted in the b_{bp} observations, with elevated values generally occurring closest to shore (Figure 6c,d). Periods of synchronous changes in chl across the shelf are observed in a few instances (e.g., May and July 2016 at WA), but overall differences among the moorings denote the patchy nature of chl distributions across the shelf. The similarities and differences between chl and b_{bp} spatial

and temporal distributions indicate variability in the types of materials dominating optical properties at the different moorings. Biogenic particles typical of productive pelagic oceanic environments have large chl and low-to-moderate b_{bp} values, whereas waters dominated by mineralogenic particles have high b_{bp} and low chl concentrations (Henderikx Freitas et al., 2016). Thus, the relationships between b_{bp} and chl in Figure 4b for samples collected between May and September at both lines indicate that nearshore b_{bp} estimates are more likely

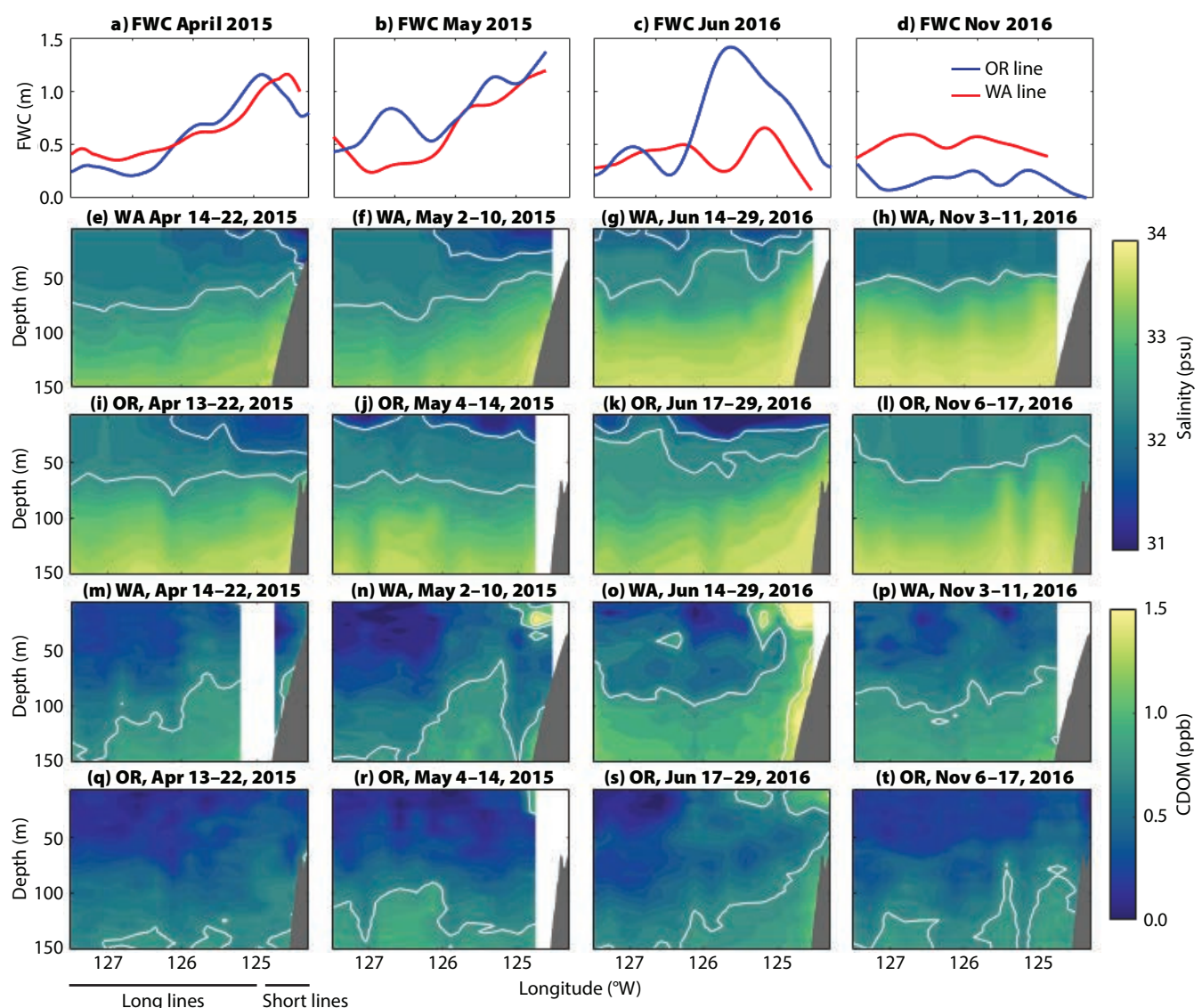


FIGURE 3. Cross-shore estimates of freshwater content, salinity, and chromophoric dissolved organic matter (CDOM) at the Washington (WA) and Oregon (OR) Endurance Lines from glider profiles for selected time periods during 2015 and 2016. Panels (a–d): the freshwater content (FWC) across the shelf; (e–h): cross-shore salinity profiles along the WA (e–h) and OR (i–l) lines where the white contours are the 32 and 32.5 psu isohalines; (m–t): cross-shore CDOM profiles along the WA (m–p) and OR (q–t) lines, where the white lines are the 0.75 and 1.25 ppb contours. Both long Endurance Line profiles (128°W to 125°W) and short Endurance Line profiles (125°W to 124.3°W) were used whenever available. Plots were made using smoothing lengths of 0.25 degrees (longitude) and 10 m (depth). White bars denote missing data.

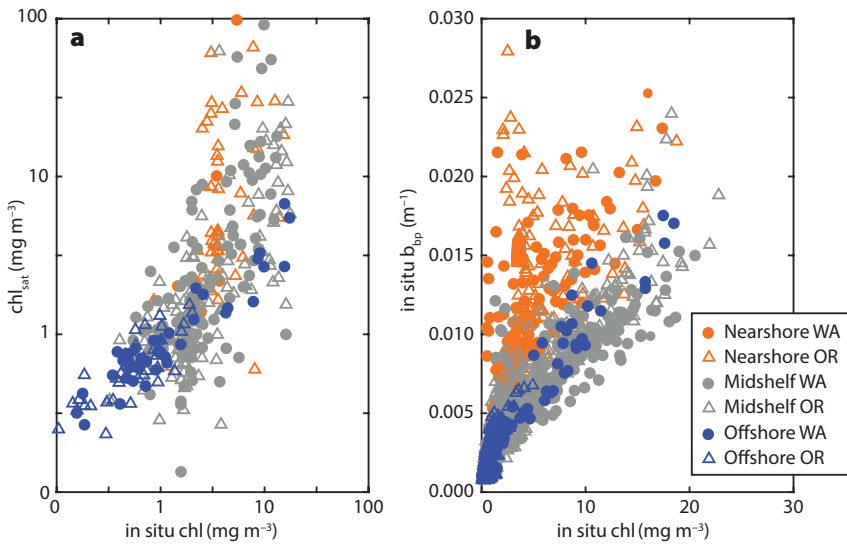


FIGURE 4. (a) Matchups between daily averages of in situ chl and chl_{sat} . Only the closest cloud-free pixel (4 km resolution) to each mooring was chosen for each available day whereas in situ chl were derived only from nighttime daily averages. Note that data availability due to cloud cover and QA/QC flags applied to satellite data led to variable matchup density between locations. (b) Correspondence between mooring optical measurements of b_{bp} and chl for samples collected between May and September 2015 and 2016. Note that nearshore samples are more likely to show high b_{bp} and low chl values, in agreement with characterization of non-phytoplankton particles.

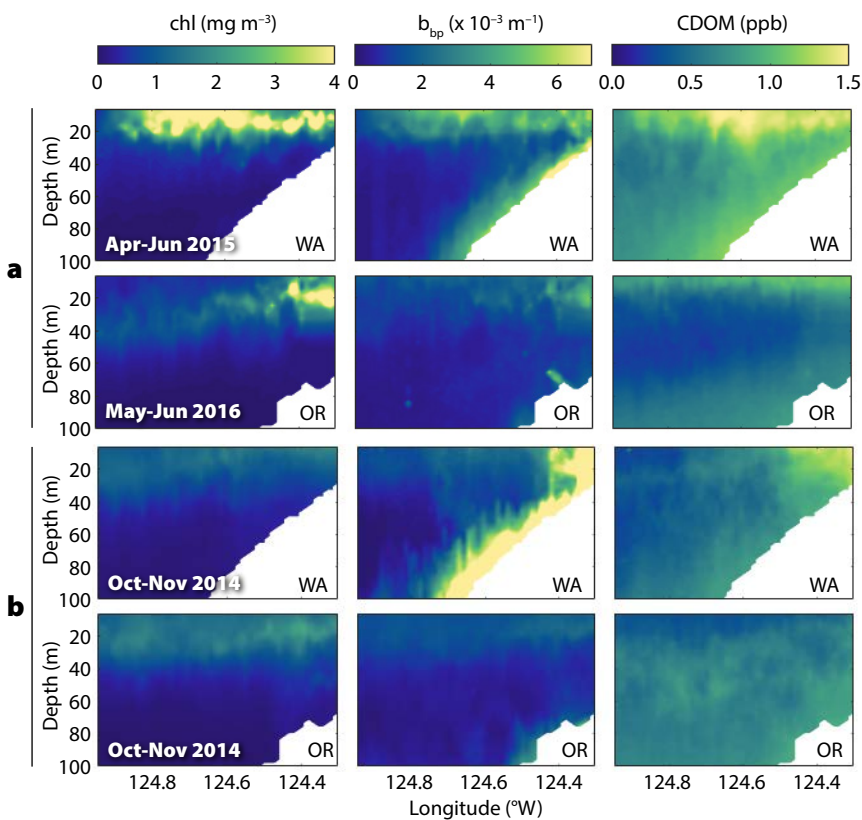


FIGURE 5. Examples of mean cross-shore sections of chl, b_{bp} , and CDOM for selected glider deployments along the WA and OR Endurance Lines. (a) Spring of 2015 (WA) and 2016 (OR). (b) Fall of 2014 for WA and OR. Ordinary kriging is used to plot the average quantities, with smoothing scales of 1 km (longitude) and 2 m (depth), and shallowest measurement of 6 m. Westernmost and easternmost longitudes are equivalent to the location of the offshore and mid-shelf moorings, respectively. Note that lack of coincident glider deployments in time largely prevented direct comparison between the two lines.

to be affected by non-phytoplankton materials (even in periods when discharge is presumably low), whereas optical properties of offshore samples are more likely to be dominated by changes in phytoplankton concentrations. These observations contextualize the relationships between chl and b_{bp} with depth and distance from shore previously shown in the glider sections (Figure 5b).

The chl variations along the OR and WA lines are comparable over the course of the upwelling season, with mid-shelf averages of chl for the May–September months of 2015 and 2016 reaching 3.34 ± 2.58 (one standard deviation) mg m^{-3} at WA and $4.61 \pm 2.65 \text{ mg m}^{-3}$ at OR. However, differences between OR and WA chl concentrations can exceed 20 mg m^{-3} at any given time during the more productive months of the years (e.g., August 2016; Figure 6a,b). Nonetheless, these values are considerably different from the average seasonal concentrations suggested from satellite estimates (Figures 1c and 2c,d). Nearshore b_{bp} patterns at WA and OR are also comparable in timing and magnitude, but differences are apparent in the mid-shelf, where WA waters show elevated backscattering compared to OR in the winter months (Figure 6c,d). The similarities nearshore are expected because both WA and OR are under the influence of riverine inputs, but mid-shelf differences may point to the broader cross-shore extent of the Columbia River plume off WA compared to coastal river plumes created by smaller rivers to the south off OR. Bathymetry differences between the two lines may also explain these mid-shelf discrepancies, as illustrated from glider observations (Figure 5). The temporal distribution of CDOM somewhat agrees with that of b_{bp} when concentrations are high, particularly during winter, whereas during the remaining periods values oscillate above a background that is larger at WA during 2015, and relatively similar at WA and OR in 2016 (Figure 6e,f). The consistently lower CDOM concentrations at the mid-shelf OR mooring compared to offshore OR between October 2015 and March 2016 (Figure 6f) are suspicious, and may indicate drift or instrument issues.

In contrast with the optical properties, consistent cross-shore gradients in temperature

are observed across WA and OR, with nearshore waters presenting the coolest overall observations. Cross-shore gradients in temperature are strongest in spring-summer, consistent with the expected effects of upwelling and solar heating, and less pronounced in fall-winter, following stronger mixing processes. Nearshore and mid-shelf temperatures are overall cooler during the upwelling season in OR, as expected given the stronger wind conditions in OR compared to WA (wind stress is on average 1.5 times stronger on the Oregon shelf compared to the Washington shelf during the 2015–2016 period; Figure 6l). Salinity patterns in OR present marked seasonal changes in nearshore values (Figure 6i), showing the most saline waters in spring-summer and the freshest values in fall-winter. Salinity values are freshest overall along the WA line, as expected given its proximity to the Columbia River (Figure 6j). Low-salinity peaks in December 2015 and January 2016 at both WA and OR inshore moorings (Figure 6i,j) agree well with CDOM maxima in Figure 6e,f. It is important to note that although the surface mooring observations cannot vertically resolve variations of physical and bio-optical properties, surface chl values have been shown to be well correlated with depth-integrated chl at the OR line (McKibben, 2016). However, we cannot exclude the importance of subsurface features such as thin layers of phytoplankton or bottom and intermediate nepheloïd layers that are not sampled by the moorings (e.g., Figure 5). Additionally, the role of upwelling in lifting isopycnals toward the coast (and therefore changing the vertical distribution of chl across the shore) as suggested between May and June 2016 in OR (Figure 5a), undoubtedly complicates interpretation of moored data that are measured at the same depth (7 m) across the shelf. Further analyses should be expanded to include OOI Profiler Mooring data in order to resolve these vertical variations. Concurrent profiler data, however, were not available for the time period of this study.

Processes Controlling Observed Variability in In Situ Optical Properties

Establishing causal links between physical and biogeochemical changes in the surface ocean is not trivial. Cumulative alongshore wind stress, a metric that represents energy input into the upwelling system over the course of each season, is plotted in Figure 7 for WA and OR for periods of 2015 and 2016. Cumulative chlorophyll values over time, which are commonly used to assess bloom initiation times (e.g., Brody et al., 2013) and to summarize and highlight major changes in local chl values (e.g., McQuatters-Gollop

et al., 2008), are also plotted in Figure 7 as cumulative chl anomaly relative to the respective time-series minimum (e.g., rapid and large increases in chl lead to increasing slopes, and small or null changes lead to flat slopes). The importance of upwelling events in driving increases in mid-shelf chl is clear at both locations, as abrupt increases in cumulative wind stress quantities are generally accompanied by steeper slopes of cumulative chl values (e.g., June 2015 and July–August 2016). In contrast, periods of flat or negative cumulative wind stress slopes (e.g., July 2015 for both WA and OR and

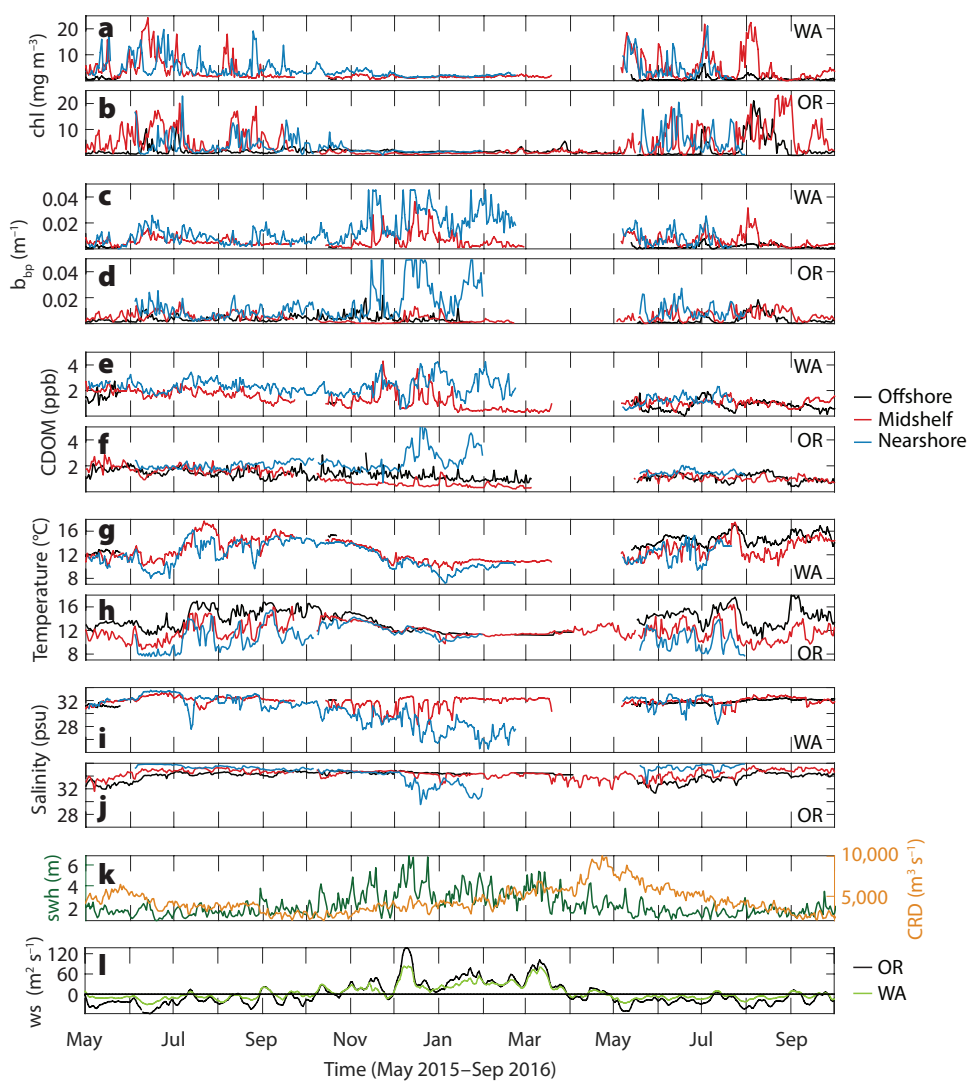


FIGURE 6. Temporal evolution of physical and optical variables at 7 m depth across the moorings of the WA and OR Endurance Lines (from daily averages). swh = significant wave height from the National Data Buoy Center (NDBC) buoy 46041. CRD = Columbia River Discharge. ws = alongshore wind stress convoluted with eight-day exponential decay as in Austin and Barth (2002). Wind stress measurements are from NDBC buoys 46041 (WA) and 46050 (OR). SWH at WA and OR buoys are well correlated with an $r^2 = 0.90$ for the 2005–2016 period.

August–September 2016 for WA) show overall flat cumulative chl anomalies. The late summer increases in cumulative chl in OR compared to WA during both years analyzed (also apparent in Figure 6a,b) may be related to the longer duration of the upwelling season at OR compared to WA. Nonetheless, the elevated chl values at WA despite much weaker upwelling-favorable winds indicate that other processes must contribute to the chl signals off WA, as reported by previous authors (e.g., Hickey and Banas, 2008). However, the latitudinal differences between chl estimates at WA and OR may not be as strong as the differences suggested from satellite data, given the relative similarity in the timing and magnitude of the variability of in situ chl estimates at the two lines (Figures 6a,b and 7). Although the moored observations alone are not sufficient to assess whether the apparent similarities in chl distribution (and the observed higher chl concentrations in OR in the summer) hold over multiple seasons and years, we hypothesize based on the evidence presented here that CDOM may be an important factor affecting the latitudinal differences observed from satellite-derived chl estimates (Figure 2). This is particularly relevant when interpreting chl_{sat} signals off the Washington coastline, given the strong interference of the CDOM-rich Columbia River plume at those locations (Palacios et al., 2009, 2012).

The OOI b_{bp} record shows the importance of biological land-ocean interactions and resuspension processes in controlling b_{bp} distributions. Salinity and b_{bp} are inversely correlated at all WA moorings ($r = -0.16$, -0.33 , and -0.53 offshore, at the mid-shelf, and inshore, respectively) and at the inshore OR mooring ($r = -0.57$). This indicates that allochthonous sources partially control b_{bp} variability particularly at the inshore moorings. However, positive (but weak) correlations are observed at the mid-shelf and offshore OR moorings ($r = 0.29$ and $r = 0.21$, respectively), indicating the added importance of pelagic phytoplankton in characterizing the bulk b_{bp} further offshore at OR, as shown in Figure 4b. Evidence for the role of mixing or resuspension processes in affecting the variability in b_{bp} is observed between November 2015 and January 2016, when increases in nearshore b_{bp} at WA and OR occur during a period of downwelling-favorable winds (Figure 6l), increased significant surface wave height conditions, and relatively low discharge (Figure 6k). Indeed, positive relationships are observed between b_{bp} and significant wave heights at the WA and OR inshore moorings ($r = 0.61$ and $r = 0.51$, respectively; correlations are the strongest at zero lag), whereas the relationships with discharge are weaker at the OR inshore mooring ($r = 0.16$), and, surprisingly, not

significant at WA. The lack of strong relationships with discharge may be related to the relatively low discharge levels observed in 2015 compared to the climatology (see Figure 1). Nonetheless, these observations indicate that river discharge alone does not explain nearshore particle distributions. No significant correlations are observed between wave heights and b_{bp} at any of the mid-shelf or offshore moorings, as expected given the constraint that increased depths impose on the particle resuspension processes.

CONCLUSIONS

Satellite observations of chl along the Washington–Oregon latitudinal range are consistent with the existing paradigm of higher annual magnitude and larger cross-shore extent of chl signals off the Washington shelf, despite reduced upwelling strength compared to Oregon. However, in situ bio-optical data for the time period of OOI data availability show relative similarity between the magnitude of the cross-shore chl distributions at WA and OR, and increased presence of suspended sediments and CDOM off WA. These observations, although temporally limited, indicate potential contamination of satellite retrievals of chl due to CDOM and suspended materials in the water column, particularly off the WA shelf, that should caution further attribution of chl_{sat} signals to differences in production. Nonetheless, the considerable differences in wind stress between WA and OR indicate that processes other than upwelling are important for determining chl distributions at WA, as previously suggested. Glider-derived data show the strong seasonal influence of the Columbia River plume as a source of freshwater to the shelf off WA and to OR offshore waters, in agreement with known shifts in wind forcing. Full water column depth analysis using profiler and additional glider data that temporally align with each other and with mooring data during key seasonal events would be needed to ascribe latitudinal gradients in chl and particle distributions to variations in productivity.

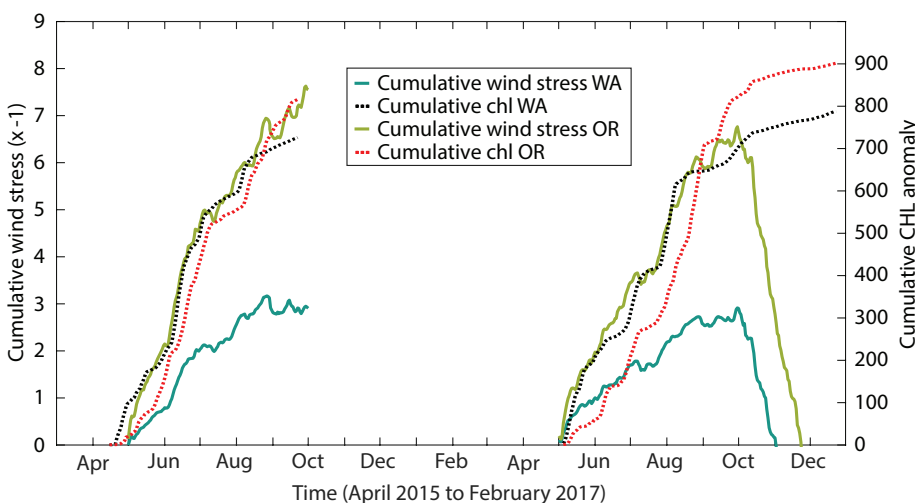


FIGURE 7. Cumulative wind stress and cumulative chl anomalies for mid-shelf observations at WA and OR moorings for mid-April to September 2015 and May to December 2016.

As the OOI time series matures, we will be better poised to discriminate between riverine impacts on particle loading and plankton productivity, and to more conclusively address the factors that lead to biogenic carbon production and export in the Northern California Current ecosystem. ☐

REFERENCES

- Austin, J.A., and J.A. Barth. 2002. Variation in the position of the upwelling front on the Oregon shelf. *Journal of Geophysical Research* 107(C11), 3180, <https://doi.org/10.1029/2001JC000858>.
- Barnes, C.A., A.C. Duxbury, and B. Morse. 1972. Circulation and selected properties of the Columbia River effluent at sea. Pp. 71–80 in *The Columbia River Estuary and Adjacent Ocean Waters: Bioenvironmental Studies*. A.T. Pruter and D.L. Alveison, eds, University of Washington Press, Seattle.
- Brody, S.R., M.S. Lozier, and J.P. Dunne. 2013. A comparison of methods to determine phytoplankton bloom initiation. *Journal of Geophysical Research* 118(5):2,345–2,357, <https://doi.org/10.1029/jgrc.20167>.
- Coble, P.G. 1996. Characterization of marine and terrestrial DOM in seawater using excitation-emission matrix spectroscopy. *Marine Chemistry* 51(4):325–346, [https://doi.org/10.1016/0304-4203\(95\)00062-3](https://doi.org/10.1016/0304-4203(95)00062-3).
- Cullen, J.J. 1982. The deep chlorophyll maximum: Comparing vertical profiles of chlorophyll *a*. *Canadian Journal of Fisheries and Aquatic Sciences* 39:791–803, <https://doi.org/10.1139/f82-108>.
- Davis, K.A., N.S. Banas, S.N. Giddings, S.A. Siedlecki, P. MacCready, E.J. Lessard, R.M. Kudela, and B.M. Hickey. 2014. Estuary-enhanced upwelling of marine nutrients fuels coastal productivity in the US Pacific Northwest. *Journal of Geophysical Research* 119:8,778–8,799, <https://doi.org/10.1002/2014JC010248>.
- Dickson, M., and P.A. Wheeler. 1995. Nitrate uptake rates in a coastal upwelling regime: A comparison of PN-specific, absolute, and Chi a-specific rates. *Limnology and Oceanography* 40, <https://doi.org/10.4319/lo.1995.40.3.0533>.
- Dierssen, H.M. 2010. Perspectives on empirical approaches for ocean color remote sensing of chlorophyll in a changing climate. *Proceedings of the National Academy of Sciences of the United States of America* 107:17,073–17,078, <https://doi.org/10.1073/pnas.0913800107>.
- Drake, D.E., and D.A. Caccione. 1985. Seasonal variation in sediment transport on the Russian River Shelf, California. *Continental Shelf Research* 4:495–514, [https://doi.org/10.1016/0278-4343\(85\)90007-X](https://doi.org/10.1016/0278-4343(85)90007-X).
- Goñi, M.A., J.A. Hatten, R.A. Wheatcroft, and J.C. Borgeld. 2013. Particulate organic matter export by two contrasting small mountainous rivers from the Pacific Northwest, USA. *Journal of Geophysical Research* 118:112–134, <https://doi.org/10.1002/jgrg.20024>.
- Gordon, H.R. 1997. Atmospheric correction of ocean color imagery in the Earth Observing System era. *Journal of Geophysical Research* 102(D14):17,081–17,106, <https://doi.org/10.1029/96JD02443>.
- Henderikx Freitas, F., D.A. Siegel, S. Maritorena, and E. Fields. 2017. Satellite assessment of particulate matter and phytoplankton variations in the Santa Barbara Channel and its surrounding waters: Role of surface waves. *Journal of Geophysical Research* 122:355–371, <https://doi.org/10.1002/2016JC012152>.
- Henderikx Freitas, F., D.A. Siegel, L. Washburn, S. Halewood, and E. Stassinos. 2016. Assessing controls on cross-shelf phytoplankton and suspended particle distributions using repeated bio-optical glider surveys. *Journal of Geophysical Research* 121:7,776–7,794, <https://doi.org/10.1002/2016JC01781>.
- Hickey, B.M., and N.S. Banas. 2003. Oceanography of the US Pacific Northwest coastal ocean and estuaries with application to coastal ecology. *Estuaries* 26(4):1,010–1,031, <https://doi.org/10.1007/BF02803360>.
- Hickey, B.M., and N.S. Banas. 2008. Why is the northern end of the California Current System so productive? *Oceanography* 21(4):90–107, <https://doi.org/10.5670/oceanog.2008.07>.
- Hickey, B.M., S. Geier, N. Kachel, and A. Macfadyen. 2005. A bi-directional river plume: The Columbia in summer. *Continental Shelf Research* 25:1,631–1,656, <https://doi.org/10.1016/j.csr.2005.04.010>.
- Hickey, B.M., L.J. Pietrafesa, D.A. Jay, and W.C. Boicourt. 1998. The Columbia River plume study: Subtidal variability in the velocity and salinity fields. *Journal of Geophysical Research* 103(C5):10,339–10,368, <https://doi.org/10.1029/97JC03290>.
- Huyer, A. 1983. Coastal upwelling in the California Current system. *Progress in Oceanography* 12(3):259–284, [https://doi.org/10.1016/0079-6611\(83\)90010-1](https://doi.org/10.1016/0079-6611(83)90010-1).
- Jonasz, M., and G. Fournier. 2011. *Light Scattering by Particles in Water: Theoretical and Experimental Foundations*. Academic Press, 704 pp.
- Kniskern, T.A., J.A. Warrick, K.L. Farnsworth, R.A. Wheatcroft, and M.A. Goñi. 2011. Coherence of river and ocean conditions along the US West Coast during storms. *Continental Shelf Research* 31(7):789–805, <https://doi.org/10.1016/j.csr.2011.01.012>.
- Maritorena, S., D.A. Siegel, and A.R. Peterson. 2002. Optimization of a semianalytical ocean color model for global-scale applications. *Applied Optics* 41(15):2,705–2,714, <https://doi.org/10.1364/AO.41.002705>.
- McKibben, S.M. 2016. *Above and Below: Oregon Coastal Phytoplankton Bloom Dynamics from Sea and Space*. PhD Thesis, Oregon State University, Corvallis, Oregon.
- McQuatters-Gollop, A., L.D. Mee, D.E. Raitsos, and G.I. Shapiro. 2008. Non-linearities, regime shifts and recovery: The recent influence of climate on Black Sea chlorophyll. *Journal of Marine Systems* 74(1):649–658, <https://doi.org/10.1016/j.jmarsys.2008.06.002>.
- Müller, P., X.-P. Li, and K.K. Niyogi. 2001. Non-photochemical quenching: A response to excess light energy. *Plant Physiology* 125(4):1,558–1,566, <https://doi.org/10.1104/pp.125.4.1558>.
- Palacios, S.L., T.D. Peterson, and R.M. Kudela. 2009. Development of synthetic salinity from remote sensing for the Columbia River plume. *Journal of Geophysical Research* 114, C00B05, <https://doi.org/10.1029/2008JC004895>.
- Palacios, S.L., T.D. Peterson, and R.M. Kudela. 2012. Optical characterization of water masses within the Columbia River plume. *Journal of Geophysical Research* 117, C11020, <https://doi.org/10.1029/2012JC008005>.
- Pak, H., G.F. Beardsley Jr., and P.K. Park. 1970. The Columbia River as a source of marine light-scattering particles. *Journal of Geophysical Research* 75(24):4,570–4,578, <https://doi.org/10.1029/JC075i024p04570>.
- Saldías, G.S., R.K. Shearman, J.A. Barth, and N. Tuñillaro. 2016. Optics of the offshore Columbia River plume from glider observations and satellite imagery. *Journal of Geophysical Research* 121:2,367–2,384, <https://doi.org/10.1002/2015JC014131>.
- Schmechtig, C., H. Claustre, A. Poteau, and F. D'Ortenzio. 2014. *Bio-Argo Quality Control Manual for the Chlorophyll-A Concentration*, Version 1.0. Ifremer, 16 pp., <https://doi.org/10.13155/35385>.
- Smith, L.M., J.A. Barth, D.S. Kelley, A. Plueddemann, I. Rodero, G.A. Ulses, M.F. Vardaro, and R. Weller. 2018. The Ocean Observatories Initiative. *Oceanography* 31(1):16–35, <https://doi.org/10.5670/oceanog.2018.105>.
- Sullivan, J.M. 2013. Measuring optical backscattering in water. Pp. 189–224 in *Light Scattering Reviews 7: Radiative Transfer and Optical Properties of Atmosphere and Underlying Surface*. J.M. Sullivan, M.S. Twardowski, J.R.V. Zaneveld, C.C. Moore, and A. Kokhanovsky, eds, Praxis Publishing Ltd.
- Thomas, A.C., and R.A. Weatherbee. 2006. Satellite-measured temporal variability of the Columbia River plume. *Remote Sensing of Environment* 100:167–178, <https://doi.org/10.1016/j.rse.2005.10.018>.
- Ware, D.M., and R.E. Thomson. 2005. Bottom-up ecosystem trophic dynamics determine fish production in the Northeast Pacific. *Science* 308(5726):1,280–1,284, <https://doi.org/10.1126/science.1109049>.
- Warner, M.D., C.F. Mass, and E.P. Salathé. 2012. Wintertime extreme precipitation events along the Pacific Northwest coast: Climatology and synoptic evolution. *Monthly Weather Review* 140:2,021–2,043, <https://doi.org/10.1175/MWR-D-11-00197.1>.
- Wetzel, M.S., and P.A. Wheeler. 2003. Production and partitioning of organic matter during simulated phytoplankton blooms. *Limnology and Oceanography* 48, <https://doi.org/10.4319/lo.2003.48.5.1808>.
- Wheatcroft, R.A., M.A. Goñi, J.A. Hatten, G.B. Pasternack, and J.A. Warrick. 2010. The role of effective discharge in the ocean delivery of particulate organic carbon by small, mountainous river systems. *Limnology and Oceanography* 55:161–171, <https://doi.org/10.4319/lo.2010.55.1.0161>.
- Zhang, X., L. Hu, and M.-X. He. 2009. Scattering by pure seawater: Effect of salinity. *Optics Express* 17(7):5,698–5,710, <https://doi.org/10.1364/OE.17.005698>.

ACKNOWLEDGMENTS

This work was funded by the National Science Foundation (OCE-1642295 to MG, AW, KS) with additional support from the Simons Foundation via the SCOPe program (AW). All matlab code for data processing and generation of figures are available upon request to the corresponding author (awhite@coas.oregonstate.edu). We are particularly grateful to Stuart Pearce at OOI for access to the glider data streams.

AUTHORS

Fernanda Henderikx Freitas is Research Associate, College of Earth, Ocean, and Atmospheric Sciences (CEOAS), Oregon State University, Corvallis, OR, USA. **Gonzalo S. Saldías** completed his PhD at CEOAS, Oregon State University, Corvallis, OR, USA, and is currently a researcher at Centro FONDAP de Investigación en Dinámica de Ecosistemas Marinos de Altas Latitudes (IDEAL), Valdivia, Chile. **Miguel Goñi** is Professor, **R. Kipp Shearman** is Associate Professor, and **Angelique E. White** (awhite@coas.oregonstate.edu) is Associate Professor, all at CEOAS, Oregon State University, Corvallis, OR, USA.

ARTICLE CITATION

Henderikx Freitas, F., G.S. Saldías, M. Goñi, R.K. Shearman, and A.E. White. 2018. Temporal and spatial dynamics of physical and biological properties along the Endurance Array of the California Current ecosystem. *Oceanography* 31(1):80–89, <https://doi.org/10.5670/oceanog.2018.113>.

Warm Blobs, Low-Oxygen Events, and an Eclipse

THE OCEAN OBSERVATORIES INITIATIVE
ENDURANCE ARRAY CAPTURES THEM ALL

By John A. Barth, Jonathan P. Fram, Edward P. Dever, Craig M. Risien,
Chris E. Wingard, Robert W. Collier, and Thomas D. Kearney



ABSTRACT. The Ocean Observatories Initiative (OOI) Endurance Array in the Northeast Pacific off the coasts of Oregon and Washington is designed to measure changes in the ocean on timescales from hours to decades. The Endurance Array is located halfway between the pole and the equator in one of the major coastal upwelling systems on our planet, the California Current System. This area is forced locally by winds, waves, tides, and freshwater inputs from rivers and, more broadly, by large-scale ocean-atmosphere phenomena from both the south, for example, the El Niño-Southern Oscillation, and the north, for example, changes originating in the subarctic Gulf of Alaska. The Endurance Array spans the continental shelf and slope and hosts a variety of platforms and sensors for measuring physical-biogeochemical oceanographic processes. After briefly introducing the unique OOI platforms and range of sensors that make up the Endurance Array, we describe three phenomena with durations spanning hours to years. These include an ocean response to the total eclipse of the Sun on August 21, 2017, the devastating effects of a low-oxygen event off central Oregon, and the appearance of an anomalously warm upper-ocean feature off the Pacific Northwest in recent years.

INTRODUCTION

The Ocean Observatories Initiative (OOI) Endurance Array spans the continental shelf and slope in the Northeast Pacific. The scientific motivation behind the array design was the need to measure and understand a wide variety of ocean-atmosphere and physical-biogeochemical processes that influence marine ecosystems in this region. Spring and summer wind-driven coastal upwellings strongly influence the Oregon and Washington shelves (R.L. Smith, 1974). Understanding gained from this upwelling region is valuable for comparisons with the other major upwelling systems around the world, including the Humboldt Current, the Benguela Current, and the Canary Current. In winter, the Oregon and Washington coasts are subject to strong wind-driven downwelling, large waves, and swift northward currents. The Columbia River, the largest source of freshwater to the US west coast, also influences the region. The oceanographic instruments and measurement platforms, and their placement across the continental margin off Oregon and Washington, were chosen to study physical-biogeochemical interactions in the ocean. Here, we describe early results from the OOI Endurance Array that demonstrate the observatory's utility for studying phenomena that change over hours to years.

The OOI Endurance Array is part of the more extensive ocean observing network in the Northeast Pacific that includes the OOI Cabled Array and the OOI Global Station Papa site (L.M. Smith et al., 2018, in this issue), the latter in partnership with a mooring maintained by the National Oceanic and Atmospheric Administration (NOAA). The Ocean Networks Canada NEPTUNE and VENUS arrays (<http://www.oceannetworks.ca>) and the NOAA-supported Northwest Association of Networked Ocean Observatories (NANOOS; <http://nanoos.org>) assets provide even greater coverage in this region. This combination of ocean observatories affords an exceptional opportunity to study coastal ocean processes and long-term change within the context of regional climate and ocean changes.

Pacific Northwest (PNW) waters are home to a diverse range of highly productive, profitable marine fisheries, including iconic species such as Dungeness crab, razor clams, salmon, groundfish, and hake. These successful fisheries rely on the injection of nutrients into the euphotic zone by upwelling and the subsequent blooms of phytoplankton that form the base of the oceanic food web. However, this productive chain of events can sometimes be altered to the detriment of fisheries by a variety of atmospheric, oceanographic, and biogeochemical processes,

as well as anthropogenic influence.

Over the last 15 years, PNW waters have been exposed to hypoxic and even anoxic events (Grantham et al., 2004; Chan et al., 2008) that have the potential to severely disrupt local fisheries. The region is also known for the appearance of harmful algal blooms that generate toxic substances that become incorporated into the ocean food chain, leading to closures of valuable recreational and commercial fisheries. These interdisciplinary ocean challenges require measuring ocean properties from physics to chemistry to biology on many different timescales, a capability of the Endurance Array.

Climate and ocean anomalies on year-to-year ("interannual") and decade-to-decade ("interdecadal") timescales influence PNW waters. In response to interannual variability forced by the El Niño-Southern Oscillation at the equator, upper-ocean stratification, ocean currents, and local winds all change in the Northeast Pacific as a result of signals that travel to the PNW through both the ocean and the atmosphere (Huyer et al., 2002). On interdecadal timescales, PNW waters are affected by the Pacific Decadal Oscillation, which manifests itself as 10–40 year cycles in upper-ocean temperature and swings between dominance by northern, "fatty" zooplankton and southern, "skinny" zooplankton (Peterson and Schwing, 2003).

ENDURANCE ARRAY MEASUREMENT PLATFORMS AND SENSORS

Coastal waters in the Northeast Pacific change on timescales from hours to decades. This huge range, almost five orders of magnitude, requires programming ocean sensors to sample at intervals on the order of minutes while deployed on platforms designed and operated to endure for decades. After a brief introduction of the overall Endurance Array design, we describe in more detail the instruments and platforms used in the array.

The Endurance Array employs a variety of oceanographic sampling platforms, including coastal surface moorings, water column profilers, and instruments on the seafloor and on a midwater platform. The Endurance Array backbone includes the Oregon Line, off Newport near 44.6°N, and the Washington Line, off Grays Harbor near 47°N (Figure 1). These lines each have three sites: one at the inner shelf (~25–30 m water depth, 4–6 km from shore, referred to as “Inshore”), the “Shelf” (~80–90 m depth, 20–30 km from shore), and the continental slope (~500–600 m depth, 60–65 km from shore, “Offshore”). All Endurance Array platforms and sites measure fundamental ocean properties such as temperature, salinity, pressure, water velocity, chlorophyll fluorescence, and dissolved oxygen. The Endurance Array sensors and platforms return data to shore via either cellular or satellite links at the sea surface for autonomous moorings or via a seafloor cable. All data were obtained from

the National Science Foundation Ocean Observatories Initiative Data Portal (<http://ooinet.oceanobservatories.org>).

Coastal surface moorings each consist of a surface buoy equipped with either a cellular or a satellite communications antenna, a mooring line supporting the delivery of power and data to instruments along the line and to the seafloor, and a seafloor instrument platform with an integrated anchor system. Moored instruments provide high temporal resolution at fixed points. Meteorological instruments (ASIMET, Star Engineering) on the buoys provide continuous measurements of winds, air temperature and humidity, and solar radiation at one-minute intervals. For this paper, solar radiation data from the sensors located onboard the large surface buoys at the Oregon and Washington Shelf and Offshore sites are used to examine the arrival of the August 2017 eclipse (Figure 1). We use wind measurements from the Oregon Shelf Site. The Endurance Oregon Inshore mooring has

an instrumented platform on the seafloor on which temperature (Sea-Bird SBE 16plusV2) and dissolved oxygen (Aanderaa Optode 4831) are measured at 15-minute intervals. Measurements are sent to a surface buoy for relay to shore via the cellular network every four hours. We use the near-bottom dissolved oxygen and temperature data from the Oregon Inshore site to examine a summer-time hypoxia event.

Profiling moorings have self-contained instrument packages that move up and down the water column and are paired adjacent to each surface mooring. They provide fine vertical resolution (~1 m) at a fixed location. The Endurance Array has four types of profilers, and we use data from one of them to describe the arrival of anomalously warm water to the Pacific Northwest, specifically an uncabled wire-following profiler (McLane Moored Profiler) located at the offshore end of the Washington line (Figure 1). Wire-following profilers carry low-power instruments that sample the water column from just below a subsurface float at 30 m depth down to 500 m, ascending and descending three times per day. We use temperature data from a profiler’s onboard conductivity-temperature-depth sensor (Sea-Bird SBE 52MP). Data are reported to a surface buoy tethered to the subsurface float and then ultimately to shore via inductive and satellite modems, respectively.

The cabled bioacoustic sensors at the Oregon Shelf and Offshore locations are three-frequency systems (38, 120, and 200 kHz), and their cable-provided power allows for frequent sampling. The bioacoustic sensors are modified Kongsberg EK60 echosounders that obtain acoustic backscatter from targets in the water column like zooplankton and fish. The bioacoustics sensors collect data every one second for 20 minutes each hour and send 100% of those data to shore via the seafloor cable. The cabled bioacoustic sensors were used to examine zooplankton migration during the August 2017 eclipse.

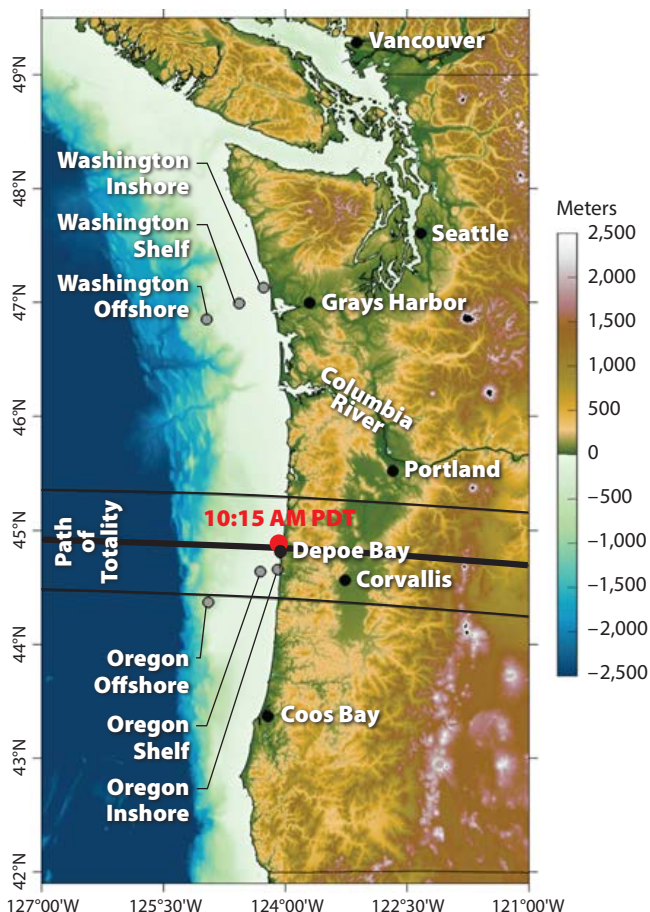


FIGURE 1. Map of the Ocean Observatories Initiative (OOI) Endurance Array located in the Northeast Pacific Ocean, spanning north and south of the Columbia River. Fixed platforms are shown as gray filled circles. The August 21, 2017, solar eclipse path of totality is shown crossing the Oregon line off Newport; the local time for the start of totality at the coast (red circle) is shown in red. Colored shades are ocean bathymetry and land topography.

THE NORTHEAST PACIFIC “WARM BLOB” REACHES THE COAST

Oceanographers have documented how air-sea interactions at high latitudes set the depth and characteristics of the surface ocean mixed layer that then subsequently affect ocean properties and ecosystem responses at latitudes to the south (e.g., for the North Pacific in Freeland, 2013; Wheeler et al., 2003; for the North Atlantic in Greene and Pershing, 2007). The OOI arrays in the Northeast Pacific extend from the global site at Station Papa in the central Gulf of Alaska, through the regional cabled array off the Pacific Northwest, to the Endurance Array on the continental slope and shelf off Oregon and Washington (L.M. Smith et al., 2018, in this issue; Figures 1 and 2). These arrays are well positioned to track long-period variations in ocean conditions, for example, El Niño/La Niña cycles and the Pacific Decadal Oscillation, between high and low latitudes in the Northeast Pacific.

During the winter of 2013–2014, the atmospheric Jet Stream shifted anomalously northward, leading to less wind-driven mixing in the central Gulf of Alaska, which subsequently led to the formation of a large region of anomalously warm surface water (Figure 2). This “warm blob” (Bond et al., 2015) was subsequently observed to be advected south and toward the Canadian and US west coasts (Peterson et al., 2017; Figure 2). Peterson et al. (2017) reported that the warm blob persisted at least through 2016.

The wire-following profiler cycling up and down three times per day at the offshore end of the Endurance Array line off Grays Harbor, Washington, captured the arrival and evolution of the warm blob as it was advected south and toward the US west coast (Figure 3). In late 2014 and early 2015, near-surface temperature anomalies exceeded 4°C, with 2°C anomalous water penetrating 150 m deep in the water column, commensurate with the depth of the continental shelf in this region. As wintertime downwelling pulled offshore waters toward shore, the

entire shelf was bathed in warm blob waters (Peterson et al., 2017).

The warm anomaly was replaced with slightly colder water at depth in spring 2015, and near-surface (~30 m) waters were cooled by the offshore advection of cold upwelled waters during summertime upwelling off the Pacific Northwest. Warm blob waters returned in fall 2015 and again persisted until the following summer. However, during winter 2015–2016, the warm blob waters went even

deeper, with 2°C anomalous water penetrating down to 250 m. This deeper extent of the large-scale warm anomalies is consistent with downward mixing and diffusion of the warm blob since its formation two years earlier. Note also that the maximum warm anomalies are at depth—the lingering signature of the surface warm blob—while the surface waters are returning ever so slightly back toward normal. During winter 2016, the 2015–2016 El Niño also influenced warm water

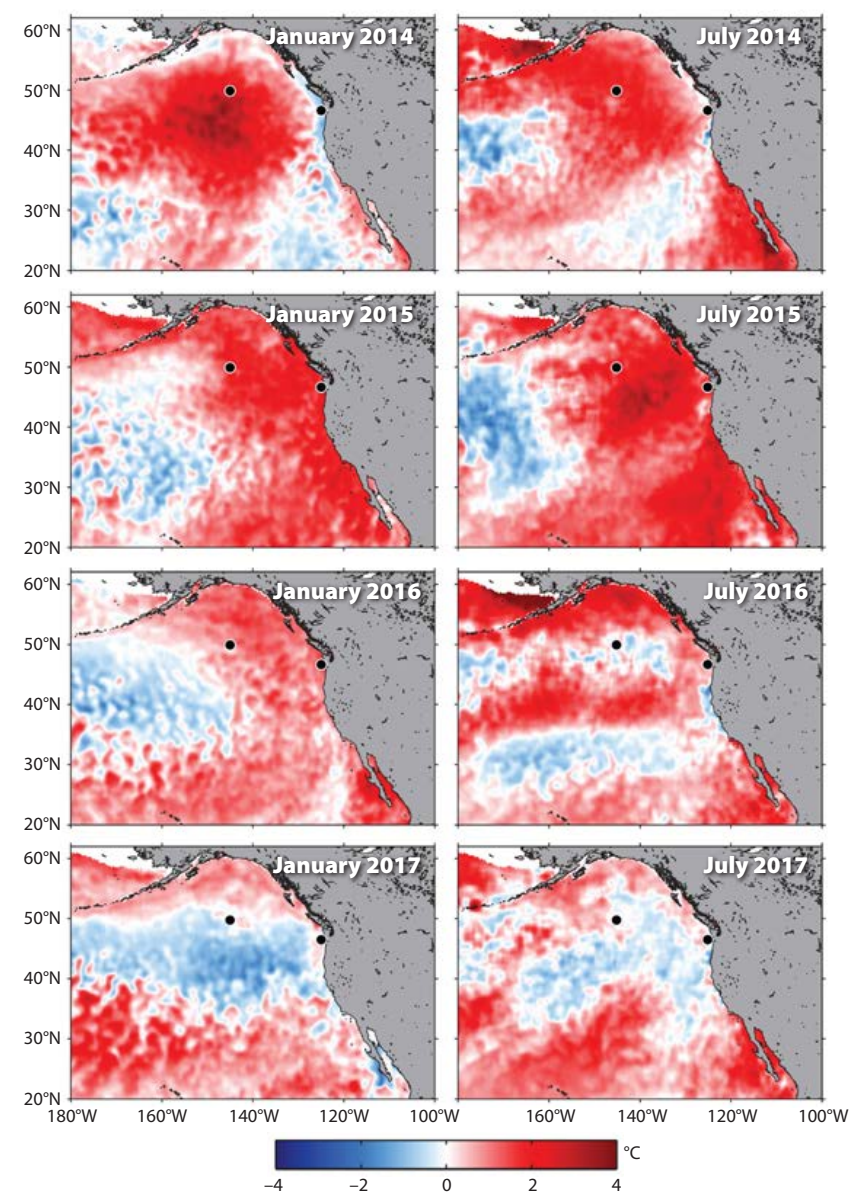


FIGURE 2. North Pacific sea surface temperature anomaly showing the evolution of the “warm blob” from its origination in winter 2013–2014 through the following four years. Satellite temperature data are from AVHRR-only Optimum Interpolation Sea Surface Temperature (OISST, <https://www.ncdc.noaa.gov/oisst/data-access>), and anomalies are computed relative to a 30-year climatology constructed from 1982 to 2011. The locations of the OOI Washington Offshore wire-following profiler mooring and the OOI Station Papa (50°N , 145°W) mooring are shown as filled black circles.

anomalies at depth.

In October 2016, an intense winter storm broke the wire-following profiler loose from its anchor. In April 2017, a replacement unit was installed during the regular Endurance Array refurbishment cruise. Data from summer and early fall 2017 show that the strength of the warm water anomaly has decreased, but it remains at depth at the edge of the continental shelf off the Pacific Northwest. During the October 2017 turnaround cruise, the wire-following profiler was upgraded to allow four profiles per day, leading to even greater data density at this site.

Since 2014, the warm blob waters have had a strong impact on the marine ecosystem off Washington, Oregon, and northern California. The warm waters were identified as contributing to enhanced harmful algal blooms (HABs) in the area (McCabe et al., 2016; McKibben et al., 2017). A toxic diatom bloom (*Pseudo-nitzschia*) led to the release of domoic acid that then appeared in one of the iconic and valuable commercial shellfish species off the US west coast, the Dungeness crab. In 2014, the commercial Dungeness crab fishery was valued at nearly \$170 million

(2014 Pacific States Marine Fisheries Commission Dungeness Crab Report, posted online at <https://www.psmfc.org/crab>). High levels of domoic acid in the crabs led to the delay (Oregon) or shutdown (California) of the commercial crab fishery during the 2015–2016 crabbing season. Delays in opening the Dungeness crab fishery hit again in late 2016. The warm blob waters also led to increased abundance of dinoflagellates and a reduced biomass of copepods and euphausiids on the Oregon shelf, the latter being an important food source for commercially and ecologically important species such as salmon (Peterson et al., 2017). See Cavole et al. (2016) for a review of other biological impacts of the 2013–2015 warm-water anomaly in the Northeast Pacific.

LOW-OXYGEN EVENT OFF CENTRAL OREGON

The surface waters of coastal upwelling zones such as the one off the Pacific Northwest are extremely productive because injection of nutrients into the surface light zone fuels a robust ocean food web. However, a potentially harmful low-oxygen layer can sometimes exist

near the seafloor beneath the productive surface waters. Near-bottom waters over the continental shelf off Oregon in the northern California Current have become increasingly hypoxic over the last decade and a half, including the appearance of anoxia in summer 2006 (Chan et al., 2008). Observed ecosystem impacts include the absence of fish and die-offs of invertebrates (Grantham et al., 2004).

Upwelling of low-oxygen, nutrient-rich source water onto the continental shelf, followed by the decay of organic matter from surface phytoplankton blooms, drives near-bottom, inner-shelf hypoxia. This process can form a pool of near-bottom water that can sometimes reach dissolved oxygen levels that are less than $\sim 62 \mu\text{Mol kg}^{-1}$ (1.4 mL L^{-1}), adversely affecting many organisms (Diaz and Rosenberg, 1995). Under “severe” hypoxia, with dissolved oxygen levels less than $\sim 22 \mu\text{Mol kg}^{-1}$ (0.5 mL L^{-1}), the condition of the commercially valuable Dungeness crab (*Cancer magister*) can deteriorate (Keller et al., 2010).

Changes in near-bottom oxygen levels off central Oregon vary through the spring-summer upwelling season, decreasing toward July and August (Adams et al., 2013). These levels can also vary on a timescale of days as the wind-driven upwelling circulation advects the low dissolved oxygen pool back and forth across the shelf. To illustrate this variability, we use data from July 2017 when several upwelling-favorable (southward) and downwelling-favorable (northward) wind events lasting from 2–10 days influenced near-bottom oxygen off Newport, Oregon (Figure 4). This late in the upwelling season, which began in late April, near-bottom dissolved oxygen levels at the bottom of the OOI Oregon Inshore Surface mooring were below the hypoxia threshold for much of the month.

Note that when winds blow to the south, the near-bottom temperature decreases due to coastal upwelling, with a slight lag relative to the wind. During these upwelling events, near-bottom oxygen usually decreases, as exemplified by

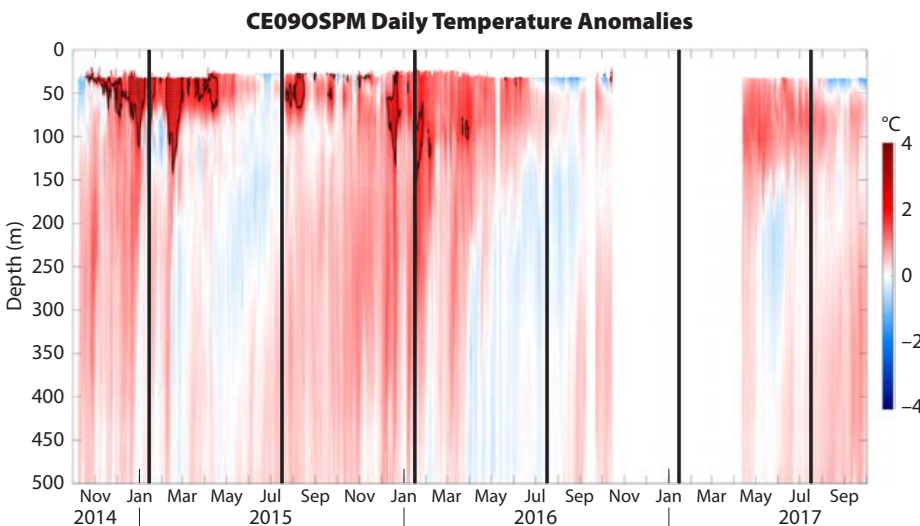


FIGURE 3. Temperature anomaly ($^{\circ}\text{C}$) as a function of time and depth from the OOI Endurance Array Washington Offshore wire-following profiler. The anomalies are computed from the “Averaged Decades” World Ocean Atlas climatology (<https://www.nodc.noaa.gov/cgi-bin/OC5/woa13/woa13.pl?parameter=t>). There are over 5,400 vertical profiles in the wire-following profiler time series. The gap in late 2016/early 2017 is when the wire-following profiler broke loose from its anchor as a result of an intense winter storm. The vertical black bars mark the times of the 2015–2017 satellite images in Figure 2.

July 23–25. Conversely, during wind relaxation or downwelling, near-bottom temperature and dissolved oxygen increase rapidly. These changes are consistent with near-bottom cold water low in dissolved oxygen being drawn toward the coast during upwelling and warm water containing more oxygen being pushed down and away from the coast near the bottom during downwelling. Note that the dissolved oxygen does not follow the winds or temperature as clearly as temperature follows the wind because the additional biological processes of photosynthesis and microbial decay raise or lower dissolved oxygen levels, respectively.

Incidentally, on July 12, 2017, scientists from the Oregon Department of Fish and Wildlife (ODFW) deployed a seafloor crab pot equipped with a video camera in 48 m of water off Newport, Oregon (<http://oregonmarinereserves.com/2017/09/06/hypoxia-central-coast>). This location is approximately 3.5 km from the OOI Oregon Inshore Mooring. Images recorded just after deployment show healthy active crabs in the pot, but starting on July 17, the crabs in the pot began to look lethargic, and by July 26 there was little to no movement in the crab pot (Figure 5). This die-off coincided with the decrease of dissolved oxygen to severely hypoxic levels starting on about July 17,

with final values on July 24 of less than $10 \mu\text{Mol kg}^{-1}$ (0.2 mL L^{-1}). The decrease in dissolved oxygen happened in two pulses of upwelling-favorable winds around July 17 and July 24. When the video-equipped crab pot was recovered on August 3, 2017, ODFW scientists recovered 30 dead and two live crabs (Kelly Corbett, ODFW, *pers. comm.*, 2017).

The hypoxic event of July 2017 demonstrates how near-bottom oceanographic data, in combination with surface winds, capture the “event-scale” response of the coastal ocean to wind forcing. The OOI Endurance Array has a wealth of other oceanographic data available to be analyzed, including near-bottom and water-column measurements of temperature, salinity, velocity, chlorophyll fluorescence, and light transmission (a measure of suspended particles). These data show just how quickly the coastal ocean can change and how ocean properties can strongly impact marine organisms.

RISING ZOOPLANKTON DURING THE 2017 TOTAL ECLIPSE OF THE SUN

On August 21, 2017, the United States experienced a total eclipse of the sun, one of only a handful visible from the continental United States over the last 60 years and the first of the twenty-first

century. The 110 km wide path of totality stretched from Oregon to South Carolina and, fortuitously, passed directly over the Newport line of the OOI Endurance Array (Figure 1). Similar to land animals, which are known to react to the appearance of darkness during a total solar eclipse, vertically migrating zooplankton also react to this irregular darkening of the sky (Kampa, 1975; Strömberg et al., 2002). Zooplankton migrate vertically each day, rising at dusk from the depths where they seek refuge from predators to the sea surface where they feed at night. At dawn, they descend again to depths of several hundred meters, depending on the species and local bottom depth. Off central Oregon, the vertically migrating zooplankton species include *Euphausia pacifica*, based on past studies of this region (e.g., Peterson and Schwing, 2003).

Knowing that the eclipse would happen and realizing that the path of totality would pass over the OOI Newport line, the Oregon State University Endurance Array team responded to requests from non-OOI scientists to reprogram the Endurance Array cabled bioacoustic sensors at the Oregon Shelf and Offshore sites to sample continuously rather than at their regular sampling rate of once per second for 20 minutes each hour in order to see whether the zooplankton off Oregon would react to the total solar eclipse. Through the OOI Engineering Change Request system, this request was

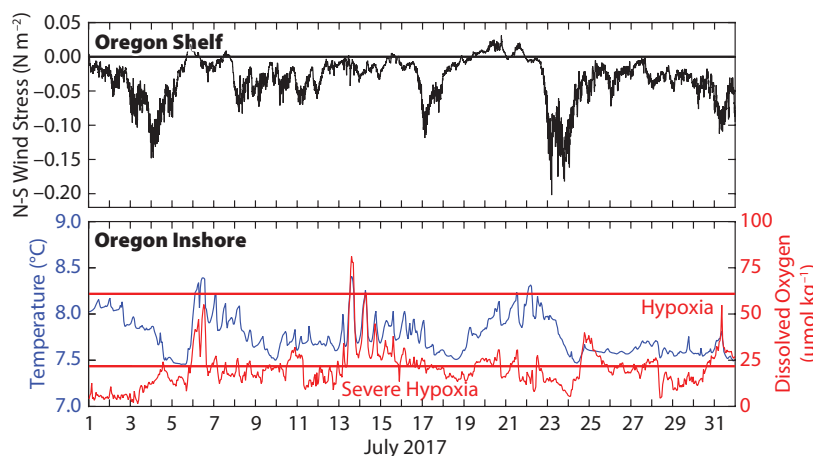


FIGURE 4. Dissolved oxygen ($\mu\text{Mol kg}^{-1}$, red) and temperature ($^{\circ}\text{C}$, blue) from near the bottom at the 25 m OOI Oregon Inshore mooring, and north-south wind stress (N m^{-2} , black) from the OOI Oregon Shelf surface mooring. Levels of dissolved oxygen for hypoxia ($\sim 62 \mu\text{Mol kg}^{-1}$, 1.4 mL L^{-1}) and “severe” hypoxia ($\sim 22 \mu\text{Mol kg}^{-1}$, 0.5 mL L^{-1}) are indicated by horizontal red lines.



FIGURE 5. This July 26, 2017, still frame is from a video showing the die-off of Dungeness crabs (*Cancer magister*) caught in an Oregon Department of Fish and Wildlife pot off Newport, Oregon (<http://oregonmarinereserves.com/2017/09/06/hypoxia-central-coast>).

reviewed, approved, and implemented in time for the eclipse. This change was possible within the power constraints of the cabled system because there are fewer power constraints on the bioacoustic instruments than when the sampling was first implemented three years earlier. Moving forward, the cabled bioacoustic sensors will continue to sample continuously.

The idea to use the OOI sensors to visualize animal behavior in the ocean captivated people's attention as the eclipse approached. With much of the pre-eclipse hype focused on humans and land-based animals, the unique view into the ocean afforded by the Endurance Array offered a new twist to an eager audience. The *Los Angeles Times* ran pre- and post-eclipse stories (Netburn, 2017) that included the whimsical headline "Poor little zooplankton—they got totally punk'd by Monday's eclipse." The story was also

picked up by National Public Radio and the Coastal Society among others.

Shortly after 9 a.m. Pacific Daylight Time (UTC minus seven hours), sensors on the OOI surface buoys measured the beginning of the decrease in incoming solar radiation (Figure 6). The partial eclipse lasted for over two hours, but the time of totality lasted just about two minutes centered on 10:16 am PDT. In response to this darkening, zooplankton began to rise in the water column above the 200 m bioacoustic sensor at the Oregon Offshore site (Figure 6). The regular diel vertical migration is evident during the days before the eclipse. The acoustic scatterers rose from around 170 m to 120 m, covering 50 m in about 45 minutes, a vertical migration speed of about 0.02 m s^{-1} . This speed is in agreement with past studies of zooplankton vertical migration speeds.

Putting data online in near-real time

is important for education and outreach, just as it is important for science. Eclipse-related data plots were online by the end of August 21, so they could be shared with the public while the eclipse was still front-page news. Follow-up stories on these data by the *Los Angeles Times* and National Public Radio were retweeted and "liked" far more than the news stories about our zooplankton migration prediction before the eclipse.

In addition to the continuously sampling, cabled bioacoustic sensors, an Endurance Array glider, two Coastal Surface Piercing Profilers (CSPP), and a variety of fixed sensors on the coastal moorings, including a spectral irradiance instrument, were programmed to run more often during the eclipse period. The CSPPs were commanded to make vertical profiles during the two minutes of totality. An underwater glider conducted continuous profiles next to the Oregon Shelf Surface Mooring during the day of the eclipse, temporarily breaking from its normal across-shelf profiling. We hope this demonstration of adaptive sampling stimulates others to utilize this OOI capability.

SUMMARY

With the examples described above, we demonstrated the utility of the OOI Endurance Array to capture oceanographic events lasting from hours to years. This OOI Endurance Array, the Cabled Array, and the Station Papa Array are all parts of a larger Northeast Pacific observing network that allows the spatial connections and the propagation of events to be studied from formation to impact. The sensors deployed on the array simultaneously measure physical, biological, and chemical parameters, allowing the study and modeling of linked physical-biogeochemical processes. The examples above provide but a glimpse of the capabilities of the OOI Endurance Array.

Further analysis and modeling of the arrival and the impact of the "warm blob" on Pacific Northwest waters can make use of the large number of moored and

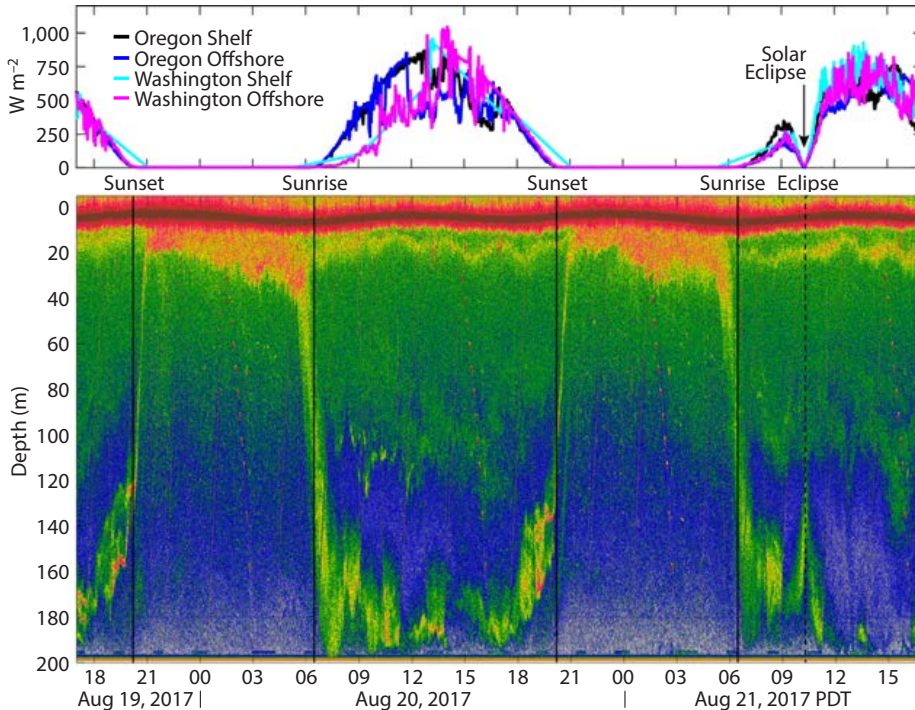


FIGURE 6. (top) Incoming shortwave radiation measured at four OOI surface moorings showing the daily cycle of sunlight; the total solar eclipse happens a little after 10 a.m. local time on August 21, 2017. (bottom) Echogram of acoustic backscatter at 200 kHz measured from the OOI Oregon Offshore midwater platform. The bioacoustic sensor is mounted on the 200 m deep midwater platform looking up; the dark red line is the acoustic return from the sea surface; other red and bright green returns are scattering off zooplankton that undergo diel vertical migration. Times of sunset and sunrise are noted by black vertical lines. The total solar eclipse is indicated by a black dashed line. The faint straight red lines traveling diagonally from top to bottom are acoustic returns off the Cabled Shallow Profiler that samples the water column nine times per day.

mobile assets on the OOI platforms in the region as well as measurements made by Ocean Networks Canada and the NOAA-supported Station Papa mooring and NANOOS instruments. Such an analysis would join and benefit from the in-depth analysis of the warm water anomalies conducted farther south in the California Current using a variety of observational platforms (e.g., Zaba and Rudnick, 2016; Cavole et al., 2016). Better yet, as the OOI time series grows over the anticipated 25–30 year life of the program, we expect to sample more interdecadal changes and add to the historic time series in the area that will allow us to better discern long-term change in the context of interdecadal variability.

The hypoxia event observed in July 2017 provides a glimpse of the strong changes driven both by the “event-scale” (2–10 days) changes in the wind and by biogeochemical processes. Variability in all ocean parameters is strong at this timescale, and the OOI Endurance Array is set up to capture this variability. Further insight and even predictive capability is possible by combining the many air-sea interface, water-column, and seafloor measurements across the OOI arrays. These data should also be used to verify and challenge our ever-improving numerical ocean circulation and biogeochemical modeling capability.

The Endurance Array was not designed for measuring the August 21, 2017, eclipse, but its sensor diversity and large footprint over the continental shelf sets it up well to measure events in unique ways. While the anticipated zooplankton migration was observed in previous eclipses, what is new and different about OOI’s eclipse sampling is synoptic coverage from multiple bioacoustic sonars as well as measurements from all of the other potentially relevant Endurance Array sensors. We look forward to a more complete analysis of this event and welcome others to dig in to these data. ☺

REFERENCES

- Adams, K.A., J.A. Barth, and F. Chan. 2013. Temporal variability of near-bottom dissolved oxygen during upwelling off central Oregon. *Journal of Geophysical Research* 118:4,839–4,854, <https://doi.org/10.1029/jgrc.20361>.
- Bond, N.A., M.F. Cronin, H. Freeland, and N. Mantua. 2015. Causes and impacts of the 2014 warm anomaly in the NE Pacific. *Geophysical Research Letters* 42(9):3,414–3,420, <https://doi.org/10.1002/2015GL063306>.
- Cavole, L.M., A.M. Demko, R.E. Diner, A. Giddings, I. Koester, C.M.L.S. Pagniello, M.-L. Paulsen, A. Ramirez-Valdez, S.M. Schwenck, N.K. Yen, and others. 2016. Biological impacts of the 2013–2015 warm-water anomaly in the Northeast Pacific: Winners, losers, and the future. *Oceanography* 29(2):273–285, <https://doi.org/10.5670/oceanog.2016.32>.
- Chan, F., J.A. Barth, J. Lubchenco, A. Kirincich, H. Weeks, W.T. Peterson, and B.A. Menge. 2008. Emergence of anoxia in the California Current large marine ecosystem. *Science* 319:920, <https://doi.org/10.1126/science.1149016>.
- Diaz, R.J., and R. Rosenberg. 1995. Marine benthic hypoxia: A review of its ecological effects and the behavioural responses of benthic macrofauna. *Oceanography and Marine Biology: An Annual Review* 33:245–303.
- Freeland, H.J. 2013. Evidence of change in the winter mixed layer in the Northeast Pacific ocean: A problem revisited. *Atmosphere-Ocean* 51:126–133, <https://doi.org/10.1080/07055900.2012.754330>.
- Grantham, B.A., F. Chan, K.J. Nielsen, D.S. Fox, J.A. Barth, A. Huyer, J. Lubchenco, and B.A. Menge. 2004. Upwelling-driven nearshore hypoxia signals ecosystem and oceanographic changes in the Northeast Pacific. *Nature* 429:749–754, <https://doi.org/10.1038/nature02605>.
- Greene, C.H., and A.J. Pershing. 2007. Climate drives sea change. *Science* 315:1,084–1,085, <https://doi.org/10.1126/science.1136495>.
- Huyer, A., R.L. Smith, and J. Fleischbein. 2002. The coastal ocean off Oregon and northern California during the 1997–8 El Niño. *Progress in Oceanography* 54(1–4):311–341, [https://doi.org/10.1016/S0079-6610\(02\)00056-3](https://doi.org/10.1016/S0079-6610(02)00056-3).
- Kampa, E. 1975. Observations of a sonic-scattering layer during the total solar eclipse, 30 June, 1973. *Deep Sea Research* 22:417–423, [https://doi.org/10.1016/0011-7471\(75\)90063-7](https://doi.org/10.1016/0011-7471(75)90063-7).
- Keller, A.A., V. Simon, F. Chan, W.W. Wakefield, M.E. Clarke, J.A. Barth, D. Kamikawa, and E.L. Fruh. 2010. Demersal fish and invertebrate biomass in relation to an offshore hypoxic zone along the US west coast. *Fisheries Oceanography* 19:76–87, <https://doi.org/10.1111/j.1365-2419.2009.00529.x>.
- Netburn, D. 2017. Poor little zooplankton—they got totally punk’d by Monday’s eclipse. *Los Angeles Times*, August 24, 2017, <http://www.latimes.com/science/sciencenow/la-sci-sn-eclipse-science-results-20180823-story.html>.
- McCabe, R.M., B.M. Hickey, R.M. Kudela, K.A. Lefebvre, N.G. Adams, B.D. Bill, F.M.D. Gulland, R.E. Thomson, W.P. Cochlan, and V.L. Trainer. 2016. An unprecedented coastwide toxic algal bloom linked to anomalous ocean conditions. *Geophysical Research Letters* 43(19):10,366–10,376, <https://doi.org/10.1002/2016GL070023>.
- McKibben, S.M., W. Peterson, A.M. Wood, V.L. Trainer, M. Hunter, and A.E. White. 2017. Climatic regulation of the neurotoxin domoic acid. *Proceedings of the National Academy of Sciences of the United States of America* 114:239–244, <https://doi.org/10.1073/pnas.1606798114>.
- Peterson, W.T., and F.B. Schwing. 2003. A new climate regime in northeast pacific ecosystems. *Geophysical Research Letters* 30, 1896, <https://doi.org/10.1029/2003GL017528>.
- Peterson, W.T., J.L. Fisher, P.T. Strub, X. Du, C. Risien, J. Peterson, and C.T. Shaw. 2017. The pelagic ecosystem in the Northern California Current off Oregon during the 2014–2016 warm anomalies within the context of the past 20 years. *Journal of Geophysical Research* 122:7,267–7,290, <https://doi.org/10.1002/2017JC012952>.
- Smith, R.L. 1974. A description of current, wind and sea level variations during coastal upwelling off the Oregon coast, July–August 1972. *Journal of Geophysical Research* 79:435–443, <https://doi.org/10.1029/JC079i003p00435>.
- Smith, L.M., J.A. Barth, D.S. Kelley, A. Plueddemann, I. Rodero, G.A. Ulses, M.F. Vardaro, and R. Weller. 2018. The Ocean Observatories Initiative. *Oceanography* 31(1):16–35, <https://doi.org/10.5670/oceanog.2018.105>.
- Strömborg, J.-O., J.I. Spicer, B. Liljebladh, and M.A. Tomasson. 2002. Northern krill, *Meganyctiphanes norvegica*, come up to see the last eclipse of the millennium? *Journal of the Marine Biological Association of the United Kingdom* 82:919–920, <https://doi.org/10.1017/S0025315402006367>.
- Wheeler, P.A., A. Huyer, and J. Fleischbein. 2003. Cold halocline, increased nutrients and higher chlorophyll off Oregon in 2002. *Geophysical Research Letters* 30, 8021, <https://doi.org/10.1029/2003GL017395>.
- Zaba, K.D., and D.L. Rudnick. 2016. The 2014–2015 warming anomaly in the Southern California Current System observed by underwater gliders. *Geophysical Research Letters* 43:1,241–1,248, <https://doi.org/10.1002/2015GL067550>.

ACKNOWLEDGMENTS

We thank all members of the Oregon State University (OSU) OOI team for their tireless efforts designing, installing, and maintaining the Endurance Array. We are grateful to the captains and crews of the research vessels that get us to sea to retrieve data and keep the Endurance Array operating. These include OSU’s research vessels *Oceanus* and *Pacific Storm* and the research vessels *Thomas G. Thompson* (University of Washington), *Sikuliaq* (University of Alaska) and *Atlantis* (Woods Hole Oceanographic Institution). We thank our University of Washington OOI colleagues who designed, installed, and maintain the midwater platform and bioacoustic sensors of the Oregon offshore cabled shallow profiler mooring. We appreciate the Oregon Department of Fish and Wildlife sharing the video and a report of Dungeness crab behavior off Newport, Oregon.

AUTHORS

John A. Barth (jack.barth@oregonstate.edu) is Professor and OOI Project Scientist, **Jonathan P. Fram** is Assistant Professor and OOI Systems Engineer, **Edward P. Dever** is Professor and Endurance PI/Project Manager, **Craig M. Risien** is OOI Technician, **Chris E. Wingard** is OOI Senior Technician, **Robert W. Collier** is Professor Emeritus, and **Thomas D. Kearney** is Endurance Project Management Assistant, all at the College of Earth, Ocean, and Atmospheric Sciences, Oregon State University, Corvallis, OR, USA.

ARTICLE CITATION

Barth, J.A., J.P. Fram, E.P. Dever, C.M. Risien, C.E. Wingard, R.W. Collier, and T.D. Kearney. 2018. Warm blobs, low-oxygen events, and an eclipse: The Ocean Observatories Initiative Endurance Array captures them all. *Oceanography* 31(1):90–97, <https://doi.org/10.5670/oceanog.2018.114>.



Power from Benthic Microbial Fuel Cells Drives Autonomous Sensors and Acoustic Modems

By Clare E. Reimers and Michael Wolf

ABSTRACT. Autonomous platforms that support low-power sensors represent one approach to expanding ocean observing. This paper describes a unique autonomous platform designed to deliver long-term sensor measurements from the benthic boundary layer at low cost. The platform, called a Benthic Observer (BeOb), is powered by energy harvested with a benthic microbial fuel cell (BMFC), and it uses an acoustic modem to both store and transmit data organized in daily reports of hourly measurements. A BeOb equipped with sensors to measure dissolved oxygen, temperature, and conductivity ~1 m above the seabed has been active for over 14 months on the Oregon slope at a location within the core of the oxygen minimum zone. During this observation period, the system's battery reserves have been kept fully charged by the BMFC. A 90-day time series of sensor data are compared to simultaneous high-frequency measurements at a neighboring Ocean Observatories Initiative cabled Benthic Experiment Package to examine the expected quality and confidence levels for seasonal or annual means of continued measurements. An ocean observing system incorporating arrays of BMFC-powered platforms transmitting to central gateway modems is proposed for future ocean-property monitoring programs. Such arrays may be especially helpful for tracking expansions of ocean oxygen minimum zones.

INTRODUCTION

Accurate, long-term, and widespread sensor measurements of essential ocean variables are needed for documenting changes in ocean conditions and circulation on both regional and global scales. Oceanic processes that are critical to the planet such as heat transport, oxygenation, acidification, and primary production may be better understood and interconnected through sustained multiscale observations. Observations are also needed to both calibrate and validate ocean models that seek to predict the influence of anthropogenic forcing, and are crucial for the detection of potentially hazardous oceanic events such as tsunami waves and harmful algal blooms. The US Ocean Observatories Initiative (OOI), highlighted in this special issue of *Oceanography*, combines Lagrangian and Eulerian sensing platforms including gliders, autonomous underwater vehicles, surface buoys, profilers, inductive mooring cables, and seafloor junction boxes to create arrays of instruments for sensing and sampling the ocean through time and in three dimensions. Although

OOI has an unprecedented variety of nearly 75 models of specialized instruments and the capability to follow transient phenomena through high-speed measurements, its coverage of large-scale phenomena measured consistently over months, years, and eventually decades, remains limited. More broadly, it is estimated that the coverage of all existing and planned international ocean observing time series stations represents only 9%–15% of the global ocean surface area (Henson et al., 2016). The greatest limiting factor for ocean observing is the high cost of installing and maintaining in situ observing assets widely distributed in the ocean.

This problem of sustaining measurements, and the larger goal of contributing to an adaptive framework for global ocean observing, encouraged us to devise a low-cost, easy-to-deploy, autonomous sensor platform well suited for expanding the spatial footprint of ocean observations. This new platform, which we call a Benthic Observer or BeOb, employs bioelectrical energy harvesting to recharge batteries and acoustics to relay

data. By operating at the seafloor, it provides observations from within the benthic boundary layer apart from the sampling reach of most gliders and floats. This article briefly describes the platform's technology and illustrates sensor temperature, conductivity, and dissolved oxygen data from a trial deployment on the Oregon slope at a site within the oxygen minimum zone (OMZ) of the Northeast Pacific. A BeOb was deployed on August 12, 2016, from R/V *Sally Ride* at 44°21'39"N, 124°56'17"W, at a target water depth of 580 m, 1.6 km south of OOI's Benthic Experiment Package CE04OSBP. The deployment was executed by winch and wire using an acoustic release (ORE Offshore) that was triggered after lowering the platform to within 10 m of the seafloor. Several cruises of opportunity connected to the OOI mission have allowed a partial retrieval of BeOb data, which are evaluated here by comparing them to contemporaneous OOI observations. The variability of water column parameters at a fixed point is also assessed and used to make recommendations for future BeOb sensor configurations. An ocean observing system incorporating arrays of networked BeOb platforms is envisioned and is fully within the capabilities of these systems.

BENTHIC OBSERVER TECHNOLOGIES

Any ocean observing platform requires a reliable power source, instrument control, a means of data recovery, and sensor systems that can produce and maintain high-quality measurements. Various approaches can meet these requirements, but numerous trade-offs influence the extent of sensor measurements throughout the ocean. BeOb incorporates a small footprint (0.28 m^2) benthic microbial fuel cell (BMFC) and a power management

platform (PMP) to harvest energy continuously and to keep two serial stacks of 3.7 V cylindrical lithium-ion batteries (three per stack) charged (total capacity 57 Wh) and ready to supply power to sensors and communication systems on board (Figure 1). With the present design, the BMFC can supply ~10–20 mW reliably over the long term. This provides the intended benefit that large, potentially hazardous, battery packs are not needed, nor do batteries need to be replaced. The 57 Wh capacity of the lithium ion batteries, combined with the BMFC, means that even fairly power-hungry sensors can be run if they are constrained to low duty cycles (e.g., 5 W for 0.2% of the time).

The BMFC harvests energy by taking advantage of the natural oxidation of organic matter by bacteria to supply electrons to an inert carbon fiber brush electrode (anode) enclosed in an anaerobic benthic chamber (Tender et al., 2002; Reimers, 2015; Reimers et al., 2017a,b). This chamber also creates a base structure for the BeOb (Figure 1). Extra “fuel”

is pre-packed inside the chamber in the form of paper packets of 20% by weight dried plankton flake (fish food) and 80% CaCO_3 (that helps buffer the pH). Electricity flows through the BMFC as electrons are passed from the anode to the cathode to reduce dissolved oxygen. Like in a battery, the voltage difference between the cathode (+) and the anode (-) depends on the chemistry surrounding the electrodes and the load placed on the cell. This voltage difference is always $\leq 0.9\text{V}$; therefore, part of the function of the PMP is to create electricity at higher voltages by passing current through a primary charge pump to a supercapacitor, to a secondary charge pump, and then on to lithium-ion batteries that are connected in series (Figure 1c; Schrader et al., 2016). The PMP microcontroller and an RS-232 buffer also draw energy from a small “micropower” charge pump that doubles the supercapacitor voltage and regulates it to 3.3 V. Other functions of the PMP are to trigger the powering and reading of sensors, run certain failsafe operations,

and time the storage of system data. The PMP electronics were uniquely designed for this application and are enclosed inside the acoustic modem housing. We have also customized the PMP software for nearly every deployment.

The acoustic modem, mounted at the center of the BeOb platform (Figure 1), serves as the instrument for data storage and recovery. The modem receives data from the PMP in daily reports configured by the user before deployment. Currently, the sensors onboard are read hourly, and the BMFC performance is assessed once daily by executing polarization tests (Logan et al., 2006) that indicate the power levels the BMFC can deliver as a function of load resistance. This information and the supercapacitor and battery voltages are items in each daily report. The modem must be prompted to transmit its stored data (nominally, we set the modem to transmit at 600 bits per second, and a one-day report = 1 kb) to a receiving modem located within a ~2 km radius. This range is constrained primarily by the power level of the transmitting modem, but it can be increased to ~5 km by using higher power levels and/or lower bit rates, and to ~20 km using repeater functionality.

For this study, we enlisted marine technician help and used shipboard 12 kHz systems on seven cruises of opportunity on four different research vessels to communicate with the Benthic Observer, and thus far have a partial 450-day-long record of recovered reports. The data retrieved illustrate that the BMFC is harvesting energy and keeping the supercapacitor and the batteries fully charged (Figure 2). This is in part because the energy being drawn to power the sensors and the PMP electronics is relatively small (~5 mW), and the more energy intensive acoustic communications (~2 W during data transmission) have been short and infrequent. To establish regular communications, other acoustic gateways would be needed, such as modems linked to nearby cabled observatories, moorings, or autonomous gliders that would then relay the

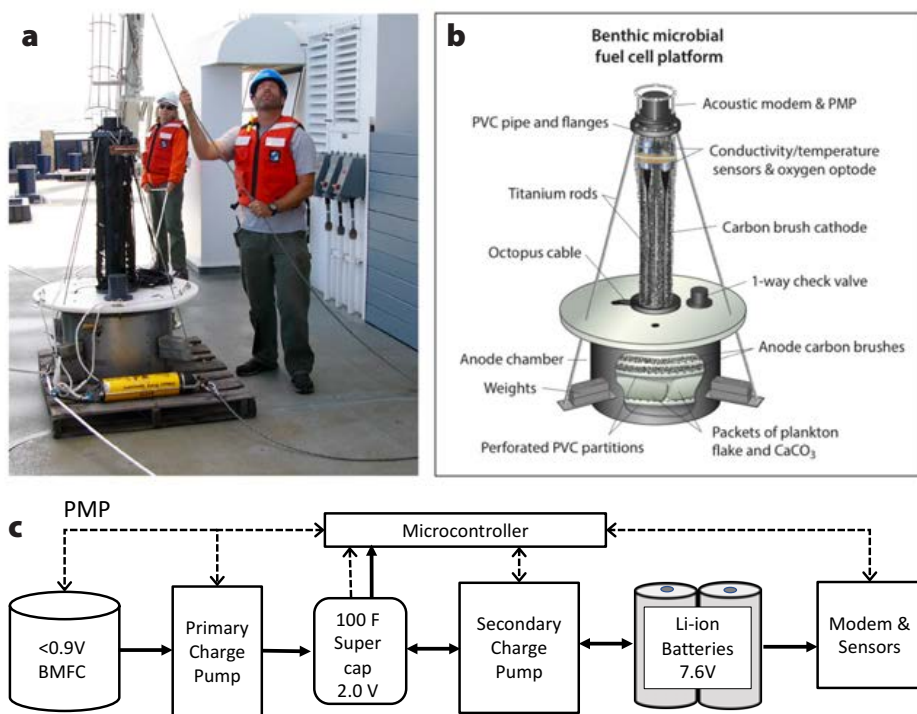


FIGURE 1. (a) The Benthic Observer platform is shown with an acoustic release before deployment in August 2016 as author C. Reimers and marine technician M. Durham (Scripps Institution of Oceanography) ready taglines and wire. (b) Components of the platform and its benthic microbial fuel cell (BMFC). (c) Schematic of the power management platform (PMP) electronics. Solid lines and arrows indicate the flow of energy. Dashed lines and arrows depict function controls and inputs from status components and sensors.

data ashore. The latter framework is envisioned should next generation Benthic Observers become integrated components of observing networks in the future. As indicated above, many other sensor configurations could be utilized on these platforms, provided their operation meets a realistic energy supply budget from the BMFC.

THE QUALITY OF BENTHIC OBSERVER SENSOR DATA FROM THE OREGON SLOPE

One of the conceptual advantages of the Benthic Observer is its ability to operate for many years unattended because it does not run out of battery power or need to be physically recovered to transfer data. Low-power sensors that can remain accurate and fully operational over the long term represent the remaining challenge for these systems. It is known from profiling float applications that many CTD sensors and oxygen sensors can maintain required (or at least correctable) accuracies in multiyear applications if they are operated mostly below the thermocline, in the dark, away from regions of enhanced biological growth (Riser et al., 2008; Takeshita et al., 2013). Following this example, we chose to mount a conductivity/temperature sensor (Aanderaa model 4319) and a dissolved oxygen/temperature sensing optode (Aanderaa model 4330) on the BeOb and to evaluate the data quality of these sensors by comparing them to similar sensors on the

OOI Oregon Slope Benthic Experiment Package (CE04OSBP) located ~1.6 km away and at the same depth (within a few meters). The BeOb optode was calibrated prior to deployment using air-saturated water and an anoxic solution of 1 M Na ascorbate and 0.5 M NaOH diluted to 10% with N₂-purged deionized water, but for the conductivity sensor we relied on the factory calibration. For comparison, the relevant OOI sensors are a Sea-Bird SBE 16plusV2 CTD and an Aanderaa model 4831 oxygen optode.

Focusing on a 90-day period where 94% of hourly measurements from the BeOb have been recovered acoustically thus far, we find that the mean, standard deviation, and range (maximum-minimum) of temperature data are nearly identical between platforms, but that

conductivity measurements from the BeOb appear systematically low, with spikes of extremely low readings probably due to contamination (biofouling or suspended sediment interference) of the unpumped Aanderaa conductivity cell (Table 1, Figure 3). Much better agreement (means within 0.005 S m⁻¹ equivalent to within 0.06 PSU) occurs in comparisons of conductivity records measured during the first month after BeOb deployment (data shown in Reimers et al., 2017b). No OOI oxygen data are shown in Figure 3c because of a faulty factory calibration of the CE04OSBP optode that gave erroneous concentrations that remain in the OOI database. We do note, however, that after this OOI sensor was replaced with a properly calibrated version on August 10, 2017, the dissolved oxygen at CE04OSBP

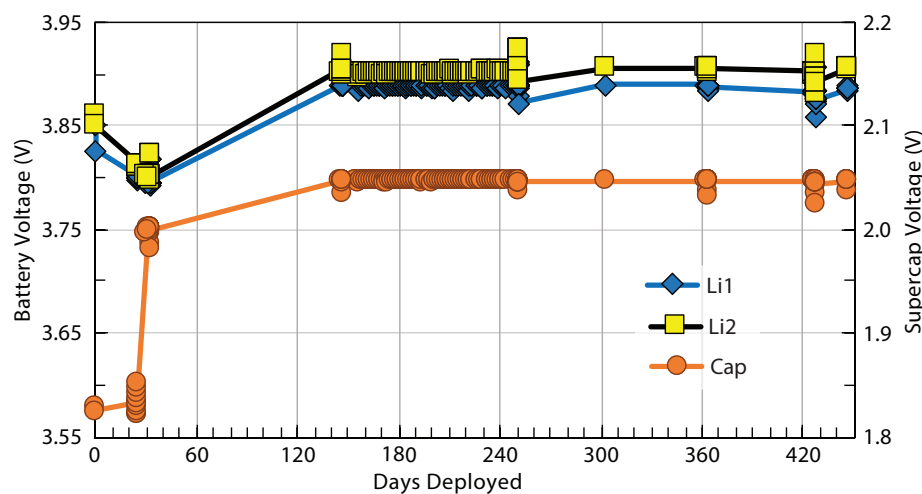


FIGURE 2. Benthic Observer battery and supercapacitor voltages measured in situ through time.

TABLE 1. Comparison of sensor data between the Benthic Observer (BeOb) and the Ocean Observatories Initiative (OOI) over a 90-day period. The mean pressure at the OOI measurement location during this period was 586 dbar.

Sensor	Number of Measurements	Mean	Standard Deviation	Variance	Autocorrelation Coefficient*	Range of Observations
BeOb temperature 1 (optode sensor)	2,031	4.9719°C	0.173	0.0299	0.9503	1.05
BeOb temperature 2 (cond. sensor)	2,031	4.9674°C	0.173	0.0298	0.9471	1.07
OOI temperature	7,626,513	5.0295°C	0.167	0.0280	1.0000	1.0299
BeOb conductivity	2,033	3.2661 S m ⁻¹	0.0226	0.00051	0.9194	0.203
OOI conductivity	7,626,513	3.2963 S m ⁻¹	0.0136	0.00018	0.9999	0.3909
BeOb oxygen ¹	2,033	11.16 (10.96) µmol L ⁻¹	2.75 (2.70)	7.54 (7.26)	0.9100	19.35 (19)

¹ With (and without) pressure correction

² This parameter is derived from the correlation of a time series against a lagged (one sample) version of itself and is influenced by sample frequency and the amount of random noise in the measurements (Box et al., 2015).

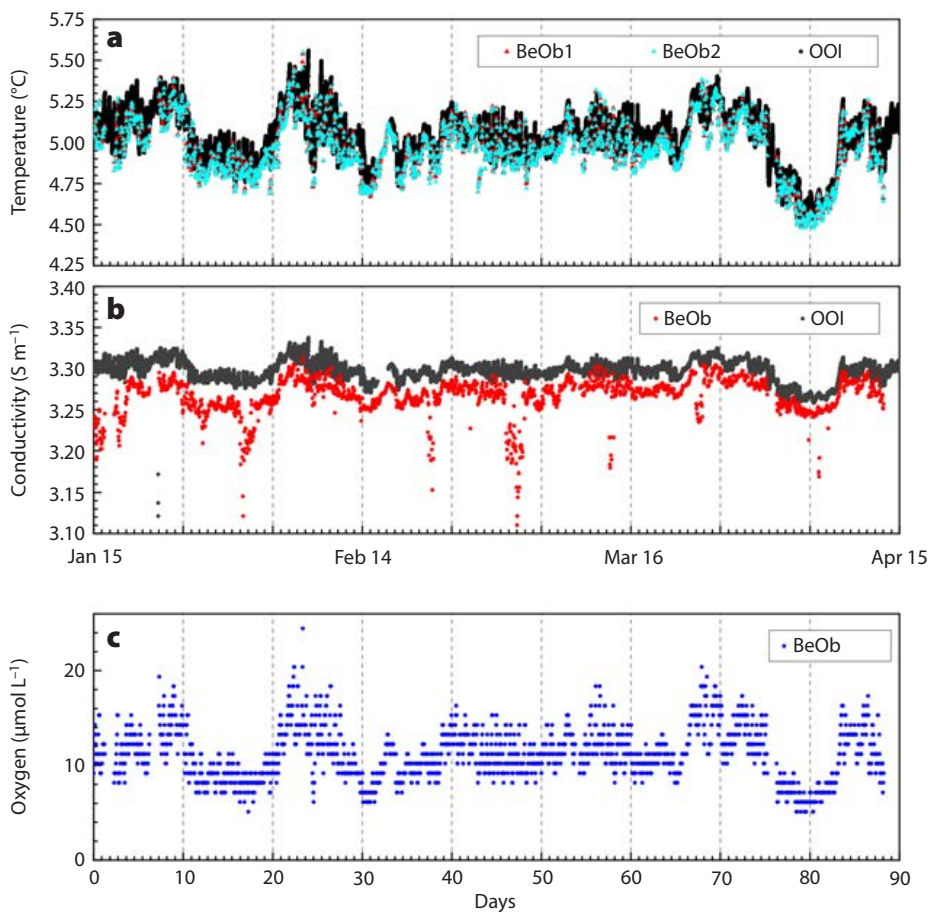


FIGURE 3. Comparative sensor data from the Benthic Observer and the OOI Oregon Slope Benthic Experiment Package (CE04OSBP). These time series were measured from January 15, 2017, to April 15, 2017, which was 154–244 days after the Benthic Observer deployment on the seafloor. OOI temperature and conductivity data are reduced to from 1 Hz to 1-minute averages in plots (a) and (b). No properly calibrated oxygen data were available from the OOI database to include in (c).

has been reported between $12 \mu\text{mol L}^{-1}$ and $38 \mu\text{mol L}^{-1}$, with similar periodicity to Figure 3c (data spanning August 10 to November 20, 2017). These OOI sensor values are generally $5\text{--}10 \mu\text{mol L}^{-1}$ higher than BeOb sensor records from both before and after August 10. Thus, there appears to be a calibration offset between the two sensors.

The oscillations in the time series of temperature, conductivity, and oxygen are interesting because they reveal semidiurnal (M2) frequencies of variation as well as two- to seven-day weatherband variations of considerable range that are highly correlated. Some of the oscillation in the BeOb oxygen record is obscured by a $\pm 1 \mu\text{mol L}^{-1}$ resolution of the optode output, but this can be improved in future experiments by simply enabling a

higher-resolution readout.

If a researcher's goal is to detect trends in ocean time series data that could signal an oceanic response to climate change, one might ask: are the Benthic Observer data reliable and frequent enough to support statistically robust analyses? This question takes on added significance in light of several studies that suggest declines in dissolved oxygen in midwater OMZs may be signaling reduced water column ventilation coupled to enhanced stratification and ocean warming over decadal timescales (Keeling et al., 2010; Helm et al., 2011; Falkowski et al., 2011; Pierce et al., 2012). To detect such trends, researchers will commonly apply generalized least squares regressions to a time series spanning several decades, or they will apply rank-based non-parametric

statistical tests to the available environmental data that may be first reduced to seasonal or annual means (Weatherhead et al., 1998; Yue et al., 2002). Without diving too deeply into the details of these tests or their pitfalls, we note that data sets without gaps or sudden shifts created by changes in instrumentation are the most useful, and the number of years of data necessary to detect trends with confidence will decrease in records with less-random noise (Weatherhead et al., 1998; Henson et al., 2016).

Table 1 suggests that the much smaller sample size of the BeOb time series compared to OOI data does not greatly alter the temporal realism of observed temperature, but that we do need to improve the quality of the direct measurement of conductivity, perhaps by switching to sensors in a pulsed-duty pumped cell and/or applying biocides to prohibit contamination, as is done routinely on Argo floats (Riser et al., 2008). A low duty cycle pump run, for example, for two seconds every hour does not add up to a significant amount of added power consumption and may help improve the long-term accuracy of inline oxygen measurements as well. With this field-based insight, we envision that the next-generation version of the Benthic Observer will be equipped with a complete pulse-pumped CTD unit and an oxygen optode to allow tracking of more highly resolved changes in oxygen at fixed points in the benthic boundary layer. Accurate CTD-O₂ time series would also allow the identification of dissolved oxygen changes on discrete potential density surfaces.

The acoustic modems of these systems are designed to support communications between platforms deployed as a network, and thus in another few years BeOb systems could be distributed throughout the full expanse of OMZs where these midwater column zones intersect the continental slope. As functioning members of ocean observing projects, future BeOb platforms would provide more spatial coverage, and could transmit data to a variety of gateways including gliders

and cable nodes. These BeOb platforms might also be modified to expedite regular recoveries, every two to three years, presumably by remotely operated vehicles. Although the BMFC technology can keep the power on, eventually biofouling and corrosion are expected to win the day, necessitating recovery, sensor recalibration, and servicing. The relative cost of these autonomous systems would still be low (the principal expense is ~\$25,000, stemming from the sensors and the acoustic modem), and they are adaptable to support nearly any form of low-power sensor with a serial output. 

REFERENCES

- Box, G.E.P., G.M. Jenkins, G.C. Reinsel, and G.M. Ljung. 2015. *Time Series Analysis: Forecasting and Control*, 5th ed., Wiley, 712 pp.
- Falkowski, P., T. Algeo, L. Codispoti, C. Deutsch, S. Emerson, B. Hales, R. Huey, W. Jenkins, L. Kump, L. Levin, and others. 2011. Ocean deoxygenation: Past, present, and future. *Eos* 92:409–420, <https://doi.org/10.1029/2011EO460001>.
- Helm, K., N. Bindoff, and J. Church. 2011. Observed decreases in oxygen content of the global ocean. *Geophysical Research Letters* 38, L23602, <https://doi.org/10.1029/2011GL049513>.
- Henson, S.A., C. Beaulieu, and R. Lampitt. 2016. Observing climate change trends in ocean biogeochemistry: When and where. *Global Change Biology* 22:1,561–1,571, <https://doi.org/10.1111/gcb.13152>.
- Keeling, R.F., A. Körtzinger, and N. Gruber. 2010. Ocean deoxygenation in a warming world. *Annual Review of Marine Science* 2:199–229, <https://doi.org/10.1146/annurev.marine.010908.163855>.
- Logan, B., B. Hamelers, R. Rozendal, U. Schröder, J. Keller, S. Freguia, P. Aelterman, W. Verstraete, and K. Rabaey. 2006. Microbial fuel cells: Methodology and technology. *Environmental Science & Technology* 40:5,181–5,192, <https://doi.org/10.1021/es0605016>.
- Pierce, S., J. Barth, R. Shearman, and A. Erofeev. 2012. Declining oxygen in the Northeast Pacific. *Journal of Physical Oceanography* 42:495–501, <https://doi.org/10.1175/JPO-D-11-0170.1>.
- Reimers, C.E. 2015. Applications of bioelectrochemical energy harvesting in the marine environment. Pp. 345–366 in *Biofilms in Bioelectrochemical Systems: From Laboratory Practice to Data Interpretation*. H. Beyenal and J.T. Babauta, eds., Elsevier, <https://doi.org/10.1002/9781119097426.ch10>.
- Reimers, C.E., C. Li, M.F. Graw, P.S. Schrader, and M. Wolf. 2017a. The identification of cable bacteria attached to the anode of a benthic microbial fuel cell: Evidence of long distance extracellular electron transport to electrodes. *Frontiers in Microbiology* 8:2055, <https://doi.org/10.3389/fmicb.2017.02055>.
- Reimers, C.E., P.S. Schrader, and M. Wolf. 2017b. Autonomous sensors powered by a benthic microbial fuel cell provide long-term monitoring of the Northeast Pacific oxygen minimum zone. *Proceedings of Oceans'17*, June 19–22, 2017, MTS/IEEE Aberdeen, UK, <https://doi.org/10.1109/OCEANSE.2017.8084602>.
- Riser, S.C., L. Ren, and A. Wong. 2008. Salinity in Argo: A modern view of a changing ocean. *Oceanography* 21(1):56–67, <https://doi.org/10.5670/oceanog.2008.67>.
- Schrader, P.S., C.E. Reimers, P. Girguis, J. Delaney, C. Doolan, M. Wolf, and D. Green. 2016. Independent benthic microbial fuel cells powering sensors and acoustic communications with the MARS underwater observatory. *Journal of Atmospheric and Oceanic Technology* 33:607–617, <https://doi.org/10.1175/JTECH-D-15-0102.1>.
- Takesita, Y., T.R. Martz, K.S. Johnson, J.N. Plant, D. Gilbert, S.C. Riser, C. Neill, and B. Tilbrook. 2013. A climatology-based quality control procedure for profiling float oxygen data. *Journal of Geophysical Research* 118:5,640–5,650, <https://doi.org/10.1002/jgrc.20399>.
- Tender, L.M., C.E. Reimers, H.A. Stecher III, D.E. Holmes, D.R. Bond, D.R. Lovley, D.A. Lowry, K. Pilobello, and S. Fertig. 2002. Harnessing microbially generated power on the seafloor. *Nature Biotechnology* 20:821–825, <https://doi.org/10.1038/nbt716>.
- Weatherhead, E.C., G.C. Reinsel, G.C. Tiao, X-L. Meng, D. Choi, W-K. Cheang, T. Keller, J. DeLuisi, D.J. Wuebbles, J.B. Kerr, and others. 1998. Factors affecting the detection of trends: Statistical considerations and applications to environmental data. *Journal of Geophysical Research* 103:17,149–17,161, <https://doi.org/10.1029/98JD00995>.
- Yue, S., P. Pilon, and G. Cavadias. 2002. Power of Mann-Kendall and Spearman's rho tests for detecting monotonic trends in hydrological series. *Journal of Hydrology* 259:254–271, [https://doi.org/10.1016/S0022-1694\(01\)00594-7](https://doi.org/10.1016/S0022-1694(01)00594-7).

ACKNOWLEDGMENTS

This research and development has been steadfastly supported by the US Office of Naval Research. We thank Paul Schrader for helping to assemble the Benthic Observer, and Jon Fram, Skip Denny, and Deb Kelley for coordination with the OOI. We also thank the resident technicians, scientists, crew and officers on R/V *Sally Ride* during its transit cruise from the shipyard in August 2016 for assisting with the Benthic Observer deployment.

AUTHORS

Clare E. Reimers (creimers@coas.oregonstate.edu) is Professor, College of Earth, Ocean, and Atmospheric Sciences, Oregon State University, Corvallis, OR, USA. **Michael Wolf** is an engineer at Teledyne Benthos, North Falmouth, MA, USA.

ARTICLE CITATION

Reimers, C.E., and M. Wolf. 2018. Power from benthic microbial fuel cells drives autonomous sensors and acoustic modems. *Oceanography* 31(1):98–103, <https://doi.org/10.5670/oceanog.2018.115>.

The Role of the Ocean Observatories Initiative in Monitoring the Offshore Earthquake Activity of the Cascadia Subduction Zone

By Anne M. Tréhu, William S.D. Wilcock, Rose Hilmo, Paul Bodin,
Jon Connolly, Emily C. Roland, and Jochen Braunmiller



Photo taken aboard R/V *Oceanus*
during cruise OC1205A, May 2012.
Photo credit: Daniel Zietlow

ABSTRACT. Geological and historical data indicate that the Cascadia subduction zone last ruptured in a major earthquake in 1700. The timing of the next event is currently impossible to predict, but recent studies of several large subduction zone earthquakes provide tantalizing hints of precursory activity. The seismometers at the Ocean Observatories Initiative (OOI) Slope Base and Southern Hydrate Ridge nodes are well placed to provide new insights into interplate coupling because they are located over a segment of the subduction zone that is nominally locked but that has been relatively active for more than a decade. Since their installation in 2014, 18 earthquakes with magnitudes up to 3.8 have been located by the Pacific Northwest Seismic Network between 44°N and 45°N in the region of the plate boundary thought to be accumulating strain. The OOI seismometers have also detected events that were not reported by the onshore seismic network. Noting that OOI data are available in real time, which is a necessary criterion for routine earthquake monitoring, and that the OOI seismometers generally have lower noise levels than campaign-style ocean bottom seismometers, there would be significant benefit to adding seismometers to existing nodes that are not yet instrumented with seismometers.

INTRODUCTION

The largest and some of the most damaging earthquakes in history have occurred in subduction zones, where one plate plunges beneath another plate. At the Cascadia subduction zone (Figure 1), which extends from northern California to Vancouver Island, the Juan de Fuca Plate is being subducted beneath the North American Plate. In several respects, Cascadia is an end member in the global spectrum of subduction zones (Wang and Tréhu, 2016). Because of the young age of the subducting plate (<15 million years), a relatively slow convergence rate (3–4 cm yr⁻¹), and abundant sediment supply that blankets subducting oceanic crust, the Cascadia plate boundary fault is hotter than most subduction megathrusts. It is also unusually free of recent earthquake activity (Figure 1).

Despite the low level of current earthquake activity, there is evidence for large (magnitude >8) historic and prehistoric earthquakes on the Cascadia megathrust. Tsunami records in Japan, coastal subsidence, and oral histories indicate there was a magnitude 8.7–9.2 earthquake at the Cascadia subduction zone on January 29, 1700 (Atwater et al., 2015). Onshore and offshore paleoseismic data indicate the occurrence of 20 large earthquakes in the past 10,000 years, with inter-event times ranging from 200 years to 1,200 years (Goldfinger et al., 2012).

The paucity of recent earthquakes can mean that the two plates are slipping past each other without generating earthquakes or that they are firmly locked together, storing elastic strain that will be released in a future large earthquake, or some combination thereof. Thermal models (e.g., Hyndman and Wang, 1993;

Cozzens and Spinelli, 2012) have been used to predict the boundary between the seismogenic zone, where the plates are cold and may be locked (temperature <350–450°C), and a deeper zone of “episodic tremor and slip” (ETS), characterized by slow slip observed in GPS data accompanied by seismic tremor (Rogers and Dragert, 2003). Figure 1 shows the position of the 450°C isotherm (short dashed line) and the updip position of ETS (short/long dashed line), which are approximately coincident and may indicate the downdip limit of seismogenic slip in major subduction zone earthquakes (Hyndman, 2013; Wang and Tréhu, 2016). Note that the Cascadia seismogenic zone lies almost entirely offshore.

Global plate models (e.g., DeMets et al., 2010) predict that ~8 m of slip perpendicular to the margin has accumulated off central Oregon since 1700. This slip deficit is large enough to generate a magnitude 8 or larger earthquake if it is released through sudden slip on the shallow (offshore) plate

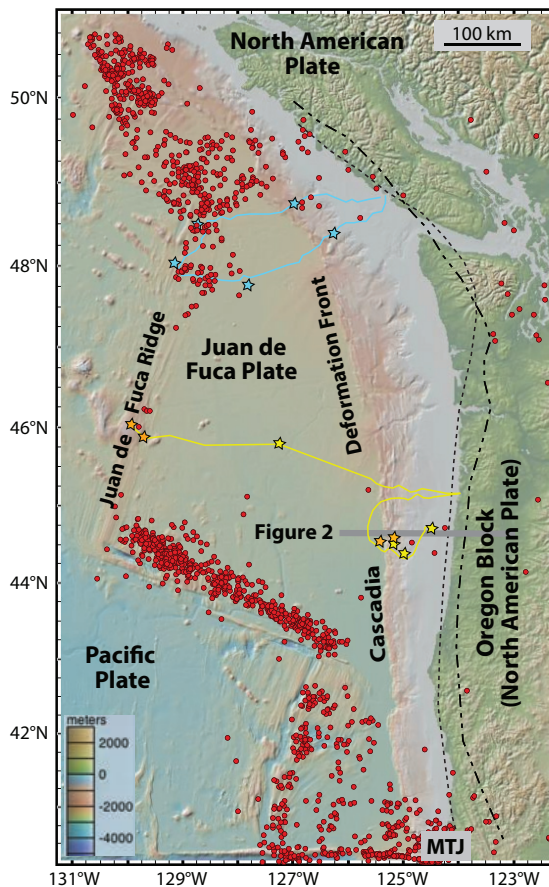


FIGURE 1. Topographic map of the US Pacific Northwest using data from the Global Multi-Resolution Topographic database accessed via GeoMapApp (<http://www.geomapapp.org>). Earthquakes with magnitudes ≥ 4 from January 1989 through August 2017 in the Advanced National Seismic System (ANSS) Comprehensive Earthquake Catalog (<https://earthquake.usgs.gov/data/comcat>) are shown as red dots. The surface trace of the boundary between the Juan de Fuca and North American Plates coincides with the abrupt deformation front seen in the topography of the continental margin. The short dashed line is the 450°C contour, the short/long dashed line is the updip limit of tremor from 2005 to 2011, and the dark gray line is the location of the cross section in Figure 2. The yellow line shows the OOI cable route. Stars show nodes with (orange) and without (yellow) seismometers. Blue lines and stars show the NEPTUNE cabled observatory.

boundary (Tréhu, 2016). To evaluate the seismic hazard in Cascadia, it is important to understand how much of the potential slip is being stored, to be released in a future great subduction zone earthquake, and how much is being accommodated through aseismic slip and small earthquakes on the plate boundary or by internal deformation of the Juan de Fuca and North American Plates. Developing this understanding requires knowledge of where offshore earthquakes occur. Moreover, recent results from subduction zone earthquakes elsewhere show that at least some earthquakes are preceded by distinctive foreshock activity and/or slow slip within the seismogenic zone (e.g., Bouchon et al., 2013; Ito et al., 2013; Burgmann, 2014). As these precursory patterns become better documented and modeled, their value for earthquake forecasting should increase.

The objective of this paper is to determine the value of seismometers located at the Ocean Observatories Initiative (OOI) Slope Base (SB) and Southern Hydrate Ridge (SHR) nodes to the detection and location of earthquakes on the Cascadia margin. Through coincidence, the OOI SB-SHR network is located near an anomalous segment of the margin that

has been the site of persistent seismicity in the magnitude 2–5 range since at least 1989 (Tréhu et al., 2015). Between November 4, 2014, when data from the OOI SB-SHR network became available through the IRIS Data Management Center, and September 30, 2017, 18 earthquakes with magnitudes up to 3.8 were reported by the Pacific Northwest Seismic Network (PNSN) between 44°N and 45°N and 125.5°W and 124°W. In addition, from November 2014 to October 2015, the Cascadia Initiative ocean bottom seismometer (OBS) network (Toomey et al., 2014) operated simultaneously with the OOI SB-SHR network, providing the opportunity to compare signal-to-noise ratios and evaluate the impact of potential expansion of the OOI seismic network.

BACKGROUND

The Challenge of Recording Seismic Waves Offshore

Earthquakes radiate seismic energy across a range of frequencies, with larger earthquakes generating relatively more low-frequency energy. The seismic waves are recorded using sensors that typically record three orthogonal components of ground motion. Development of portable broadband sensors in the 1980s greatly

expanded the ability of onshore seismologists to record seismic waves at many locations and across a wide frequency band, improving their ability to resolve Earth structure and earthquake source processes. Expansion of this capability to the ocean has been difficult because of the exceptionally low shear strength of marine sediments and the high noise levels generated by nonlinear interactions and direct effects of ocean waves (e.g., Webb, 1998). Moreover, conventional OBS designs include power, buoyancy, timing control, and data recording in a single package. The resulting bulky package is more susceptible to narrow-band frequency resonances and is more attractive to seafloor fauna, which disturb the instrument, generating signals, termed “bio-bumps,” that can obscure local earthquakes. Many of these noise sources are potentially mitigated by OOI sensors because on the Cascadia margin they are buried in seafloor sediments and separated from the power and recording hardware.

The Challenge of Locating Offshore Earthquakes

An earthquake is located by determining the arrival times of the seismic waves it generates on a network of seismometers. Accurate determination of source latitude and longitude requires a good azimuthal distribution of seismic stations around an earthquake and knowledge of the velocity with which seismic waves travel through the rocks from the source to the receiver. Both requirements are problematic when only onshore data are available to locate small earthquakes on the shallow part of subduction zone plate boundaries, which are generally offshore. Moreover, the crustal thickness and velocity structure change dramatically across the continent-ocean margin (Figure 2), which is generally not taken into account for routine earthquake monitoring.

To interpret the tectonic implications of earthquakes, it is important to determine their depth. A general rule of thumb for resolving depth from observed travel

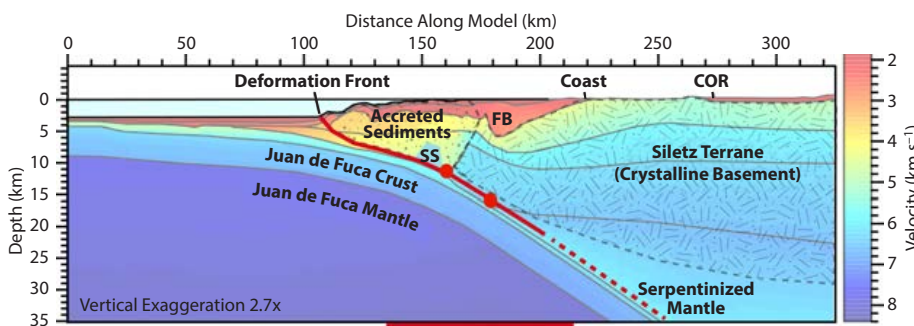


FIGURE 2. Interpreted cross section through the Cascadia subduction zone near latitude 44.65°N. The velocity model of Gerdemann et al. (2000) is overlaid by a geologic interpretation. The red line represents the plate boundary (dashed where the modeled plate boundary temperature is >450°C). Red dots indicate the projected positions of the two magnitude 4.7–4.8 earthquakes of 2004. The projected position of a subducted seamount (SS) based on magnetic anomaly data is also shown (Figure 3A). The basement rocks of the upper plate in this region are formed by mafic rocks of the Siletz terrane, anomalously thick oceanic crust that was accreted to North America ~50 million years ago and that is slowly moving northward and rotating relative to the core of North America, effectively acting as a microplate known as the Oregon Block (McCaffrey et al., 2007). Seaward of the Siletz terrane, the upper plate is composed of folded and faulted accreted sediments and slope sediments captured in basins formed through deformation and uplift of the margin. The seaward edge of the Siletz terrane is overlain by a forearc basin (FB). The red bar along the base of the figure indicates the region shown in Figure 4.

times is that the horizontal distance to the closest station should not exceed the depth. This condition is nearly always violated when land stations record offshore events. Offshore seismic stations are required to locate earthquake epicenters accurately, obtain better estimates of source depth, and decrease the earthquake detection threshold. Although conventional OBSs (from which data are downloaded when the instrument is recovered) can be used to revise depth estimates post facto, real-time data are needed for routine earthquake monitoring.

Recent Seismicity on the Central Oregon Margin

Figure 3A shows a map of all earthquakes from January 1, 1989, through September 3, 2017, with magnitudes ≥ 3 between 43.5°N and 45.5°N and 126°W and 123°W . The data are from the US Geological Survey Advanced National Seismic System-Comprehensive Earthquake Catalog (ANSS-ComCat; see Figure 1 caption), which includes events reported by the PNSN and other regional

networks. While earthquakes are scattered throughout this region, most seismicity has occurred in clusters labeled N, S_A, and S_B. The largest event in these clusters was a magnitude 4.8 earthquake in cluster S_A in July 2004 and a magnitude 4.7 earthquake in cluster N in August 2004 (Tréhu et al., 2008). These two events were large enough to generate low-frequency energy within the noise notch (see below), permitting determination of the source mechanism and depth through moment tensor inversion of the waveforms recorded by regional seismic networks. From moment tensor inversion, with additional support from travel-time analysis of secondary seismic phases (pP, PmP, and SmS) observed on distant and regional seismic stations, Tréhu et al. (2008) concluded that these were low-angle thrust earthquakes that occurred on or near the plate boundary.

When smaller earthquakes in these clusters are relocated (Tréhu et al., 2015, and references therein), either by determining their depth relative to the two larger earthquakes or by including OBS

data when available, they define a surface dipping about 12° to the east (Figure 4), corresponding to the plate boundary identified in previous controlled source imaging experiments (Figure 2). This activity may result from grinding of a buried seamount against the seaward edge of crystalline basement (labeled “Siletz terrane” in Figure 2). Cluster S_B was first identified as being distinct from S_A when four nearly identical earthquakes with magnitudes of 2.8–3.4 occurred on January 25, 2013. The three clusters continue to produce earthquakes large enough to be detected by the onshore network at a rate of about six events per year.

In map view, earthquake locations obtained through these detailed studies are similar to those obtained through PNSN analyses, although the clusters are better defined. The earthquake depths and their relationship to the plate boundary structure, however, are significantly affected by the lack of offshore stations and by the simplified velocity models used in routine PNSN analysis (Figure 4).

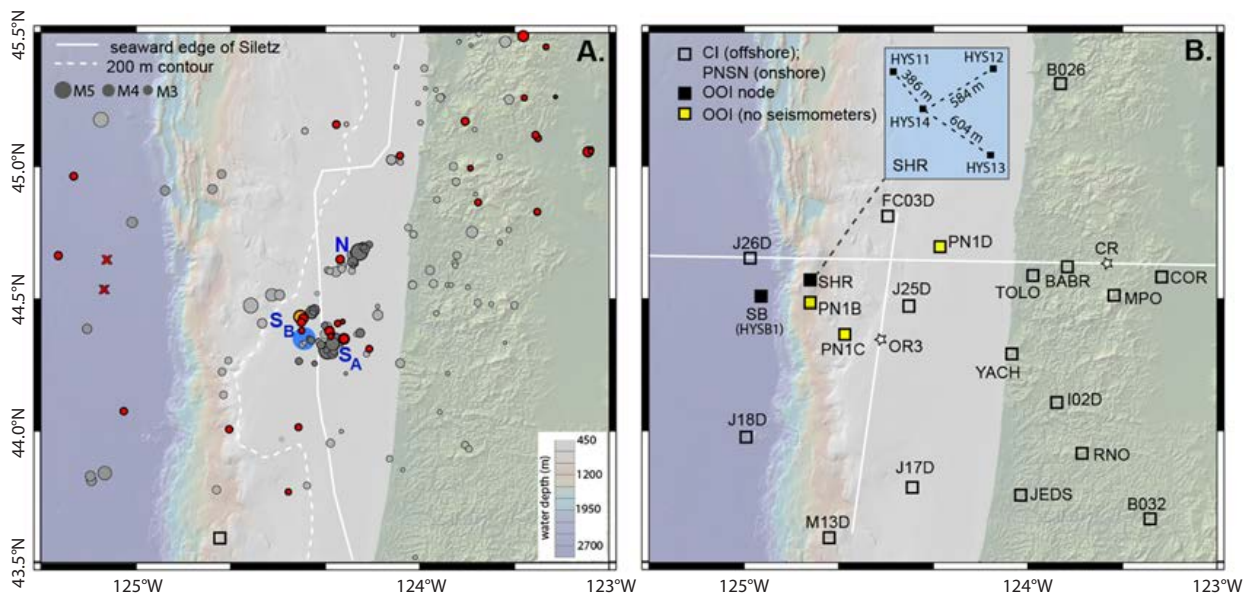


FIGURE 3. (A) Seismicity in the central Cascadia subduction zone. Dark gray circles mark earthquakes relocated as discussed by Tréhu et al. (2015); light gray circles are epicenters from the Pacific Northwest Seismic Network (PNSN) catalog prior to 2015 that have not been relocated; red dots denote earthquakes reported by PNSN from January 2015 through September 2017. Dot sizes are proportional to magnitude. N, S_A, and S_B indicate clusters of seismicity discussed in the text. The blue circle marks a subducted seamount inferred based on magnetic anomaly data (Tréhu et al., 2015). (B) Ocean Observatory Initiative (OOI) nodes and Cascadia Initiative (CI) and PNSN seismic stations used for this study. The inset shows the configuration of the four-station OOI array at Southern Hydrate Ridge (SHR); those labeled HYS11–13 are short period seismometers, and HYS14 is a broadband seismometer. Broadband seismometer HYSB1 is at node Slope Base (SB). White lines show the locations of two-dimensional velocity models discussed by Gerdemann et al. (2000); stars locate one-dimensional velocity models used in this study. Velocity models are shown in Supplementary Figure S5.

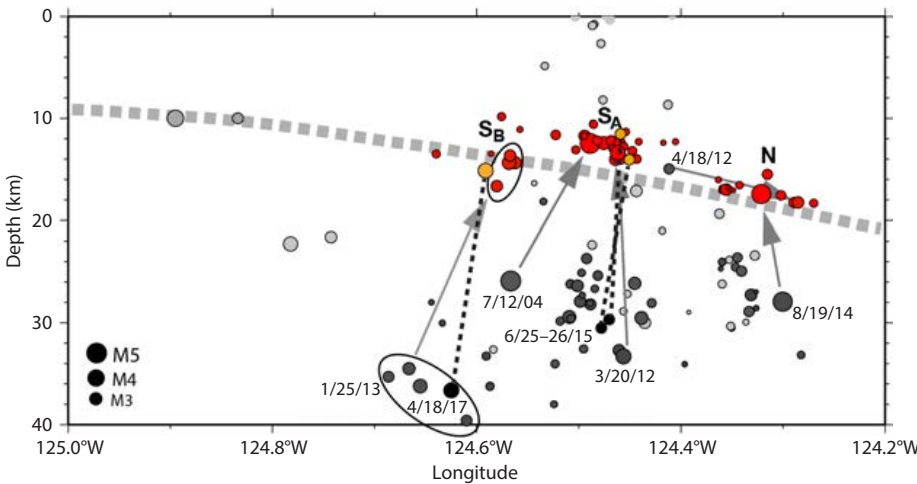


FIGURE 4. Cross section showing earthquake depths compared to the plate boundary in Figure 2. Circle radius is proportional to magnitude. Events in red were relocated by Tréhu et al. (2015); dark gray circles show PNSN locations for these events. Light gray circles are catalog events that were not relocated either because they were too small or they occurred prior to 2000 when there were too few stations (e.g., larger events west of 124.8°W). Relocations done for this study are in orange. Clusters labeled N, S_A, and S_B are discussed in the text and shown in map view in Figure 3A. Gray arrows (from Tréhu et al., 2015) and dashed lines (this study) illustrate relocated depths for selected events.

RESULTS OF NEW ANALYSES ENABLED BY THE OOI SEISMOMETERS

To examine the impact of including OOI stations in routine operations and the potential of augmenting the offshore array by instrumenting additional existing OOI nodes with seismometers, we compare OOI and OBS noise levels and look at three “case studies” of earthquakes occurring since 2014. Figure 3B shows the locations of OOI nodes, Cascadia Initiative OBSs, land seismic stations, and velocity models used in this study.

Noise Levels

Considerable effort has been devoted to understanding the characteristics of seismic noise in the ocean to improve recordings of teleseismic earthquakes on broadband OBSs (Webb, 1998). Broadband seismometers are best deployed in boreholes (Montagner et al., 1994; Collins et al., 2001), but where they are not available, shallow burial is preferred to emplacement on the seafloor because it ensures good ground coupling and shields the seismometer from ocean currents.

All seismic stations of the SB-SHR network are buried. The broadband stations

at SHR and SB were placed beneath the seafloor following an approach described by Romanowicz et al. (2003). A section of PVC pipe was inserted into the sediments to form a caisson, the sediments were evacuated from inside, the seismic sensor was enclosed in a spherical housing and placed at the bottom of the caisson so as not to touch the walls (online Supplementary Figure S1), and the caisson was covered with glass beads flush with the seafloor. The three short-period sensors at SHR are contained in narrow titanium cylinders that were buried by inserting them into a groove gouged by the arm of a remotely operated vehicle (Supplementary Figure S2); the groove was then filled with glass beads.

Figure 5A compares noise power spectra from the vertical channel of the two OOI broadband seismometers with those from a station located 20 km inland (BABR) and from three autonomous seafloor OBSs from the Cascadia Initiative experiment. From 0.1 Hz to 3 Hz, the noise spectra are dominated by microseism peaks, which have higher amplitudes at the seafloor stations compared to the land station because they are generated by nonlinear interactions of ocean

waves (Webb, 1998). At frequencies immediately below the microseism peak, there is a low-noise notch on all stations except for J25C. This is the signal band used for inversion of waveform data to obtain moment tensor estimates. At the seafloor stations, the noise level increases at lower frequencies because the pressure perturbations from infragravity waves (long-wavelength ocean waves) reach the seafloor. In shallow water, the infragravity wave noise extends to higher frequencies and impinges on, and in the case of station J25C eliminates, the low-noise notch. Processing techniques can remove this noise from the vertical channel using data from the horizontal channels or a coincident seafloor pressure sensor (e.g., Crawford and Webb, 2000).

From 3 Hz to 20 Hz, the noise levels onshore and at three of the five seafloor stations, including the two OOI stations, are remarkably similar (Figure 5A). This signal band is needed to pick travel times of P- and S-waves from local earthquakes. Figure 5B shows noise levels at 5 Hz recorded by Cascadia Initiative and OOI seismometers as a function of water depth. For the Cascadia Initiative OBSs, the noise levels are quite scattered, but increase markedly at shallower depths. This likely reflects poor coupling of the sensors to the seafloor, noise induced by components of the OBS package in the presence of strong ocean currents, and frequent impulsive signals due to biological activity, which can number in the thousands per day at water depths <500 m (Williams et al., 2010). Burying the seismometers, as was done for the OOI instruments, shields the sensors from currents and fauna, leading to lower noise levels at higher frequencies.

Modeling the Impact of Offshore Stations on Detection Levels Using Site-Specific Noise Characteristics

Figure 6 shows the results of applying the method of McNamara et al. (2016) to develop a series of magnitude detection threshold maps for different seismic

network configurations by combining site-specific spectral noise characteristics with simple earthquake source and wave propagation models. If the ground motion at a station from a model earthquake exceeds the noise model at any frequency, we infer that the station detects the earthquake. Detections at four stations result in a network detection and hence a locatable earthquake. To investigate potential improvements in detection capability that might result from adding offshore stations to the current onshore seismic network, we used modal noise profiles derived from OOI and Cascadia Initiative stations, which represent the most likely noise levels at hypothetical sites. We also use modal noise values for PNSN onshore stations.

These maps represent a best-case scenario because a signal just above noise does not guarantee an automatic detection; in practice, signal must exceed noise by some (difficult to quantify) amount. However, the method is consistent and objective, and thus useful for comparing network detection performance. Figure 6A shows the detection threshold from the onshore seismometers and current OOI SB-SHR and Axial Seamount (see Wilcock et al., 2018, in this issue) networks using noise profiles computed for a randomly selected month. The detection threshold is very low onshore and shows how clusters of

stations can further reduce the detection threshold locally in regions of particular interest. Offshore, the detection threshold increases smoothly with increasing distance from the network, with locally lower-magnitude detection thresholds in

the immediate vicinity of the OOI networks. Figure 6B shows how an ambitious offshore network of buried seismometers would impact the detection threshold, assuming noise levels characteristic of OOI sites and a station distribution

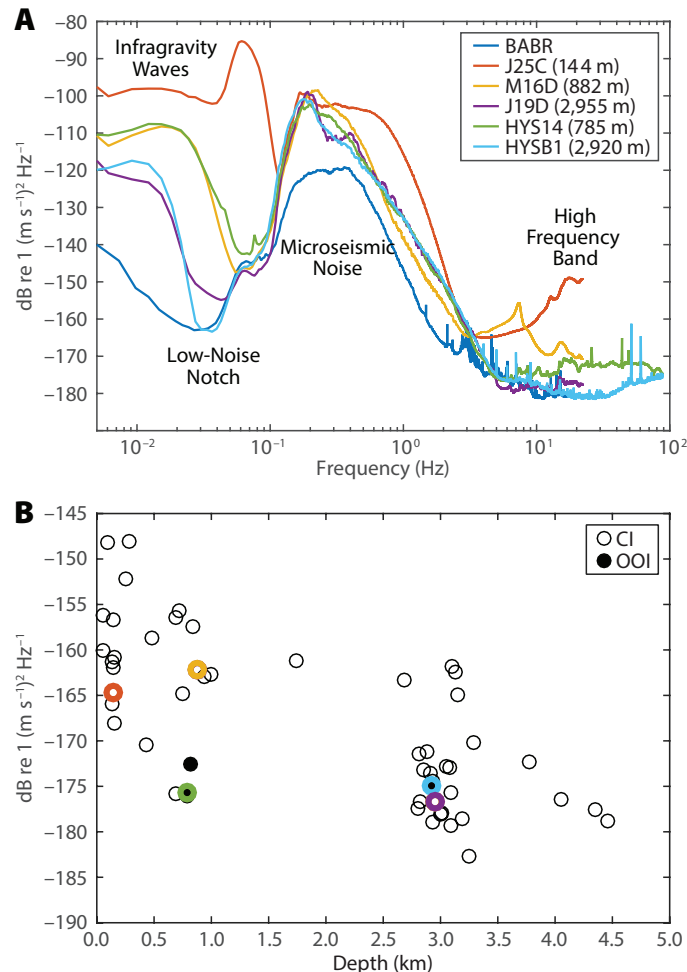


FIGURE 5. (A) Velocity power spectra for background noise on the vertical broadband channels of selected PNSN (BABR, CI (J25C, J19D, M16D), and OOI (HYS14, HYSB1) sites, with water depths indicated. Spectra were calculated with one-hour data windows over one year; median values are plotted. (B) Median noise levels at 5 Hz as a function of instrument depth for all Cascadia Initiative OBSs deployed in 2014–2015 and for the OOI stations. Color corresponds to sites shown in (A).

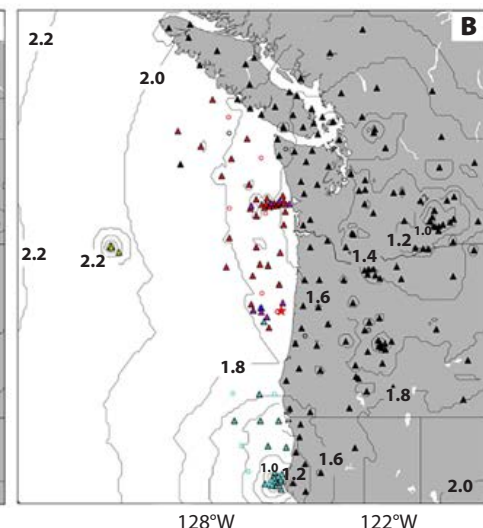
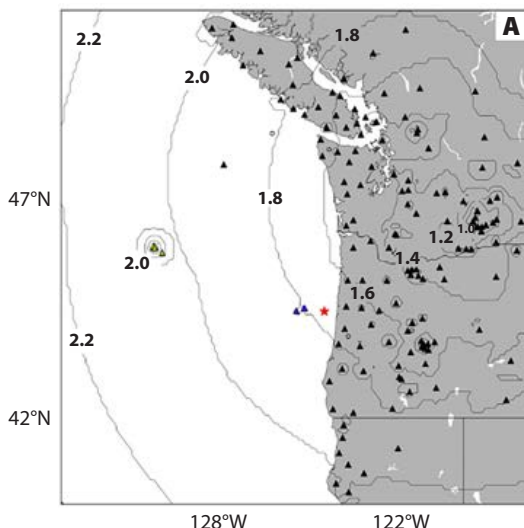


FIGURE 6. (A) Magnitude detection threshold in Cascadia using existing onshore stations and offshore cabled seismometers (OOI and NEPTUNE networks). Contours show the minimum magnitude that would be detected by at least four stations (see text for details). Black triangles are onshore seismic stations. Circles are stations that did not contribute to any of the four detections used to determine the threshold. The red star marks the approximate location of interplate earthquakes (Figure 3A). (B) As for (A), but with stations added at additional existing OOI nodes (violet triangles) and at Cascadia Initiative OBS locations along the margin in 2012 (red triangles) and 2013 (cyan triangles).

similar to the Cascadia Initiative network along the Cascadia subduction margin.

This exercise indicates that improvement in the detection threshold for offshore earthquakes along the continental margin is decreased, although a significant decrease in the magnitude detection threshold would require a large investment. However, it is important to note that this analysis considered only detectability. The impact of offshore stations on the resolution of earthquake source depth, a parameter that is important for understanding the tectonic and hazard implications of seismicity, is discussed in the next section. It also does not include the impact of T-phases on detections, as discussed in the penultimate section.

The Importance of Close Stations for Determining Earthquake Depth: Case Study of the June 25–26, 2015, Earthquakes

The PNSN catalog includes two magnitude 2.5 earthquakes on June 25 and 26 with locations in cluster S_A and nominal source depths of about 30 km. To relocate these events, we picked P and S arrival times from seismic stations within about 120 km of the epicenter, including the OOI stations, Cascadia Initiative OBSs,

and onshore stations. Figure 7A compares data from broadband OOI station HYS14 in the SHR network to data from onshore broadband station BABR. Both stations were located about 60 km from the earthquake and show clear, impulsive P- and S-wave arrivals, and the signal-to-noise ratio is similar in the 1–20 Hz frequency band. Although not shown here, signal-to-noise ratios are also similar at SB (broadband station HYSB1) and on short-period stations HYS11–13 in the SHR network.

Figure 7B compares the P-waves recorded on HYSB1 and HYS14 to P-waves recorded on several Cascadia Initiative OBSs, including J25D, which was the station closest to the epicenter. Although P and S first arrivals are impulsive on J25D, the signal-to-noise ratio at distances >50 km is quite variable. While this may be due in part to the radiation pattern of the earthquake, it may also be due to effects of soil-structure interaction, bottom current activity, and other noise sources that affect OBSs more strongly than the buried OOI seismometers, as discussed in the previous section. Note that although FC03D is closer to the source than HYS14, and J17D is closer than HYSB1, the noise levels are lower at

the OOI site than at the Cascadia Initiative site for both of these station pairs.

Earthquakes were located in one-dimensional velocity models. All stations were normalized to sea level by applying station corrections based on the velocity of the uppermost layer in the model (2.5 km s^{-1}) to correct for different station elevations. This results in station corrections that range from -1.23 s for OBS station J10D to 1.15 s for onshore station B032 and is equivalent to removing the Coast Range and filling the ocean with sediment.

Results for the event on June 25, 2015, at 20:25 based on two different one-dimensional P-wave velocity models were compared. See Supplementary Figure S3 for details. The first model was extracted from a two-dimensional velocity model of the continental margin derived from controlled-source imaging at the position marked OR3 in Figure 3B. The second model is appropriate for the Coast Range (CR on Figure 3B) and is similar to the model used by PNSN to locate earthquakes in this region. For both models, we assumed a ratio of P-wave to S-wave velocity of 1.77, which is a typical value for crustal rocks, although it is low for marine sediments. To test the sensitivity

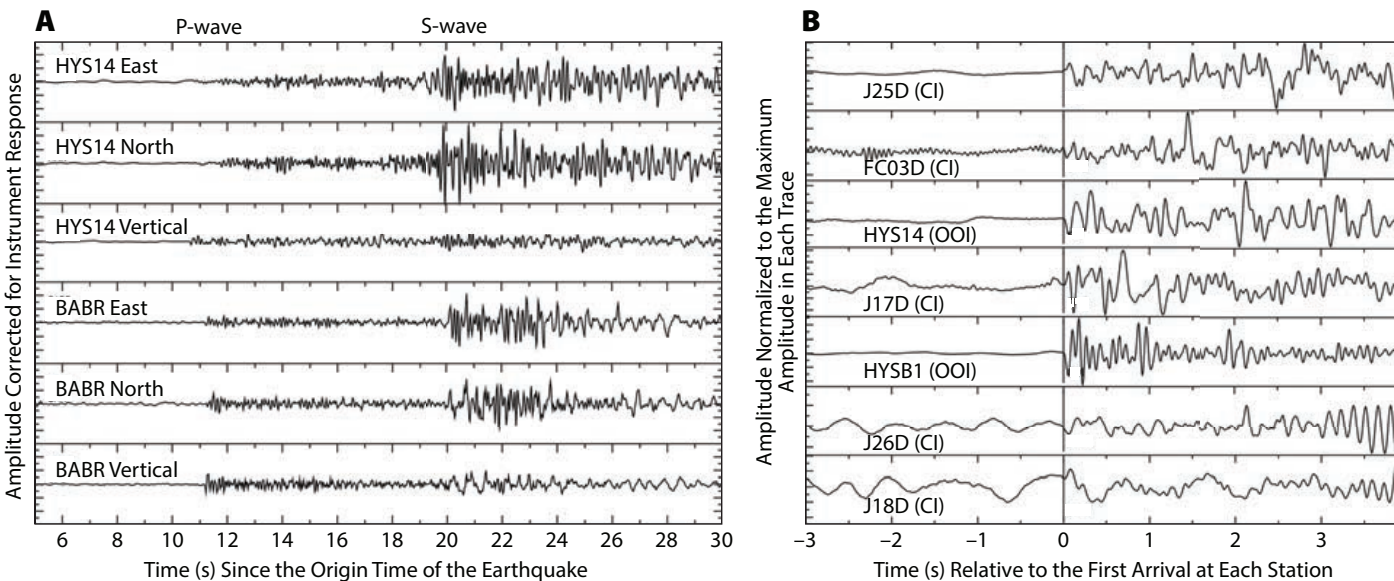


FIGURE 7. Waveforms for the July 25, 2016, earthquake in cluster S_A. Data have been high-pass filtered at 1 Hz to remove microseismic noise. (A) Comparison of three-component broadband waveforms for stations HYS14 and BABR. (B) P-waveforms recorded on the vertical component of OOI and OBS broadband seismometers ordered with source-receiver distance (17–93 km) increasing from top to bottom. Waveforms are aligned on the P-arrival pick.

of the solution to source depth, we determined the best-fitting source latitude, longitude, and origin time for a series of fixed source depths and compared the misfit for the different velocity models and various subsets of data.

The effect of velocity model uncertainty on the source latitude and longitude is small. All solutions are within about 2 km of each other (and of the epicenter reported by PNSN), which is consistent with the nominal horizontal uncertainties. The best-fit source depth, however, depends strongly on the velocity model, with model OR3 leading to shallow source depths (<15 km) and model CR leading to deeper depths (>30 km). Moreover, the misfit for OBS station J25D, located ~17 km from the epicenter, is small only for depths of 8–13 km independent of the velocity model used. Addition of seismometers to existing OOI nodes that do not currently have them (Figure 3B) would be of great benefit for improving the depth resolution when locating earthquakes along this anomalously active segment of the margin.

A Test of the Broadband Data from the OOI Seismometers: The April 15, 2017, Earthquake

The magnitude 3.8 event in subcluster S_B on April 15, 2017, was large enough to generate long-period waves suitable for moment tensor inversion. Results of that analysis are shown in Figure 8. Data at periods of 12–20 s and velocity model OR3 were used for the inversion. Stable moment tensor inversions near coasts, where the microseismic noise is strong, require using seismic waves in the frequency band of the low-noise notch (Figure 5A), which are not excited strongly enough to rise above background noise levels for earthquakes with magnitudes less than about 3.2.

Figure 8A shows several examples of the data and the waveforms predicted for the best-fitting solution, which has a depth of 12 km, and for a solution with a depth of 36 km, which is close to the depth in the

PNSN catalog (38 km). Figure 8B shows the focal mechanism (type of faulting in the source region) of the best-fit solution along with azimuthal data coverage. Figure 8C shows the residual for the inversion as a function of depth and the focal mechanism for the solution at each depth. If the OOI data are not included, the misfit decreases by ~0.05 s at each depth and the focal mechanism and source depth are not significantly different. The increased misfit when OOI data are included is likely due to higher noise levels on the horizontal components of the OOI broadband seismometers. Although inclusion of the OOI data did not significantly affect the moment tensor solution in this case, this exercise demonstrated that the

OOI broadband data are useful for low-frequency waveform modeling.

We conclude that this earthquake was a thrust event near the plate boundary. The fault dip appears to be ~45° on either an east-dipping or west-dipping plane. The focal mechanism is similar to that of a magnitude 3.8 earthquake in cluster S_A on March 20, 2012 (Tréhu et al., 2015), and somewhat different from that of the two larger earthquakes in 2004 (Tréhu et al., 2008). These results suggest a scenario in which the subducted seamount is acting as an asperity (lock on the fault) that is generating earthquakes around its edges or in the lower crust of the upper plate (Wang and Bilek, 2011). The implications of these observations for estimates of

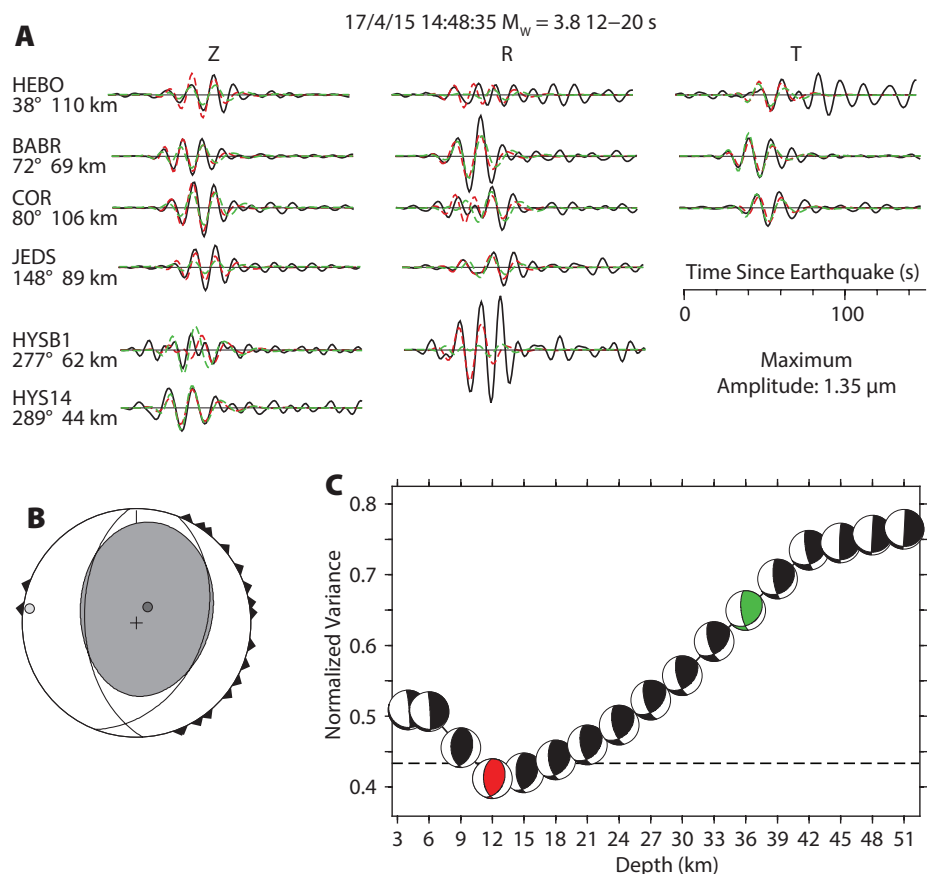


FIGURE 8. Moment tensor inversion for the April 15, 2017, magnitude 3.8 earthquake. (A) Examples of observed (black lines) long period waveforms (12–20 s period) compared to waveforms predicted for the preferred solution at 12 km depth (red dashed lines) and at 36 km depth (green dashed lines). In addition to the two OOI stations, 15 onshore broadband stations were used to obtain this solution. (B) Best-fit source mechanism, including a minor non-double couple component that is likely due to noise, has a nearly horizontal compression axis oriented at 275° and indicates thrust faulting on a plane dipping ~45°. Triangles on the outside of the focal sphere indicate azimuth of stations used. (C) Normalized variance and corresponding best-fit double couple solution as a function of assumed source depth. Red and green mechanism diagrams correspond to red and green seismograms in (A).

Cascadia earthquake hazard are unclear, and continued monitoring of this region with improved capability to resolve the source depth and mechanism is needed.

Events Detected by the OOI Network That Are Not Reported by Onshore Networks

We visually scanned all data collected from January 1 to August 15, 2017, at stations HYS11-14 and HYSB1 to determine if any local signals were recorded across the SB-SHR network that were not reported by the PNSN. Visual scans are a preliminary step toward identification of potential “templates” for automated searching of the data for additional earthquakes (Morton and Bilek, 2015) and other seismic signals. The dense network of stations at the summit of SHR (inset in Figure 3B) was designed, in part, to detect possible seismic tremor or low-frequency earthquakes generated by pulses of fluid motion associated with known methane vents.

We detected two small events in 2017, one on January 4 and one on April 18, that were clearly recorded across the OOI array

and were not reported by the land network because they were not clearly recorded on enough stations to trigger a detection (Supplementary Figure S4). These events have been tentatively located ~50 km northwest of station HYSB1 (Figure 3B) and may represent earthquakes in the subducting plate as it approaches the deformation front. A number of earthquakes in this general region have been reported in the past, including a magnitude 5.8 event in 1973 (Spence, 1989). The OOI seismic stations at SB, SHR, and Axial Seamount have the potential to decrease the detection threshold and improve the accuracy of earthquake locations within this part of the Juan de Fuca Plate, improving knowledge of the tectonics of this region and the relationship between intraplate deformation and subduction.

Another type of event recorded on the OOI SB-SHR network, but not onshore, is energy from submarine earthquakes that couples into the SOFAR channel and produces a packet of energy that follows the P (primary) and S (secondary) waves. These are generally known as T (tertiary) phase. Figure 9 shows aftershocks

associated with a swarm of earthquakes (including two events with magnitudes of 5.8 and 5.9) on the Blanco Transform Fault on June 1, 2015. In the hour following the magnitude 5.8 event, the ANSS ComCat catalog includes six earthquakes (the smallest of magnitude 3.9). During that same time period, T-phases from more than 20 smaller amplitude events were detected on the OOI network. Future work includes determination of magnitudes based on T-phase amplitudes (e.g., Dziak, 2001) to increase the magnitude range available for detailed analysis of swarm characteristics, which can provide clues to in situ stress state and earthquake dynamics.

CONCLUSIONS

The OOI seismometers contribute significantly to the ability of the regional seismic network in the Pacific Northwest to monitor the temporal evolution of seismic activity. Offshore sensors are critical for determining earthquake source depths, which are important for understanding Cascadia interplate dynamics. The OOI data are available immediately and can be incorporated into routine locating procedures, unlike data from traditional ocean bottom seismometers. Moreover, data quality is comparable to that recorded on coastal stations, unlike data from ocean bottom seismometers, for which local effects of seafloor currents, biological activity, and OBS-sediment coupling differences due to different package designs can lead to considerable variability in the effective signal-to-noise ratio. Although the magnitude detection threshold based only on P- and S-waves is significantly decreased primarily in the immediate vicinity of the stations, analysis of T-phases, recorded only on offshore stations, promises to decrease the detection levels for earthquakes occurring throughout the region. Expansion of the seismic network to the three active nodes on the central Cascadia margin that are not presently equipped with seismometers would improve depth resolution for events along a segment of the margin that has been

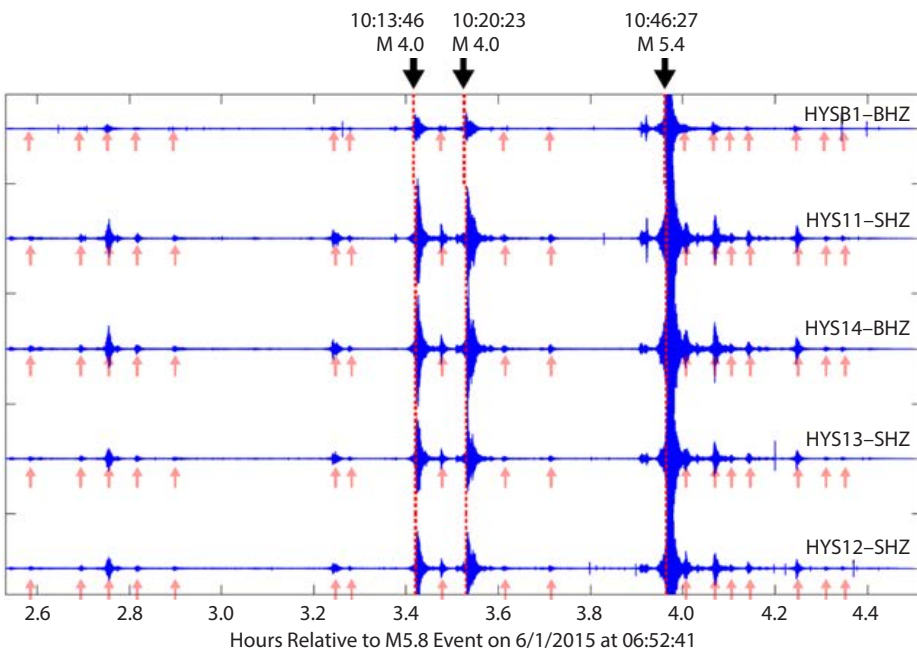


FIGURE 9. T-phases recorded on the vertical component of the OOI SB-SHR network from a swarm of earthquakes on the Blanco Transform Fault that occurred on June 1, 2015. The red dashed lines show T-phases from earthquakes in the ANSS Comprehensive Earthquake Catalog. Time and magnitude are indicated. The pink arrows show T-phases interpreted to be from additional, smaller earthquakes.

anomalously seismically active for the past several decades when compared with segments to the north and south. Significant expansion of the cabled network would be necessary to provide equivalent capability along the entire margin. ↗

SUPPLEMENTARY MATERIALS

Supplementary Figures S1–S5 are available online at <https://doi.org/10.5670/oceanog.2018.116>.

REFERENCES

- Atwater, B.F., S. Musumi-Rokkaku, K. Satake, Y. Tsuji, K. Ueda, and D.K. Yamaguchi. 2015. *The Orphan Tsunami of 1700: Japanese Clues to a Parent Earthquake in North America*, 2nd ed. US Geological Survey Professional Paper 1707, Seattle, University of Washington Press, 135 pp, <https://pubs.er.usgs.gov/publication/pp1707>.
- Bouchon, M., V. Durand, D. Marsan, H. Karabulut, and J. Schmittbuhl. 2013. The long precursory phase of most large interplate earthquakes. *Nature Geoscience* 6:299–302, <https://doi.org/10.1038/geo1770>.
- Burgmann, R. 2014. Warning signs of the Iquique earthquake. *Nature* 512:258–259, <https://doi.org/10.1038/nature13655>.
- Collins, J.A., F.L. Vernon, J.A. Orcutt, R.A. Stephen, K.R. Peal, F.B. Wooding, F.N. Speiss, and J.A. Hilderbrand. 2001. Broadband seismology in the oceans: Lessons from the Ocean Seismic Network Pilot Experiment. *Geophysical Research Letters* 28(1):49–52, <https://doi.org/10.1029/2000GL011638>.
- Crawford, W.C., and S.C. Webb. 2000. Identifying and removing tilt noise from low-frequency (<0.1 Hz) seafloor vertical seismic data. *Bulletin of the Seismological Society of America* 90:952–963, <https://doi.org/10.1785/0119990121>.
- Cozzens, B.D., and G.A. Spinelli. 2012. A wider seismogenic zone at Cascadia due to fluid circulation in subducting oceanic crust. *Geology* 40(10):899–902, <https://doi.org/10.1130/G33019.1>.
- deMets, C., R.G. Gordon, and D.F. Argus. 2010. Geologically current plate motions. *Geophysical Journal International* 181(1):1–80, <https://doi.org/10.1111/j.1365-246X.2009.04491.x>.
- Dziak, R. 2001. Empirical relationship of T-wave energy and fault parameters of Northeast Pacific ocean earthquakes. *Geophysical Research Letters* 28:2,537–2,540, <https://doi.org/10.1029/2001GL012939>.
- Gerdemann, M., A.M. Tréhu, E.R. Flueh, and D. Klaeschen. 2000. The continental margin off Oregon from seismic investigations. *Tectonophysics* 329:79–97, [https://doi.org/10.1016/S0040-1951\(00\)00190-6](https://doi.org/10.1016/S0040-1951(00)00190-6).
- Goldfinger, C., C.H. Nelson, A. Morey, J.E. Johnson, J. Gutierrez-Pastor, A.T. Eriksson, E. Karabanov, J. Patton, E. Gracia, R. Enkin, and others. 2012. *Turbidite Event History: Methods and Implications for Holocene Paleoseismicity of the Cascadia Subduction Zone*. US Geological Survey Professional Paper 1661-F, Reston, VA, 332 pp, https://pubs.usgs.gov/pp/1661f/pp1661f_text.pdf.
- Hyndman, R.D. 2013. Down-dip landward limit of Cascadia great earthquake rupture. *Journal of Geophysical Research* 118(10):5,530–5,549, <https://doi.org/10.1002/jgrb.50390>.
- Hyndman, R., and K. Wang. 1993. Thermal constraints on the zone of major thrust earthquake failure: The Cascadia subduction zone. *Journal of Geophysical Research* 98(B2):2,039–2,060, <https://doi.org/10.1029/92JB02279>.
- Ito, Y., R. Hino, M. Kido, H. Fujimoto, Y. Osada, D. Inazu, Y. Ohta, T. Ilinuma, M. Ohzono, S. Miura, and others. 2013. Episodic slow slip events in the Japan subduction zone before the 2011 Tohoku-Oki earthquake. *Tectonophysics* 600:14–26, <https://doi.org/10.1016/j.tecto.2012.08.022>.
- McCaffrey, R., A.I. Qamar, R.W. King, R. Wells, G. Khazaradze, C.A. Williams, C.W. Stevens, J.J. Vollink, and P.C. Zwick. 2007. Fault locking, block rotation and crustal deformation in the Pacific Northwest. *Geophysical Journal International* 169(3):1,315–1,340, <https://doi.org/10.1111/j.1365-246X.2007.03371.x>.
- McNamara, D.E., C. von Hillebrandt-Andrade, J.-M. Saurel, V.R. Huerfano, and L. Lynch. 2016. Quantifying 10 years of improved earthquake-monitoring performance in the Caribbean region. *Seismological Research Letters* 87:26–36, <https://doi.org/10.1785/0220150095>.
- Montagner, J.-P., J.-F.O. Karczewski, B. Romanowicz, S. Bouaricha, P. Lognonné, G. Roult, E.O. Stutzmann, J.-L. Thirot, J. Brion, B. Dole, and others. 1994. The French Pilot Experiment OFM-SISMOBS: First scientific results on noise level and event detection (1994). *Physics of the Earth and Planetary Interiors* 84(1):321–336, [https://doi.org/10.1016/0031-9201\(94\)90050-7](https://doi.org/10.1016/0031-9201(94)90050-7).
- Morton, E.A., and S.L. Bilek. 2015. Preliminary event detection of earthquakes using the Cascadia Initiative data. *Seismological Research Letters* 86(5):1,270–1,277, <https://doi.org/10.1785/0220150098>.
- Rogers, G., and H. Dragert. 2003. Episodic tremor and slip on the Cascadia subduction zone: The chatter of silent slip. *Science* 300:1,942–1,943, <https://doi.org/10.1126/science.1084783>.
- Romanowicz, B., D. Stakes, R. Uhrhammer, P. McGill, D. Neuhauser, T. Ramirez, and D. Dolenc. 2003. The MOBB experiment: A prototype permanent off-shore ocean bottom broadband station. *Eos, Transactions American Geophysical Union* 84(34):325–332, <https://doi.org/10.1029/2003EO340002>.
- Spence, W. 1989. Stress origins and earthquake potentials in Cascadia. *Journal of Geophysical Research* 94(B3):3,076–3,088, <https://doi.org/10.1029/JB094iB03p03076>.
- Toomey, D.R., R.M. Allen, A.H. Barclay, S.W. Bell, P.D. Bromirski, R.L. Carlson, X. Chen, J.A. Collins, R.P. Dziak, B. Evers, and others. 2014. The Cascadia Initiative: A sea change in seismological studies of subduction zones. *Oceanography* 27(2):138–150, <https://doi.org/10.5670/oceanog.2014.49>.
- Tréhu, A.M. 2016. Source parameter scaling and the Cascadia paleoseismic record. *Bulletin of the Seismological Society America* 106:904–911, <https://doi.org/10.1785/0120150272>.
- Tréhu, A.M., J. Braunmiller, and E. Davis. 2015. Seismicity of the central Cascadia continental margin near 44.5°N: A decadal view. *Seismological Research Letters* 86:819–829, <https://doi.org/10.1785/0220140207>.
- Tréhu, A.M., J. Braunmiller, and J.L. Nabelek. 2008. Probable low-angle thrust earthquakes on the Juan de Fuca-North America plate boundary. *Geology* 36:127–130, <https://doi.org/10.1130/G24145A.1>.
- Wang, K., and S.L. Bilek. 2011. Do subducting sea-mounts generate or stop large earthquakes? *Geology* 39:819–822, <https://doi.org/10.1130/G31856.1>.
- Wang, K., and A.M. Tréhu. 2016. Invited review paper: Some outstanding issues in the study of great megathrust earthquakes—The Cascadia example. *Geodynamics* 98:1–18, <https://doi.org/10.1016/j.jog.2016.03.010>.
- Webb, S.C. 1998. Broadband seismology and noise under the ocean. *Reviews of Geophysics* 36(1):105–142, <https://doi.org/10.1029/97RG02287>.
- Wilcock, W.S.D., R.P. Dziak, M. Tolstoy, W.W. Chadwick Jr., S.L. Nooner, D.R. Bohnenstiehl, J. Caplan-Auerbach, F. Waldhauser, A.F. Arnulf, C. Baillard, and others. 2018. The recent volcanic history of Axial Seamount: Geophysical insights into past eruption dynamics with an eye toward enhanced observations of future eruptions. *Oceanography* 31(1):114–123, <https://doi.org/10.5670/oceanog.2018.117>.
- Williams, M.C., A.M. Tréhu, and J. Braunmiller. 2010. Local earthquake detection in marine environments using seismic signal parameters. *Eos, Transactions American Geophysical Union* 91, Abstract S53A-1965.

ACKNOWLEDGMENTS

Support for this work was provided by the US National Science Foundation (NSF) through grants to Oregon State University. NSF supports the OOI seismic network through a contract with the University of Washington. Support was also provided by the US Geological Survey through its support of the Pacific Northwest Seismic Network. The University of Washington also acknowledges support from the Gordon and Betty Moore Foundation. Data from the OOI, Cascadia Initiative, and PNSN stations used in this study are freely available from the IRIS Data Management Center (<https://ds.iris.edu/ds/nodes/dmc>).

AUTHORS

Anne M. Tréhu (trehu@coas.oregonstate.edu) is Professor, College of Earth, Ocean and Atmospheric Sciences, Oregon State University, Corvallis, OR, USA. William S.D. Wilcock is Jerome M. Paros Endowed Chair in Sensor Networks, Rose Hilmo is a graduate student, Paul Bodin is Research Professor, Jon Connolly is Software Engineer, and Emily C. Roland is Assistant Professor, all at the College of the Environment, University of Washington, Seattle, WA, USA. Jochen Braunmiller is Research Assistant Professor, School of Geosciences, University of South Florida, Tampa, FL, USA.

ARTICLE CITATION

Tréhu, A.M., W.S.D. Wilcock, R. Hilmo, P. Bodin, J. Connolly, E.C. Roland, and J. Braunmiller. 2018. The role of the Ocean Observatories Initiative in monitoring the offshore earthquake activity of the Cascadia subduction zone. *Oceanography* 31(1):104–113, <https://doi.org/10.5670/oceanog.2018.116>.

THE RECENT VOLCANIC HISTORY OF AXIAL SEAMOUNT

Geophysical Insights into Past Eruption Dynamics with
an Eye Toward Enhanced Observations of Future Eruptions

By William S.D. Wilcock, Robert P. Dziak,
Maya Tolstoy, William W. Chadwick Jr.,
Scott L. Nooner, DelWayne R. Bohnenstiehl,
Jacqueline Caplan-Auerbach, Felix Waldhauser,
Adrien F. Arnulf, Christian Baillard, Tai-Kwan Lau,
Joseph H. Haxel, Yen Joe Tan, Charles Garcia,
Samuel Levy, and M. Everett Mann



“ The 2015 eruption at Axial Seamount was the first to be recorded by an in situ cabled observatory, and Axial is now the best-monitored submarine volcano on Earth. ”

ABSTRACT. To understand the processes that form oceanic crust as well as the role of submarine volcanoes in exchanging heat and chemicals with the ocean and in supporting chemosynthetic biological communities, it is essential to study underwater eruptions. The world’s most advanced underwater volcano observatory—the Ocean Observatories Initiative Cabled Array at Axial Seamount—builds upon ~30 years of sustained geophysical monitoring at this site with autonomous and remote systems. In April 2015, only months after the Cabled Array’s installation, it recorded an eruption at Axial Seamount, adding to the records of two prior eruptions in 1998 and 2011. Between eruptions, magma recharge is focused beneath the southeast part of the summit caldera, leading to steady inflation and increasing rates of seismicity. During each eruption, the volcano deflates over days to weeks, coincident with high levels of seismicity as a dike is emplaced along one of the volcano’s rifts and lava erupts on the seafloor. Cabled Array seismic data show that motions on an outward-dipping ring fault beneath the caldera accommodate the inflation and deflation. Eruptions appear to occur at a predictable level of inflation; hence, it should be possible to time deployments of additional cabled and autonomous instrumentation to further enhance observations of the next eruption.

INTRODUCTION

There is a long history of supporting volcano observatories on land, where studies are motivated by the dual goals of mitigating the risks of eruptions and improving our scientific understanding of the role volcanoes play in transferring material and heat from the mantle and in forming Earth’s crust. Investigations of volcanoes combine discrete studies to characterize their structures and past eruptive histories with ongoing monitoring of ground deformation, seismicity,

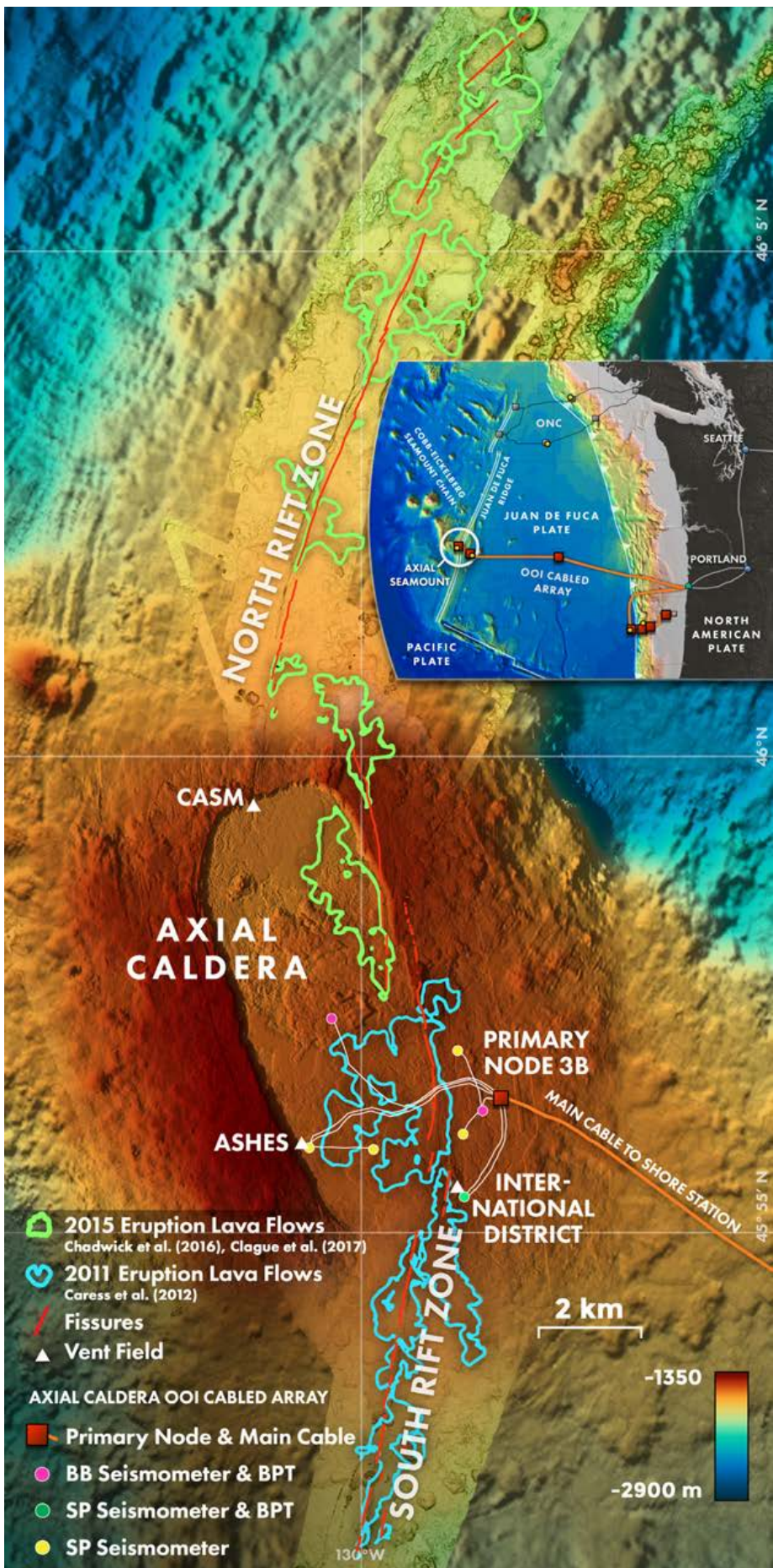
and the emissions of gas and geothermal fluids. Most volcanoes erupt infrequently and irregularly, and monitoring requires a commitment to long-term observations to characterize baseline behavior, detect early precursors of unrest, and record periods of activity.

In the ocean, studies of deepwater volcanoes are motivated by scientific goals. Volcanism at oceanic spreading centers replaces ~60% of the Earth’s surface on timescales of ~100 million years. Understanding this process requires observations of diking-eruptive events

and the “quantum events of upper oceanic crustal accretion” (Delaney et al., 1998). Hydrothermal systems on submarine volcanoes transport heat and chemicals into the ocean and feed chemosynthetic biological communities in a setting that may replicate the environment in which life first evolved on Earth and potentially elsewhere (Martin et al., 2008). Volcanic eruptions can reinvigorate existing hydrothermal vent fields and lead to the formation of event plumes, giant pulses of hydrothermal fluid that rise high in the water column from short-lived sources (Baker et al., 1999). Event plumes may flush out microorganisms from a subseafloor biosphere that is otherwise hard to sample (Summit and Baross, 1998). Rapid response cruises have been organized to study submarine eruptions detected remotely by their seismicity (Duennebier et al., 1997; Cowen et al., 2004). However, because the timescales for diking, the onset of eruptions, and the formation of event plumes are hours to days, expeditions that arrive on site after a week or more are limited to observing the aftermath of these key processes.

These timing considerations motivated the installations of the Ocean Observatories Initiative (OOI) Cabled Array at Axial Seamount (Figure 1), an active volcano in the Northeast Pacific Ocean at the intersection of the Juan de Fuca Ridge oceanic spreading center and Cobb-Eickelberg seamount chain.

FACING PAGE. View of Axial Seamount from the south showing additional sensors that could be usefully added prior to the next eruption. Bathymetry from Clague et al. (2017). Lava flow outlines and Ocean Observatories Initiative Cabled Array geophysical instrumentation are as for Figure 1. Created by the University of Washington Center for Environmental Visualization



Axial Seamount rises ~1 km above the surrounding seafloor, and its summit is characterized by an elongated 8 km × 3 km caldera that hosts three high-temperature hydrothermal vent fields. Extensional rifts on the north and south flanks form segments of the Juan de Fuca Ridge that overlap in the caldera (Embley et al., 1990). The summit is underlain by an extensive and well-imaged magma body at 1–2 km depth that extends well beyond the northern and southern limits of the caldera (West et al., 2001; Arnulf et al., 2014).

The OOI Cabled Array at Axial Seamount is the most advanced underwater volcano observatory in the world (Kelley et al., 2014), and its siting benefits from over 30 years of expeditionary studies and sustained efforts to support near-continuous geophysical monitoring. During its first year of operation in 2015, the Cabled Array captured an eruption of the volcano in real time, adding to the records of two prior eruptions that were detected in 1998 and 2011.

In this paper, we review the geophysical observations of the three eruptions, each of which was recorded by a different configuration of sensors. Over its lifetime, the OOI Cabled Array will likely record more eruptions; the geodetic observations to date imply that eruptions will be predictable on timescales of one to a few years. With this in mind, we conclude by discussing how the observatory might be enhanced prior to the next eruption.

FIGURE 1. Bathymetric chart of Axial Seamount showing the configuration of geophysical instrumentation on the Ocean Observatories (OOI) Cabled Array and the location of fissures and lava flows associated with the 2011 (Caress et al., 2012) and 2015 (Chadwick et al., 2016; Clague et al., 2017) eruptions. The inset figure shows the location of Axial Seamount in the Northeast Pacific Ocean, the configuration of the OOI Cabled Array, and six hydrophones on the OOI and Ocean Networks Canada (ONC) cabled observatories (yellow circles) used to locate hydroacoustic events on April 24, 2011 (Figure 4c). Modified from Manalang and Delaney (2016), created by the University of Washington Center for Environmental Visualization

OBSERVATIONS PRIOR TO THE 1998 ERUPTION

Axial Seamount was first mapped with multibeam bathymetry and side-scan sonar systems in the early 1980s, and submersible-based studies of seafloor geology and hydrothermal venting commenced at the summit in 1983 (Chase et al., 1985; Butterfield et al., 1990). Sustained geophysical monitoring of Axial Seamount started in 1987 with the deployment of a bottom pressure recorder (BPR) near the center of the summit caldera (Fox, 1990). One or more BPRs were recovered and redeployed each summer. In 1996, these instruments were incorporated into the NOAA New Millennium Observatory (NeMO), a precursor to the OOI Cabled Array, that sought to obtain time-series observations of the interactions between volcanic activity and hydrothermal venting (Hammond et al., 2015).

The seismic networks on land in the Pacific Northwest are not sensitive enough to monitor volcanism on the Juan de Fuca Ridge, but because seismic signals propagate efficiently in the ocean sound channel, regional hydroacoustic monitoring provides an effective means for monitoring ocean spreading centers. In late 1991, NOAA was provided access to the US Navy Sound Surveillance System (SOSUS), a network of multiple element hydrophone arrays, for the purpose of monitoring the Juan de Fuca and Gorda Ridges for seismicity (Fox et al., 1994; Dziak et al., 2011); in 1993, the analysis became near-real time.

There was evidence from a short eight-day deployment of three ocean bottom seismometers (OBSs) in 1985 that Axial Seamount was seismically quite active (Jacobson et al., 1987), and from the onset of SOSUS monitoring in 1991, the rates of seismicity were clearly increasing. Over six years prior to the 1998 eruption, the SOSUS system, which had a detection threshold of magnitude ~ 2.5 (Fox et al., 1994; Dziak et al., 2011), recorded ~ 800 earthquakes concentrated in swarms (Dziak and Fox, 1999a; Figure 2b). A two-month

microearthquake survey with three OBSs in 1994 confirmed that seismicity rates were high (Tolstoy et al., 2002), and 400 earthquakes were located in the southern part of the caldera (Figure 3a).

1998 ERUPTION

The 1998 eruption at Axial Seamount started on January 25, and over 11 days SOSUS detected more than 8,000 earthquakes. Seismicity commenced at the summit and then, during the first two days, epicenters traced the southward propagation of a dike for ~ 50 km at a velocity of $\sim 0.9 \text{ m s}^{-1}$ for the first ~ 20 km and then at $\sim 0.2 \text{ m s}^{-1}$ (Figure 4a). Seismicity continued at the summit and southern end of the south rift for about a week after the migration ceased (Dziak and Fox, 1999b).

The BPR at the center of the caldera recorded a few centimeters of uplift starting 2.2 hours after seismicity began (Chadwick et al., 2013) followed by the onset of deflation 1.1 hours later. Over 3.2 m of deflation took place over six days, with most of it occurring in the

first two days as the dike propagated (Fox, 1999). A second BPR in the southeast caldera was caught in a lava flow very shortly after the onset of deflation at the central caldera (Fox et al., 2001). From these observations it was inferred that the dike took about three hours to propagate from the magma chamber to the seafloor (Fox, 1999; Chadwick et al., 2013).

Two five-element temperature moorings, extending 115 m above the seafloor, detected temperature anomalies within hours that peaked at 0.6°C and declined over two weeks (Baker et al., 1999). A response cruise that arrived on site 18 days after the eruption onset did not find an event plume over the caldera but found event-plume-like chemistry in a plume off-axis to the southwest. This led to speculation that the event plume discharge may have been sheared by strong currents (Lupton et al., 1999).

Differences between pre- and post-eruption bathymetry, coupled with side-scan data and seafloor observations, show that lava flows extended from the southeast caldera about 11 km down the

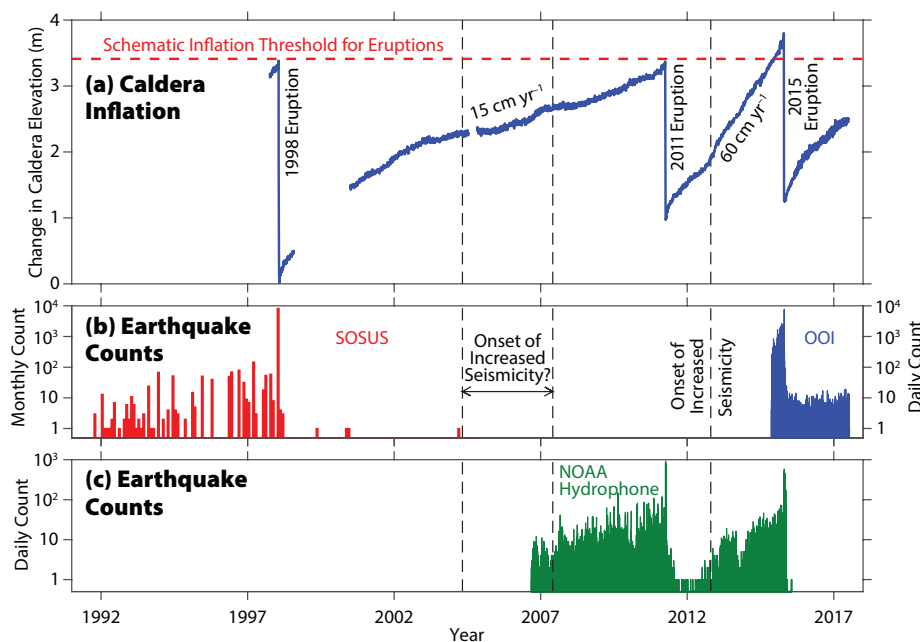


FIGURE 2. Long-term record of volcano inflation and deflation and earthquake counts at Axial Seamount. (a) Relative elevation at the center of the caldera (blue line) measured by combining data from continuously recording bottom pressure recorders with campaign-style calibration measurements from a mobile pressure recorder (modified from Nooner and Chadwick, 2016). (b–c) Histograms of earthquake counts plotted on logarithmic scales showing earthquakes detected per month by SOSUS (recreated from Dziak and Fox, 1999a), autonomous ocean bottom hydrophones (Caplan-Auerbach et al., 2017), and the OOI Cabled Array seismic network (Wilcock et al., 2016).

south rift (Embley et al., 1999; Chadwick et al., 2013). Interestingly, there is no evidence for an eruption at the southern end of the dike. The lava flow volume was estimated at $31 \times 10^6 \text{ m}^3$ and the volume of deflation at $207 \times 10^6 \text{ m}^3$, indicating that most of the magma removed from the summit reservoir was intrusive (Chadwick et al., 1999, 2013).

Following the 1998 eruption, seismicity at Axial Seamount declined dramatically (Dziak and Fox, 1999a), and over the next decade, SOSUS detected fewer than 10 earthquakes on the volcano. Starting two weeks after the 1998 eruption, three deployments of between four and 10 OBSs and ocean bottom hydrophones (OBHs) monitored microseismicity for 15 months

(Sohn et al., 2004). Only 140 microearthquakes were detected, an earthquake rate that is ~5% of that observed with a smaller network four years prior to the eruption (Tolstoy et al., 2002).

2011 ERUPTIVE CYCLE

Immediately following the 1998 eruption, the bottom pressure observations document a period of rapid re-inflation that is attributed either to recharge from secondary magma bodies or to poroelastic and viscoelastic re-equilibration following a sudden drop in pressure in the magma chamber (Nooner and Chadwick, 2009). After a two-year hiatus, bottom pressure observations resumed in 2000 with the addition of regular surveys using a mobile pressure recorder carried by a remotely operated vehicle. These surveys were designed to measure the difference in elevation between a set of benchmarks in and near the caldera and a reference benchmark on the volcano's flank (Chadwick et al., 2006). The resulting time series of calibrated bottom pressure records (Figure 2a) show an average inflation rate of $\sim 15 \text{ cm yr}^{-1}$ from 2000 to 2010 (Chadwick et al., 2012).

In the mid-2000s the SOSUS system became less reliable, and in 2008 the stations most useful for monitoring Axial Seamount went offline permanently. To continue the long-term observations, up to four autonomous NOAA OBHs were continuously operated in the caldera starting in 2006 (Dziak et al., 2012). The data show that the rates of microseismicity increased progressively over the five years of observations leading up to the 2011 eruption (Figure 2c).

Data from the autonomous hydrophones, however, were not available in real time, so in the absence of SOSUS monitoring, the 2011 eruption was not detected until new lava flows were discovered on the seafloor in July 2011 (Carey et al., 2012). The chronology of the eruption on April 6 was subsequently inferred from autonomous BPRs and OBHs (Chadwick et al., 2012; Dziak et al., 2012). There were several short-term precursors.

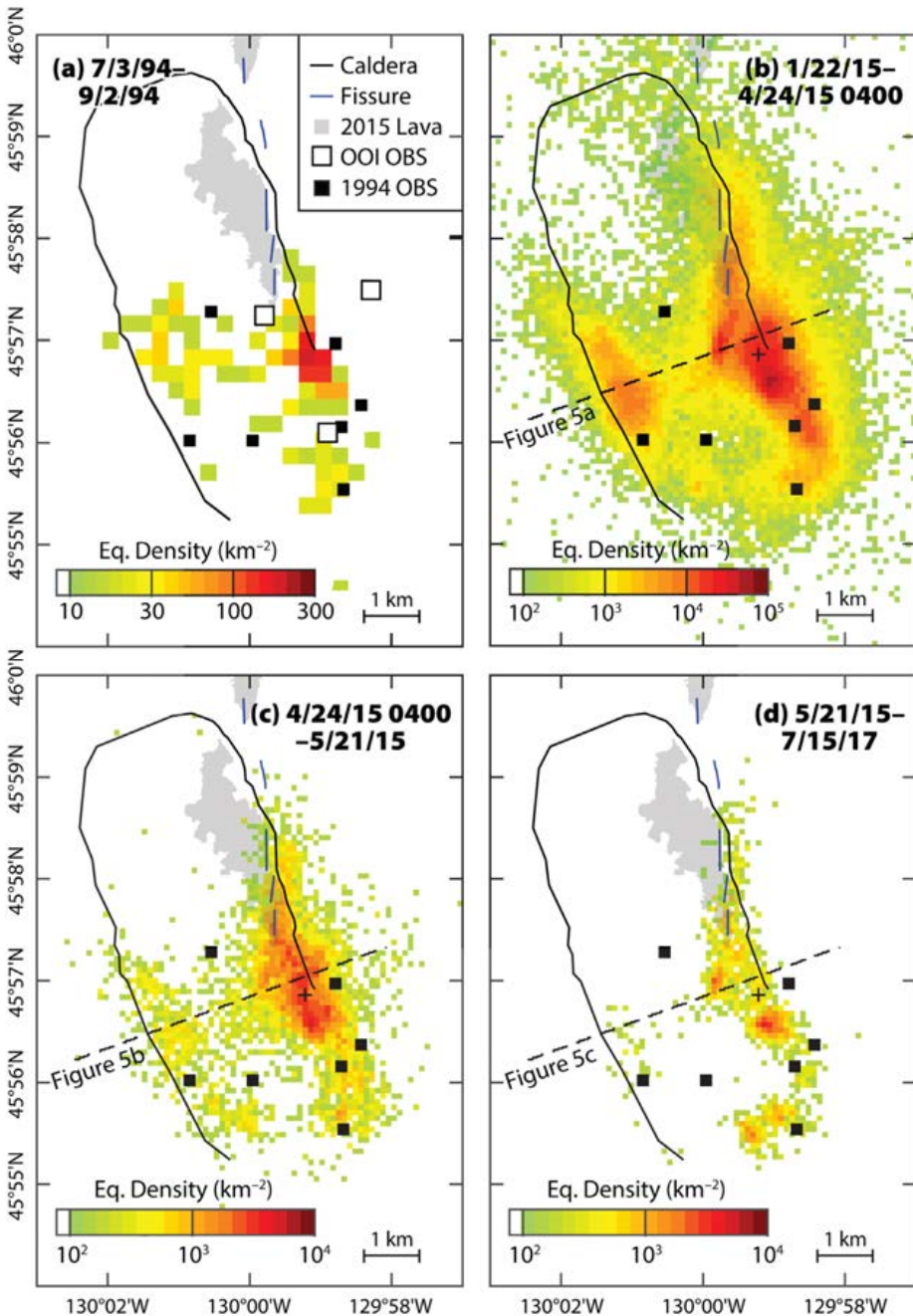


FIGURE 3. Maps showing the density of earthquake epicenters for (a) two months in 1994 (Tolstoy et al., 2002), and for the OOI Cabled Array seismic network for (b) the three months immediately prior to the 2015 eruption, (c) the 27-day duration of the 2015 eruption, ending when explosions ceased and the volcano started to re-inflate, and (d) the first 14 months of re-inflation. Note that the color scale for earthquake density is logarithmic, with threshold and color scales differing between plots.

For a few months leading up to the eruption, the rate of inflation steadily increased. Bursts of volcanic tremor, likely linked to subsurface magma movements, commenced several days beforehand. About eight hours before the eruption, the amplitude of short-term noise on the pressure recorders doubled.

The 2011 eruption itself shows many similarities to the 1998 eruption (Chadwick et al., 2013). The onset of seismicity occurred 2.6 hours before the eruption started, and acoustic amplitudes then increased rapidly, peaking 0.5 hours before the eruption, coincident with 7 cm of dike-induced uplift in the central caldera. The total deflation in the center of the caldera for the 2011 eruption was about 2.4 m, less than in 1998, but the duration of deflation and the time for acoustic amplitudes to decay were similar to those of the earlier eruption.

Because one of the three OBHs deployed at the time of the eruption was trapped in 2011 lava, there are no earthquake locations to track the propagation of the dike (Dziak et al., 2012). Fresh lava flows were found extending from the center of the caldera to about 10 km south. About 30 km south of the caldera, bathymetric difference maps delineated a 5 km-long pillow ridge with a maximum thickness of 140 m that postdates the 1998 eruption and is reasonably inferred to be part of the 2011 eruption (Caress et al., 2012). The northern eruption occupied many of the same eruptive fissures as the 1998 eruption and has a similar footprint and volume ($33 \times 10^6 \text{ m}^3$), while the more southern lava flow has a volume of $66 \times 10^6 \text{ m}^3$. The total volume of deflation estimated using a point source elastic deformation model is $147 \times 10^6 \text{ m}^3$, of which about two-thirds was erupted (Chadwick et al., 2012). Thus, while smaller in total volume than the 1998 eruption, the volume of extruded lavas was much higher in 2011.

OOI CABLED ARRAY AND 2015 ERUPTION

Shortly after the 2011 eruption, Chadwick et al. (2012) postulated that eruptions of Axial Seamount occur at a threshold level of inflation and stated that if the volcano re-inflated in the same pattern as observed after the 1998 eruption, it could be ready to erupt again in 2018. The initial pattern of re-inflation at Axial was similar to the prior eruption, but by 2013 it was clear that the inflation was continuing at a higher rate of $\sim 60 \text{ cm yr}^{-1}$ (Figure 2a) due to increased magma supply. This observation led in September 2014 to a revised forecast that the volcano would erupt in 2015 (Chadwick and Nooner, 2014). The earthquake rate measured by the NOAA OBHs also started to increase in fall 2012 (Caplan-Auerbach et al., 2017) and then increased up to the time of the 2015 eruption more quickly than observed prior to the 2011 eruption (Figure 2c), consistent with the higher rate of re-inflation. The earthquake rates just before the eruptions were similar in 2011 and 2015.

Installation of the OOI Cabled Array at Axial Seamount was completed late in the summer of 2014, with the observatory coming on line that fall (Kelley et al., 2014). The system

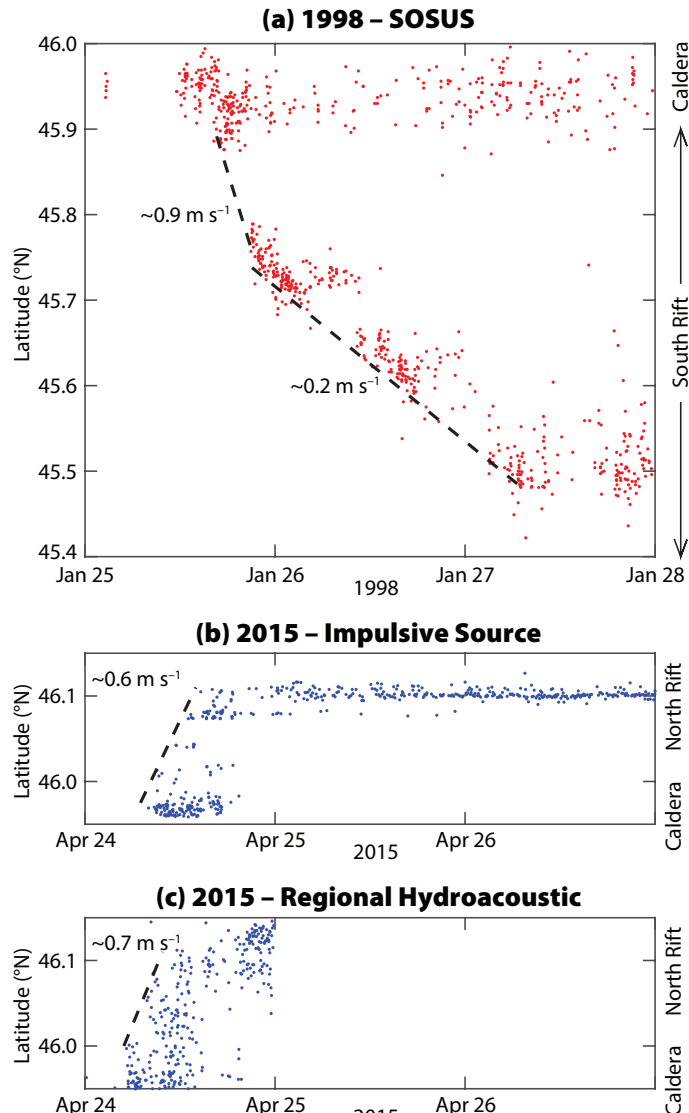


FIGURE 4. Migration of earthquakes and impulsive seafloor signals for the 1998 and 2015 eruptions. (a) Latitude of SOSUS epicenters for the first three days of the 1998 eruption (Dziak and Fox, 1999b). (b) Latitude of eruption-related seafloor impulsive signals determined with the OOI Cabled Array caldera seismic network for the 2015 eruption. (c) Latitude of earthquakes and seafloor impulsive signals for the first day of the 2015 eruption determined with hydrophones from the OOI and ONC cabled observatories (see Figure 1 inset).

incorporates geophysical instrumentation on both the Cascadia margin (Tréhu et al., 2018, in this issue) and Axial Seamount. At the summit of Axial Seamount, the footprint of the observatory (Figure 1) spans the southern half of the caldera where the 1998 and 2011 eruptions initiated. The seismic component of the observatory includes seven three-component seismic stations; five are short period instruments that are attached to leveled triangular baseplates (Figure S1a), and two are broadband instruments in spherical housings that are co-located with hydrophones (Figure S1b). The broadband stations sit on basaltic seafloor and are surrounded by sandbags to improve coupling. When the observatory was installed, three of the seismic

stations were co-located with geodetic sensors that measure bottom pressure and seafloor tilt (Figures 1 and S1c). These instruments are complemented by autonomous BPRs at several other sites. A fourth cabled bottom pressure and tilt instrument was added at the ASHES (Axial Seamount Hydrothermal Emission Study) vent field in summer 2017.

The rates of seismicity were already high when the OOI Cabled Array came online in November 2014, and the number of earthquakes detected by this system increased from a few hundred per day to about two thousand per day a month before the eruption (Figure 2b; Wilcock et al., 2016). The presence of a local seismic network on top of the volcano has allowed over 100,000 earthquakes to be located. Their distributions before, during, and after the eruption (Figure 3b–d) are similar to one another and to the distribution observed in 1994 (Figure 3a), although after the eruption a larger proportion of the earthquakes occur at the southern end of the caldera and a smaller proportion on the west wall. The majority of the earthquakes are concentrated below the east wall of the caldera, with the highest density near the centroid of inflation determined from the bottom pressure data (Nooner and Chadwick, 2016). There is also a high density of earthquakes near the west wall and beneath the southern end of the caldera. Cumulatively, these earthquakes define an outward-dipping ring fault

(Figure 5) that accommodates some of the uplift of the caldera prior to an eruption and then, by reversing the direction of fault motion, some of the subsidence during an eruption (Wilcock et al., 2016).

The rate of seismicity decreased slightly two weeks before the eruption, but the only seismic precursor was tremor starting six hours beforehand, a markedly shorter warning than seen for the 2011 eruption. The onset of increased seismicity on April 24 preceded peak seismic amplitudes and the onset of deflation by about two hours. The total amount of deflation was similar to 2011, but the volcano deflated more quickly (Nooner and Chadwick, 2016), with the majority of earthquakes occurring during the ~10-hour seismic “crisis.”

One unexpected observation from this eruption was the detection of tens of thousands of impulsive water-borne signals (Wilcock et al., 2016; Tolstoy et al., 2018, in this issue) that started within hours of the seismic crisis and continued for nearly a month, ceasing when the bottom pressure data showed that the volcano started to re-inflate and the seismicity rates reached very low levels. The mechanism for these signals is uncertain, but they are clearly related to lava erupting on the seafloor. The impulsive signals can be located by modeling the times of the water column reverberations. They can be spatially linked to lava flows, and the majority were located ~10–15 km along the north rift where thick pillow

flows were subsequently discovered. The OOI hydrophones at the summit of Axial Seamount also recorded diffuse events in the later stages of the eruption that were interpreted as possible explosive submarine ash eruptions (Caplan-Auerbach et al., 2017).

The earthquake locations show that early in the eruption, earthquakes migrated 2–3 km south from the northeast edge of the caldera before stalling near the northern limit of the two prior eruptions (Wilcock et al., 2016). The locations show no evidence of the dike propagating northward along the north rift. This is a result of the limited footprint of the seismic network, the high noise levels generated by local earthquakes, and shadowing from the axial magma chamber that extends well to the north of the caldera and would lie in the path of seismic waves traveling from earthquakes on the north rift.

There is evidence for northward dike propagation based on the onset time of the impulsive signals as a function of their latitude (Figure 4b). Using these data to get the dike propagation rate requires an untested assumption that the interval between the passage of the dike and the onset of impulsive signals is constant. A more robust estimate of the dike propagation speed can be obtained from regional hydroacoustic locations. In combination, the hydrophones on the OOI Cabled Array and the Ocean Networks Canada NEPTUNE cabled observatory

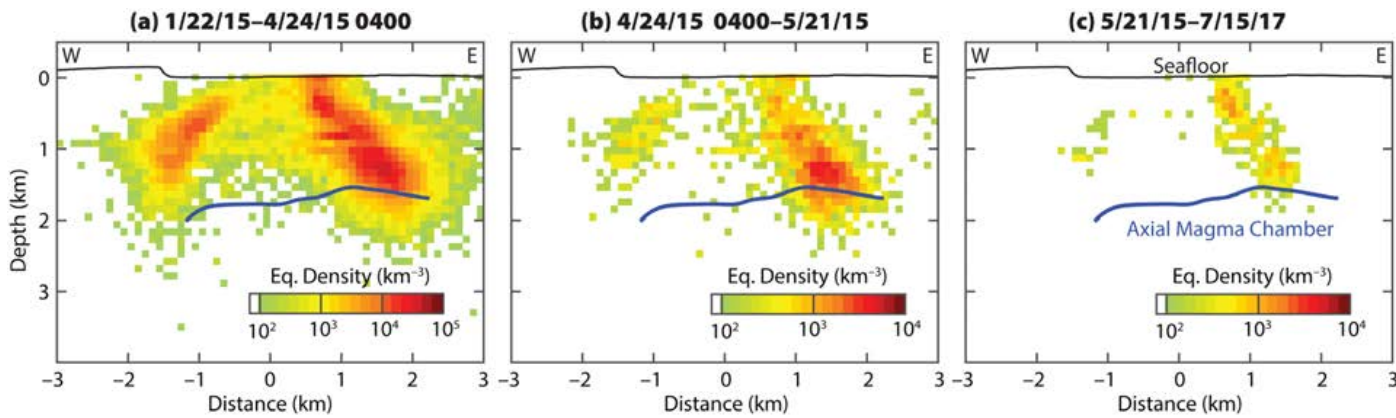


FIGURE 5. Vertical cross sections oriented WSW-ENE across the southern caldera (dashed lines in Figure 3b–d), showing the density of earthquake hypocenters lying within 0.5 km of the cross section for the same time intervals (a) before, (b) during, and (c) after the eruption as shown in Figure 3b–d.

provide a reasonable geometry for triangulating locations on Axial Seamount (Figure 1 inset). Hydroacoustic locations obtained for April 24 (Figure 4c) suggest that northward dike propagation started early in the seismic crisis, coincident with the onset of deflation, and that the dike propagated at $\sim 0.7 \text{ m s}^{-1}$, possibly slowing near its northern end, as was observed for the 1998 dike.

The larger number of bottom pressure measurement sites for the 2015 eruption from an array of 10 seafloor benchmarks permitted calculation of more complex source geometries than was possible for prior eruptions. The best fitting source was a steeply dipping prolate-spheroid, with a co-eruption decrease in volume of $2.88 \times 10^8 \text{ m}^3$ (Nooner and Chadwick, 2016). Just over half of that volume erupted onto the seafloor, mostly in the northern lava flows (Chadwick et al., 2016); the rest was inferred to have filled a 24 km-long, 2–3 m-wide dike. The large width is consistent with the rapid deflation observed (Nooner and Chadwick, 2016).

FUTURE OF VOLCANO MONITORING AT AXIAL

Volcano monitoring at Axial Seamount has contributed substantially to our understanding of submarine volcanism. Along with the East Pacific Rise at $9^{\circ}50'N$ (Tolstoy et al., 2006), it is one of only two sites on an oceanic spreading center where more than one eruption has been observed and the only site where geodetic and seismic observations have been obtained concurrently through an eruption. As of summer 2017, the volcano has recovered about half of the deflation that occurred during the 2015 eruption, with the rate of inflation declining from $\sim 1 \text{ m yr}^{-1}$ immediately after the eruption to $\sim 0.40 \text{ m yr}^{-1}$ recently. If the volcano continues to inflate at $\sim 0.40 \text{ m yr}^{-1}$, another eruption is expected in three years, but the inflation rate may vary. Interestingly, the volcano remains seismically quiet. Because the level of inflation has already exceeded that at which seismicity rates started to increase prior to

the 2015 eruption and is similar to that at which the seismicity rate was increasing prior to the 2011 eruption (Figure 2), we infer that the rate of seismicity will soon start to increase, providing another indicator of the time to the next eruption.

One lesson learned from monitoring seismicity at Axial Seamount is the importance of nested observations. The cabled seismometer and hydrophone

new opportunities for understanding the mechanics of submarine dike events by constraining the depth and style of faulting and measuring variations in the speed of propagation.

Another goal for the next eruption should be to enhance hydrothermal observations. At present, the Cabled Array incorporates a variety of instrumentation in the ASHES and International District

“Along with the East Pacific Rise at $9^{\circ}50'N$, [Axial Seamount] is one of only two sites on an oceanic spreading center where more than one eruption has been observed and the only site where geodetic and seismic observations have been obtained concurrently through an eruption.”

network at the summit has provided an unprecedented data set that is being mined to understand the dynamics of a submarine caldera as well as the source of eruption-generated sounds. However, the network did not detect earthquakes associated with the northward propagation of the dike that fed the most voluminous lava flows. Regional hydroacoustic monitoring with the OOI and Ocean Networks Canada hydrophones constrained the rate of propagation for the 2015 dike (Figure 4c), but distant hydroacoustic observations cannot easily distinguish between shallow earthquakes and impulsive seafloor events, and they provide only a weak constraint on source depth (Dziak and Fox, 1999b). For the next eruption, the cabled seismic and regional hydroacoustic observations should be complemented by temporary deployments of OBSs to cover the northern part of the caldera and upper portions of north and south rifts and the moored hydrophones that encircle the seamount (title page and Figure S2). This would provide

vent fields (Figure 1), but no significant perturbations were observed in these hydrothermal vents for the 2015 eruption because the dike and the lava flows were located well to the north of these fields. Because it is unknown whether the next dike will be emplaced on the north or south rift, deploying sensors in the CASM (Canadian American Seamount) vent field at the north end of the caldera (Figures 1 and S2 and title page) would ensure that at least one monitored vent field is close to the next dike.

Although numerous event plumes have been observed after formation either by response cruises or serendipity, their formation mechanism remains unclear and has been alternatively attributed to cooling lava flows (Palmer and Ernst, 1998), cooling dikes (Lowell and Germanovich, 1995), or the release of mature hydrothermal fluids already present in the crust (Cann and Strens, 1989). One approach to studying both steady-state and event plumes would be to build upon water column temperature observations from the

1998 eruption (Baker et al., 1999) and install moorings in and near the caldera (title page and Figure S2). Alternatively, ocean gliders could be deployed to survey the hydrothermal plumes as is done at many of the other OOI observatory sites.

Manalang and Delaney (2016) explore the feasibility of adding a resident autonomous underwater vehicle at Axial Seamount. It would dock to the Cabled Array to recharge batteries and download data, and utilize a network of acoustic transponders to navigate and communicate while executing missions (title page and Figure S2). If event plumes form above thick lava flows, such as those found down the rifts in 2011 and 2015, mobile platforms may be the most practical means of observing the eruption in progress and event plumes during their formation. An acoustic transponder network could also complement an expanded set of bottom pressure measurements by enabling horizontal geodesy between pairs of transponders that would further constrain models of caldera inflation and measure the extension that occurs when dikes are emplaced.

The 2015 eruption at Axial Seamount was the first to be recorded by an in situ cabled observatory, and Axial is now the best-monitored submarine volcano on Earth. More was learned about Axial Seamount's internal plumbing in 2015 than in the previous eruptions because of the many multidisciplinary observations enabled by the cabled network. The 2015 eruption also showed where knowledge gaps exist and where any new monitoring assets might be deployed to learn even more in the future. Ultimately, the real-time data provided through OOI will enable better preparation for future eruptions both on an annual timescale by deployment of additional autonomous sensors as the volcano nears its critical state, and on an hourly timescale through deployment and rapid sampling of all available Cabled Array assets as seismic and geodetic signals indicate an eruption is imminent or underway. 

SUPPLEMENTARY MATERIALS

Supplementary Figures S1 and S2 are available online at <https://doi.org/10.5670/oceanog.2018.117>.

REFERENCES

- Arnulf, A.F., A.J. Harding, G.M. Kent, S.M. Carbotte, J.P. Canales, and M. Nedimovic. 2014. Anatomy of an active submarine volcano. *Geology* 42(8):655–658, <https://doi.org/10.1130/G35629.1>.
- Baker, E.T., C.G. Fox, and J.P. Cowen. 1999. In situ observations of the onset of hydrothermal discharge during the 1998 submarine eruption of Axial Volcano, Juan de Fuca Ridge. *Geophysical Research Letters* 26(23):3,445–3,448, <https://doi.org/10.1029/1999GL002331>.
- Butterfield, D.A., G.J. Massoth, R.E. McDuff, J.E. Lupton, and M.D. Lilley. 1990. Geochemistry of hydrothermal fluids from Axial Seamount hydrothermal emissions study vent field, Juan de Fuca Ridge: Subseafloor boiling and subsequent fluid-rock interaction. *Journal of Geophysical Research* 95(B8):12,895–12,921, <https://doi.org/10.1029/JB095iB08p12895>.
- Cann, J.R., and M.R. Strens. 1989. Modeling periodic megaplume emission by black smoker systems. *Journal of Geophysical Research* 94(B9):12,227–12,237, <https://doi.org/10.1029/JB094iB09p12227>.
- Caplan-Auerbach, J., R.P. Dziak, J. Haxel, D.R. Bohnenstiehl, and C. Garcia. 2017. Explosive processes during the 2015 eruption of Axial Seamount, as recorded by sea-floor hydrophones. *Geochemistry, Geophysics, Geosystems* 18(4):1,761–1,774, <https://doi.org/10.1002/2016GC006734>.
- Caress, D.W., D.A. Clague, J.B. Paduan, J.F. Martin, B.M. Dreyer, W.W. Chadwick Jr., A. Denny, and D.S. Kelley. 2012. Repeat bathymetric surveys at 1-metre resolution of lava flows erupted at Axial Seamount in April 2011. *Nature Geoscience* 5(7):483–488, <https://doi.org/10.1038/ngeo1496>.
- Chadwick, W.W., Jr., D.A. Clague, R.W. Embley, M.R. Perfitt, D.A. Butterfield, D.W. Caress, J.B. Paduan, J.F. Martin, P. Sasnett, S.G. Merle, and A.M. Bobbitt. 2013. The 1998 eruption of Axial Seamount: New insights on submarine lava flow emplacement from high-resolution mapping. *Geochemistry, Geophysics, Geosystems* 14(10):3,939–3,968, <https://doi.org/10.1002/ggge.20202>.
- Chadwick, W.W., Jr., R.W. Embley, H.B. Milburn, C. Meining, and M. Stapp. 1999. Evidence for deformation associated with the 1998 eruption of Axial Volcano, Juan de Fuca Ridge, from acoustic extensometer measurements. *Geophysical Research Letters* 26(23):3,441–3,444, <https://doi.org/10.1029/1999GL900498>.
- Chadwick, W.W., Jr., and S.L. Nooner. 2014. Slide from a talk at the Monterey Bay Aquarium Research Institute (MBARI). *Blog to Chronicle Eruption Forecasts at Axial Seamount*, https://www.pmel.noaa.gov/eoi/axial_blog.html.
- Chadwick, W.W. Jr., S.L. Nooner, D.A. Butterfield, and M.D. Lilley. 2012. Seafloor deformation and forecasts of the April 2011 eruption at Axial Seamount. *Nature Geoscience* 5(7):474–477, <https://doi.org/10.1038/ngeo1464>.
- Chadwick, W.W., Jr., S.L. Nooner, M.A. Zumberge, R.W. Embley, and C.G. Fox. 2006. Vertical deformation monitoring at Axial Seamount since its 1998 eruption using deep-sea pressure sensors. *Journal of Volcanology and Geothermal Research* 150(1):313–327, <https://doi.org/10.1016/j.jvolgeores.2005.07.006>.
- Chadwick, W.W., Jr., J.B. Paduan, D.A. Clague, B.M. Dreyer, S.G. Merle, A.M. Bobbitt, D.W. Caress, B.T. Philip, D.S. Kelley, and S.L. Nooner. 2016. Voluminous eruption from a zoned magma body after an increase in supply rate at Axial Seamount. *Geophysical Research Letters* 43(23):12,063–12,070, <https://doi.org/10.1002/2016GL071327>.
- Chase, R., J. Delaney, J. Karsten, H. Johnson, S. Juniper, J. Lupton, S. Scott, V. Tunnicliffe, R. Hammond, and R. McDuff. 1985. Hydrothermal vents on an axis seamount of the Juan de Fuca ridge. *Nature* 317(5999):212–214, <https://doi.org/10.1038/313212a0>.
- Clague, D.A., J.B. Paduan, D.W. Caress, W.W. Chadwick Jr., M. Le Saout, B.M. Dreyer, and R.A. Portner. 2017. High-resolution AUV mapping and targeted ROV observations of three historical lava flows at Axial Seamount. *Oceanography* 30(4), <https://doi.org/10.5670/oceanog.2017.426>.
- Cowen, J.P., E.T. Baker, and R.W. Embley. 2004. Detection of and response to mid-ocean ridge magmatic events: Implications for the subsurface biosphere. Pp. 227–243 in *The Subseafloor Biosphere at Mid-Ocean Ridges*. W.S.D. Wilcock, E.F. DeLong, D.S. Kelley, J.A. Baross, and S.C. Cary, eds, *Geophysical Monograph Series*, vol. 144, American Geophysical Union, Washington, DC.
- Delaney, J.R., D.S. Kelley, M.D. Lilley, D.A. Butterfield, J.A. Baross, W.S.D. Wilcock, R.W. Embley, and M. Summit. 1998. The quantum event of oceanic crustal accretion: Impacts of diking at mid-ocean ridges. *Science* 281(5374):222–230, <https://doi.org/10.1126/science.281.5374.222>.
- Duennebier, F.K., N.C. Becker, J. Caplan-Auerbach, D.A. Clague, J. Cowen, M. Cremer, M. Garcia, F. Goff, A. Malahoff, G.M. McMurtry, and others. 1997. Researchers rapidly respond to submarine activity at Loihi Volcano, Hawaii. *Eos, Transactions American Geophysical Union* 78(22):229, <https://doi.org/10.1029/97EO00150>.
- Dziak, R.P., and C.G. Fox. 1999a. Long-term seismicity and ground deformation at Axial Volcano, Juan de Fuca Ridge. *Geophysical Research Letters* 26(24):3,641–3,644, <https://doi.org/10.1029/1999GL002326>.
- Dziak, R.P., and C.G. Fox. 1999b. The January 1998 earthquake swarm at Axial Volcano, Juan de Fuca Ridge: Hydroacoustic evidence of sea-floor volcanic activity. *Geophysical Research Letters* 26(23):3,429–3,432, <https://doi.org/10.1029/1999GL002332>.
- Dziak, R.P., S.R. Hammond, and C.G. Fox. 2011. A 20-year hydroacoustic time series of seismic and volcanic events in the Northeast Pacific Ocean. *Oceanography* 24(3):280–293, <https://doi.org/10.5670/oceanog.2011.79>.
- Dziak, R.P., J.H. Haxel, D.R. Bohnenstiehl, W.W. Chadwick Jr., S.L. Nooner, M.J. Fowler, H. Matsumoto, and D.A. Butterfield. 2012. Seismic precursors and magma ascent before the April 2011 eruption at Axial Seamount. *Nature Geoscience* 5(7):478–482, <https://doi.org/10.1038/ngeo1490>.
- Embley, R.W., K.M. Murphy, and C.G. Fox. 1990. High-resolution studies of the summit of Axial Volcano. *Journal of Geophysical Research* 95(8):12,785–12,812, <https://doi.org/10.1029/JB095iB08p12785>.
- Embley, R.W., W.W. Chadwick Jr., D. Clague, and D. Stakes. 1999. 1998 eruption of Axial Volcano: Multibeam anomalies and sea-floor observations. *Geophysical Research Letters* 26(23):3,425–3,428, <https://doi.org/10.1029/1999GL002328>.

- Fox, C.G. 1990. Evidence of active ground deformation on the mid-ocean ridge: Axial Seamount, Juan de Fuca Ridge, April–June 1988. *Journal of Geophysical Research* 95(B8):12,813–12,822, <https://doi.org/10.1029/JB095iB08p12813>.
- Fox, C.G. 1999. In situ ground deformation measurements from the summit of Axial Volcano during the 1998 volcanic episode. *Geophysical Research Letters* 26(23):3,437–3,440.
- Fox, C.G., W.W. Chadwick Jr., and R.W. Embley. 2001. Direct observation of a submarine volcanic eruption from a sea-floor instrument caught in a lava flow. *Nature* 412(6848):727–729, <https://doi.org/10.1038/35089066>.
- Fox, C.G., R.P. Dziak, H. Matsumoto, and A.E. Schreiner. 1994. Potential for monitoring low-level seismicity on the Juan de Fuca Ridge using military hydrophone arrays. *Marine Technology Society Journal* 27(4):22–30.
- Hammond, S.R., R.W. Embley, and E.T. Baker. 2015. The NOAA vents program 1983 to 2013: Thirty years of ocean exploration and research. *Oceanography* 28(1):160–173, <https://doi.org/10.5670/oceanog.2015.17>.
- Jacobson, R.S., L.D. Bibee, R.W. Embley, and S.R. Hammond. 1987. A microseismicity survey of Axial Seamount, Juan de Fuca Ridge. *Bulletin of the Seismological Society of America* 77(1):160–172.
- Kelley, D.S., J.R. Delaney, and S.K. Juniper. 2014. Establishing a new era of submarine volcanic observatories: Cabling Axial Seamount and the Endeavour Segment of the Juan de Fuca Ridge. *Marine Geology* 352:426–450, <https://doi.org/10.1016/j.margeo.2014.03.010>.
- Lowell, R., and L. Germanovich. 1995. Dike injection and the formation of megaplumes at ocean ridges. *Science* 267(5205):1804, <https://doi.org/10.1126/science.267.5205.1804>.
- Lupton, J., E. Baker, R. Embley, R. Greene, and L. Evans. 1999. Anomalous helium and heat signatures associated with the 1998 Axial Volcano Event, Juan de Fuca Ridge. *Geophysical Research Letters* 26(23):3,449–3,452, <https://doi.org/10.1029/1999GL002330>.
- Manalang, D., and J.R. Delaney. 2016. Axial seamount—restless, wired and occupied: A conceptual overview of resident AUV operations and technologies. Paper presented at OCEANS 2016 MTS/IEEE, September 19–23, 2016, Monterey, CA, <https://doi.org/10.1109/OCEANS.2016.7761305>.
- Martin, W., J. Baross, D. Kelley, and M.J. Russell. 2008. Hydrothermal vents and the origin of life. *Nature Reviews Microbiology* 6:805–814, <https://doi.org/10.1038/nrmicro1991>.
- Nooner, S.L., and W.W. Chadwick Jr.. 2009. Volcanic inflation measured in the caldera of Axial Seamount: Implications for magma supply and future eruptions. *Geochemistry, Geophysics, Geosystems* 10(2), Q02002, <https://doi.org/10.1029/2008GC002315>.
- Nooner, S.L., and W.W. Chadwick Jr. 2016. Inflation-predictable behavior and co-eruption deformation at Axial Seamount. *Science* 354(6318):1,399–1,403, <https://doi.org/10.1126/science.aaa4666>.
- Palmer, M.R., and G.G.J. Ernst. 1998. Generation of hydrothermal megaplumes by cooling of pillow basalts at mid-ocean ridges. *Nature* 393(6686):643–647, <https://doi.org/10.1038/31397>.
- Sohn, R.A., A.H. Barclay, and S.C. Webb. 2004. Microearthquake patterns following the 1998 eruption of Axial Volcano, Juan de Fuca Ridge: Mechanical relaxation and thermal strain. *Journal of Geophysical Research* 109, B01101, <https://doi.org/10.1029/2003JB002499>.
- Summit, M., and J.A. Baross. 1998. Thermophilic sub-seafloor microorganisms from the 1996 North Gorda Ridge eruption. *Deep Sea Research Part II* 45(12):2,751–2,766, [https://doi.org/10.1016/S0967-0645\(98\)00092-7](https://doi.org/10.1016/S0967-0645(98)00092-7).
- Tolstoy, M., F.L. Vernon, J.A. Orcutt, and F.K. Wyatt. 2002. Breathing of the seafloor: Tidal correlations of seismicity at Axial Volcano. *Geology* 30(6):503–506, [https://doi.org/10.1130/0091-7613\(2002\)030<0503:BOSTC>2.0.CO;2](https://doi.org/10.1130/0091-7613(2002)030<0503:BOSTC>2.0.CO;2).
- Tolstoy, M., W.S.D. Wilcock, Y.J. Tan, and F. Waldhauser. 2018. A tale of two eruptions: How data from Axial Seamount led to a discovery on the East Pacific Rise. *Oceanography* 31(1):124–125, <https://doi.org/10.5670/oceanog.2018.118>.
- Tolstoy, T., J.P. Cowen, E.T. Baker, D.J. Fornari, K.H. Rubin, T.M. Shank, F. Waldhauser, D.R. Bohnenstiehl, D.W. Forsyth, R.C. Holmes, and others. 2006. A sea-floor spreading event captured by seismometers. *Science* 314(5807):1,920–1,922, <https://doi.org/10.1126/science.113950>.
- Tréhu, A.M., W.S.D. Wilcock, R. Hilmo, P. Bodin, J. Connolly, E.C. Roland, and J. Braunmiller. 2018. The role of the Ocean Observatories Initiative in monitoring the offshore earthquake activity of the Cascadia subduction zone. *Oceanography* 31(1):104–113, <https://doi.org/10.5670/oceanog.2018.116>.
- West, M., W. Menke, M. Tolstoy, S. Webb, and R. Sohn. 2001. Magma storage beneath Axial Volcano on the Juan de Fuca mid-ocean ridge. *Nature* 413(6858):833–836, <https://doi.org/10.1038/35101581>.
- Wilcock, W.S.D., M. Tolstoy, F. Waldhauser, C. Garcia, Y.J. Tan, D.R. Bohnenstiehl, J. Caplan-Auerbach, R.P. Dziak, A.F. Arnulf, and M.E. Mann. 2016. Seismic constraints on caldera dynamics from the 2015 Axial Seamount eruption. *Science* 354(6318):1,395–1,399, <https://doi.org/10.1126/science.aah5563>.
- Christian Baillard** is Research Associate, School of Oceanography, University of Washington, Seattle, WA, USA. **Tai-Kwan Lau** is Applied Mathematician, and **Joseph H. Haxel** is Assistant Professor, both at Oregon State University/Cooperative Institute for Marine Resources Studies, and NOAA/PMEL, Newport, Oregon, USA. **Yen Joe Tan** is a graduate student at Lamont-Doherty Earth Observatory of Columbia University, Palisades, NY, USA. **Charles Garcia** is a graduate student in the School of Oceanography, University of Washington, Seattle, WA, USA. **Samuel Levy** is a graduate student in the Department of Marine, Earth, and Atmospheric Sciences, North Carolina State University, Raleigh, NC, USA. **M. Everett Mann** is a graduate student in the Department of Earth and Atmospheric Sciences, Cornell University, Ithaca, NY, USA.
- ARTICLE CITATION**
- Wilcock, W.S.D., R.P. Dziak, M. Tolstoy, W.W. Chadwick Jr., S.L. Nooner, D.R. Bohnenstiehl, J. Caplan-Auerbach, F. Waldhauser, A.F. Arnulf, C. Baillard, T.-K. Lau, J.H. Haxel, Y.J. Tan, C. Garcia, S. Levy, and M.E. Mann. 2018. The recent volcanic history of Axial Seamount: Geophysical insights into past eruption dynamics with an eye toward enhanced observations of future eruptions. *Oceanography* 31(1):114–123, <https://doi.org/10.5670/oceanog.2018.117>.

ACKNOWLEDGMENTS

We thank John Delaney, Deborah Kelley, and the OOI Cabled Array team for their efforts to design, install, and operate the Cabled Array. This work was supported by the National Science Foundation under awards OCE-1536219, 1536320, 1546616, 1356216, 1635276, and 1357076. This paper is Pacific Marine Environmental Laboratory contribution number 4715.

AUTHORS

William S.D. Wilcock (wilcock@uw.edu) is Jerome M. Paros Endowed Chair in Sensor Networks, School of Oceanography, University of Washington, Seattle, WA, USA. **Robert P. Dziak** is Acoustics Program Manager, National Oceanic and Atmospheric Administration/Pacific Marine Environmental Laboratory (NOAA/PMEL), Newport, OR, USA. **Maya Tolstoy** is Professor, Lamont-Doherty Earth Observatory of Columbia University, Palisades, NY, USA. **William W. Chadwick Jr.** is Professor, Oregon State University/Cooperative Institute for Marine Resources Studies, and NOAA/PMEL, Newport, Oregon, USA. **Scott L. Nooner** is Associate Professor, University of North Carolina Wilmington, Wilmington, NC, USA. **DelWayne R. Bohnenstiehl** is Associate Professor, Department of Marine, Earth, and Atmospheric Sciences, North Carolina State University, Raleigh, NC, USA. **Jacqueline Caplan-Auerbach** is Associate Professor, Geology Department, Western Washington University, Bellingham, WA, USA. **Felix Waldhauser** is Lamont Research Professor, Lamont-Doherty Earth Observatory of Columbia University, Palisades, NY, USA. **Adrien F. Arnulf** is Research Associate, Institute for Geophysics, Jackson School of Geosciences, University of Texas, Austin, TX, USA.

A Tale of Two Eruptions

HOW DATA FROM AXIAL SEAMOUNT LED TO A DISCOVERY ON THE EAST PACIFIC RISE

By Maya Tolstoy,
William S.D. Wilcock,
Yen Joe Tan, and
Felix Waldhauser

ABSTRACT. Mid-ocean ridge volcanism generates two-thirds of the surface of our planet and plays an important role in chemical exchange with the overlying ocean, yet little is known about the dynamic processes involved in mid-ocean ridge eruptions. This is largely due to the costs and challenges of deploying long-term instrumentation on the seafloor, particularly those that transmit data to shore in real time and would allow the scientific community to respond to and coalesce around a particular event. The 2015 eruption at Axial Seamount, which lies along the Juan de Fuca Ridge in the Northeast Pacific Ocean, resulted in the first in situ, real-time geophysical data collected during a mid-ocean ridge eruption. The results provided insights into the caldera fault structure and response to a seafloor-spreading episode, and also confirmed the origin of seismically recorded impulsive signals that are associated with fresh lava erupting onto the seafloor. This confirmation of a seismic signal associated with erupting lava led to revisiting data from an eruption almost a decade earlier and a fundamental new view of seafloor spreading at fast-spreading ridges thousands of kilometers from Axial Seamount. This example illustrates the point that even though cabled observatories are necessarily bound to a specific location, their results can have significant implications for understanding systems that are quite different, in far reaches of the globe.

Fresh lava from a 2006 East Pacific Rise eruption overlying lava from an older seafloor eruption. Photo credit:
Dan Fornari/Woods Hole Oceanographic Institution/NSF

Real-time, open-access geophysical data collected from the deep-sea floor have long held great promise for understanding dynamic seafloor processes, in particular, mid-ocean ridge eruptions. The benefits of streaming data live to the science community include the ability to respond quickly to events of interest, the ability to monitor instrument status, and the collective engagement of the interested community. While the benefits of having access to real-time data are obvious to scientists studying a particular site, it is perhaps less obvious how these data can also benefit understanding of seafloor processes far away in analogous settings.

In April 2015, a seafloor eruption at Axial Seamount was captured live on geophysical instruments attached to the Ocean Observatories Initiative (OOI) Cabled Array (Wilcock et al., 2018, in this issue, and references therein). The eruption came just months after live-streaming seismic data had become openly available, and two days after conclusion of a workshop that discussed science at Axial Seamount. Community engagement was high, as an eruption was forecast to be imminent. The ability to geophysically observe a seafloor eruption live for the first time generated substantial excitement, and different signals were discussed, analyzed, and shared rapidly through emails as new data were received. Although a formal discussion platform did not exist, the email list grew and generated a dynamic collective discussion that brought multiple perspectives to interpreting the event unfolding at Axial Seamount. This was the real-time event the community had been preparing for.

One observation of a waterborne impulsive signal was discussed at length and interpreted to be associated with lava erupting onto the seafloor (Wilcock et al., 2016). Such signals had previously been hypothesized as being associated with seafloor eruptions (e.g., Caplan-Auerbach and Duennebier, 2001; Schlindwein and Riedel, 2010), but not clearly demonstrated as such in the field. The timing of the multiple water bounce arrivals (Figure 1) on

multiple instruments allowed rapid estimation of the source locations. Initial locations were soon confirmed to be associated with new lava flows (Chadwick et al., 2016). The exact cause of these signals is yet to be determined (Tan et al., 2016; Wilcock et al., 2016), but they could be related to steam explosions (Perfit et al., 2003; Chadwick et al., 2016), pillow implosions or degassing (Caplan-Auerbach and Duennebier, 2001; Schlindwein and Riedel, 2010), other lava-seawater interactions, or a mix of causes (Figure 2). Regardless of the cause, these signals provide a newly ground truthed way to establish the timing of lava reaching the seafloor, a critical factor in understanding eruption dynamics.

As a result of this observation, data from the only previous in situ seismically observed seafloor eruption, at 9°50'N on the East Pacific Rise (Tolstoy et al., 2006), were revisited. These data were limited to three ocean bottom seismometers, in part because two-thirds of the original array was buried in the lava flow. However, a number of the recovered instruments also had hard drive issues unrelated to the eruption that were not known until after recovery, illustrating another important limitation of non-real-time data. Therefore, analysis of available earthquake data was quite limited. The eruption period was dominated by many small impulsive seismic events that were not consistent with earthquake travel times between instruments, and thus were thought to perhaps be isolated

small events happening very near individual instruments.

On reexamining the East Pacific Rise data, it was clear these signals were not small local earthquakes, but instead impulsive signals similar to those observed during Axial Seamount's eruption. When these waterborne arrivals were revisited, their locations correlated remarkably well with the previously mapped lava flows (Soule et al., 2007; Tan et al., 2016), addressing a long-standing debate about the timing of that eruption, and providing a whole new insight into how mid-ocean ridges erupt. The results showed that the majority of the lava erupted within a matter of days in January 2006; flows could even be tracked moving down the flanks of the ridge axis. Most interesting was the timing of the eruption with respect to the largest earthquakes, which suggested that the East Pacific Rise erupted largely in response to the rupture of the plate rather than in response to buildup of magma pressure (Tan et al., 2016). This is in contrast to what is expected at most volcanoes, where magma pressure is solely driving the seismic and eruptive activity, and different to what was observed at Axial Seamount in 2015.

Of particular note when comparing the geophysical signals leading up to and during both eruptions is the difference in timing of the magmatic tremor. At Axial Seamount, six hours of tremor (inferred to be magma movement) preceded the seismic crisis that led to the eruption (Wilcock et al., 2016). At the East Pacific

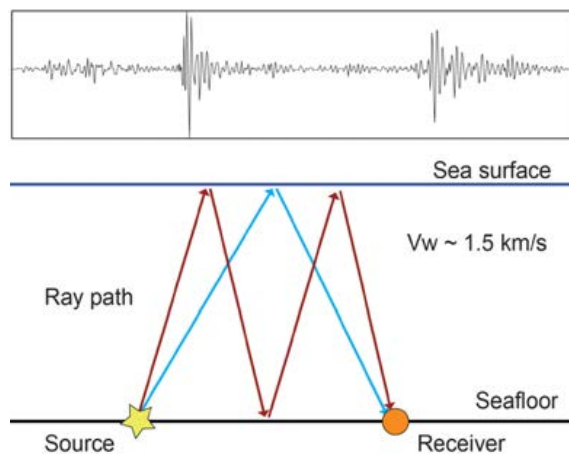


FIGURE 1. Illustration of ray paths taken by the first two arrivals of the waterborne impulsive signal observed to be associated with lava eruption, with an example waveform show at the top. The blue ray is the first arrival and the red ray is the second arrival. At Axial Seamount, more than two arrivals were often observed associated with a single event (Wilcock et al., 2016). With good knowledge of the regional water depth, the velocity of sound in water, and signal arrival times, the events could be accurately located using multiple instruments.

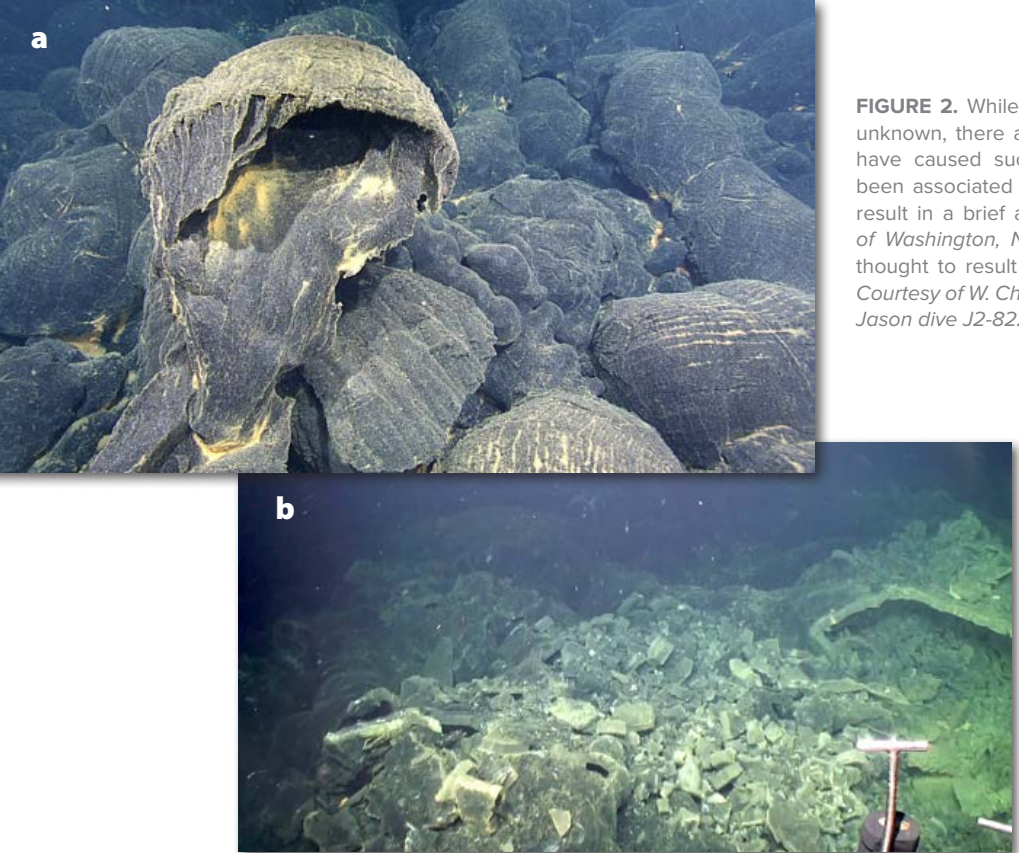


FIGURE 2. While the exact source of the impulsive signals is still unknown, there are multiple examples of lava features that might have caused such signals. (a) A drained pillow that may have been associated with degassing or other phenomenon that might result in a brief acoustic source. Courtesy of D. Kelley, University of Washington, NSF/OOI-ROPOS dive R1863 (TN326). (b) Rubble thought to result from a steam explosion (Chadwick et al., 2016). Courtesy of W. Chadwick, NOAA-Pmel and Oregon State University, Jason dive J2-822 (TN327).

Perfit, M.R., J.R. Cann, D.J. Fornari, J. Engels, D.K. Smith, W.I. Ridley, and M.H. Edwards. 2003. Interaction of sea water and lava during submarine eruptions at mid-ocean ridges. *Nature* 426:62–65, <https://doi.org/10.1038/nature02032>.

Schlindwein, V., and C. Riedel. 2010. Location and source mechanism of sound signals at Gakkel ridge, Arctic Ocean: Submarine Strombolian activity in the 1999–2001 volcanic episode. *Geochemistry, Geophysics, Geosystems* 11, Q01002, <https://doi.org/10.1029/2009GC002706>.

Soule, S.A., D.J. Fornari, M.R. Perfit, and K.H. Rubin. 2007. New insights into mid-ocean ridge volcanic processes from the 2005–2006 eruption of the East Pacific Rise, 9°46'N–9°56'N. *Geology* 35:1,079–1,082, <https://doi.org/10.1130/G23924A.1>.

Tan, Y.J., M. Tolstoy, F. Waldhauser, and W.S.D. Wilcock. 2016. Dynamics of a sea-floor spreading episode at the East Pacific Rise. *Nature* 540:261–265, <https://doi.org/10.1038/nature20116>.

Tolstoy, M., J.P. Cowen, E.T. Baker, D.J. Fornari, K.H. Rubin, T.M. Shank, F. Waldhauser, D.R. Bohnenstiehl, D.W. Forsyth, R.C. Holmes, and others. 2006. A sea-floor spreading event captured by seismometers. *Science* 314(5827):1,920–1,922, <https://doi.org/10.1126/science.1133950>.

Wilcock, W.S.D., M. Tolstoy, F. Waldhauser, C. Garcia, Y.J. Tan, D.R. Bohnenstiehl, J. Caplan-Auerbach, R.P. Dziak, A.F. Arnulf, and M.E. Mann. 2016. Seismic constraints on caldera dynamics from the 2015 Axial Seamount eruption. *Science* 354(6318):1,395–1,399, <https://doi.org/10.1126/science.aaa5563>.

Wilcock, W.S.D., R.P. Dziak, M. Tolstoy, W.W. Chadwick Jr., S.L. Nooner, D.R. Bohnenstiehl, J. Caplan-Auerbach, F. Waldhauser, A.F. Arnulf, C. Baillard, and others. 2018. The recent volcanic history of Axial Seamount: Geophysical insights into past eruption dynamics with an eye toward enhanced observations of future eruptions. *Oceanography* 31(1):114–123, <https://doi.org/10.5670/oceanog.2018.117>.

ACKNOWLEDGMENTS

The authors thank W. Chadwick and D. Kelley for making Figure 2 photographs available, and J. Karson and an anonymous reviewer for comments that substantially improved the manuscript. This work was supported by the National Science Foundation under awards OCE-1536320, OCE-1536219, and OCE-0961594.

AUTHORS

Maya Tolstoy (tolstoy@ldeo.columbia.edu) is Professor, Lamont-Doherty Earth Observatory of Columbia University, Palisades, NY, USA.

William S.D. Wilcock is Jerome M. Paros Endowed Chair in Sensor Networks, School of Oceanography, University of Washington, Seattle, WA, USA. **Yen Joe Tan** is a graduate student and **Felix Waldhauser** is Professor, Lamont-Doherty Earth Observatory of Columbia University, Palisades, NY, USA.

ARTICLE CITATION

Tolstoy, M., W.S.D. Wilcock, Y.J. Tan, and F. Waldhauser. 2018. A tale of two eruptions: How data from Axial Seamount led to a discovery on the East Pacific Rise. *Oceanography* 31(1):124–125, <https://doi.org/10.5670/oceanog.2018.118>.

Rise, however, approximately one hour of tremor (long-period events) followed the initiation of the seismic crisis. The tremor at the East Pacific Rise appeared within tens of minutes following the largest earthquakes recorded at the site in a decade (Dziak et al., 2009), and ended 36 minutes prior to lava first reaching the seafloor (Tan et al., 2016). This timing is consistent with the tremor resulting from magma response to failure of the plate boundary. This contrast in relative timing of the tremor to the seismic crisis implies that at Axial Seamount, magma pressure played a key role in the timing of the eruption, whereas at the East Pacific Rise, the buildup of tectonic stress due to plate pull led to rupture of the plate boundary. It is possible that magma pressure may also have contributed to initiation of the eruption at the East Pacific Rise, but the timing of the eruption is interpreted as largely responding to the rupture.

Comparison of the seafloor eruptions shows that they represent two end members: Axial Seamount displays classic ring-fault caldera dynamics (Wilcock et al., 2016), while the East Pacific Rise demonstrates that mid-ocean ridge eruptions can result from a “tear”

in the seafloor (Tan et al., 2016). While the East Pacific Rise at 9°50'N is viewed as a “typical” fast-spreading ridge, Axial Seamount by contrast is a feature of the Cobb-Eickelberg hotspot that interacts with the intermediate-spreading Juan de Fuca Ridge. This fundamental difference between ridge-based hotspot volcanism and non-hotspot-influenced mid-ocean ridge magmatism remains to be demonstrated elsewhere and at other spreading rates. However, it provides an exciting template to test these two models, both in further eruptions at Axial Seamount and eruptions elsewhere on the deep seafloor.

REFERENCES

- Caplan-Auerbach, J., and F. Duennebier. 2001. Seismic and acoustic signals detected at Lo'ihi Seamount by the Hawai'i Undersea Geo-Observatory. *Geochemistry, Geophysics, Geosystems* 2, 1024, <https://doi.org/10.1029/2000GC000113>.
- Chadwick, W.W., Jr., J.B. Paduan, D.A. Clague, B.M. Dreyer, S.G. Merle, A.M. Bobbitt, D.W. Caress, B.T. Philip, D.S. Kelley, and S.L. Nooner. 2016. Voluminous eruption from a zoned magma body after an increase in supply rate at Axial Seamount. *Geophysical Research Letters* 43:12,063–12,070, <https://doi.org/10.1002/2016GL071327>.
- Dziak, R.P., D.R. Bohnenstiehl, H. Matsumoto, M. Fowler, J. Haxel, M. Tolstoy, and F. Waldhauser. 2009. January 2006 seafloor-spreading event at 9°50'N, East Pacific Rise: Ridge dike intrusion and transform fault interactions from regional hydroacoustic data. *Geochemistry, Geophysics, Geosystems* 10, Q06T06, <https://doi.org/10.1029/2009GC002388>.

SIDE BAR Axial Seamount Biology Catalog By Katie Bigham

http://www.interactiveoceans.washington.edu/story/Biology_at_Axial_Seamount

The deep waters overlying the Juan de Fuca Plate host amazing life forms, yet rarely are they viewed by humans, nor are most well documented digitally. Undergraduate participants in the University of Washington VISIONS '14 educational program (http://interactiveoceans.washington.edu/story/VISIONS_14) recognized this lack of available information on deep-sea organisms that live in perpetual darkness in some of the most extreme environments on Earth. This experiential learning opportunity for undergraduates took place during the 85-day construction cruise for the National Science Foundation's Regional Cabled Array, a component of the Ocean Observatories Initiative (OOI). During the VISIONS programs, students stood daily watches inside remotely operated vehicle (ROV) control labs, working alongside scientists, engineers, and the ship and ROV teams, to conduct their own research and outreach projects, and to learn about ship life.

In 2014, seven undergraduates saw a need, based on their watch-standing experience, for a comprehensive resource to address their continual question: what do you think that animal is? An online biology catalog was conceived as a resource for both scientists and the public to make it easier to identify animals observed during the annual cruises and in the video and digital still imagery streaming live back to shore from the Regional Cabled Array. As an initial effort, the students focused on the OOI cabled site called Axial Seamount, an active underwater volcano that erupted in 1998, 2011, and 2015 (see Wilcock et al., 2018, in this issue), to create a resource for identifying organisms. Thus, the Axial Seamount Biology Catalog was born.

"Best hit" high-definition video and digital still images collected by ROV-mounted cameras from 2011 to 2017 have been logged, edited, and documented by VISIONS students. The catalog currently contains images and video of 39 species, including octopuses, crabs, jellies, sea stars, and fish. Along with the video and images, students researched and compiled short descriptions of the animals' feeding habits, behaviors, and

environmental ranges. Entries include animals observed in the water column, on the seafloor, and interacting with Regional Cabled Array infrastructure.

The catalog was designed so that it could be expanded and improved over time. Indeed, on operation and maintenance cruises in 2015 and 2017, undergraduates continued to refine and add to its content. Student contributor backgrounds range from oceanography to biology, business, music, and engineering. The project has engaged students in the research process, provided a wealth of sea-going experiences, and led to the creation of a one-of-a-kind resource for Northeast Pacific biology. The resulting continually growing repository of HD video and digital still imagery is being used by numerous scientists, educators, news agencies, and documentary producers.

Images and videos from the Axial Seamount Biology Catalog can be viewed on the OOI Regional Cabled Array's website (see url above). Visitors with an interest, or expertise in, these deep-sea organisms are encouraged to suggest additions or revisions. Work is underway to include entries from coastal research sites as the current student contributors compile more images and information.

REFERENCE

Wilcock, W.S.D., R.P. Dziak, M. Tolstoy, W.W. Chadwick Jr., S.L. Nooner, D.R. Bohnenstiehl, J. Caplan-Auerbach, F. Waldhauser, A.F. Arnulf, C. Baillard, and others. 2018. The recent volcanic history of Axial Seamount: Geophysical insights into past eruption dynamics with an eye toward enhanced observations of future eruptions. *Oceanography* 31(1):114–123, <https://doi.org/10.5670/oceanog.2018.117>.

AUTHOR

Katie Bigham (bighamkt@uw.edu) is Oceanographer, University of Washington, Seattle, WA, USA.

ARTICLE CITATION

Bigham, K. 2018. Axial Seamount Biology Catalog. *Oceanography* 31(1):127, <https://doi.org/10.5670/oceanog.2018.119>.

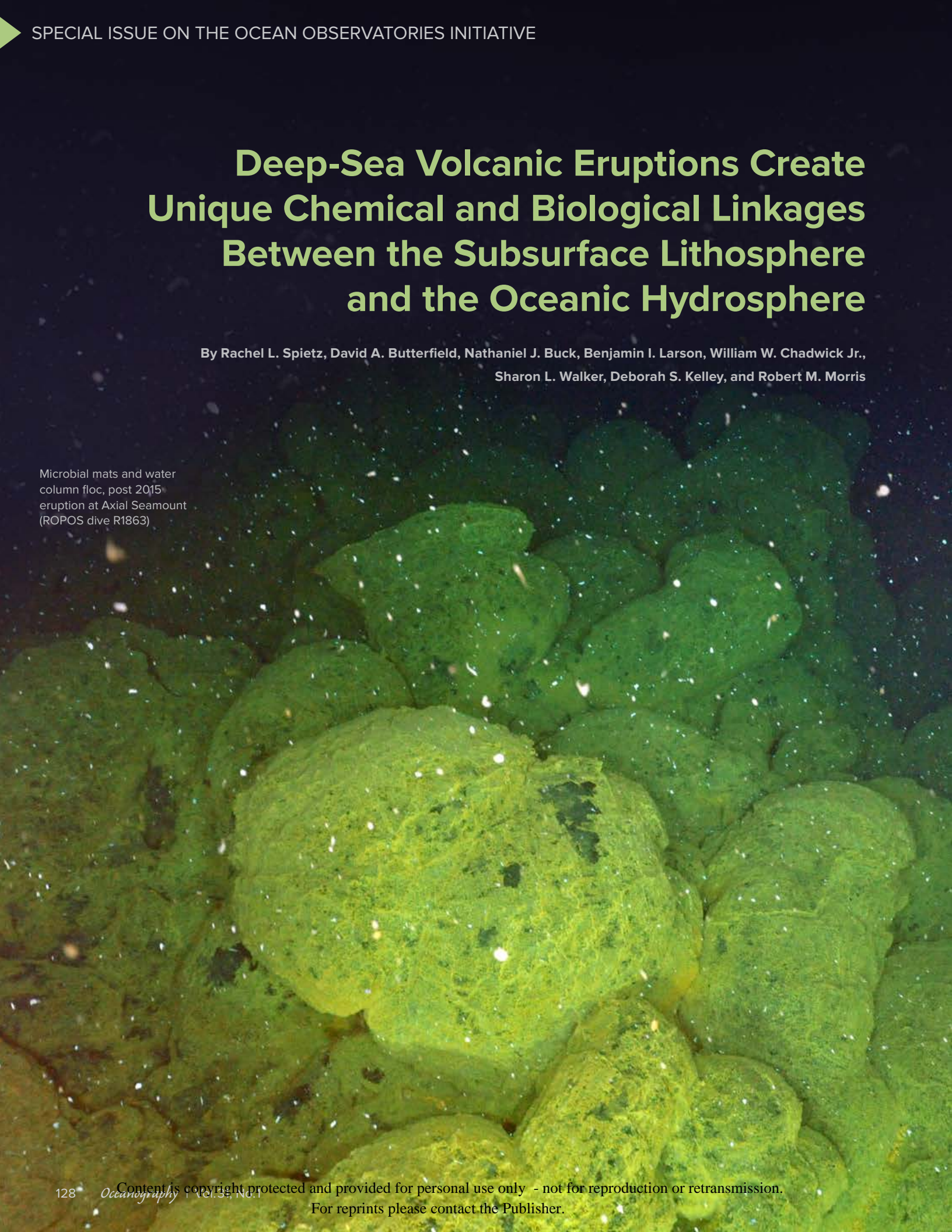
FIGURE 1. This *Graeledone* octopus was photographed near the Escargot hydrothermal vent at Axial Seamount during VISIONS '14 with the remotely operated vehicle ROPOS. Water depth is 1,515 m. Photo credit: NSF-OOI/UW/CSSF; Dive R1723; V14



Deep-Sea Volcanic Eruptions Create Unique Chemical and Biological Linkages Between the Subsurface Lithosphere and the Oceanic Hydrosphere

By Rachel L. Spietz, David A. Butterfield, Nathaniel J. Buck, Benjamin I. Larson, William W. Chadwick Jr.,
Sharon L. Walker, Deborah S. Kelley, and Robert M. Morris

Microbial mats and water column floc, post 2015 eruption at Axial Seamount (ROPOS dive R1863)



ABSTRACT. In April 2015, pressure recorders, seismometers, and hydrophones attached to the Ocean Observatories Initiative (OOI) Cabled Array on Axial Seamount detected, in real time, a volcanic eruption predominantly located along the north rift zone (NRZ). Real-time detection enabled a rapid response cruise to augment OOI data with ship-based physical, chemical, and biological sampling of the eruption and the new lava flows. The combined data set demonstrates the synergistic value of real-time monitoring combined with rapid response efforts that sample beyond the boundaries of a fixed cabled array. These combined data show that the 2015 eruption gave rise to chemically and microbiologically variable hydrothermal plumes over new NRZ lava flows, reflecting chemical and biological linkages between the subsurface lithosphere and the oceanic hydrosphere. The warmest and least diluted plume near the new lava flows was 0.119°C above background seawater and hosted thermophilic and hyperthermophilic taxa that are typically identified in hydrothermal fluids emanating from the warm subsurface. Cooler and more diluted hydrothermal plumes farther from a hydrothermal fluid source were 0.072°–0.078°C above background seawater and hosted mesophilic and psychrophilic taxa that are typically identified in neutrally buoyant plumes at persistent hydrothermal venting sites. Potentially chemosynthetic microbial lineages, including Epsilonproteobacteria, Gammaproteobacteria, and Methanococcales, were positively correlated with elevated temperature anomalies. These data suggest that hydrothermal fluid flow through new lava flows on the NRZ supported diverse microbial communities for several months following the 2015 eruption and that subsurface heterogeneity contributed to the structure of unique hydrothermal-plume-hosted microbial communities.

BACKGROUND

Axial Seamount is the largest and most active volcano on the Juan de Fuca Ridge spreading center. Annual research cruises have collected chemical, geological, and biological data at Axial Seamount for more than three decades, making this one of the longest time series for a deep-sea volcanically driven hydrothermal system. In 1998, an eruption on Axial's south rift zone was remotely detected by US Navy hydrophones (Dziak and Fox, 1999; Chadwick et al., 2013). Axial Seamount erupted again in 2011 along the south rift zone, resulting in lava flows inside and outside the caldera with numerous “snow blower” vents that emitted white floc from dense eruption-associated microbial mats (Caress et al., 2012; Meyer et al., 2013; Kelley et al., 2014). In 2014, the Ocean Observatories Initiative (OOI) completed installation of a regional cabled observatory that spans the Juan de Fuca Plate with nodes at Axial Seamount

that include over 20 cabled instruments within the caldera (Kelley et al., 2016).

The OOI Cabled Array detected in real time the most recent eruption, which started on April 24, 2015, and lasted for several weeks (Nooner et al., 2016; Wilcock et al., 2016). These data were critical for identifying new lava flows, capturing for the first time the locations and timing of earthquakes and explosive events as they occurred. The data suggest that activity was focused along Axial's north rift zone (NRZ), and this location was confirmed by depth changes detected by bathymetric resurveys and remotely operated vehicles in July and August 2015 (Chadwick et al., 2016; Kelley et al., 2016). The thickest new lava flows were covered by microbial mats, and there were numerous sites of hydrothermal flow (Chadwick et al., 2016; Kelley et al., 2016). The bathymetric and visual observations detected 11 new lava flows from at least 13 new fissures along the NRZ and within Axial

caldera (Chadwick et al., 2016), with a combined volume of $1.48 \times 10^8 \text{ m}^3$, making the 2015 eruption the largest volume of lava documented since data collection began in the mid-1980s. The morphology and chemical composition of separate lava flows varied from thin sheet flows within the caldera to much thicker and more evolved (lower MgO) pillow lava along the NRZ (Chadwick et al., 2016).

Eruptive events at mid-ocean ridges are responsible for high fluxes in heat, chemicals, and biological matter from the subsurface (Baker et al., 1987; Butterfield et al., 1997; Delaney et al., 1998). Previous studies show that abrupt changes in the seafloor's physical and chemical environment and the overlying water column follow eruptive events and influence the structure and activity of local microbial communities (Huber et al., 2002, 2003). For example, fresh basalt in areas of hydrothermal flow after eruptive events is rapidly colonized by microbes (Gulmann et al., 2015). These benthic biofilms are dominated by chemolithoautotrophs (Meyer et al., 2013) that support seafloor communities at hydrothermal systems for months to years following eruptions (Tunnicliffe et al., 1997).

Eruptions can produce new venting of hydrothermal fluids due to increased permeability of the crust and new heat sources such as subseafloor magma and freshly erupted lava fields that are still cooling (Baker, 1998; Baker et al., 2004). Neutrally buoyant hydrothermal plumes from long-lived vents are a mixture of entrained background seawater and <0.01% of subsurface-derived hydrothermal fluid (Lupton et al., 1985). A recent high-resolution spatial study of hydrothermal vent plumes along the Eastern Lau Spreading Center suggests that ubiquitous deep-sea microbes populate plume microbial communities, while the contribution of subsurface microbial taxa to plume communities is secondary as

a result of extreme dilution within the hydrothermal plume (Sheik et al., 2015). Yet, some subsurface bacteria, such as sulfur-oxidizing Epsilonproteobacteria, demonstrate strong distance-decay relationships within plumes, with high abundances near the source of hydrothermal flow, and they can be considered indicators of hydrothermal activity (Djurhuus et al., 2017). While distance-decay relationships and high rates of entrainment of background deep-sea microbial communities primarily structure plume microbial communities, the geochemical and physical environment of the subsurface source fluids also impose selective pressures on microbial community composition over time (Huber et al., 2007; Opatkiewicz et al., 2009; Anderson et al., 2013).

Newly established links between the seafloor and subsurface magma sources,

as the result of a deep-sea eruption, have the potential to create variable subseafloor hydrothermal conditions that alter overlying seawater non-uniformly, which may be reflected in the structure of microbial communities in newly formed eruptive hydrothermal plumes. We use physical, chemical, and biological data to characterize hydrothermal plume heterogeneity above new lava flows along the NRZ at Axial Seamount. Our data indicate that differences in subsurface environments associated with new lava flows can create geochemically unique hydrothermal plumes that harbor distinct microbial communities comprised of both deep-ocean and subsurface lineages. This has the potential to significantly impact deep-ocean microbiology, as mid-ocean ridges span 65,000 km of Earth's surface and are responsible for approximately 70% of the volcanic activity on Earth.

RESULTS AND DISCUSSION

Physical and Chemical

Characterization of Distinct Post-Eruption Hydrothermal Plumes

A rapid response cruise was added to the previously planned R/V *Thompson* TN327 expedition to survey the geology, chemistry, and microbiology of new lava flows. CTD tow-yo surveys above the new NRZ lava flows collected continuous measurements for depth, temperature, salinity, and turbidity. Potential temperature and turbidity anomalies verified the presence of near-seafloor hydrothermal plumes 50–100 m thick extending horizontally several kilometers over the northernmost new lava flows (Methods in online Supplementary Materials, Figure 1A, Table 1). It is estimated that 92% of the erupted volume was accounted for in the three northernmost lava flows (#8–#10 using the numbering scheme

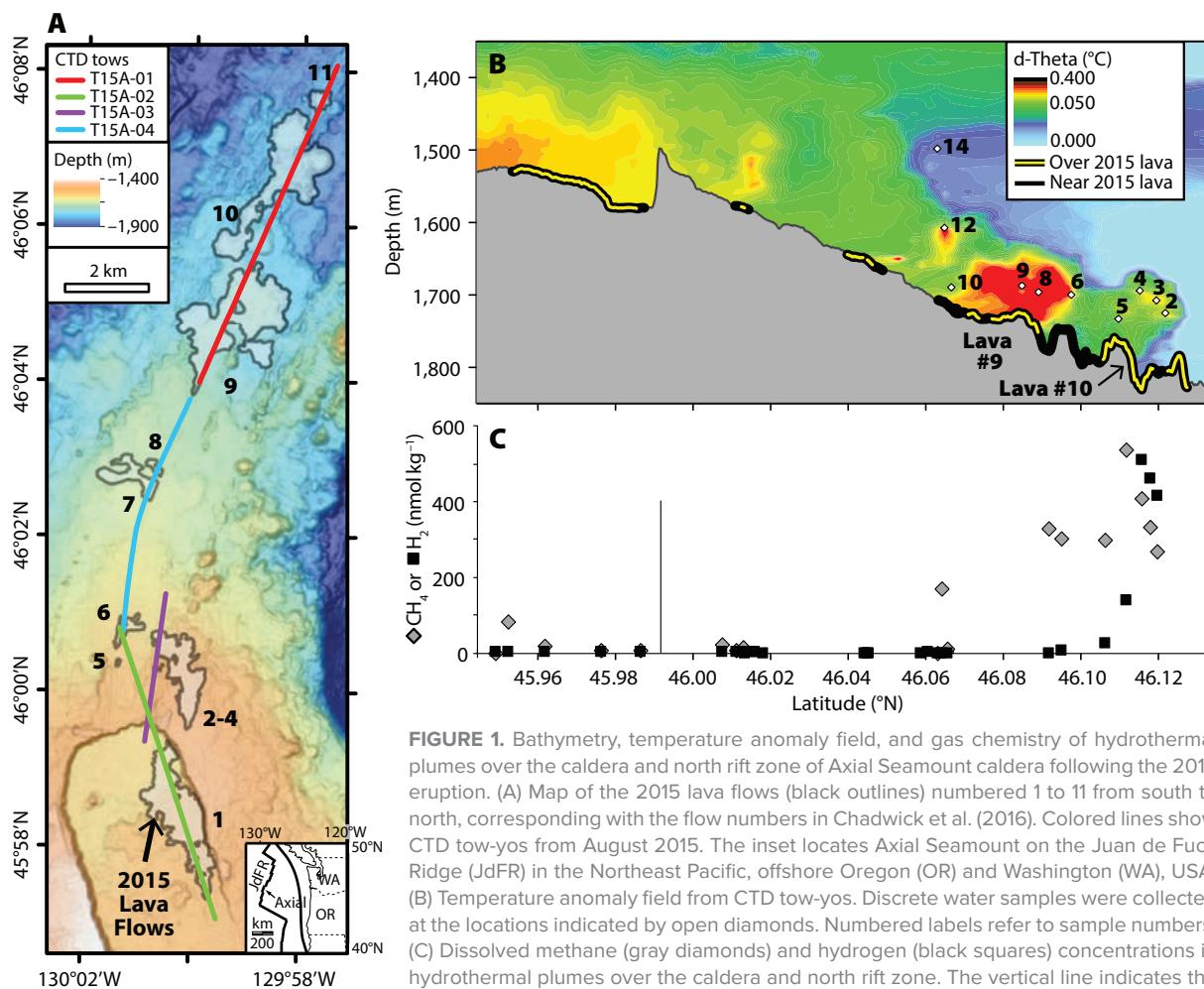


FIGURE 1. Bathymetry, temperature anomaly field, and gas chemistry of hydrothermal plumes over the caldera and north rift zone of Axial Seamount caldera following the 2015 eruption. (A) Map of the 2015 lava flows (black outlines) numbered 1 to 11 from south to north, corresponding with the flow numbers in Chadwick et al. (2016). Colored lines show CTD tow-yos from August 2015. The inset locates Axial Seamount on the Juan de Fuca Ridge (JdFR) in the Northeast Pacific, offshore Oregon (OR) and Washington (WA), USA. (B) Temperature anomaly field from CTD tow-yos. Discrete water samples were collected at the locations indicated by open diamonds. Numbered labels refer to sample numbers. (C) Dissolved methane (gray diamonds) and hydrogen (black squares) concentrations in hydrothermal plumes over the caldera and north rift zone. The vertical line indicates the northern boundary of Axial caldera.

from south to north following Chadwick et al., 2016). Hydrothermal plumes above these thicker northern flows had higher temperature anomalies than plumes overlying thinner new flows within Axial caldera or elsewhere along the NRZ. The plumes over new lava flows #9 and #10 (46.08°N and 46.11°N, respectively) were sampled for further characterization of plume chemistry and microbial microbiology. A total of 44 water-column samples from the caldera, NRZ, and background seawater were analyzed shipboard for methane and hydrogen concentrations. DNA was extracted from a subset of 12 water-column samples, and the microbial community was characterized by 16S rRNA gene sequencing (Methods in online Supplementary Materials).

Temperature and turbidity anomalies, as well as methane and hydrogen concentrations, were not uniform along the NRZ (Figure 1B,C) and showed regions of variability above lava flows #9 and #10 (Table 1). The hydrothermal plume above lava flow #9 (samples 6, 8, and 9) had the highest temperature and turbidity anomalies, measured as ΔNTU (nephelometric turbidity units; Figure 1B, Table 1). The plume over lava flow #10 (samples 2, 3, 4, and 5) was characterized by the highest hydrogen and methane concentrations compared to any other plume along the NRZ or within Axial caldera but had lower temperature and turbidity anomalies than in the plume over lava flow #9 (Figure 1B,C, Table 1). Two samples (10 and 12) were collected within the broader plume, not above a new lava flow, to compare lava-associated plumes with the non-lava associated plume (Figure 1B). Non-lava temperature anomalies were similar to those over lava flow #10 (average 0.078°C), but turbidity anomalies were lower than in both lava-associated plumes ($\Delta\text{NTU} = 0.024$ vs. >0.039). Similarly, methane concentrations in the non-lava plumes were lower than in the lava-associated plumes, and hydrogen concentrations were near zero (Table 1). One background sample was collected at the

NRZ (sample 14) where temperature and turbidity anomalies were not detected. Two additional background samples were collected 24 km northeast of Axial Seamount and at depths corresponding to plume samples above lava flows #9 and #10 (1,500 m and 1,700 m).

Differences in plume conditions above the two NRZ lava flows indicate variability in the subsurface geology, chemistry, and microbiology. While no obvious differences in lava morphology or composition were detected between flows #9 and #10 (Chadwick et al., 2016), the microbial mats covering lava flows were thicker and more orange in color on lava flow #9 relative to lava flow #10. Additionally, the sharp increase in plume hydrogen and methane concentrations over lava flow #10 indicates differences in the chemistry, and possibly microbiology, over the two flows.

Hydrothermal fluids enriched in reduced chemical species fuel high rates of microbial productivity, which are commonly more productive than photosynthetically driven parts of the ocean (Lutz et al., 1994; McCollom and Shock, 1997; Shock and Holland, 1997; McCollom, 2000). Geochemical models predict that most chemosynthetic primary production within vent plumes occurs when

concentrations of hydrogen and sulfide are highest. This condition can occur in the early stages of hydrothermal plume development (McCollom, 2000). Microbial characterization of persistent vent plumes shows that sulfur- and hydrogen-oxidizing autotrophic bacteria dominate vent fluids at their source and are present in diffuse-flow fluids (Sunamura et al., 2004; Anantharaman et al., 2013; Anderson et al., 2013; Mattes et al., 2013). Understanding the heterogeneity in the hydrothermal plumes associated with new lava flows from the 2015 eruptive event is important when considering biogeochemical models of deep-sea eruptions.

Microbiological Characterization of Distinct Post-Eruption Hydrothermal Plumes

To understand how microbial community structure relates to environmental heterogeneity within post-eruptive hydrothermal plumes, we characterized microbial communities in discrete samples collected from the plumes over lava flows #9 and #10, in non-lava associated samples, and in background seawater. Non-metric multidimensional scaling of microbial operational taxonomic units derived from 16S rRNA gene sequence

TABLE 1. Physical and chemical measurements. Discrete samples are categorized by region and match sample numbers as indicated in Figure 1.

Region	Sample (ID)	Depth (m)	Temperature anomaly (°C)	Turbidity anomaly (ΔNTU)	CH_4 (nmol kg ⁻¹)	H_2 (nmol kg ⁻¹)
Lava flow #10	2	1,725	0.070	0.057	333	461
	3	1,708	0.082	0.054	406	508
	4	1,694	0.081	0.039	536	140
	5	1,733	0.054	0.035	297	25
Lava flow #9	6	1,700	0.113	0.134	301	4
	8	1,696	0.121	0.202	NA	NA
	9	1,687	0.122	0.241	NA	NA
Non-lava	10	1,689	0.059	0.024	8	0
	12	1,607	0.096	0.024	168	0
Background	14	1,498	0.012	0.005	NA	NA
	1500	1,500	-0.012	0.001	BDL	1
	1700	1,700	0.000	0.001	1	1

NA = not available (data not collected). BDL = below detection limit. ΔNTU = turbidity anomaly in nephelometric turbidity units.

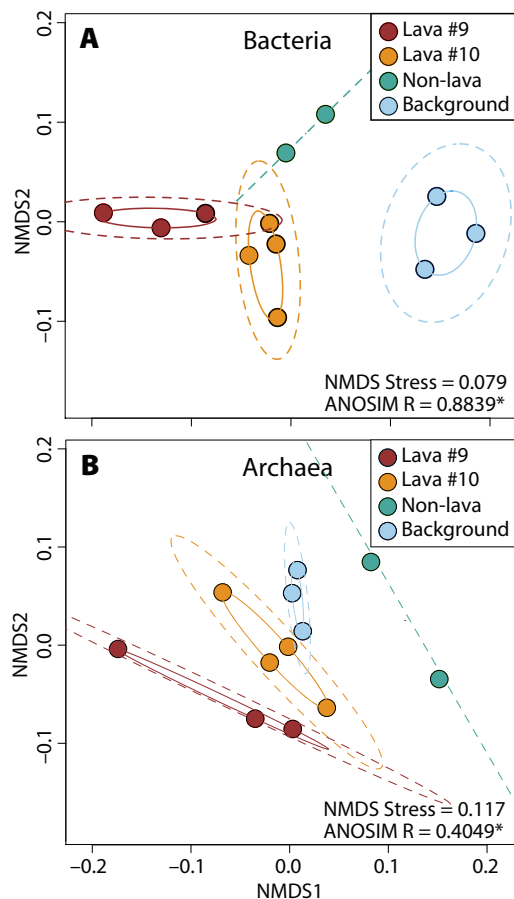
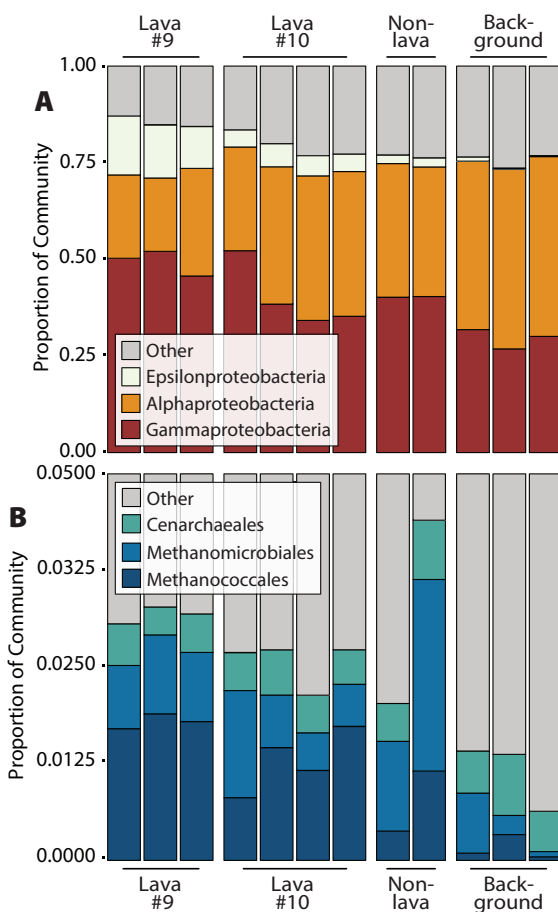


FIGURE 2. Non-metric multidimensional scaling plot of the differences between microbial communities across sampling regions at Axial Seamount following the 2015 eruption. Microbial communities were assessed for (A) bacterial and (B) archaeal composition. Points represent individual samples, and the colors of points represent four distinct sampling regions (above lava flow #10, lava flow #9, or non-lava seafloor, and background seawater not influenced by hydrothermal activity). Solid lines define a convex hull of the set of samples within a group while the dashed-lines show a dispersion ellipse using the standard deviation of sample point scores under a 95% confidence limit. An asterisk indicates $p < 0.01$.



analyses indicates that bacterial community composition was unique within each region (Figure 2A, ANOSIM global $R = 0.8839$, $p < 0.01$). The four regions sampled were also significantly distinct in terms of their archaeal communities (Figure 2B, ANOSIM global $R = 0.4049$, $p < 0.01$). Dispersion ellipses demarcating the standard deviations of sample points within each region indicate that microbial community composition was distinct in each of the four regions sampled.

Distinct bacterial communities were identified over the four different sampling regions even at a broad taxonomic level (Figure 3, Figure S1). The most abundant classes of bacteria were Alphaproteobacteria, Gammaproteobacteria, and Epsilonproteobacteria (Figure 3A). Gammaproteobacteria were dominant in plume regions (40.0% to 49.3%). Alphaproteobacteria dominated communities in background seawater, averaging 45.5% of the bacterial 16S rRNA gene sequences recovered from these samples. Many of the top bacterial classes were strongly correlated with temperature and turbidity anomalies, both indicators of hydrothermal input (Table S1). The Gammaproteobacteria and Epsilonproteobacteria had strong normal relationships with anomalies of temperature (adjusted R^2 : 0.63 and 0.67, respectively) and turbidity (adjusted R^2 : 0.57 and 0.96, respectively) across all 12 samples, while the Alphaproteobacteria had a strong inverse relationship with temperature and turbidity anomalies (adjusted R^2 : 0.78 and 0.74, respectively; Table S1).

Shifts in archaeal communities were also evident, though patterns in distribution were most noticeable among three low abundance orders: Methanococcales, Methanomicrobiales, and Cenarchaeales (Figure 3B). Methanococcales were most abundant in the near-seafloor plume over lava flow #9 (average 1.8%), where temperature anomalies were highest and where there were elevated methane and hydrogen concentrations, and over lava flow #10 (average 1.4%) where temperature anomalies were lower but methane and hydrogen concentrations were highest. Their contribution to archaeal communities decreased significantly in non-lava samples (average 0.8%) and in background seawater (0.2%). The Methanococcales also had the highest correlations with temperature and turbidity anomalies (adjusted R^2 : 0.82 and 0.55, respectively; Table S2). Cultivation-based studies have isolated thermophilic and

FIGURE 3. Proportions of key (A) bacterial classes and (B) archaeal orders detected along the north rift zone of Axial Seamount following the 2015 eruption. Samples are ordered by decreasing turbidity anomaly, a proxy for hydrothermal circulation, from left to right. Samples are classified into four distinct sampling regions: above lava flow #9, lava flow #10, non-lava, and background samples not influenced by hydrothermal activity.

hyperthermophilic hydrogen-consuming Methanococcales with temperature requirements well above the temperature of the hydrothermal plume fluids from which they were sampled (Holden et al., 1998; Summit and Baross, 1998; Topcuoglu et al., 2016). The implication from these studies is that mesophilic and thermophilic microorganisms in the heated subsurface environment are released into seawater (Delaney et al., 1998; Holden et al., 1998; Summit and Baross, 1998).

Strictly methanogenic Methanomicrobiales were most abundant in the non-lava associated samples and least abundant in background seawater. Most members of the Methanomicrobiales are psychrophilic or mesophilic and can use either hydrogen or formate as

electron donors for methanogenesis and acetate as a carbon source (Liu, 2010). It is important to note that while the Methanomicrobiales were most numerous in the non-lava region, their relative abundance compared to other archaeal orders was low (1.82% of archaeal sequences) and that the detection of a 16S rRNA gene sequence in the environment does not imply activity. Therefore, Methanomicrobiales may persist longer than thermophilic and hyperthermophilic methanogens in hydrothermal plumes that cool and become more dilute with entrained seawater, but are likely not contributing as much to methanogenesis within the plume, as indicated by the lower concentrations of methane in mid-plume samples. Methane-oxidizing microbes are known to dominate hydrothermal

plumes at Axial Seamount (Mattes et al., 2013), suggesting that they may contribute to the drawdown in methane in the non-lava associated samples. These data suggest that temperature-dependent niche partitioning among subseafloor methane-producing Methanococcales and Methanomicrobiales is evident in newly formed lava-associated plumes.

Indicator analyses of bacterial taxa detected over new lava flows and in background seawater also suggest that there are detectable differences in species adapted to differences in subsurface temperatures. There were significant increases in the relative abundance of Epsilonproteobacteria in hydrothermal plumes (Figure 4). On average, they accounted for 13.2% of the bacterial community in the higher-temperature

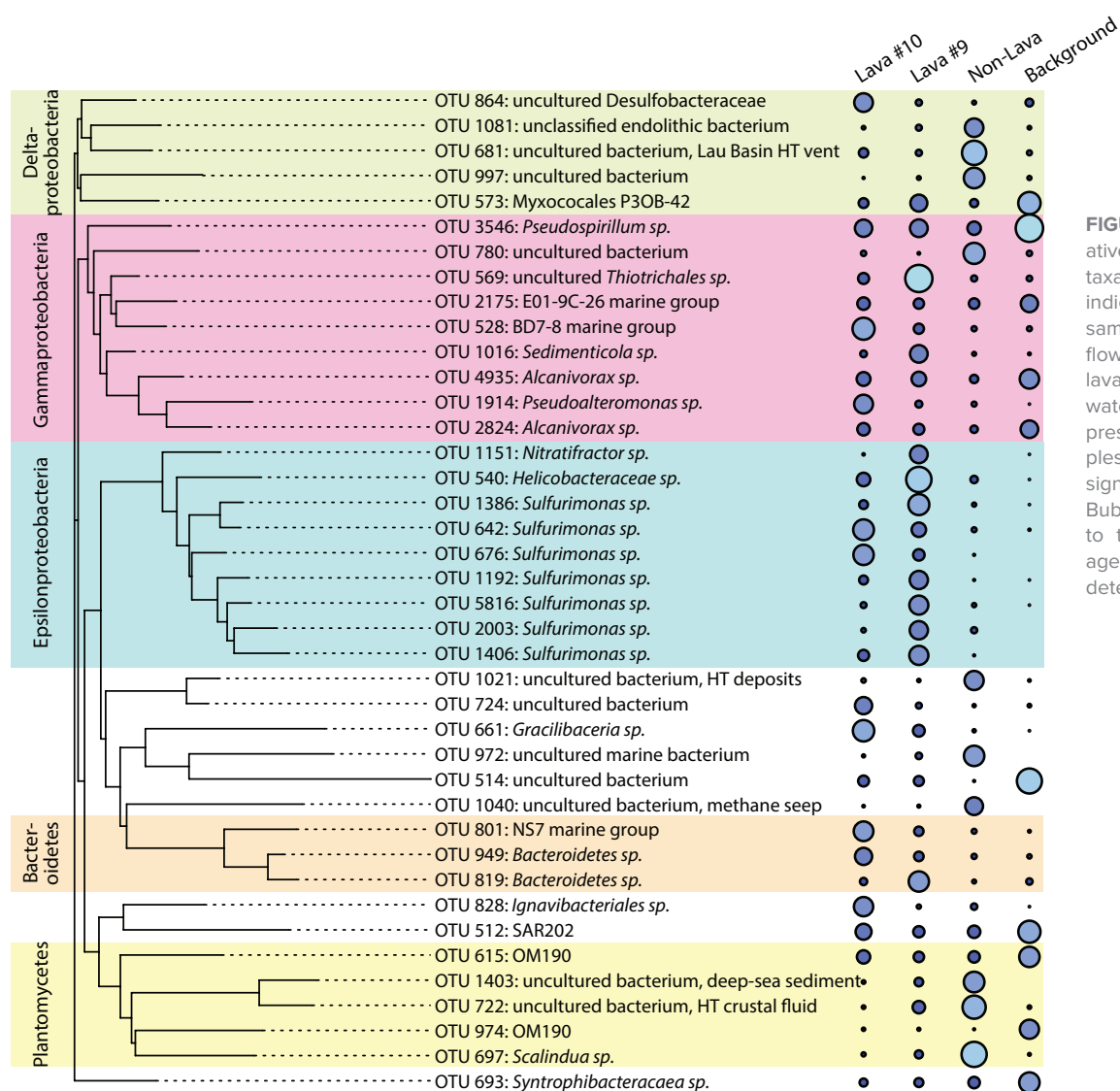


FIGURE 4. Phylogeny and relative abundances of bacterial taxa identified as significant indicators for each distinct sampling region: above lava flow #9, lava flow #10, non-lava, and background seawater. All indicator taxa were present in at least three samples, and indicator values were significant at $\alpha < 0.05$. Bubble size is proportional to the log-transformed average abundance of sequences detected within a region.

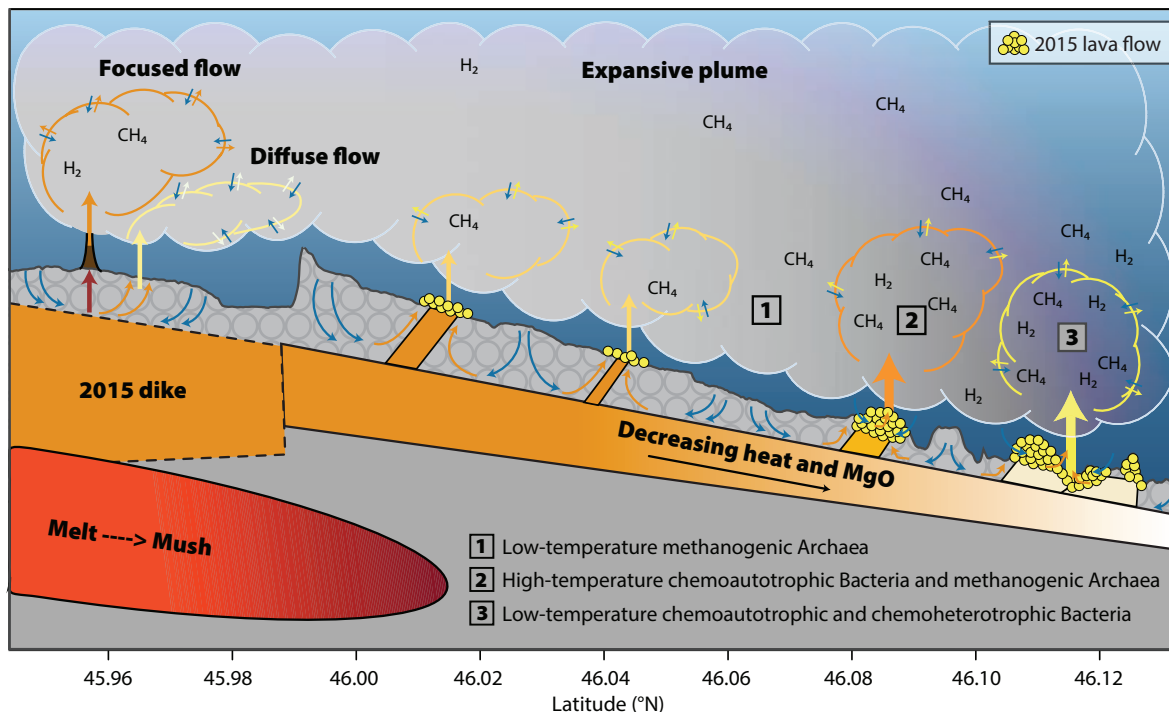


FIGURE 5. Conceptual model showing the different sources of hydrothermal plumes and the implications for overlying seawater microbial communities and chemistry, with interpretation of subsurface processes modified from Chadwick et al. (2016). The weight of arrows corresponds to the estimated relative magnitude of hydrothermal input to plumes. Colors outlining distinct plumes correspond to the relative temperature of the plume, with white being cool and orange being hotter. Lines outlining non-buoyant plumes are theoretical boundaries that are not necessarily distinct but rather gradients between regions of hydrothermal input from the subsurface and background seawater. Numbered boxes indicate microbial functional groups strongly associated with each plume region. Note that the vertical axis is exaggerated to show detail.

plume over lava flow #9 and only 0.6% in background seawater. Indicator analyses suggest that thermophilic taxa from the Epsilonproteobacteria, including *Sulfurimonas* sp., are significant indicators in these plumes. These data support the hypothesis proposed by Djurhuus et al. (2017) that members of the mesophilic/thermophilic sulfur-oxidizing Epsilonproteobacteria are strong indicators of hydrothermal activity. We add that individual taxa within the Epsilonproteobacteria demonstrate preferences for different temperature ranges or subsurface geochemistry, which affects the distribution of different taxa across plumes of varying origin (Figures 3 and 4).

CONCLUSIONS

Real-time data from the OOI Cabled Array at Axial Seamount enabled a rapid response expedition to characterize the geochemistry and microbiology of

post-eruptive hydrothermal plumes overlying new lava flows from the 2015 eruption. Our results suggest that differences in the hydrothermal sources associated with distinct lava flows and their subsurface feeder dikes create near-seafloor plume environments that are chemically and microbiologically distinct from upper, non-buoyant hydrothermal plumes. We present a conceptual model that incorporates different hydrothermal venting sites over new lava flows to highlight differences in plume chemistry and microbiology at Axial Seamount (Figure 5). In the model, we attribute differences in microbiology to differences in subseafloor microbial communities injected into the water column, differences in the degree of mixing due to seawater entrainment, and differences in residence time in the plume. These findings extend our knowledge, indicating that post-eruptive hydrothermal output over new lava flows can continue to influence

deep-sea processes for months following an eruption and that the influence on deep-sea chemistry and microbiology is heterogeneous. ☐

SUPPLEMENTARY MATERIALS

Methods, Figure S1, and Tables S1 and S2 are available online at <https://doi.org/10.5670/oceanog.2018.120>.

REFERENCES

- Anantharaman, K., J.A. Breier, C.S. Sheik, and G.J. Dick. 2013. Evidence for hydrogen oxidation and metabolic plasticity in widespread deep-sea sulfur-oxidizing bacteria. *Proceedings of the National Academy of Sciences of the United States of America* 110(1):330–335, <https://doi.org/10.1073/pnas.1215340110>.
- Anderson, R.E., M.T. Beltrán, S.J. Hallam, and J.A. Baross. 2013. Microbial community structure across fluid gradients in the Juan de Fuca Ridge hydrothermal system. *FEMS Microbiology Ecology* 83(2):324–339, <https://doi.org/10.1111/j.1574-6941.2012.01478.x>.
- Baker, E.T. 1998. Patterns of event and chronic hydrothermal venting following a magmatic intrusion: New perspectives from the 1996 Gorda Ridge eruption. *Deep Sea Research Part II* 45(12):2,599–2,618, [https://doi.org/10.1016/S0967-0645\(98\)00085-X](https://doi.org/10.1016/S0967-0645(98)00085-X).
- Baker, E.T., G.J. Massoth, and R.A. Feely. 1987. Cataclysmic hydrothermal venting on the Juan de Fuca Ridge. *Nature* 329:149–151, <https://doi.org/10.1038/329149a0>.

- Baker, E.T., R.P. Lowell, J.A. Resing, R.A. Feely, R.W. Embley, G.J. Massoth, and S.L. Walker. 2004. Decay of hydrothermal output following the 1998 seafloor eruption at Axial Volcano: Observations and models. *Journal of Geophysical Research* 109, B01205, <https://doi.org/10.1029/2003JB002618>.
- Butterfield, D.A., I.R. Jonasson, G.J. Massoth, R.A. Feely, K.K. Roe, R.E. Embley, J.F. Holden, R.E. McDuff, M.D. Lilley, and J.R. Delaney. 1997. Seafloor eruptions and evolution of hydrothermal fluid chemistry. *Philosophical Transactions of the Royal Society A* 355(1723):369–386, <https://doi.org/10.1098/rsta.1997.0013>.
- Caress, D.W., D.A. Clague, J.B. Paduan, J.F. Martin, B.M. Dreyer, W.W. Chadwick Jr., A. Denny, and D.S. Kelley. 2012. Repeat bathymetric surveys at 1-metre resolution of lava flows erupted at Axial Seamount in April 2011. *Nature Geoscience* 5(7):483–488, <https://doi.org/10.1038/ngeo1496>.
- Chadwick, W.W., Jr., D.A. Clague, R.W. Embley, M.R. Perfit, D.A. Butterfield, D.W. Caress, J.B. Paduan, J.F. Martin, P. Sasnett, S.G. Merle, and A.M. Bobbitt. 2013. The 1998 eruption of Axial Seamount: New insights on submarine lava flow emplacement from high-resolution mapping. *Geochemistry, Geophysics, Geosystems* 14(10):3,939–3,968, <https://doi.org/10.1002/ggge.20202>.
- Chadwick, W.W., Jr., J.B. Paduan, D.A. Clague, B.M. Dreyer, and S.G. Merle. 2016. Voluminous eruption from a zoned magma body after an increase in supply rate at Axial Seamount. *Geophysical Research Letters* 5:63–70, <https://doi.org/10.1002/2016GL071327>.
- Delaney, J.R., D.S. Kelley, M.D. Lilley, D.A. Butterfield, J.A. Baross, W.S.D. Wilcock, R.W. Embley, and M. Summit. 1998. The quantum event of oceanic crustal accretion: Impacts of diking at mid-ocean ridges. *Science* 281(5374):222–230, <https://doi.org/10.1126/science.281.5374.222>.
- Djurhuus, A., S. Mikalsen, H. Giebel, and A. Rogers. 2017. Cutting through the smoke: Free-living bacterial diversity in deep-sea hydrothermal plumes. *Royal Society Open Science* 4:160829, <https://doi.org/10.1098/rsos.160829>.
- Dziak, R.P., and C.G. Fox. 1999. Long-term seismicity and ground deformation at Axial Volcano, Juan de Fuca Ridge. *Geophysical Research Letters* 26(24):3,641–3,644, <https://doi.org/10.1029/1999GL002326>.
- Gulmann, L.K., S.E. Beaulieu, T.M. Shank, K. Ding, W.E. Seyfried, and S.M. Sievert. 2015. Bacterial diversity and successional patterns during biofilm formation on freshly exposed basalt surfaces at diffuse-flow deep-sea vents. *Frontiers in Microbiology* 6:901, <https://doi.org/10.3389/fmicb.2015.00901>.
- Holden, J.F., M. Summit, and J.A. Baross. 1998. Thermophilic and hyperthermophilic microorganisms in 3–30°C hydrothermal fluids following a deep-sea volcanic eruption. *FEMS Microbiology Ecology* 25:33–41, <https://doi.org/10.1111/j.1574-6941.1998.tb00458.x>.
- Huber, J.A., D.A. Butterfield, and J.A. Baross. 2002. Temporal changes in archaeal diversity and chemistry in a mid-ocean ridge subseafloor habitat. *Applied and Environmental Microbiology* 68(4):1,585–1,594, <https://doi.org/10.1128/AEM.68.4.1585-1594.2002>.
- Huber, J.A., D.A. Butterfield, and J.A. Baross. 2003. Bacterial diversity in a subseafloor habitat following a deep-sea volcanic eruption. *FEMS Microbiology Ecology* 43:393–409, <https://doi.org/10.1111/j.1574-6941.2003.tb01080.x>.
- Huber, J.A., D.B. Mark Welch, H.G. Morrison, S.M. Huse, P.R. Neal, D.A. Butterfield, and M.L. Sogin. 2007. Microbial population structures in the deep marine biosphere. *Science* 318(5847):97–100, <https://doi.org/10.1126/science.1146689>.
- Kelley, D.S., J.R. Delaney, and S.K. Juniper. 2014. Establishing a new era of submarine volcanic observatories: Cabling Axial Seamount and the Endeavour Segment of the Juan de Fuca Ridge. *Marine Geology* 352:426–450, <https://doi.org/10.1016/j.margeo.2014.03.010>.
- Kelley, D.S., J.R. Delaney, and the Cabled Array Team. 2016. NSF's Cabled Array: A wired tectonic plate and overlying ocean. *OCEANS 2016 MTS/IEEE Monterey, OCE 2016*, <https://doi.org/10.1109/OCEANS.2016.7761398>.
- Liu, Y. 2010. Methanomicrobiales. Pp. 583–593 in *Handbook of Hydrocarbon and Lipid Microbiology*. K.N. Timmis, ed., Springer Berlin Heidelberg, https://doi.org/10.1007/978-3-540-77587-4_45.
- Lupton, J.E., J.R. Delaney, H.P. Johnson, and M.K. Tivey. 1985. Entrainment and vertical transport of deep-ocean water by buoyant hydrothermal plumes. *Nature* 316(6029):621–623, <https://doi.org/10.1038/316621a0>.
- Lutz, R.A., T.M. Shank, D.J. Fornari, R.M. Haymon, M.D. Lilley, K.L. Von Damm, and D. Desbruyeres. 1994. Rapid growth at deep-sea vents. *Nature* 371:633–634, <https://doi.org/10.1038/371663a0>.
- Mattes, T.E., B.L. Nunn, K.T. Marshall, G. Proskurowski, D.S. Kelley, O.E. Kawka, D.R. Goodlett, D.A. Hansell, and R.M. Morris. 2013. Sulfur oxidizers dominate carbon fixation at a biogeochemical hot spot in the dark ocean. *The ISME Journal* 7(12):2,349–2,360, <https://doi.org/10.1038/ismej.2013.113>.
- McCollom, T.M. 2000. Geochemical constraints on primary productivity in submarine hydrothermal vent plumes. *Deep Sea Research Part I* 47(1):85–101, [https://doi.org/10.1016/S0967-0637\(99\)00048-5](https://doi.org/10.1016/S0967-0637(99)00048-5).
- McCollom, T.M., and E.L. Shock. 1997. Geochemical constraints on chemolithoautotrophic metabolism by microorganisms in seafloor hydrothermal systems. *Geochimica et Cosmochimica Acta* 61(20):4,375–4,391, [https://doi.org/10.1016/S0016-7037\(97\)00241-X](https://doi.org/10.1016/S0016-7037(97)00241-X).
- Meyer, J.L., N.H. Akerman, G. Proskurowski, and J.A. Huber. 2013. Microbiological characterization of post-eruption “snowblower” vents at axial seamount, Juan de Fuca Ridge. *Frontiers in Microbiology* 4:153, <https://doi.org/10.3389/fmicb.2013.00153>.
- Nooner, S.L., and W.W. Chadwick Jr. 2016. Inflation-predictable behavior and co-eruption deformation at Axial Seamount. *Science* 354(6318):1399–1403, <https://doi.org/10.1126/science.aah4666>.
- Opatkiewicz, A.D., D.A. Butterfield, and J.A. Baross. 2009. Individual hydrothermal vents at Axial Seamount harbor distinct subseafloor microbial communities. *FEMS Microbiology Ecology* 70(3):413–424, <https://doi.org/10.1111/j.1574-6941.2009.00747.x>.
- Sheik, C.S., K. Anantharaman, J.A. Breier, J.B. Sylvan, K.J. Edwards, and G.J. Dick. 2015. Spatially resolved sampling reveals dynamic microbial communities in rising hydrothermal plumes across a back-arc basin. *The ISME Journal* 9(6):1,434–1,445, <https://doi.org/10.1038/ismej.2014.228>.
- Shock, E.L., and M.E. Holland. 1997. Geochemical energy sources that support the subsurface biosphere. Pp. 153–165 in *The Subseafloor Biosphere at Mid-Ocean Ridges*. W.S.D. Wilcock, E.F. Delong, D.S. Kelley, J.A. Baross, and S.C. Cary, eds., American Geophysical Union, Washington, DC.
- Summit, M., and J.A. Baross. 1998. Thermophilic subseafloor microorganisms from the 1996 North Gorda Ridge eruption. *Deep Sea Research Part II* 45(12):2,751–2,766, [https://doi.org/10.1016/S0967-0645\(98\)00092-7](https://doi.org/10.1016/S0967-0645(98)00092-7).
- Sunamura, M., Y. Higashi, C. Miyako, J.I. Ishibashi, and A. Maruyama. 2004. Two bacteria phylotypes are predominant in the Suiyo Seamount hydrothermal plume. *Applied and Environmental Microbiology* 70(2):1,190–1,198, <https://doi.org/10.1128/AEM.70.2.1190-1198.2004>.
- Topcuoglu, B.D., L.C. Stewart, H.G. Morrison, D.A. Butterfield, J.A. Huber, and J.F. Holden. 2016. Hydrogen limitation and syntrophic growth among natural assemblages of thermophilic methanogens at deep-sea hydrothermal vents. *Frontiers in Microbiology* 7:1240, <https://doi.org/10.3389/fmicb.2016.01240>.
- Tunnicliffe, V., R.W. Embley, J.F. Holden, D.A. Butterfield, G.J. Massoth, and S.K. Juniper. 1997. Biological colonization of new hydrothermal vents following an eruption on Juan de Fuca Ridge. *Deep-Sea Research Part I* 44(9–10):1,627–1,644, [https://doi.org/10.1016/S0967-0637\(97\)00041-1](https://doi.org/10.1016/S0967-0637(97)00041-1).
- Wilcock, W.S.D., M. Tolstoy, F. Waldhauser, C. Garcia, Y.J. Tan, D.R. Bohnenstiel, J. Caplan-Auerback, R.P. Dziak, A.F. Arnulf, and M.E. Mann. 2016. Seismic constraints on caldera dynamics from the 2015 Axial Seamount eruption. *Science* 354(6318):1,395–1,399, <https://doi.org/10.1126/science.aah5563>.

ACKNOWLEDGMENTS

We would like to thank the crew of R/V *Thompson* (TN326 and TN327) and the operational teams for the remotely operated vehicles ROPOS (TN326) and *Jason* (TN327). This research was supported by the National Science Foundation (NSF) through a Graduate Research Fellowship to R. Spietz, an NSF-OCE award to R. Morris and A. Ingalls (OCE-15584830), and a RAPID award to W. Chadwick (OCE-1546616), D. Butterfield (OCE-1546695), and J. Huber (OCE-1547004). Joint Institute for the Study of the Atmosphere and Ocean (JISAO), NOAA Cooperative Agreement and NA15OAR4320063, contribution number 2017-0107. PMEL contribution number 4718. Sequences have been deposited in NCBI's Short Read Archive under SRA accession: SRP127560.

AUTHORS

Rachel L. Spietz is currently Postdoctoral Research Associate, Montana State University, Bozeman, MT, USA. **David A. Butterfield** is Senior Research Scientist, **Nathaniel J. Buck** is Research Scientist, and **Benjamin I. Larson** is Research Scientist, all at the Joint Institute for the Study of the Atmosphere and Ocean, University of Washington, and the National Oceanic and Atmospheric Administration, Pacific Marine Environmental Laboratory (NOAA-PMEL), Seattle, WA, USA. **William W. Chadwick Jr.** is Oceanographer and **Sharon L. Walker** is Oceanographer, both at NOAA-PMEL, Newport, OR, USA. **Deborah S. Kelley** is Professor and **Robert M. Morris** (morrisrm@uw.edu) is Associate Professor, both in the School of Oceanography, University of Washington, Seattle, WA, USA.

ARTICLE CITATION

Spietz, R.L., D.A. Butterfield, N.J. Buck, B.I. Larson, W.W. Chadwick Jr., S.L. Walker, D.S. Kelley, and R.M. Morris. 2018. Deep-sea volcanic eruptions create unique chemical and biological linkages between the subsurface lithosphere and the oceanic hydrosphere. *Oceanography* 31(1):128–135, <https://doi.org/10.5670/oceanog.2018.120>.

SIDE BAR

Get Engaged with the Ocean Observatories Initiative

By Greg A. Ulses, Leslie M. Smith, and Timothy J. Cowles

The Ocean Observatories Initiative (OOI) is an open community resource supported by the National Science Foundation (NSF) (Smith et al., 2018, this issue). Free access is provided to all OOI data through online interfaces (Vardaro and McDonnell, 2018, in this issue). Independent of an NSF-funded project, individual scientists can use OOI data to address specific scientific hypotheses, or to augment existing research projects. For example, publicly accessible OOI data can provide key resources for model simulations, as well as data to augment shipboard research or field research projects. Scientists conducting research in the regional domains of the OOI are encouraged to consider these opportunities and reach out to OOI staff to discuss how their research may be included in OOI cruise opportunities.

The OOI will grow, change, and reach its full utility as it is shaped by input from its user community. Here, we summarize some of the ways to interact with the OOI and its data.

USING OOI DATA

The primary way to engage with the OOI is to use its data. All OOI data are freely available for download as quickly as they can be made accessible (Vardaro and McDonnell, 2018, in this issue). The only requirement when using OOI data is to cite OOI as the data source. Full details of the OOI Usage Policy can be found on the OOI website (<http://oceanobservatories.org>).

OOI data have a wide range of possible applications, only some of which could be represented in this special issue of *Oceanography*. We encourage potential users to dive into this rich data resource.

SEEKING FUNDING TO ENGAGE WITH THE OOI

NSF is accepting OOI-related proposals through the core science and technology programs, and several awards have already been made. Scientists are encouraged to propose new applications and approaches, including, but not limited to (1) connection of new instruments and platforms onto the observatory network, (2) modification of sampling rates and missions for existing instrumentation, (3) execution of ancillary work during normally scheduled OOI cruises, (4) testing specific hypotheses with OOI data, and

(5) creation of educational programs using both OOI infrastructure and data (e.g., McDonnell et al., 2018, in this issue). For more information on the NSF proposal process, contact the NSF program officer for your science or technology program.

Adding Infrastructure

Infrastructure in the form of instruments or additional cabled nodes may be added to the OOI. On the Cabled Array, additional power and bandwidth are available to power the instrumentation and transmit data back to shore. Some uncabled platforms have the ability to provide power for instruments and telemeter data. However, most assets added to the uncabled components of the OOI will need to be self-powered and self-recording. When instrumentation is added to the OOI infrastructure, the data collected are also integrated into the OOI Cyberinfrastructure. The proposing scientists will have embargoed access to the data of the added instrument(s) for the first year, but the data thereafter will be a part of the OOI community resource available to all.

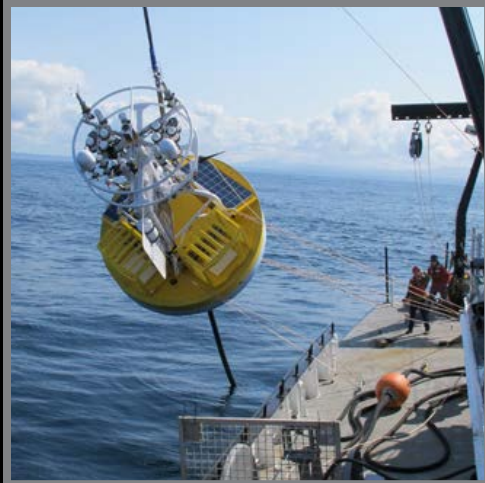
Adjusting Sampling Rates

Researchers are welcome to propose modifications to the sample rates of existing observatory instrumentation. The OOI instruments sample at “baseline sampling rates,” which were established with community input to address the long-term observational goals and objectives documented in the OOI Science Prospectus (<http://oceanobservatories.org/science-plan>). If the mooring platforms had additional available power upon deployment, the instruments were set to sample to the available power levels. These are called “as-deployed sampling rates.” Full details of OOI sampling strategies are contained in the OOI Observation and Sampling Approach document (<http://oceanobservatories.org/observation-and-sampling-approach>).

Researchers can propose modification of sampling rates to address science questions if they are lower than the as-deployed sampling rates and do not go below the OOI Science Prospectus baseline sampling rates. Any approved changes would need to be timed with deployment cycles for the specific mooring or array.

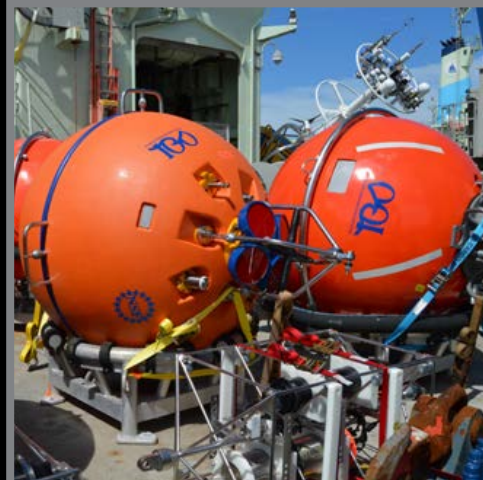
HD Video camera views “Mushroom” vent on the Axial Seamount. *Image credit:* NSF-OOI/UW/ISS; Dive R1835; V15





Coastal Surface Mooring is deployed at the Endurance Array. *Image credit: OOI Endurance Array Program, OSU*

Subsurface Flotation Buoys await on deck for deployment at the Irminger Sea Array. *Image credit: OOI Global Array Program, WHOI*



Coastal Profiler Mooring is lined up for recovery at the Pioneer Array. *Image credit: OOI Pioneer Array Program, WHOI*

Ships of Opportunity

Frequently, there are extra berths available on OOI maintenance cruises, as well as opportunities to take additional samples. Any proposed and approved additional activities would have to fit into the existing cruise schedule, be conducted by available personnel, and be subject to vessel size and safety restrictions. Proposals to spend extra days on station, add remotely operated vehicle dives, or visit remote sites could add unsustainable costs to the cruise and impact completion of OOI activities. All supplemental cruise activities must be added to the cruise plan, be pre-approved by OOI program management, and be subject to weather or safety concerns by the chief scientist and captain.

Using OOI Data and Testing Hypotheses

NSF welcomes proposals from researchers who wish to use OOI data only to answer science questions. These proposals do not require any modifications to be made to the observatory.

SUPPLEMENTAL ANALYSIS OF WATER SAMPLES

During maintenance cruises, CTD casts are conducted prior to deployment and following recovery of most OOI assets (glider deployments may involve a single reference CTD cast). Water samples are collected at multiple depths and analyzed for oxygen (Winkler), chlorophyll α fluorescence and pigment distribution, nitrate/nitrite (and potentially a full nutrient suite), total dissolved inorganic carbon and total alkalinity, pH, and salinity. Often there is sufficient water taken to support additional assays. Note that sensors used on CTD rosette casts are specific to the deployment vessel. For details of ship instrumentation, see the UNOLS website (<https://www.unols.org>). Researchers who require additional instrumentation of a specific type should contact the OOI project manager or project scientists to see if replicates can be arranged, or include the instrumentation request in an NSF proposal.

USING COMMUNITY-DEVELOPED TOOLS

Community-developed tools are an ever-expanding set of free resources shared by the OOI user community via the OOI website. Many of these tools consist of Python scripts that help transform raw OOI data into more usable forms, plot OOI netCDF data sets (courtesy of the OOI Data Team), convert broadband hydrophone files (courtesy of Pete Cable, Raytheon), and download specific portions of raw CAMHD data (courtesy of Tim Crone, Lamont-Doherty Earth Observatory).

USING OPEN SOURCE SENSOR ALGORITHMS

Sensor algorithms are free for the community to download and use with OOI raw data, or to adapt for their own observational data. The algorithm code used to generate each data product in the OOI Cyberinfrastructure system can be found in the ion-functions GitHub repository (https://github.com/oceanobservatories/ion-functions/tree/master/ion_functions/data). These modules, and the functions therein, represent the transforms and calculations used to provide the various OOI data products.

SUMMARY

The various OOI sites equipped with fixed and mobile instrumented platforms, along with over 200 freely available data products, provide users with a range of opportunities to explore new research questions, inform policy development based on extended time series of observations, and offer the public new insights into the how ocean processes contribute to our planetary system. We invite your engagement!

References

- McDonnell, J., A. deCharon, C.S. Lichtenwalner, K. Hunter-Thomson, C. Halversen, O. Schofield, S. Glenn, C. Ferraro, C. Lauter, and J. Hewlett. 2018. Education and public engagement in OOI: Lessons learned from the field. *Oceanography* 31(1):138–146, <https://doi.org/10.5670/oceanog.2018.122>.
- Smith, L.M., J.A. Barth, D.S. Kelley, A. Plueddemann, I. Rodero, G.A. Ulles, M.F. Vardaro, and R. Weller. 2018. The Ocean Observatories Initiative. *Oceanography* 31(1):16–35, <https://doi.org/10.5670/oceanog.2018.105>.
- Vardaro, M.F., and J. McDonnell. 2018. Accessing OOI data. *Oceanography* 31(1):36–37, <https://doi.org/10.5670/oceanog.2018.106>.

Authors

Greg A. Ulles is Ocean Observatories Initiative (OOI) Director, and **Leslie M. Smith** (lsmith@oceanleadership.org) is OOI Science Communicator, both at the Consortium for Ocean Leadership, Washington, DC, USA. **Timothy J. Cowles** is Professor Emeritus, Oregon State University, Corvallis, OR, USA.

Article Citation

Ulles, G.A., L.M. Smith, and T.J. Cowles. 2018. Get engaged with the Ocean Observatories Initiative. *Oceanography* 31(1):136–137, <https://doi.org/10.5670/oceanog.2018.121>.

Education and Public Engagement in OOI

Lessons Learned from the Field

By Janice McDonnell, Annette deCharon, C. Sage Lichtenwainer,
Kristin Hunter-Thomson, Catherine Halversen, Oscar Schofield, Scott Glenn,
Carrie Ferraro, Carla Lauter, and James Hewlett



“ To build the most user-friendly way for professors and researchers to access OOI data for undergraduate teaching, EPE created a suite of effective tools through an iterative development cycle. ”

ABSTRACT. The Ocean Observing Initiative (OOI) was designed to advance understanding of complex oceanographic processes by acquiring large quantities of data at six key locations in the world ocean. The OOI Education and Public Engagement (EPE) Implementing Organization has built an educational cyberinfrastructure and developed interactive tools targeted for undergraduate-level learners that enable easy access to OOI data, images, and video. To develop the suite of OOI education tools, EPE used an iterative design process, including needs assessment, tool prototyping, and usability testing in undergraduate classrooms. Data visualization and concept mapping tools were envisioned as a way to help undergraduates link concepts students see in oceanography textbooks to real-world phenomena. A Data Investigation Builder (DIB) was constructed to assist professors in designing data activities. During the usability testing, professors provided valuable feedback that allowed EPE to improve the tools. Based on the lessons learned from EPE, in 2016 we developed a new prototype set of Data Explorations that were more modular and easier to integrate into an undergraduate lecture or problem set. This paper reviews how the EPE toolset was developed, including establishment of requirements for the tools and incorporation of lessons learned from the user needs assessment and the results of usability testing of prototype tools.

INTRODUCTION

A growing number of geoscience research programs collect high volumes of data using advanced technologies, especially in oceanography. One such program is the National Science Foundation (NSF) Ocean Observatories Initiative (OOI), which has constructed observational and computational infrastructure to provide sustained ocean measurements for the study of climate variability, ocean circulation, ecosystem dynamics, air-sea exchange, seafloor processes,

and plate-scale geodynamics for the coming decades. The OOI is already advancing our ability to understand the natural world by acquiring large quantities of data to address complex oceanographic processes at six locations of interest in the world ocean.

Expanded access to online data provides geoscience professors with myriad opportunities to engage undergraduate learners through the use of real-world data sets, models, and simulations of oceanographic processes. By directly

manipulating data, learners are challenged to construct meaning and develop a deeper understanding of a topic or phenomenon. This type of learning also encourages student inquiry and helps develop practical science skills (Hays et al., 2000; Adams and Matsumoto, 2009). Working with real data helps students develop interest in, motivation for, and identity with respect to science (National Science Board, 2007). Moreover, analyzing data and identifying patterns have become core skills in the workplace and for civic engagement in the twenty-first century (Oceans of Data Institute, 2015).

Despite the benefits and opportunities of having students work with real data, undergraduate teaching is often not data intensive (Krumhansel et al., 2013). Limited experience and exposure to different data types and sources can cause students to struggle in their courses, and they may purposefully avoid the use and evaluation of data in their everyday lives. Cognitive studies reveal that students who are not regularly exposed to data manipulation often fail to see patterns emerging across scientific experiments, frequently ignoring anomalous data or distorting them to match their personal beliefs (Chinn and Brewer, 1998). Studies also indicate that students need to learn more about the types of conclusions that scientists can draw from observations,

FACING PAGE. From left to right: Cheryl Greengrove (University of Washington Tacoma), Deborah Kelley (University of Washington Seattle), Alan Trujillo (Palomar College), and Rus Higley (Highline College) explore teaching with data at the Rutgers University Inn and Conference Center, New Brunswick, NJ.

what kinds of evidence are needed to support scientific ideas, and how that evidence can be gathered and interpreted (Sampson and Clark, 2008).

To support data literacy and enhance critical thinking skills, undergraduates need to transition from working with small, typically self-collected data sets to large, professionally collected data sets (Kastens, 2011) such as those provided by the OOI. Student-collected data can spur discussion of “data ownership” (i.e., provenance) and how data provide evidence for claims, interpretations, and conclusions (Hug and McNeill, 2008).

However, the transition from using data they collected to using professionally collected data can be very challenging for students. They need to shift from using familiar to unfamiliar analysis tools, from hands-on experiences to gaining context from metadata, and from simple to complex lines of reasoning (Kastens, 2011). Supporting students while they transition to using professionally collected data can be challenging for professors too, as there is often a lack of adequate tools to help students in the classroom easily digest and manipulate large data sets.

With these challenges in mind, the OOI

Education and Public Engagement (EPE) Implementing Organization worked to build an educational cyberinfrastructure and develop interactive tools to enable easy access to OOI data, images, and video in formal learning environments. Toward this end, we explored methodologies for effectively integrating data into learning strategies and creating data visualization tools to teach twenty-first century science skills and practices in undergraduate classrooms. To build the most user-friendly way for professors and researchers to access OOI data for undergraduate teaching, EPE created a suite of effective tools through an iterative development cycle. This paper reviews how the EPE toolset was developed, including how the requirements for the tools were established, and how we folded in lessons learned from the user needs assessment and results from the usability testing of the prototype tools. Our experiences will help future developers interested in learning about effective processes for building their own educational tools and content.

A Brief History of Education and Public Engagement in OOI

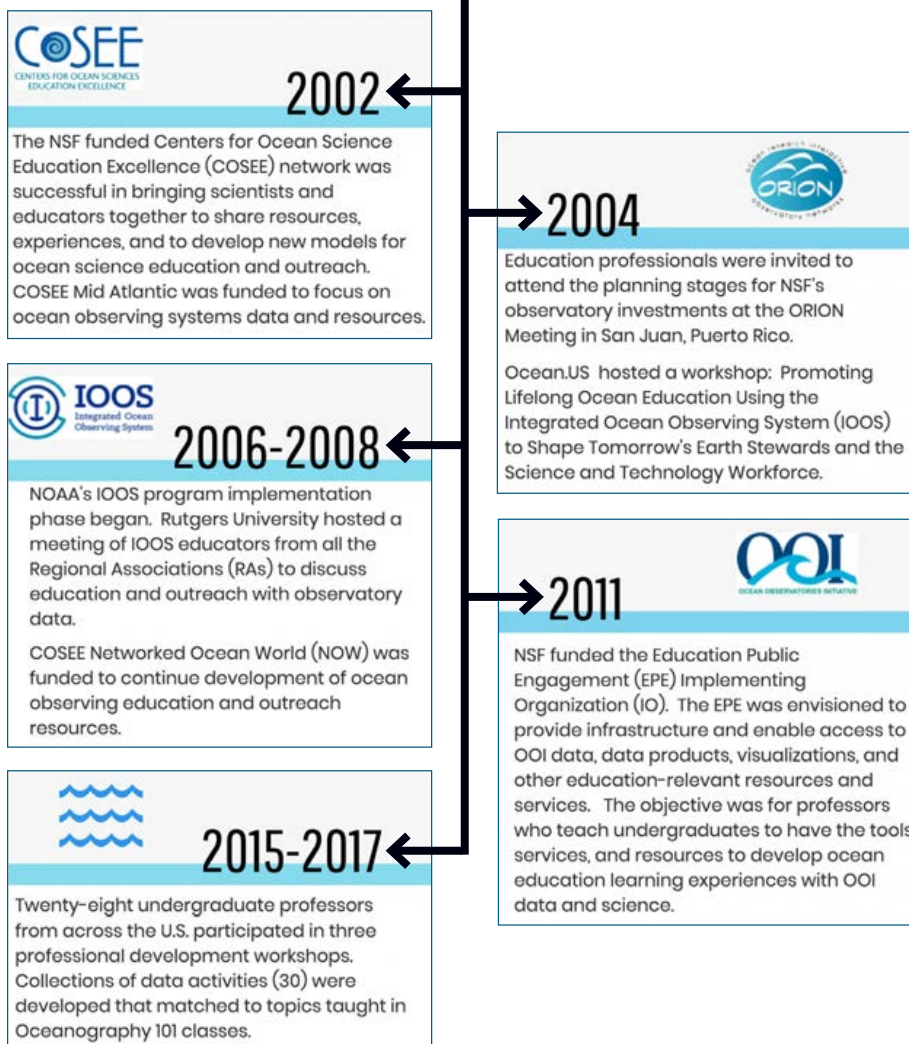


FIGURE 1. The progression of thinking about using data in teaching and learning.

and information translation facility that would be tasked with transforming OOI research results, technology innovations, and data into ready-to-use forms for a variety of education and outreach audiences.

In 2011, NSF funded the EPE Implementing Organization (IO) for the OOI. The overarching objective was to develop tools and approaches that leverage the unique science and engineering capacities of OOI. EPE IO's charge was to facilitate and support education and outreach; however, the team was not supported to create educational projects or products per se. Based on NSF guidance, the primary focus of the OOI project was on developing infrastructural tools to support undergraduate education. The EPE team was led by Rutgers University and included the University of Maine, Raytheon Web Solutions, and education liaisons from the other previously awarded IOs: The University of Washington, Scripps Institution of Oceanography, and Oregon State University.

THE PROCESS: BUILDING EPE TOOLS FOR UNDERGRADUATE STUDENT LEARNING

EPE used an iterative design process to support the use of OOI data in undergraduate teaching (Figure 2). The EPE team conducted user needs assessments and usability tests, and developed a number of prototype tools with professors who teach undergraduates.

Needs assessments consisted of phone interviews in 2011 and 2012 with professors who were teaching undergraduates as well as a national survey in 2012 ($n = 133$; response rate 14%). We focused on understanding undergraduate teaching practices employed at the time and collecting example summaries of how data were used in undergraduate classrooms. These data were synthesized into recommendations to aid OOI software developers in designing tools that would enable undergraduates to interpret and analyze oceanographic data. Overall,

assessment results showed professors were interested in using data sets to connect important themes and concepts in introductory oceanography courses. They wanted simple, clearly defined variables that are easily grasped by students. They preferred temporally based and easily manipulated data and visualization tools that allowed for easy downloading of outputs. Finally, they requested metadata to bring the context of data into student-centered activities while supporting

conceptual understanding.

These professors also recommended that EPE develop tools for creating basic statistics (e.g., calculation of mean, standard deviation, standard error, correlation coefficient, regression line), interpolating data, and helping students visualize time-series data sets (McDonnell et al., 2015). The professors also supported the development of a specialized tool that would allow them to create lessons using OOI data, rate



FIGURE 2. The OOI Education and Public Engagement (EPE) used a development process that included needs assessment of the professors, prototyping of data activities, and testing with undergraduates.

or review colleagues' lessons, and copy and edit lessons created by others. They suggested that EPE continue to develop and refine the Concept Mapper, developed earlier by COSEE Ocean Systems (deCharon et al., 2013). The Concept Mapper was highly regarded by the professors, who recognized its high potential for teaching oceanographic concepts. They also expressed the need for help in deciphering the extensive and jargon-heavy vocabulary of the OOI program. This request spurred development of the Vocabulary Navigator, which uses backend ontologies (deCharon et al., 2015) to display and describe connections among various components of the OOI using a concept-map format.

During 2012–2014, EPE developed requirements for its prototype tools and conducted usability testing on early prototypes. "Think Aloud" testing was used to solicit feedback from undergraduate professors at universities and community colleges. Think Aloud is a method of user testing that involves asking users to think out loud as they perform a task. The protocol included collecting information on the backgrounds of the users/testers, and asking them to review time-series visualizations, "glider" tools, and the preliminary Vocabulary Navigator. EPE also conducted a demonstration of pilot EPE tools in collaboration with the NSF-funded Community College Undergraduate Research Initiative (CCURI) network.

EPE OCEAN EDUCATION PORTAL

The primary goal of the EPE effort was to develop an online Ocean Education Portal (<http://education.oceanobservatories.org>) to support the creation and sharing of educational resources by undergraduate faculty. The EPE portal includes a suite of tools (Table 1) that enable faculty to create custom activities online for group or individual projects that can be used either during lectures or as homework assignments. The site also includes a variety of resources to facilitate using OOI data to teach oceanography concepts.

EPE tools were designed to help students understand and visualize how ocean data and research findings are tied to key oceanography concepts. For example, the Data Investigation Builder (DIB) is designed for learners to collect and interpret their own data and/or explore research data sets to answer questions, as described by Manduca and Mogk (2002). The DIB tool assists professors in drafting student learning objectives, identifying and visualizing OOI data sets and, most importantly, creating research challenges for undergraduates to pursue. Thus, the Education Portal was designed to help students explore scientific practices (e.g., developing a conceptual model or diagram), analyze OOI data sets, construct written explanations of phenomena observed in the data, and develop new questions based on OOI data.

IMPLEMENTING EPE TOOLS: HOW CAN THE TOOLS BE USED IN UNDERGRADUATE TEACHING?

The collection of tools developed by EPE effectively integrates OOI data into undergraduate teaching, as demonstrated by results of our pilot tests (Hunter-Thomson et al., 2017). However, there is still much work to be done to facilitate the use of OOI data in education. Pilot testers stated that EPE data visualization tools provided their students with examples of how oceanographic data are collected, graphed, and analyzed. The tools also allow students to see how data can be graphed and visualized for better analysis.

During the EPE development phase, a collection of five lessons were created in the Education Portal, entitled Ocean-Atmosphere Interactions During Storms, Salinity Matters, Seasonality in the Ocean, Is Overfishing Creating a Population Bottleneck?, and Ocean Acidification. These prototype lessons employed other data sets from NOAA as placeholders for OOI data, which were not yet available. EPE conducted formative evaluation, surveying both the professors ($n = 8$) and undergraduates participating

in the pilot. Professors reported that these types of lessons broadened students' views from local to more regional/global perspectives. This observation was common among the CCURI community college faculty whose students had collected data locally before learning about the OOI program.

Finally, undergraduate survey results demonstrate that they need more guidance and support to learn how to interpret graphs. Students found the graphs difficult to read and interpret (e.g., the axes were sometimes unclear; more captions, key terms, visualizations, videos, and maps were needed to understand data sources; photos of instruments were requested; McDonnell et al., 2015). Some key outcomes include:

- **Data visualization tools are most critical to successfully integrating OOI into undergraduate classrooms.**

Professors and their students agreed that there is great value to the types of tools developed by EPE; however, they need additional effort to increase their reliability and usability. There is broad agreement that bringing traditional textbook discussions of oceanographic concepts alive with OOI data would be of great value to students. Thus, more research and evaluation should be conducted to ascertain whether or how data interactions impact student learning and their likelihood of pursuing scientific careers.

- **Lack of model content or OOI-specific data visualization tools was a significant barrier to the success of the EPE.**

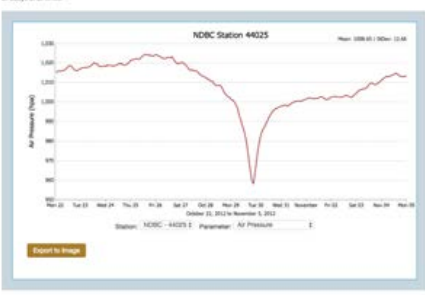
The OOI construction funds for EPE were limited to tool development and could not be applied to classroom lesson development. However, supplemental NSF funding has supported the successful development of the classroom exemplars used in our CCURI pilot demonstration. Although the simultaneous development of the OOI Cyberinfrastructure/Data Portal and the EPE tools initially complicated the use of OOI data streams to test the tools and demonstrate their utility,

TABLE 1. A description of EPE tools.

Educational Data Visualization Tools

NDBC buoy observations of Superstorm Sandy

Created by: Sean Linternemer
This interactive allows you to investigate several variables measured by NOAA buoys deployed off the East-Atlantic coast, including: 44027 (approximately 200 miles off the coast of New Jersey), 44028 (approximately 100 miles off the coast of North Carolina), and 44029 (approximately 100 miles off the coast of South Carolina). Users can investigate the oceanic and atmospheric conditions before, during, and after Superstorm Sandy traveled through the region. Note, data may not be available for all buoys at all times.



Air Pressure (hPa)

NDBC Station 44025

Mean: 1009.00 | StdDev: 12.46

Station: NDBC - 44025 E Parameter: Air Pressure

Export to Image

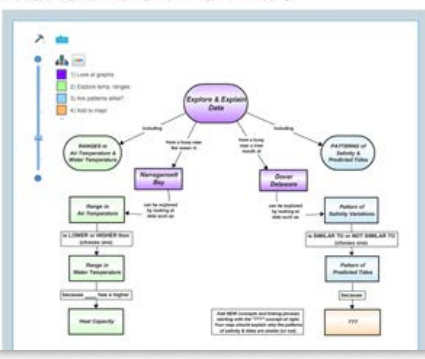
Description. Provide simple interfaces to interact with OOI datasets. A collection of five interactive visualization tools was designed to be intuitive and adaptable to professors' teaching goals.

Key Features. One example is the "Simple Time Series" tool, which is used to select instruments and date ranges. This allows students to explore changes in environmental conditions over time (e.g., hurricanes, seasons).

Concept Mapper

Using Concept Maps to Explore & Explain Data

Created by: Sean Linternemer
Concept maps that can be used to guide students through exploring and explaining data. It can be presented in sequence by turning these icons on/off: [1] Looking at the graphs (purple); [2] Exploring the temperature ranges (green); [3] Assessing similarity in patterns of salinity and tides (blue); and [4] Explaining these patterns by adding concepts and linking phrases to the map (orange).



Exploring & Explaining Data

Assessing Similarity in Patterns of Salinity and Tides

Explaining These Patterns by Adding Concepts and Linking Phrases to the Map

Range in Air Temperature

Range in Water Temperature

Water Temperature

Salinity

Heat Capacity

Nonnegative Bay

Normal Distribution

Pattern of Predicted Values

Pattern of Actual Variations

Similar to or Not Similar to

Pattern of Predicted Values

Normal Distribution

Nonnegative Bay

Range in Water Temperature

Range in Air Temperature

Water Temperature

Salinity

Heat Capacity

Exploring & Explaining Data

Assessing Similarity in Patterns of Salinity and Tides

Explaining These Patterns by Adding Concepts and Linking Phrases to the Map

Range in Air Temperature

Range in Water Temperature

Water Temperature

Salinity

Heat Capacity

Nonnegative Bay

Normal Distribution

Pattern of Predicted Values

Pattern of Actual Variations

Similar to or Not Similar to

Pattern of Predicted Values

Normal Distribution

Nonnegative Bay

Range in Water Temperature

Range in Air Temperature

Water Temperature

Salinity

Heat Capacity

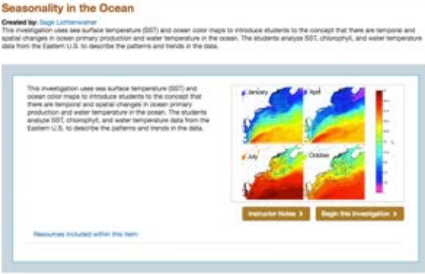
Description. Allows users to build connected diagrams of their knowledge, using shapes to represent concepts and arrows to describe the relationships between them.

Key Features. Concept maps are widely used in education to aid or evaluate students' contextual understanding of topics.

Data Investigation Builder (DIB)

Seasonality in the Ocean

Created by: Sean Linternemer
This investigation uses sea surface temperature (SST) and ocean color maps to introduce students to the concept that there are temporal and spatial changes in primary productivity and water temperature in the oceans. The students analyze SST, chlorophyll, and water temperature data from the Eastern U.S. to describe the patterns and trends in the data.



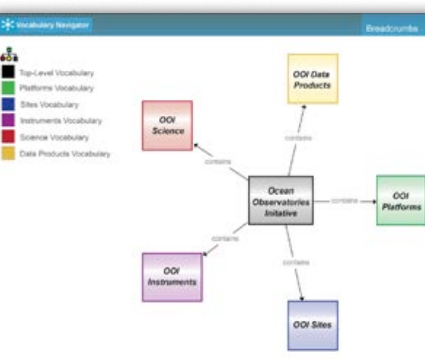
Instructor Notes > Begin the Investigation >

Description. Resources—including OOI data visualizations, images, videos, and concept maps—can be assembled into learning modules. These lessons can also be shared with colleagues.

Key Features. Well-defined steps help educators develop lessons using OOI data. The tool promotes effective education practices by supporting students' use of data-based evidence to answer prompting questions.

Vocabulary Navigator

Vocabulary Navigator



Top-Level Vocabulary

Platform Vocabulary

Sites Vocabulary

Instruments Vocabulary

Science Vocabulary

Data Products Vocabulary

OOD Science

OOD Data Products

OOD Instruments

OOD Platforms

OOD Observatories Initiative

OOD Sites

Description. Provides an intuitive and visual way to explore OOI's infrastructure. Its five interlinked vocabularies include terms and images from high-level science themes to specific data products.

Key Features. Based on organizational structures used in information and computer sciences, these vocabularies were designed to meet users' needs by placing information into relevant context, while promoting self-directed discovery.

it was possible to conduct some limited testing with National Data Buoy Center data. Experience, user feedback, and supplemental support have all contributed to the capability for integrating OOI data into the visualization tools.

- **Continue to develop EPE tools to support inquiry-based learning.**

CCURI professors felt the DIB could be an asset for engaging in active learning and teaching. They recommended that EPE provide support for professors to create more data activities and resources, including pedagogical support for both online and face-to-face implementations. They suggested that EPE focus development on the data visualization and concept mapping tools, as they felt those tools had the most potential. Finally, they recommended EPE provide training and marketing of its tools to the community.

- **Additional professional development support for professors using the tools is needed.**

EPE tools should be iterated and refined based on the types of instruction being used by undergraduate professors. For example, instructions to students will differ based on whether they are being used

online autonomously or facilitated by a professor as part of classroom lectures. Lessons should be progressive and scaffolded to help students get the experience they need with data while also helping to build their confidence and skills. Scaffolding refers to a variety of instructional techniques used to move students progressively toward stronger understanding and, ultimately, greater independence in the learning process.

BEYOND EPE: DATA EXPLORATIONS PROJECT

Based on lessons learned from EPE, we developed a new prototype set of Data Explorations in 2016 (<http://explorations.visualocean.net>). These activities are more modular and thus easier to integrate into an undergraduate lecture or problem set. Through hands-on workshops, professors from diverse institutions—including community colleges, primarily undergraduate institutions, and minority-serving institutions—became engaged in the Data Explorations project. Overall, 28 professors participated in three OOI workshops focused on biological productivity (May 2016), properties of seawater (May 2017), and tectonics and seamounts (June 2017). Participants developed implementation plans for subsequent academic years

based on the knowledge levels of their students and their course setups (e.g., face-to-face, hybrid).

Each event focused on developing effective teaching practices for using OOI data assets and customized data visualization tools. To build a community of practice among participating professors, we focused on developing content exemplars that use OOI data. Another workshop objective was to provide pedagogical guidance to professors who often do not have much opportunity to learn about effective teaching practices.

Data Explorations employed the Learning Cycle model developed by the Lawrence Hall of Science at the University of California, Berkeley, where instruction is organized to be consistent with what is known about how people learn (see Box 1). The student-centered explorations developed in this workshop were designed to connect new content to students' prior knowledge, elicit questions and explanations, provide opportunities for exploration and discussion of ideas with peers, and apply students' understanding to new situations (Lawson, 2002; Bybee et al., 2006; Brown and Abell, 2007).

To help facilitate integration of OOI data into undergraduate teaching, we identified connections between themes in

Box 1. The Learning Cycle Explained

INVITATION - Initiates the learning task and sets the context. It sparks interest, and spurs learners to recall and retrieve past connections that may be relevant to present learning experiences.

EXPLORATION - Involves exploration of real phenomena driven mainly by learners' interest and questions, followed by discussion about discoveries, results, ideas, and questions. Provides a common base of experiences for learners to develop new concepts and skills.

CONCEPT INVENTION - After interest and attention is focused, learners actively process the experience, review evidence and data gathered through exploration, and try to make sense of it.

APPLICATION - Armed with new ideas, learners apply new knowledge and skills to solving a problem or meeting a challenge, transferring their new knowledge to unfamiliar contexts in the world.

REFLECTION - After trying out new ideas in different settings, learners reflect on how their original notions have been or need to be modified. It invites them to monitor and regulate their own evolving understanding, and generate new questions.

oceanography textbooks commonly used in lower division classes (e.g., “101 level”) and the OOI science themes. To enable easy adoption in community college and university 101-level oceanography courses, we purposely linked our data explorations to one of the most used textbooks in the United States, *The Essentials of Oceanography* (Trujillo and Thurman, 2016). A complete cross reference between this textbook’s themes and OOI data can be found on the Data Explorations website.

ANATOMY OF A DATA EXPLORATION

Data Explorations are designed as in-class, group explorations and take 15–20 minutes to complete. One such example data activity is highlighted in Figure 3. The learning objective for each Exploration is closely tied to the Learning Cycle, with different data activities designed to be used at specific Learning Cycle phases. Thus, the learning objective and the questions students will address vary across each Exploration.

The Explorations each include a description of the student objective and data tips for the student to begin interacting with data. The activity also includes questions to prompt interpretation and analysis, facilitating each student’s ability to digest and make sense of the data. Annotated background images and resources provide context. In addition, professors are encouraged to use the EPE concept-mapping tool to assess prior knowledge and reflect on knowledge gained.

Example Data Interactive from The OOI Data Explorations Project

Seasonal Variation of Surface Salinity

Explore and analyze patterns in how surface salinity changes over time.

This activity has the following variations:

Exploration

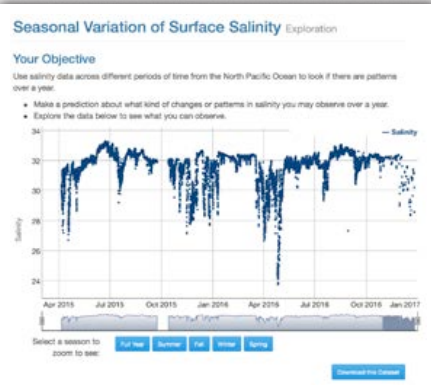
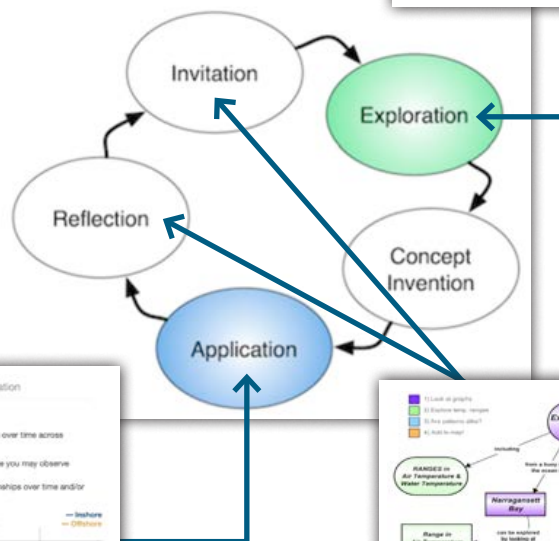
Use salinity data across different periods of time from the North Pacific Ocean to look if there are patterns over a year.

Application

Use salinity data across different time periods to determine if there are relationships over time across different regions of the ocean.

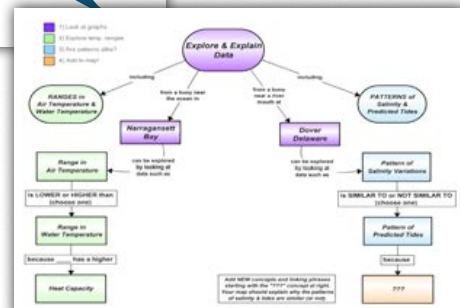
Application

The application phase focuses on comparing patterns to determine relationships in the data in time and space.



Exploration

The exploration phase focuses on exploring data to see what you can observe.



Concept Maps

Concept maps can be used to support the learning cycle—especially invitation and reflection phases.

FIGURE 3. An example of one of the data activities, Seasonal Variation of Surface Salinity, from the 30 developed as part of the Data Explorations project. The data activities were largely devoted to the “Exploration” and “Application” phases of the Learning Cycle and associated question prompts. In “Exploration,” the learner focuses on observations that can be made from the data. In “Application,” the learner focuses on comparing spatial and temporal patterns and relationships in the data. The Concept Mapper tool was frequently used to support learning, especially during the “Invitation” and “Reflection” phases.

Professors can use Data Explorations activities to augment concepts already included in their courses. For example, if they teach about seasonal variation of sea surface salinity, they can use data activities tied to relevant OOI data sets and interactive visualizations. Given that each Data Explorations activity includes multiple options, professors can tailor them to support the learning objectives and the abilities of their students.

LOOKING FORWARD AND NEXT STEPS

We hope the community of professors using OOI data in their classrooms will continue to expand over the coming years. As we further develop content, in-person and online courses, and tutorials, we hope that leaders will emerge who are excited about engaging students in OOI data and science. We invite new partners to participate and will continue to add content to the Data Explorations website as funding allows. Finally, we will work with educational researchers and practitioners to refine our Data Explorations model, building a critical mass of exemplars and sharing effective practices in the educational literature. Our EPE experience shows that the oceanographic community needs to continue improving its data tools to support educational needs, thereby reducing barriers to accessing and understanding science content. The community needs to be able to build/update tools and content (lessons) as OOI evolves. We recommend a continued focus on developing new data activities and providing professional development to continue to expand a user base for OOI education. ☺

REFERENCES

- Adams, L.G., and G. Matsumoto. 2009. Commentary: Enhancing ocean literacy using real-time data. *Oceanography* 22(2):12–13, <https://doi.org/10.5670/oceanog.2009.55>.
- Brown, P.L., and S.K. Abell. 2007. Examining the learning cycle. *Science and Children* 44:58–59.
- Bybee, R.W., J. Taylor, A. Gardner, P. Van Scotter, J. Carlson Powell, A. Westbrook, and N. Landes. 2006. *The BSCS 5E Instructional Model: Origins, Effectiveness, & Application*. BSCS, Colorado Springs, CO, 80 pp., https://uteach.wiki.uml.edu/file/view/Uteach_5Es.pdf/355111234/Uteach_5Es.pdf.
- Chinn, C.A., and W. Brewer. 1998. An empirical test of a taxonomy of responses to anomalous data in science. *Journal of Research in Science Teaching* 35(6):623–654, [https://doi.org/10.1002/\(SICI\)1098-2736\(199808\)35:6<623::AID-TEA3>3.0.CO;2-0](https://doi.org/10.1002/(SICI)1098-2736(199808)35:6<623::AID-TEA3>3.0.CO;2-0).
- deCharon, A., L. Duguay, J. McDonnell, C. Peach, C. Companion, C. Herren, P. Harcourt, T. Repa, C. Ferraro, P. Kwon, and others. 2013. Concept mapping workshops: Helping ocean scientists represent and communicate science. *Oceanography* 26(1):98–105, <https://doi.org/10.5670/oceanog.2013.08>.
- deCharon, A., L. Smith, and C. Companion. 2015. Characterizing complex marine systems and technology using visualized vocabularies. *Marine Technology Society Journal* 49(4):53–63, <https://doi.org/10.4031/MTSJ.49.4.2>.
- Hays, J.D., S. Pfirman, B. Blumenthal, K. Kastens, and W. Menke. 2000. Earth science instruction with digital data. *Computers & Geosciences* 26(6):657–668, [https://doi.org/10.1016/S0098-3004\(99\)00101-6](https://doi.org/10.1016/S0098-3004(99)00101-6).
- Hug, B., and K.L. McNeill. 2008. Use of first-hand and second-hand data in science: Does data type influence classroom conversations? *International Journal of Science Education* 30(13):1,725–1,751, <https://doi.org/10.1080/09500690701506945>.
- Hunter-Thomson, K., S. Lichtenwalner, and J. McDonnell. 2017. Incorporating observatory data into oceanography courses. *Eos* 98, <https://doi.org/10.1029/2017EO087369>.
- Kastens, K. 2011. Learning to learn from data. *Earth and Mind: The blog*, <http://serc.carleton.edu/earthandmind/posts/datalearningpro.html>.
- Krumhansl, R., A. Busey, K. Krumhansl, J. Foster, and C. Peach. 2013. *Visualizing Oceans of Data: Educational Interface Design*. 8 pp., <http://www.oceansofdata.org/sites/oceansofdata.org/files/MTS-2013.pdf>.
- Lawson, A.E. 2002. The learning cycle. Pp. 51–76 in *A Love of Discovery: Science Education—The Second Career of Robert Karplus*. R.G. Fuller, ed., Springer.
- Manduca, C.A., and D.W. Mogk. 2002. *Using Data in Undergraduate Science Classrooms: Final Report on An Interdisciplinary Workshop Held at Carleton College, April 2002*. Carleton College, Science Education Resource Center.
- Matsumoto, G., J. Bursek, R. Czujko, A. deCharon, S. Franks, S. Gilman, A. Holt-Cline, D. Keith, D. Malmquist, J. McDonnell, and others. 2006. *Ocean Research and Interactive Observatory Networks (ORION) Education and Public Awareness Draft Strategic Plan*. http://oceaneleadership.org/wp-content/uploads/2009/07/OOI_ORIONEducationPlan_4_0.pdf.
- McDonnell, J., S. Lichtenwalner, S. Glenn, C. Ferraro, K. Hunter-Thomson, and J. Hewlett. 2015. The challenges and opportunities of using data in teaching from the perspective of undergraduate oceanography professors. *Marine Technology Science Journal* 49(4):76–85, <https://doi.org/10.4031/MTSJ.49.4.9>.
- National Science Board. 2007. *A National Action Plan for Addressing the Critical Needs of the U.S. Science, Technology, Engineering, and Mathematics Education System*. National Science Foundation, Arlington, VA.
- Oceans of Data Institute. 2015. *Building Global Interest in Data Literacy: A Dialogue Workshop Report*. Oceans of Data Institute, 24 pp., <http://oceansofdata.org/our-work/building-global-interest-data-literacy-dialogue-workshop-report>.
- Pfirman, S., F. Lawrenz, G. Chin-Leo, K. St. John, R. Kinzler, S. Pompea, and B. Herbert. 2011. COSEE Decadal Review Committee Report. <http://www.cosee.net/files/coseenetc/COSEE Decadal Review Report final 092411 3.pdf>.
- Sampson, V., and D. Clark. 2008. Assessment of the ways students generate arguments in science education: Current perspectives and recommendations for future directions. *Science Education* 92(3):447–472, <https://doi.org/10.1002/sce.20276>.
- Simoniello, C., L. Spence, N. Deans, and J. McDonnell. 2010. Developing an education and outreach program for the US IOOS: Eyes on the ocean, hands-on learning. *Marine Technology Society Journal* 44(6):176–184.
- Trujillo, A., and H. Thurman. 2016. *Essentials of Oceanography*, 12th ed. Pearson Press, 624 pp.

ACKNOWLEDGMENTS

We would like to acknowledge the support of the OOI data team, Michael Vardaro, Lori Garzio, Friedrich Knuth, Michael Smith, and Leila Belabassi; the Raytheon Web Solutions team, Sean Graham, Allan Yu, and Joe Wieclawek; and the Consortium for Ocean Leadership office, especially Andrea McCurdy. We thank Debi Kilb, Alison Fundis, and Craig Risien, who served as EPE liaisons during the project. We greatly appreciate advice and support from Cheryl Peach and Liesl Hotaling. We especially thank Lisa Rom for her support and guidance over the years.

AUTHORS

Janice McDonnell (mcdonnel@marine.rutgers.edu) is an Educator in the Department of Marine and Coastal Sciences, Rutgers University, New Brunswick, NJ, USA. **Annette deCharon** is Senior Marine Outreach Education Scientist, University of Maine, Darling Marine Science Center, Walpole, ME, USA. **C. Sage Lichtenwalner** is Research Programmer, Department of Marine and Coastal Sciences, Rutgers University, New Brunswick, NJ, USA. **Kristin Hunter-Thomson** is Program Director of Dataspire and Teaching Instructor, Department of Human Ecology, Rutgers University, New Brunswick, NJ, USA. **Catherine Halversen** is Senior Program Director, Lawrence Hall of Science, University of California, Berkeley, Berkeley, CA, USA. **Oscar Schofield** is Professor, **Scott Glenn** is Professor, and **Carrie Ferraro** is Education and Outreach Program Coordinator, all in the Department of Marine and Coastal Sciences, Rutgers University, New Brunswick, NJ, USA. **Carla Lauter** is Research Associate, University of Maine, Darling Marine Science Center, Walpole, ME, USA. **James Hewlett** is Professor, Finger Lakes Community College, Canandaigua, NY, USA.

ARTICLE CITATION

McDonnell, J., A. deCharon, C.S. Lichtenwalner, K. Hunter-Thomson, C. Halversen, O. Schofield, S. Glenn, C. Ferraro, C. Lauter, and J. Hewlett. 2018. Education and public engagement in OOI: Lessons learned from the field. *Oceanography* 31(1):138–146, <https://doi.org/10.5670/oceanog.2018.122>.

SIDE BAR

Seastate: Experiential C-STEM Learning Through Environmental Sensor Building

By Deborah S. Kelley and Daniel Grünbaum

Students at Clallam Bay School on the Olympic Peninsula are mentored by Seastate science instructor Kevin Eyer as they try soldering for the first time during building of a temperature sensor.

Photo Credit: D. Kelley, University of Washington



A new experiential learning program called "Seastate" (<http://seastate.ocean.washington.edu>) has been established at the University of Washington (UW) to increase K20 (K12 plus higher education) computing, science, technology, engineering, and math (C+STEM) knowledge. The program's objectives focus on student-driven design, building, and implementation of sensors to address locally relevant environmental problems. In partnership with the West Sound STEM Network and with funding from the State of Washington, the goal is to mentor K12 teachers from 18 school districts on Kitsap Peninsula, Washington, in sensor building and marine science. In addition, the UW School of Oceanography curriculum includes a hands-on Ocean Technology program (https://www.ocean.washington.edu/story/OTP_Home) that includes a multiyear class sequence and opportunities for UW students to mentor K12 teachers and students in environmental sensing, augmented with core knowledge about local marine environments directly impacting their communities. Our experience shows that coupling hands-on activities with deployment of sensors in the field is a particularly effective way to promote computational skills and environmental literacy among underrepresented minority communities.

K12 teachers and students gain C+STEM skills and confidence by constructing their own inexpensive environmental sensors. They initially assemble temperature sensors and install them in local environments to learn the basics of sensor building, circuitry, and microprocessor functions used to assess environmental variability across a range of timescales. Other instruments include sensors for measuring light penetration through water and vegetation and for colorimetric pH assays; webcams for quantification of animal activities and distributions; weather sensors for measurements such as UV index, barometric pressure, and relative humidity; and GPS position sensors. This program introduces teachers and students to microcontroller hardware and sensor interaction via Python, which is used across all levels of computing, from microcontrollers in embedded systems to high-level scientific computing.

As part of this effort, elementary students used their sensors to monitor temperatures in a classroom tank containing salmon fry and in a local creek so that they could release the salmon under similar environmental conditions. Similarly, sixth grade students deployed temperature sensors and collected dissolved oxygen, pH, turbidity, and flow rate data on a nearby creek for comparison with earlier data to understand how this habitat has changed over the past 15 years. Middle school students used their sensors to investigate how temperatures on land and in nearby natural bodies of water differed, enhancing understanding of ecological relationships among organisms.

Content is copyright protected and provided for personal use only - not for reproduction or retransmission.

Oceanography | March 2018

147

For reprints please contact the Publisher.

in local ponds. High school students designed and built two moorings to carry "weatherboard" sensors for measuring light intensity and temperature from the sea surface to shallow underwater depths. These data will be used to develop models for selection of eelgrass restoration sites along Straits of Juan de Fuca shorelines. Through Seastate, student-collected data about local phenomena will be uploaded and analyzed by teachers and students across the region, creating a rich environment to interactively explore their data and share online stories about discoveries and lessons learned.

In the UW Ocean Technology program, students gain foundational knowledge of methods used to observe ocean characteristics, what sensors measure, what temporal and spatial sampling resolution is required to address scientific questions, and how these translate into sensor engineering requirements. Students gain practical engineering and project management skills that help them understand and critically assess design and execution of instrumentation, including critical path planning involving conceptual, preliminary, and final design evaluations and development of budgets and milestones. Students work individually or in teams during sensor design, construction, and testing prior to installation.

A student-designed and -built cabled observatory dubbed Exploration and Remote Instrumentation by Students (ERIS, <https://www.ocean.washington.edu/story/ERIS>), located off of the UW School of Oceanography dock, emulates the National Science Foundations' Ocean Observatories Initiative (OOI) Cabled Array (<http://oceanobservatories.org/array/cabled-array>). Similar to the Cabled Array, the sensors installed on ERIS provide continuous data streams for analysis and interpretation, with scaling opportunities to the OOI. Coupling of these programs, involving instrument design and construction, data collection, and development of data analytical and visualization skills, will place students in strong positions to take full advantage of rapidly evolving sensor and data technologies that are transforming how we monitor and interact with our dynamic planet.

ARTICLE CITATION

Kelley, D.S., and D. Grünbaum. 2018. Seastate: Experiential C-STEM learning through environmental sensor building. *Oceanography* 31(1):147, <https://doi.org/10.5670/oceanog.2018.123>.

AUTHORS

Deborah S. Kelley is Professor (dskelley@uw.edu) and **Daniel Grünbaum** is Professor, both at the University of Washington, School of Oceanography, Seattle, WA, USA.

Are You a Marine Major or Minor?

By Simon Boxall

After my last column in *Oceanography* in September 2017 (<https://doi.org/10.5670/oceanog.2017.305>), in search of inspiration, ideas for new articles have flooded in, which, like buses, seem to always arrive in groups. Some from readers (with my thanks), and some from the fathomous depths of my own mind. On a contemporary topic, Alan Mix (TOS president) and Ellen Kappel (my long-suffering editor) suggested looking at how a wide range of undergraduate programs are building a marine science focus into their curricula. I say contemporary, as we have just seen the latest (and possibly best) offering from Sir David Attenborough in his recently aired *Blue Planet II*. As with many such noteworthy documentary series, the interest in studying for a degree in oceanography or marine biology has consequently seen a measurable boost as young people become inspired by oceanic adventures and the great unknown. But the benefit of programs like *Blue Planet* is that they also provide an elegant public platform for our science and highlight its importance in twenty-first century society, identifying issues from plastic pollution in the sea to climate change.

In an ideal world we might see a plethora of bright students electing to study marine science at the undergraduate level, but it is still a relatively small number of universities around the world that offer such degrees. Many still focus on graduate degree or research pathways. In addition, many prospective students have an interest in the ocean but perhaps do not want to major in science, nor do they have the right background for a full degree in science, or indeed want to follow a pure science or maths pathway. The last of this group will form a significant number of our graduate cohort, and so exposure to some marine science at the undergraduate level is important for

future recruitment. In addition, future professionals in science, engineering, law, and politics who have some exposure to marine science will bring the core issues of the subject to the fore.

So it is simple—provide subsidiary courses or minors in marine sciences that students from a wide range of disciplines could follow and benefit from. In the distant past when I did my degree (with just three other students!), other undergraduates also took some of our marine science modules as a part of their maths, chemistry, or physics degrees, swelling numbers to over 80 in some modules. It has to be said, and with due respect to my professors of the time, while the four of us lapped up the details of advanced ocean dynamics and tidal theory, it was a touch on the dry side for the other students. The interest back then was inspired by the adventures of Jacques Cousteau aboard *Calypso* rather than today's David Attenborough and his *Alucia*. Many students taking subsidiary units were disappointed to discover that there were no field expeditions to the sun-soaked coasts of the Mediterranean, with dinner on the aft deck chatting about science over a glass of wine while barbecuing Jacques's latest discovery from the deep. There was a lot of (difficult) maths and theory to deal with first, and many never returned to the subject to reach the more hedonistic stages...

Today, students from other degree courses do take some of my own first-year modules, and they come from a wide variety of disciplines. As well as the expected geologists and environmental scientists, I have biochemists, geographers, mathematicians, engineers, and even the occasional law student. Ensuring that the a priori knowledge needed fits with such a diverse cohort can at times be challenging. I need to ensure that our oceanography major students can progress to higher

levels while still making the course interesting to the others, for whom it may be their only foray into marine science. It is important to ensure there is a good mix of theory and practice, and while our teaching vessel doesn't have a barbecue and operates in the slightly cooler English Channel, it does offer an inspiring window on the subject for all students. My own school offers joint degrees with marine science as a minor with subjects like geography. However, in the UK we have yet to fully embrace the concept of a minor concentration. There are set pathways, but the option of, say, a degree in physics with a minor of your choice is still some way off.

There are two issues with this. In order to fulfill the basic needs of the major (or main degree), there are some essential units that every marine scientist, chemist, or geographer needs to cover. In the United States and many other countries, it takes at least four years to earn a bachelor's degree, but in the UK, most degrees are awarded in three years (with growing pressure from government to reduce this period to an accelerated two years). While the core material for a four-year program can still be covered and allow a student to concentrate in a minor subject area, this becomes difficult to achieve within a three-year period. In my School of Ocean and Earth Science, we have to think carefully about what unit a student can drop whenever a new unit is introduced.

The second issue—timetables—is more frustrating. As with many universities, our timetables work within our departments, which is great if students wanting to undertake units outside their own subject stay within the department. However, if the student wants a cross-department experience, it becomes a logistical nightmare. It is often made worse by the fact that, in many cases, the

marine science school is remote from the university's main campus, involving a 20- or 30-minute bus journey between lectures. My school has moved departments twice and is about to undergo a new change in 2018. Twenty years ago, marine science was in the same department as environmental science and geography. This meant that a third of students in our first- and some second-year courses were from these subjects and we saw a good cross-fertilization of subjects. We then became a Faculty of Natural and Environmental Science, which strangely didn't include environmental science (hang on...it gets even stranger...). At that stage, interfaculty timetabling meant that only the most determined students from environmental science or geography could attend marine science courses. In addition, increased student numbers across the university and more units actually meant more restricted timetables and less choice, which is very much the case in other universities. We have actually gone back on options rather than forward. The good news is that we are reforming departments in 2018 and will once again encompass environmental science and geography, along with midwifery (I said it gets stranger...). I guess midwives might benefit from a first-year module in oceanography for those ever-popular water births? Nothing worse than an unexpected tsunami in the birthing pool.

There is a genuine desire for more cross-faculty units from our university hierarchy, but the reality is that a major leap across departments is difficult. This brings us to the alternative—taking examples from what is a very cool subject (we are slightly biased) and building them into other subjects. Wave theory in physics is an example where ocean waves are much more exciting than bits of string, the ocean provides an excellent applied mathematics focus for calculus, and the subject of international issues of marine resources is a very hot and contemporary item for economics and politics majors. After some level of success in trying to get examples of marine science into our

school (pre-university) curriculum, we should be working in our own universities to introduce some of our subject into other university undergraduate schools, and not just in science. At Southampton, some of our staff are shared with other departments, for example, with engineering, with archeology, and with maritime law. It is often easier to timetable a member of staff than it is to timetable 150 students all doing differing pathways. In addition, for short three-year programs it does not detract from the core material needed in a particular subject.

The perfect solution? Well, there is still an issue. Persuading an academic to increase teaching load, and in another department, is never going to be easy when we are under more and more time pressure. Marine science is being introduced in science departments in other universities in the UK that don't have a tradition or track record in the field. The number of colleagues who move to join departments of biology, chemistry, geography, environmental science, and engineering is on the rise. They are not only taking their marine research into these new departments but are also building a marine focus into their teaching so that individual units now consider issues such as marine renewables, coastal defenses, sustainable marine ecosystems, and numerical ocean modeling. These subjects are part of their core teaching role, and they do provide a way of introducing some of the concepts of marine science to non-oceanographers. Having come from more traditional schools and departments of marine science, these instructors are also well placed to signpost enthusiastic students into the field at the graduate level. It all lacks one thing—if a university doesn't have a fully developed marine science department, it is also unlikely to have the best component of our subject, a boat or research ship.

In the United States, Canada, and Bermuda, a growing number of summer schools open to undergraduates enable them to experience fieldwork firsthand. These programs provide training and

experience that build on initial interest that may be sparked by one or two modules with a marine focus in their undergraduate programs. In Europe, although there are postgraduate summer schools, there are very few that target undergraduates. Ironically, we are very good at targeting students pre-university, but there seems to be a gap at the undergraduate level. We are about to embark on a project with the British Council in the UK to bring a group of British and German students together for a short residential course to improve their ocean literacy, with a focus on rising sea levels and plastic litter. The objective would be to build on their diverse degree programs and consider not just the science but also socioeconomic issues.

If the answer to more inclusion of marine subjects in a wide range of undergraduate programs is introducing staff with marine backgrounds, then there will be a need to increase access to the exciting facilities and opportunities at the more traditional marine science schools across the globe. Such an effort will need funding—resources do not come cheap—but the benefits to the subject should be significant in the long term. I know that Alan Mix is keen to discover more, as am I, and so following on from my previous request for topics to be covered, we would be very interested in understanding what other academics' experiences have been in introducing ocean or marine science into non-marine science programs. Please email us with your experiences, and if there is sufficient response, we will provide a follow-up article on this subject in the near future.

And if anyone can think of an oceanographic link into midwifery, I'd love to hear about it. 

ARTICLE CITATION

Boxall, S. 2018. Are you a marine major or minor? *Oceanography* 31(1):148–149, <https://doi.org/10.5670/oceanog.2018.103>.

AUTHOR

Simon Boxall (sr2@noc.soton.ac.uk) is Associate Professor, Ocean and Earth Science, University of Southampton, National Oceanography Centre, Southampton, UK.

CAREER PROFILES Options and Insights

HEATHER HAVENS | Vice President, Program Development, National Defense Industrial Association (hhavens@ndia.org)

Degree: When, where, what, and what in?

In college, I studied biology at Agnes Scott College with the intention of going into the medical field. The summer before my senior year, I took a course through the School for Field Studies in the Turks and Caicos Islands that focused on marine resource studies. That experience changed my career path trajectory, and I went on to study marine science in graduate school as a result. I earned my MS in marine science from the University of South Carolina, with a focus on physical-biological oceanographic interactions and the effectiveness of the boundaries of an existing marine protected area in protecting a snapper spawning ground along the Belize Barrier Reef. I went on to earn my PhD in marine science, with a focus on physical oceanography, from the University of South Florida. My doctoral work focused on combining real-time oceanographic data with numerical models to investigate various problems in the Tampa Bay estuary ranging from maritime transportation to search and rescue operations and environmental water quality issues.

Did you stay in academia at all, and if so, for how long?

I did not stay in academia after earning my doctorate. While I enjoyed the research and fieldwork associated with getting my doctorate degree, I had a desire to transition from academia to policy. I wanted to use my scientific training to translate data and research findings into easy-to-understand policy positions, so I began considering postdocs and fellowships that involved marine policy.

After earning my doctorate degree, I was awarded a fellowship on Capitol Hill and moved to Washington, DC. The John

A. Knauss Marine Policy Fellowship is sponsored by the NOAA Sea Grant program. During the 12-month fellowship, I was immersed in marine policy at the national level.

The one-year Knauss fellowship places graduate students in an office in either the executive or the legislative branch of the government. I chose the legislative branch and was placed in the office of a US Representative from the central coast of California. During my fellowship, the Deepwater Horizon incident occurred, and I was thrown into preparations for Congressional committee hearings focusing on efforts to cap the oil spill, followed by the subsequent cleanup efforts. One thing I noticed throughout hearings was the involvement of the US Coast Guard and the US Navy in the government response efforts. Both services were providing not only ships and personnel, but also oceanographic and meteorological data to assist in the response effort. From that experience, I became interested in the military's role in providing what I now know to be called "maritime domain awareness" data to the local and federal governments involved in the response efforts.

How did you go about searching for a job outside of the university setting?

Many organizations send out weekly or monthly job postings for a particular career field. A few months before the end of my fellowship, I signed up for a number of these listservs and started receiving job announcements focused on ocean policy. Applying to jobs through these announcements, as well as through networking connections that I had gained during my time on Capitol Hill, I was able to interview for several ocean policy positions. It was not until I had gone through



several interviews that I realized that the job I really was looking for was one that allowed me to "get back into the science" and meet my goal of translating research data into policy positions, now with a broadened focus of including the defense industry in my job search, based on my fellowship experience.

It was difficult to turn down a couple of job offers at very reputable organizations, and risk possibly not finding a job once my fellowship was over, but in the end, it paid off. I was fortunate to be hired by a large defense company on a Navy contract to translate oceanographic modeling and simulation data into environmental policy.

Is this the only job (post-academia) that you've had? If not, what else did you do?

After three years on the environmental policy contract with the Navy, I sought out an opportunity with a smaller defense company to work on another defense contract, this time focusing on Arctic policy and the impacts to the Navy as this region becomes less ice covered.

What is your current job? What path did you take to get there?

Currently, I am Vice President of Program Development at the National Defense Industrial Association (NDIA). It is a

501(c)3 nonprofit association that strives to connect academia, industry, and government to provide innovative solutions that advance the national security and defense needs of the nation. I sought out this job to broaden my horizons and to learn more about the nonprofit sector.

What did your oceanographic education (or academic career) give you that is useful in your current job?

Even though my current job no longer exclusively focuses on oceanography, I still use aspects of my education and training in my daily work. My graduate education set me up with the expertise to be able to translate data and research findings into policy positions. My current job requires that I communicate effectively with high level federal and administration officials using skills that I gained on Capitol Hill during my marine policy fellowship.

Is there any course or other training you would have liked to have had as part of your graduate education to meet the demands of the job market?

I had some exposure to science writing and communication training when in graduate school, but I would have benefited from a formal course in these areas. I would have also welcomed a graduate-level mentoring program, perhaps one that paired me with a career professional, to better prepare me as I transitioned from academia to policy.

Is the job satisfying? What aspects of the job do you like best/least?

My job is very satisfying and rewarding. As a scientist, I enjoy being able to connect other scientists and researchers in academia with scientists in the Department of Defense and elsewhere in the US government. I'm also responsible for developing and coordinating program development initiatives and long-range

strategic objectives. This means that part of my job entails traveling to conferences and seminars that feature cutting-edge technology or innovative thinking. I am fortunate to be able to stay engaged with the scientific community while also engaging with industry and government.

Do you have any recommendations for new grads looking for jobs?

My advice, and this is not specific to my field, would be to take advantage of any and all opportunities that are presented to you, whether you think they will be helpful to your current career path or not. My path involved a summer study program in college, an internship in grad school, and a post-graduate fellowship to arrive at my current professional occupation. Sometimes the path you think you're meant to be on can diverge and you can find yourself going in a completely different, but maybe more interesting, direction. ☎

ANDREAS KRUPKE | Scientist III, Verification & Validation Department, Thermo Fisher Scientific (andreas.krupke@thermofisher.com)

Degree: When, where, what, and what in?

In 2013, I earned my PhD in biochemistry at the Max-Planck-Institute for Marine Microbiology in Bremen, Germany. My thesis focused on linking molecular biology with mass spectrometry, allowing me to discover an ecologically important group of marine cyanobacteria (UCYN-A) living in symbiosis with a eukaryotic cell and to provide the first physiological insights into this unique relationship.

Did you stay in academia at all, and if so, for how long?

After my PhD, I completed a 1.5-year postdoc position at the Woods Hole Oceanographic Institution (WHOI). During my tenure at WHOI, my work focused on open-ocean environments where I investigated the microbial

phosphorus redox cycle. I also worked on a project to understand how bacterial infochemicals impact particle degradation in the ocean.

How did you go about searching for a job outside of the university setting?

When I started my search, I knew I wanted to be a bench scientist. I began by reading job descriptions to determine what skills were required for an industry position, and then comparing those requirements to my own skill set. This early research helped me define what jobs interested me outside of academia and what proficiencies were needed to be a viable applicant. In parallel, I reached out to individuals who held relevant industry positions to learn about their careers, day-to-day work responsibilities, and transitions into the private sector. I



strongly recommend the “informational interview” approach, as the conversations are relaxed and no one feels pressured to discuss specific job offers—this approach helps you build a professional network outside academia that can result in specific job referrals down the road. I also spent time networking as part of a local biotech “meet up” group, and I attended seminars at nearby universities relating to careers outside academia.



Graduate Student and Early Career Resources

<https://tos.org/opportunities>

The Oceanography Society has created a web page with resources relevant to ocean sciences graduate students and early career scientists. This portal contains links to information on jobs, fellowships, scholarships, and ship time/fieldwork opportunities, as well as links to useful articles. New resources are added regularly, so please be sure visit this site often!

Oceanography Student News

<https://tos.org/opportunities>



Have you read the latest issue of Oceanography Student News? Each newsletter includes a regular column by the student representative to the TOS Council, profiles of TOS student members, information about student activities related to TOS-sponsored meetings, and links to relevant student resources and articles in *Oceanography* magazine. Feel free to forward the links to the newsletters to other students, or print out a copy and post it on your department bulletin board. Any questions? Email TOS Student Rep Stefanie Mack at studentrep@tos.org.

Is this the only job (post-academia) that you've had? If not, what else did you do?

This is my second job outside academia. My first role was a research scientist position in the R&D department at Thermo Fisher Scientific in San Jose, California, where I tested and developed technologies to link capillary electrophoresis to mass spectrometry for protein analysis (e.g., ZipChip Interface coupled to QE-Biopharma instrument). This position was very similar to my academic endeavors, as I spent most of my time in the lab and also presented project developments to my team members. I enjoyed this work, but was also interested in learning more about the business side of Thermo Fisher's operations.

What is your current job? What path did you take to get there?

I am a Scientist III in the Verification & Validation department at Thermo Fisher Scientific in South San Francisco, California. My main responsibility is to assure that products under development (e.g., capillary electrophoresis instruments) meet distinct quality and performance requirements before official release. I meet with colleagues from the R&D and business departments at Thermo Fisher in order to get both sides to agree regarding product specifications, which I then use to design, plan, and execute test protocols for upcoming products. Day to day, I spend some time in the lab trouble-shooting instruments and software. The remaining time I spend interfacing with others in my department to discuss results and key findings. There are also opportunities to develop and write research proposals internally at Thermo Fisher to acquire internal funding for additional innovative projects.

What did your oceanographic education (or academic career) give you that is useful in your current job?

My current job requires that I work effectively in an interdisciplinary environment with teams from various backgrounds

such as engineering, biochemistry, and product management. I also need to be comfortable using and connecting new technologies with one another and translating scientific data into written forms and presentations. My academic background gave me experience in all of the above. Specifically, I give credit to the numerous hours I spent in the lab tinkering with new instruments, as well as the time I dedicated to publishing my projects.

Is there any course or other training you would have liked to have had as part of your graduate education to meet the demands of the job market?

If I were to go back to graduate school, I would take courses in product management and financial planning for commercializing products from the R&D stage to market. These are areas I touch upon on a daily basis, and have had to learn more about as I go along.

Is the job satisfying? What aspects of the job do you like best/least?

My job is satisfying because I can learn about cutting-edge technologies, especially ones that are not yet publicly available. I also find it rewarding to interact with teams who bring in expertise from R&D, business, marketing, and sales. Navigating through such terrain can be challenging, as I need to convey information to audiences with different agendas and vocabularies, but at the same time these challenges enable me to constantly gain new knowledge and skills.

Do you have any recommendations for new grads looking for jobs?

Identify aspects in your graduate role you like the most—what excites you? Conduct informational interviews, and network inside as well as outside academia. This will give you valuable information about the types of positions out there and the skills needed to help you strategize your next steps to land the job you like. ☘



THE
OCEANOGRAPHY
SOCIETY

FREE
STUDENT
MEMBERSHIP!

Join TOS

**Make connections,
advance your career,
enrich your research**

The Oceanography Society (TOS) was founded in 1988 to advance oceanographic research, technology, and education, and to disseminate knowledge of oceanography and its application through research and education. TOS promotes the broad understanding of oceanography, facilitates consensus building across all the disciplines of the field, and informs the public about ocean research, innovative technology, and educational opportunities throughout the spectrum of oceanographic inquiry. TOS welcomes members from all nations. Any individual, business, or organization interested in ocean sciences is encouraged to join and to participate in the activities and benefits of the society.

The membership period is January 1st through December 31st of each year. Upon joining, new members will receive access to back issues of *Oceanography* magazine for that membership period.

Membership Options

Regular Membership [\$60]. Available to oceanographers, scientists, or engineers active in ocean-related fields, or to persons who have advanced oceanography by management or other public service.

Student Membership [Free!]. Available for students enrolled in an oceanography or ocean-related program at the baccalaureate or higher level.

Early Career Membership [\$30]. Available to non-student oceanographers, scientists, or engineers active in ocean-related fields, or to persons who have advanced oceanography by management or other public service who have received their highest degree within the past three years.

Sponsoring Membership [\$110]. Available to individuals who wish to provide enhanced support annually. In the US, \$50 of the annual dues in this category is tax-deductible as a charitable contribution, as are any additional contributions, over and above the annual regular membership dues.



New!

Call for Corporate and Institutional TOS Members

[Starting at \$300] TOS invites all corporate or non-profit organizations interested in the ocean sciences to join as members in this category. With the implementation of a flexible pricing strategy, TOS hopes to attract small "start-ups" as well as larger companies and institutions. Check out the list of benefits at:

<https://tos.org/corporate-and-institutional-members>

Please send any suggestions for organizations that you think could be good prospects for corporate or institutional membership to Jenny Ramarui (jenny@tos.org).

Visit <https://tos.org> and click on join TOS

to complete your application!

Content is copyright protected and provided for personal use only—not for reproduction or retransmission.

For reprints please contact the Publisher.

 The Oceanography Society
1 Research Court, Suite 450
Rockville, MD 20850, USA

ADDRESS SERVICE REQUESTED

Non Profit Org.
U.S. Postage
PAID
Washington, DC
Permit No. 251



OCEAN OPTICS XXIV

Valamar Lacroma Hotel | Dubrovnik, Croatia | October 7–12, 2018

Join your colleagues in fall 2018 to explore and expand the many facets of ocean color remote sensing and optical oceanography, including basic research, technological development, environmental management, and policy. Visit the website below to join the email list and receive updates.

Abstract submission deadline: **May 4, 2018**

<https://oceanopticsconference.org>

CALL FOR
NOMINATIONS!

The Jerlov Award

Awarded in Recognition of Contribution Made to
the Advancement of Our Knowledge of the Nature
and Consequences of Light in the Ocean

Nominations due » **June 1, 2018**

Learn more at » <https://tos.org/jerlov-award>

